CHANGES IN VASOACTIVE INTESTINAL PEPTIDE (VIP) AMOUNT IN CYSTIC FIBROSIS

by

Poliana Anna Semaniakou

Submitted in partial fulfilment of the requirements

for the degree of Doctor of Philosophy

at

Dalhousie University

Halifax, Nova Scotia

November 2020

TABLE OF CONTENTS

LIST OF TABLES

LIST OF FIGURES

ABSTRACT

Cystic Fibrosis (CF) is the most common lethal genetic disease in Caucasians, which results from mutations in the CFTR gene. Cystic Fibrosis - Related Diabetes (CFRD) affects more than 50% of adults with CF. The complex etiology of CFRD is poorly understood and differs from type 1 or type 2 diabetes. The major physiological agonist of the CFTR chloride channel is the Vasoactive Intestinal Peptide (VIP), a 28-amino acid neuropeptide that functions as a neuromodulator and neurotransmitter secreted by intrinsic neurons innervating exocrine glands. VIP has also insulinotropic effects on pancreatic beta cells, augmenting glucose-dependent insulin secretion. Previous studies from our lab have demonstrated the molecular role of VIP in CFTR regulation, both *in vivo* and *in vitro.* Interestingly, exocrine glands from CF patients have sparse VIPergic innervation compared to healthy individuals, but the mechanism behind this phenomenon remains unknown.

The main goal of my PhD research was to investigate changes in VIP content in exocrine tissues in F508del/F508del mice, and determine if VIP depletion was related to CF disease progression. Furthermore, we examined the mechanism of this reduction in neuronal level. Lastly, we asked if the decreased VIP amount in the pancreas could contribute to CFRD pathophysiology.

Our data showed a significant decrease in the VIP content throughout all exocrine tissues that was not linked to inflammation and/or to disease progression but was rather an early onset of CF disease. This VIP reduction was due to a disruption of the intrinsic innervation network. Importantly, nerves co-expressing VIP and Acetylcholine were reduced in density. In the pancreas, we found low levels of VIP due to reduced pancreatic innervation, starting at an early disease stage, which may initiate the development of CFRD through down-regulation of insulin and glucagon secretion.

While most of the research is centered on how to cure the basic CFTR defects, the link of the dysfunctional nervous system to the disease progression is yet a thirst for knowledge. Our pioneer data provide fundamental knowledge to boost our understanding on neuronal alterations in CF and how this can affect the pathophysiology of CF and CFRD.

LIST OF ABBREVIATIONS USED

ABC – ATP-binding Cassette

ABC – Avidin/Biotinylated Complex

ACh – Acetylcholine

AE – Anion Exchanger

AMs – Alveolar Macrophages

ASL – Airway Surface Liquid

AVPNs – Airway Vagal Preganglionic Neurons

Bcc – Burkholderia cepacia complex

BSA – Bovine Serum Albumin

CaCC – Calcium Activated Chloride Channel

cAMP – 3',5'-Cyclic Adenosine Monophosphate

CB – Chronic Bronchitis

CChs – Catecholamines

CCK – Cholecystokinin

CD-25 – Interleukin-2 receptor alpha chain

CF – Cystic Fibrosis

CFRD – Cystic Fibrosis Related Diabetes

CFTR – Cystic Fibrosis Transmembrane conductance Regulator

ChAT – Anti-Choline Acetyltransferase

CHE – CFTR High Expresser cells

CNS – Central Nervous System

COPD – Chronic Obstructive Pulmonary Disease

CUBIC – Clear Unobstructed Brain/Body Imagining Cocktail

CVA – Crypt to Villus Axis

DAB – 3, 3 Diaminobenzidine HRP Substrate

DIOS – Distal Intestinal Obstruction Syndrome

EC1, EC2, and EC3 – Extracellular Loops

ECP – Eosinophil Cationic Protein

EGF – Epidermal Growth Factor

EL1 – Fecal Elastase-1

ENaC – Epithelial Sodium Channel

GH – Growth Hormone

GHFR – Glucagon Growth Hormone Releasing Factor

GI – Gastrointestinal track

GIP – Gastric Inhibitor Peptide

GLP-1 – Glucagon-Like Peptide-1

GLP-2 – Glucagon-Like Peptide 2

GLUT2 – Glucose Transporter 2

GPCRs – G Protein-Coupled Receptors

IC1, IC2, and IC3 – Intracellular Loops

ICAM-1 – Intercellular Adhesion Molecule 1

iFABP – intestinal Fatty-Acid-Binding Protein

IFN-γ – Interferon Gamma

IgG – Immunoglobulin G

IgM – Immunoglobulin M

IHC – Immunohistochemistry

IL-1 – Interleukin 1

IL-2 – Interleukin 2

IL-8 – Interleukin 8

IMs – Interstitial Macrophages

KO – Knockout

LL-37 – Cathelicidin Antimicrobial Peptide

MCC – Mucociliary Clearance

MCP-1 – Monocyte Chemotactic Protein 1

MI – Meconium Ileus

MIP-2 – Macrophage-Inflammatory Protein 2

MUC2 and MUC7 – Gel-Forming Mucins 2 and 7

MUC5B – Gel-Forming Mucin 5B

MUC5B and MUC5AC – Gel-Forming Mucins 5B and 5AC

NANC – Non-Adrenergic, Non-Cholinergic

NBC – Na^+ - HCO_3^- Cotransporter

NBD1 and NBD2 – Nucleotide Binding Domain 1 and 2

NEP – Neutral Endopeptidase

NKCC1 – Na^+ - K^+ - Cl^- Cotransporter

NOS – Nitric Oxide Synthase

NPY – Neuropeptide Y

ORCCs – Outwardly Rectifying Cl- Channels

PCL – Periciliary Layer

PERT – Pancreatic Enzyme Therapy

PFA – Paraformaldehyde

PGP 9.5 – Protein Gene Product 9.5

PHI – Peptide Histidine Isoleucine

PHM – Peptide Histidine Methionine

PI – Pancreatic Insufficient

PKA – Protein Kinase A

PKA and PKC – Protein Kinase A and C

PL – Placental Lactogen

PLC – Phospholipase C

PNS – Peripheral Nervous System

Po – Open State Probability

PRL – Prolactin

PTA – Phosphate-Triton Azide Buffer

QPIT – Quantitative Pilocarpine Iontophoresis Test

R – Regulatory Domain

S100A12 – Calgranulin C

S100A8/S100A9 – Calprotectin

SDS – Sodium Dodecyl Sulfate

SLC 26A9 – Solute Carrier 26A9

SMGs – Submucosal Glands

SP – Substance P

Th – T helper cells

TMB – 3,3’,5,5’-Tetramethylbenzidine

TMD1 and TMD2 – Transmembrane Domain 1 and 2

TNF-α – Tumor Necrosis Factor α

UCHL1 – Ubiquitin Carboxy-terminal Hydrolase L1

VAChT – Vesicular Acetylcholine Transporter

VIP – Vasoactive Intestinal Peptide

WT – Wild-Type

YY – Peptide Tyrosine Tyrosine

ACKNOWLEDGEMENTS

Accomplishing this Ph.D. degree was made possible through the support of great people surrounding me.

First of all, I would like to express my sincere gratitude to my supervisor, Dr. Valerie Chappe, who trusted me from the very first moment and gave me the opportunity to develop my scientific knowledge. Dr. Chappe, I am so grateful to you for the continuous support, motivation, and constructive criticism throughout the project, for encouraging me through the vicissitudes, but also for inspiring me intellectually and personally through your strong personality as a woman in science.

Next, I would like to extend my appreciation and respect to a high calibre scientist and an amazing person, Dr. Roger Croll, who has been a real father over the past five years. Dr. Croll, thank you for the many hours of research discussion, your innovative ideas, unwavering enthusiasm in science, and your significant contribution to this project. Most importantly, thank you for your psychological support and always being there for me.

Moreover, I am thankful to the excellent members of my Supervisory Committee Meeting, Dr. Younes Anini, Dr. Yassine El Hiani, and Dr. Christian Lehmann. Without your continuous mentorship, comprehensive advice, insightful remarks, and expertise, this dissertation would not have been possible. Dr. Anini, thank you for your guidance and endless patience with all the ELISA experiments, and also for providing me with the opportunity to teach in your course. You are an inspiring professor and an amazing mentor. Dr. El Hiani, I deeply thank you not only for your valuable feedback throughout my research, but also for being a good friend. Our conversations always provided me with strong incentives to not give up during the hardships of my Ph.D. Dr. Lehmann, thank you for all your contribution on my research and your support during my comprehensive exam. Another special thanks to Dr. Juan Ianowski for accepting to become my external examiner and taking the time to review my thesis.

I would also like to kindly thank Dr. Elizabeth Cowley, Dr. Marie-Soleil Beaudoin, Dr. Cindy Penney, Haitham Fathalla, and Diane Cox for trusting me with the opportunity to convert my theoretical knowledge into practical experience: because of your guidance, I have

been able to change my teaching philosophy, which is now grounded in encouraging and motivating my students to learn in a collaborative environment. In addition to that, I would not be able to boost my teaching experience without the Certificate in University Teaching and Learning that is being run by Dr. Jill McSweeney. Jill, I truly have never seen such a bright presence as an instructor, so full of life and enthusiasm. You have been so inspiring – and now I also want to pursue a career as an educator. Words can not express how grateful I feel for all of your support.

Thank you Stephen Whitefield for all of your training at the confocal microscopy facilities of Dalhousie University (Cellular & Molecular Digital Imaging Facility), Dr. Arnaud Gaudin for your excellent guidance with Imaris Software, Patricia Colp for your continuous help and understanding with the immunohistochemistry experiments (Pathology Department, Dalhousie University), Eva Rogerson and Purnima Narayanan from the animal facility care of Dalhousie University for all of your help with the mice handling and monitoring.

This research was possible because of the support of the funding agents: Cystic Fibrosis Foundation, Cystic Fibrosis Canada, NSERC, PhaseBio Pharmaceuticals, CIHR, Department of Physiology and Biophysics entrance award and travel grants, as well as the Faculty of Medicine Scholarship (Dalhousie University).

I would not have been able to survive the stress through these five years if it were not for my colleagues who have become close friends. You helped turn tears into laughter and frustration to be transformed into motivation - each one of you has a special place in my heart. Many thanks to Maral, Shekufeh, Danielle, Jillian, and Diogo. I love you so much.

My appreciation also extends to my friends outside my lab life: Mrs. Xanthoula and Mr. Nick, Mrs. Nota, Dr. Xanthi and Dr. Dimitris, Dr. Evi and Dr. Evangelos, Mrs. Niki and Dr. Bill, Father Theodore and Presvytera Hara, Peter, Athena, Niovi, Elvira, Cody, Vicky, Maria, and Flora. I feel blessed for your unconditional love and for making me feel at home in Halifax and supporting me in all the steps I have taken. I will be forever grateful, and I wish I will be able one day to repay the kindness you have shown me.

To my friends in Athens who never minded the transatlantic distance: Thank you for always being there for me during the happy moments and difficulties of my Ph.D. “Though miles may lie between us, we’re never far apart, for friendship doesn’t count the miles, it’s measured by the heart.” Thank you Castalia, Vana, Eirini, Vasilis, Meletis, Evi, Anna, Katerina, Valia, Dr. Amalia, Mrs. Eugenia and Mr. Vaggelis. I am grateful to have you all in my life. Your endless love kept me going.

I owe the biggest thanks to my parents, who as immigrants themselves, despite their struggles and sacrifices, raised me to have moral values and a strong work ethic and taught me how important effort, perseverance, determination, faith, and patience are. Despite the miles between us these years, through thoughts and prayers my parents were always by my side, day and night. Mom and dad, I love you and I apologize for all of the anxiety and “heart attacks” I gave you. I also want to thank my beloved sister Konstantina and my cousin Marinela who both deeply supported me amid my many anxious moments and fears. You believed in me and that always gave me hope that I could accomplish this chapter in my life. All of you helped keep me going.

Lastly, and most importantly, I want to avow, in all humility, that God was by my side and sustained me throughout my journey. Among the biggest blessings I received was the presence and support of my spiritual father, Father Maximos – thank you so much for everything. I am indebted to you for all the times you saved me from giving up on my Ph.D., for all your countless prayers and endless generosity.

CHAPTER 1: INTRODUCTION

1. CYSTIC FIBROSIS (CF)

Cystic fibrosis, is the most common lethal autosomal recessive disorder in the Caucasian population, affecting one in 2,500 to 3,000 newborns, and approximately 100,000 people live with this condition worldwide (Middleton et al., 2019). CF arises from the deficiency or absence of the cystic fibrosis transmembrane conductance regulator (CFTR) chloride channel from the apical membrane of epithelial cells, caused by mutations in the CFTR gene that encodes the CFTR protein. This protein controls the flow of salt and fluids in and out of cells. If CFTR is dysfunctional, it causes a buildup of thick and viscous mucus that covers the lungs and the gut, leading to malabsorption of nutrients and severe airway disease with chronic inflammation and bacterial infection (Rey et al., 2019).

In 1938, CF was differentiated from celiac disease and named "cystic fibrosis of the pancreas" by Andersen (Andersen, 1938; Davis, 2006). At that time, patients with CF did not live longer than 6 months. Interestingly, while the main reason of death was airway infection and inflammation, scientists believed that etiology of the disease was mucus obstruction of the exocrine pancreatic ducts. In 1959, Paul di Sant' Agnese, discovered the sweat electrolyte defect, and the standardization of the sweat test shed light on the belief of CF as a mainly mucus disorder (Gibson et al., 1959; Wine, 2010). Almost thirty years later, in 1983, the impaired chloride transport was recognized as the basic defect in CF, with a real milestone, the discovery of the CFTR gene responsible for CF, by Riordan *et al.* in 1989 (Riordan et al., 1989).

Since the gene was discovered, more than 2,000 mutations have been reported and the most common mutation, present in almost 90% of CF patients, is the F508del CFTR mutation. The era of CFTR gene discovery brought an explosion of basic and clinical research that led to fundamental therapeutic progress. Nowadays, the median life expectancy varies from 40 to >52 years old (https://www.cysticfibrosis.ca/our-programs/cf-registry), with the highest in Canada, which is an astonishing improvement from only 6 months in 1938 (Riordan et al., 1989; Rommens et al., 1989).

As CFTR is expressed in various organs, CF is a multisystem disease affecting the lungs, the sinuses, the gastrointestinal track, the liver, the pancreas, the hepatobiliary and the reproductive systems (Figure 1.1). The main cause of morbidity and mortality is respiratory failure due to thick tenacious mucus accumulation in the airways, leading to chronic infection and inflammation as well as acute pulmonary exacerbations. The approval of the first triple-combination therapy, Elexacaftor/Tezacaftor/Ivacaftor (Trikafta), for CF patients aged 12 and older who have at least one copy of the F508del mutation, and regardless of their second mutation, was a monumental improvement targeting almost 90% of the patients. In September of 2020 Vertex Pharmaceuticals announced positive trials completed in a younger age group, 6-11 years old. Also, more trials are ongoing for children 6 months and up (*Vertex Announces Positive Phase 3 Study for TRIKAFTA® (Elexacaftor/Tezacaftor/Ivacaftor and Ivacaftor) in Children Ages 6-11 Years With Cystic Fibrosis to Support Submissions for Global Regulatory Approvals | Vertex Pharmaceuticals*, 2020).

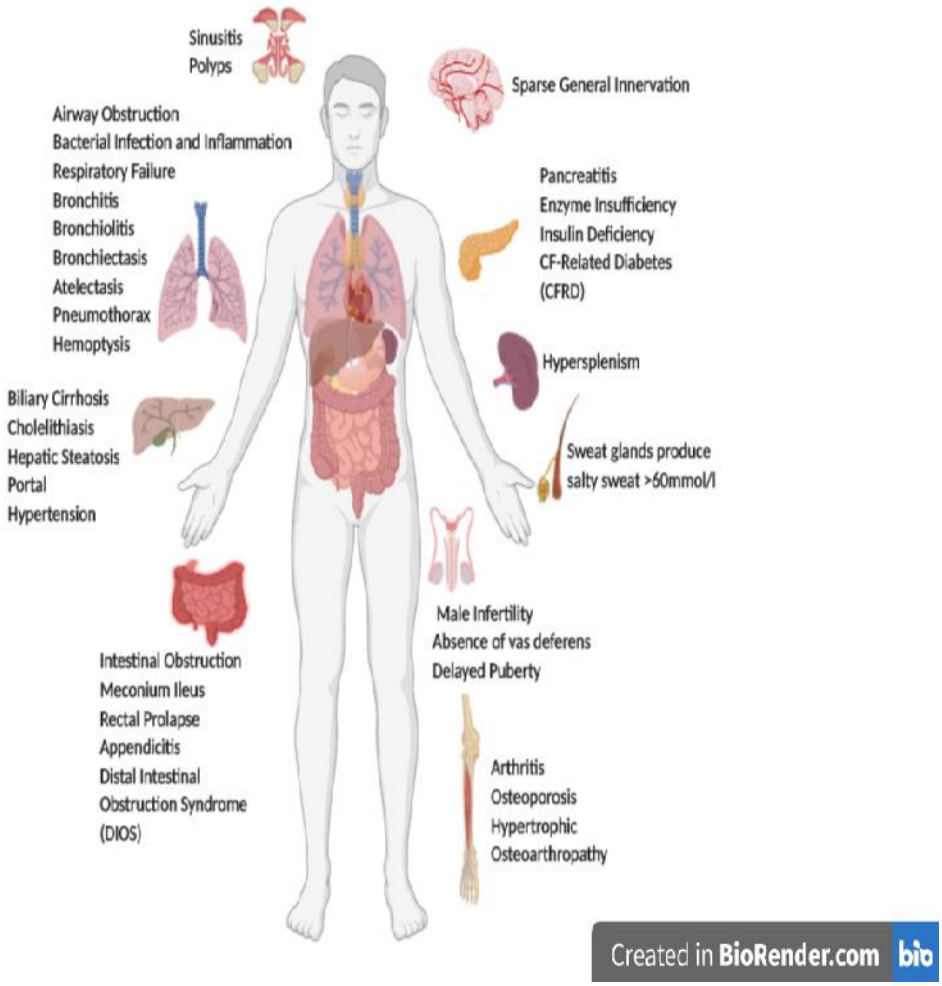

Figure 1.1: Cystic Fibrosis is a multifactorial disease.

As CFTR is expressed in various organs, CF is a multisystem disease affecting the lungs, the sinuses, the gastrointestinal track, the liver, the pancreas, the hepatobiliary and the reproductive systems

However, while Trikafta has a great impact on the lung function markers and also improves the overall quality of life, it is a very expensive therapy and, consequently, access poses a challenge for many (Middleton et al., 2019). Despite the tremendous

research progress, CF still remains a life threatening complex disease, and with the increased longevity additional co-morbidities to respiratory failure, such as CF-Related Diabetes (CFRD), are increasing.

1.1 Types of CFTR Mutations

The CFTR gene is located on the long 'q' arm of chromosome 7 at position 31 (7q31), spanning approximately 230kb of genomic DNA with 27 exons. It encodes a large glycoprotein of 1,480 amino acids which has a molecular weight of ~170,000 Da. CFTR, also known as ABCC7, belongs to the ATP-binding cassette membrane transporter superfamily (ABC) of proteins. It consists of two transmembrane domains (TMD1 and TMD2), each containing six transmembrane α-helices, that form the pore of the channel through which ions travel across the membrane, two nucleotide binding domains (NBD1 and NBD2) that bind and hydrolyze ATP for channel gating and a large cytoplasmic regulatory (R) domain that regulates channel function by protein kinase A (PKA) and C (PKC)-dependent phosphorylation. CFTR channel function is directly activated by phosphorylation of the R domain through PKA phosphorylation which is enhanced by PKC phosphorylation (Alcolado et al., 2011; Alcolado et al., 2014; Alshafie et al., 2014; Chappe F.et al., 2008; Chappe et al., 2012; Vankeerberghen et al., 2002).

The CFTR mutations reported in the CFTR gene affect the synthesis of the CFTR protein, its transport to the apical membrane of epithelial cells, gating of the channel and conductance of the chloride ions, the amount and the stability of the CFTR protein present at the cell surface. Depending on their specific impact on the CFTR protein, there

are seven categories of mutations. Class I, nonsense frameshift mutations: no CFTR protein synthesis which accounts for 10% of disease-causing mutations; Class II, missense-amino acid or deletion: altered CFTR trafficking/processing defect having almost 90% prevalence; Class III, missense-amino acid change: defective channel regulation/altered gating that represents 4% of CFTR mutations; Class IV, missense-amino acid change: defective channel conductance having less than 2% prevalence: Class V, missense-splicing defect: reduced amount of CFTR proteins, Class VI, missense-amino acid change: diminished CFTR stability at the cell surface, and Class VII: entirely no mRNA synthesis. recently described by De Boeck (2020). Similar to class I, there is no mRNA transcription (De Boeck, 2020; Elborn, 2016). Class I, II, III and VII produce more severe phenotypes due to a lack or very low amount of CFTR proteins, while Class IV, V and VI are characterized by a milder phenotype as they still permit a residual amount of CFTR protein synthesis.

1.1.1 ΔF508 Mutation: The Most Common Mutation in Cystic Fibrosis

Among Class II mutations, the F508del *CFTR* mutation is the most frequent in CF patients worldwide. Approximately 50% of patients with CF are homozygous for the F508del mutation, and 90% of them are heterozygous, having a single copy of F508del in combination with another *CFTR* mutation (Ghelani et al., 2020; Lukacs et al., 2011). Based on the 2018 Canadian CF registry annual data report, 42.7% of Canadians are homozygous for the F508del and 40.5% heterozygous

(https://www.cysticfibrosis.ca/about-us/publications-and-financials) (*Cystic Fibrosis Canada*, 2018).

The F508del mutation is a three base-pair deletion in exon 10 of the *CFTR* gene, resulting in the absence of a single amino acid phenylalanine (F) at position 508, located in the Nucleotide Binding Domain 1 (NBD1) of the CFTR protein. This leads to defective trafficking of newly assembled CFTR proteins, due to misfolding, retention inside the cell and eventual degradation by the ubiquitin-proteasome machinery. Consequently, inducing dramatic reduction or absence of mature CFTR protein at the epithelial cell surface to perform its chloride ion conductance activity (Penque et al., 2000). However, very few F508del-CFTR proteins escape from the proteosomal degradation, mature and reach the plasma membrane (Lukacs et al., 2011; Okiyoneda et al., 2010). F508del cell surface expression and stability is temperature-sensitive and impeded at 37^{o}C. Scientists have tried to rescue this temperature-sensitive conformational defect of F508del-CFTR proteins at lower temperature (20^{o}C - 30^{o}C), by chemical chaperons such as glycerol or other molecules (Alcolado et al., 2011; Chappe et al., 2012; Denning et al., 1992; Kopito, 1999; Lukacs et al., 2011; Rafferty et al., 2009), and with trafficking correctors such as Lumacaftor and Tezacaftor which are now part of approved CF patients' therapy (Donaldson et al., 2018; Lopes-Pacheco, 2020; Taylor-Cousar et al., 2017; Van Goor et al., 2011; Wainwright et al., 2015). In addition to impaired folding and stability, F508del-CFTR has a gating defect. Its open probability (Po) is very low, approximately one third that of wild-type CFTR (Cai et al., 2011). The current combination of clinically approved drugs

known as Trikafta, includes two trafficking corrector molecules (Lumacaftor and Tezacaftor) and a potentiator of CFTR gating (Ivacaftor).

1.2 CFTR: A Regulator of Fluid Secretion

Epithelial cells are characterized by two membranes where different proteins are expressed: (a) the apical membrane that faces the external environment of the tissue or inward to the lumen, and functions as a physical and chemical barrier preventing pathogens to get to the blood stream, (b) the basolateral membrane attached to the serous or mucosal part of the tissues. The basolateral membrane is divided from the apical membrane by tight junction proteins that play a significant role in maintaining the polarity of the cell as well as orienting the transepithelial movement of fluid and ions, from the basolateral to the apical membrane, during secretion/absorption processes.

CFTR functions as a cAMP-dependent chloride channel, and a bicarbonate channel, expressed at the apical membrane of epithelial and serous cells responsible for fluid and electrolytes secretion. Other than a chloride channel, CFTR has supplementary functions as a regulator of other ion channels and transporters such as the outwardly rectifying Cl^- channels (ORCCs) and most significantly as a regulator of epithelial sodium channel (ENaC) (Morales et al., 1999; Peckham et al., 2018).

In secretory epithelia, fluid secretion depends on the active transport of chloride (Cl^-) mainly regulated by the CFTR chloride channel and other Cl^- channels in the apical membrane. Cl^- accumulation inside the cells happens above electrochemical equilibrium, by the Cl^- entry across the basolateral membrane of the cell through the $Na^+K^+2Cl^-$

(NKCC1) active co-transporter that uses the inward Na^+ chemical gradient generated by the activity of the Na^+/K^+-ATPase at the basolateral membrane. Especially, the NKCC1 co-transporter brings 1 Na^+, 1 K^+ and 2 Cl^- ions into the cell, K^+ is recycled back to the interstitium via the K^+ channels located at the basolateral membrane and Na^+ is constantly pumped out of the cell through the Na^+/K^+-ATPase, leading to chloride accumulation inside the cell. At the apical cell surface, active Cl^- secretion from the CFTR channel, into the lumen, initiates the driving force for Na^+ transport across the epithelium through the paracellular pathway, generating NaCl (salt) assembling, that in turn moves water either paracellularly or transcellularly through aquaporins (Frizzell et al., 2012; Saint-Criq et al., 2017). Recent studies have shown that in some epithelial cells a basolateral Cl^-/HCO^-_3 anion exchanger (AE) collaborates with a Na^+-bicarbonate co-transporter (NBC) leading to Cl^- accumulation through an alternative route (Saint-Criq et al., 2017). Lastly, CFTR also regulates bicarbonate (HCO_3^-) secretion which is critical for the pH of fluid in the extracellular space. In some tissues (e.g., pancreas), other Cl^- channels additionally to CFTR, such as calcium activated Cl^- channels (CaCC), the solute carrier family 26 member 9 (SLC26A9) and TMEM16A (also known as anoctamin-1; ANO1) may be co-present and stimulate Cl^- secretion (Danahay et al., 2020; Schroeder et al., 2008).

In the sweat glands, CFTR is expressed in both secretory coil and reabsorptive duct epithelium (Saint-Criq et al., 2017). ENaC is co-localized with CFTR at the apical membrane of the reabsorptive duct epithelial cell, and in concert they modulate NaCl reabsorption from duct lumen into the epithelial cells (Ertongur-Fauth et al., 2014;

Frizzell et al., 2012). Afterwards, the basolateral Na^+/K^+-ATPase pump drives intracellular Na^+ out of the cell and into the bloodstream, generating a transepithelial electrochemical gradient allowing Cl^- absorption. The duct epithelium has a high conductance for ions and low permeability to water, enabling reabsorption of salt in excess of water. As a result, sweat is diluted allowing body cooling by evaporation, and therefore only a small amount of salt is lost from the body. In CF, the sweat duct is unable to absorb Cl^- because of the dysfunctional CFTR, preventing Na^+ transport. NaCl reabsorption is very minimal, resulting in highly increased sweat Cl^- concentration (>60 mmol/L *vs.* <40mmol/L in healthy subjects) (Baker, 2019; Frizzell et al., 2012; Quinton, 2007).

In the airways, CFTR is expressed in epithelial cells and submucosal glands of the conducting airways, stimulating fluid secretion, and contributing to the airway surface liquid (ASL) hydration and pH regulation. Accordingly, keeping airways sterile via an effective mucociliary clearance that will be described in more detail below (see section 2.1). In CF disease, CFTR channel dysfunction in the airways epithelium leads to an imbalance between salt and water secretion/absorption mechanism, and thus reduced ASL volume and pH regulation, accumulation of viscous mucus, favoring bacteria growth and causing airway obstruction.

In the small intestine, CFTR is highly expressed primarily in epithelial cells of the duodenum villi, while moderately expressed in the large intestine (colon). Secretion process is the same as in the airway epithelia: transcellular transport of chloride and sodium, and movement of water either passively through the paracellular route and/or by osmosis. CFTR-mediated secretion maintains luminal surface liquid composition that

is important for optimizing nutrition, enzymatic activity, and disposal of non-necessary luminal products. In CF, altered anion secretion due to abnormal CFTR function causes meconium ileus, severe intestinal obstruction, and long term constipation (Frizzell et al., 2012; Saint-Criq et al., 2017).

In the pancreas, CFTR expression is localized in the exocrine ductal cells. In pancreatic acinar cells Cl^- secretion is performed through CACC chloride channels. In ductal cells, CFTR secretes both Cl^- and HCO_3^- and works in concert with a Cl^-/HCO_3^- apical exchanger (SLC26A3/A6) to increase HCO_3^- accumulation in the ductal lumen, and allowing Cl^- transport across the apical membrane. In turn, Na^+ migrates paracellularly in presence of transepithelial bicarbonate secretion, generating an osmotic driving force on the luminal surface, which stimulates water movement outside the cell and makes a HCO_3^- -rich highly alkaline pancreatic juice important for enzyme digestion and overall pancreatic function. This “juice” migrates to the small intestine where it promotes fat digestion. Defective CFTR function in the pancreas impairs bicarbonate secretion in the lumen, consequently inducing an acidic environment, which then evokes viscous mucus accumulation, and enzymatic precipitation that in turn causes ductal obstruction. Pancreas is eventually completely destroyed and replaced by fibrous cysts, hence the original name “Cystic Fibrosis of the pancreas” before the CFTR gene discovery (Davis, 2006; Frizzell et al., 2012; Saint-Criq et al., 2017). Pancreatic insufficiency is one of the common CF disease manifestations.

1.2.1 The Sweat Gland and Defective Sweating in CF

The sweat gland plays an important role in thermoregulation, controlling the sweat production in our body. Sweat is composed of salt and water and under heat conditions, skin temperature is elevated. Therefore, our body produces diluted sweat, which in turn evaporates and helps body temperature to cool down. There are approximately 4 million sweat glands in our body while forehead, palms and feet soles contain the highest number of glands (Baker, 2019; Cui et al., 2015; Saint-Criq et al., 2017). In addition to thermoregulation, sweat glands are important for skin health, maintaining its homeostasis via secretion of antimicrobial peptides (LL-37, lactoferrin, dermicidin) (Baker, 2019; Saint-Criq et al., 2017). Increased NaCl reabsorption abnormalities from sweat in CF patients have been broadly studied and the Cl^- concentration in the sweat, evaluated by the Quantitative Pilocarpine Iontophoresis Test (QPIT), still constitutes the most reliable pathophysiological marker for the diagnosis of CF disease. Sweat Cl^- concentrations higher than 60 mEq/l define CF disease while in healthy individuals sweat Cl^- values are <40 mEq/l. Sweat glands are excellent for studying CFTR dysfunction as they are easily accessible and free of inflammation or infection.

CF sweat glands are characterized by dysfunctional Cl^- reabsorption and CF patients sweat 3-5 times more than healthy people (Quinton, 2007). In humans, sweat glands are controlled by adrenergic, cholinergic, and peptidergic innervation (Heinz-Erian et al., 1985; Hodge et al., 2018; Wang et al., 2016). Most of the fluid secretion is regulated by the β-adrenergic stimulation, which is CFTR-dependent while the sympathetic cholinergic innervation utilizes acetylcholine and is CFTR independent (Cui et al., 2015; Quinton,

2007; Saint-Criq et al., 2017).

In CF, the non-CFTR dependent cholinergic and Ca^{2+}-mediated fluid production from the secretory coil functions normally with sweat secretion rates almost similar between CF and non-CF individuals (Sato et al., 1984). However, the β-adrenergic and cAMP-mediated CFTR-dependent sweat secretion is absent, because of the mutated CFTR that is highly expressed in the apical membrane of sweat ducts regulating salt reabsorption. This finding was demonstrated by Sato and Sato (1984) when trying to increase salt absorption in CF glands by triggering them with isoproterenol (a β-adrenergic agonist) with no success (Sato et al., 1984; Sato et al., 1988). The sweat duct was unable to absorb Cl^- which in turn impedes Na^+ transport and consequently decreased salt absorption that leads to elevated sweat chloride concentration, the hallmark of CF disease (Quinton, 2007; Sato et al., 1988; Wine et al., 2013). The evaporimeter and bubble imagining assays methods for quantifying secretion rates from individually sweat glands, have been used to determine levels of CFTR function by measuring C-sweat rates (the sweat that is produced in β-adrenergic response) and differentiate CF from carriers and carriers from healthy subjects (Kim et al., 2016).

1.3 Infection and Inflammation in CF

Defective or absence of the CFTR channel from the apical membrane of epithelial cells in exocrine tissues leads to defective fluid secretion which in turn causes mucus accumulation, and thus bacterial infection and/or inflammation, tissue remodeling and obstruction. Progressive lung disease with respiratory failure is a major clinical concern

that causes 95% of morbidity and mortality in patients with CF. Lung disease begins very early in life of patients with CF, and *Staphylococcus aureus* is the most common lung pathogen in CF children (Esposito et al., 2019; Filkins et al., 2015; Pittman et al., 2015). Sputum culture is used to diagnose pathogens in lower respiratory track of CF patients and especially in the young age, as is less invasive than bronchoalveolar lavage (Burns et al., 2014). The disease develops over recurrent exacerbations of pulmonary infections caused by infection with bacterial species including *Staphylococcus aureus*, *Haemophilus influenza*, *Pseudomonas aeruginosa* and the Burkholderia cepacia complex (Bcc) (Festini et al., 2006; Tarran et al., 2001). *P. aeruginosa* is the most persistent in human lungs with CF and chronic pulmonary infection is inevitable, despite antibiotic therapies, with biofilm-forming cells of a mucoid phenotype in more severe advanced infections. It is hypothesized that since *Staphylococcus aureus* is detected from a very early age, it is the one that initiates lung alterations allowing *P. aeruginosa* to chronically infect the patients causing severe infiltration and alveolar thickening, severe peribronchial infiltration, complete lumen diffusion and finally respiratory failure (Bayes et al., 2016; Li et al., 2017). Recent studies are trying to understand the airway microbiome and utilize it as an indication of lung disease severity (Caverly et al., 2015; Cuthbertson et al., 2020; O'Toole, 2018). More specifically, Cuthbertson *et al.* (2020) studied the microbiota in CF patients with various grades of lung function and diverse antibiotic treatment. The authors revealed a connection between reduced microbiota diversity with increased persistence of specific bacterial taxa (*P. aeruginosa*), and declined lung function. However, airways of CF patients with a better lung function, were characterized by an increased dominance

of obligate anaerobes bacterial taxa (e.g. *Prevotella*, *Porphyromonas*, and *Veillonella*) (Cuthbertson et al., 2020).

In addition, CF lungs are characterized by defective bacterial clearance and high expression levels of pro-inflammatory cytokines in the sputum of CF patients that induce inflammation: TNF-α, IL-1α, IL-1β, L-6, IL-8, IL-17, IL-33, GM-CSF, G-CSF, and HMGB-1. Also, recent studies have shown that hypoxic epithelial necrosis stimulates neutrophilic inflammation through the IL-1 receptor, suggesting a critical link of IL-1 signaling pathway between mucus-plugged airways and inflammation in early CF lung disease (Balázs et al., 2019). In contrary, the anti-inflammatory cytokine IL-10 is down-regulated in CF. Thus, airway obstruction is associated with neutrophilic inflammation, that is usually observed from a young age, yet in the absence of bacterial infection (Balázs et al., 2019; Khan et al., 2019).

Macrophages were initially described in 1892 by Metchnikoff as the key players in the primary innate immune response. Macrophages function through phagocytosis of microorganisms and secretion of pro-inflammatory and antimicrobial mediators. They are present in all mammalian organs however, the heterogeneous populations of macrophages with distinct phenotypic specializations are distributed in a tissues-specific manner. In the lung, macrophages are the most commonly found immune cells that play a significant role in bacteria clearance from the airways. There are two distinct macrophage populations: Alveolar Macrophages (AMs) and Interstitial Macrophages (IMs). Alveolar Macrophages are found in the airway lumen in close contact with epithelial cells of alveoli. These macrophages are considered as the first line of host

defense that play a significant role in maintaining lung homeostasis. The second and less described macrophage population is interstitial macrophages whish reside in the lung parenchyma and exert immunoregulatory activities (Bruscia et al., 2016; Liegeois et al., 2018). Based on activation status, Alveolar Macrophages are classified into 2 groups: classically activated macrophages (M1) involved in initiating and sustaining inflammation and alternatively activated macrophages (M2) which are associated with anti-inflammatory, immunoregulatory and tissue-repair properties as well as playing roles in fibrotic pathology and allergic conditions (Bruscia et al., 2016). Imbalance in the population of M1 and M2 macrophages has been reported to be involved in the pathogenesis of CF (Tarique et al., 2017). More specifically, macrophage phenotype in CF alters during CF development, as a consequence of plasticity, characterized by increased production of pro-inflammatory cytokines, elastase, and increased concentrations of the monocyte chemotactic protein 1 (MCP-1). Studies in CF mice have shown that macrophages are unable to degrade internalized pathogens such as *P. aeruginosa* and *Bcc* (Li et al., 2017; Semaniakou et al., 2019). The input of macrophages polarization and plasticity in CF disease progression is still undefined. Macrophages express CFTR in low levels and its inhibition in wild-type macrophages leads to a CF-macrophage behaviour, implying that macrophages alterations in CF could be partially due to dysfunctional CFTR (Lévêque et al., 2017; Turton et al., 2020).

In the CF intestine, one of the earliest disease manifestation is obstruction of the last part of ileum or proximal large intestine, named meconium ileus (MI) appearing in 15–20% of CF newborns, and distal intestinal obstruction syndrome (DIOS) seen in 25% of adults

(Zielenski et al., 1999). As CFTR is highly expressed across the intestinal track, especially in the duodenum, consequences of defective CFTR are severe intestinal obstruction, including mucus accumulation, goblet cell hyperplasia, crypt dilatation and elongation. Also, intestinal inflammation has been described by elevated inflammatory markers such as the human calcium-binding S100 proteins, calprotectin (S100A8/S100A9), IL-8, albumin, lactoferrin, IL-1, IgM, IgG, neutrophil elastase, TNF-α, eosinophil cationic protein (ECP), ICAM-1, CD-25, IL-2 and IFN-γ (Allali et al., 2012; Enaud et al., 2019; Raia et al., 2000; Smyth, 2000).

More specifically, the S100 proteins are ideal markers for identifying acute infectious exacerbations and especially S100A12 (calgranulin C) which is a serum marker, found in phagocytes and directly related to inflammation (Allali et al., 2012; Smyth, 2000; Werlin et al., 2010; Xia et al., 2018). S100A8 and S100A9 proteins are expressed in different immune cell types (e.g., neutrophils, monocytes, macrophages etc.) following their activation. Accordingly, secretion of IL-1, which is elevated in CF intestine, stimulates calprotectin release (Allali et al., 2012). While intestinal inflammation has been reported, the exact mechanism of this intestinal inflammation is not clear yet. A recent study demonstrated a link between the gut microbiota and the intestinal inflammation in CF children while the microbiota composition differed based on the inflammation status of CF subjects (Enaud et al., 2019). CF patients that had higher than normal levels of calprotectin were characterized by increased bacterial expression such as *Staphylococcus spp*., and *Streptococcus spp*., and decreased expression of others such as *Bacteroides spp*., *Ruminococcus spp*., and *Coprococcus spp*.

Gut microbiota is important for the immune response of the entire body during postnatal development and as CF abnormal luminal environment affects the microbiome of the gut, it contributes to microbial dysbiosis, that in turn could impact levels of inflammation in the intestine. Lastly, a study in F508del mice showed altered intestinal structure compared to the wild-type mice. Some characteristics in the ileum of CF mice were: increased crypt to villus axis (CVA) height, increased cell density, muscularis externa thickness, and presence of many goblet cells (Bazett et al., 2015; Semaniakou et al., 2020).

In the exocrine pancreas, defective anion transport leads to reduced ductal fluid secretion, and consequently, ducts are dilated by enzyme precipitation and mucus accumulation with the presence of eosinophilic secretions, neutrophils, and macrophages. This severe inflammation and fatty infiltration, in turn, causes ductal plugging, acinar damage and fibrosis, destroys gradually the exocrine pancreas leading to complete atrophy and pancreatic development (Gibson-Corley et al., 2016; Wilschanski et al., 2013). The endocrine pancreatic tissue is intact, spared from the surrounding exocrine destruction with fewer acinar cells and zymogen granules. Insulin-immunoreactive islets are mostly localized in the intact lobular tissue without alterations in the amount of produced insulin or glucagon cells (Gibson-Corley et al., 2016). In a recent study from Hart *et al.* (2018), was shown increased expression of IL-6, IL-1β, CXCL10, TNF-α and IFN-γ in human CF islets (Hart et al., 2018).

Pancreatic alterations start *in utero* and after birth the destruction of small ducts, which leads to large duct dilation, persists (Wilschanski et al., 2013). A study from Abu-El-Haija

et al. (2012) in fetal and newborn $Cftr^{-/-}$ and $Cftr^{F508del/F508del}$ pigs, that shares many pathological characteristics with human CF pancreas, demonstrated that tissue damage starts *in utero* and pro-inflammatory, complement cascade, pro-apoptotic, and pro-fibrotic pathways are involved (Abu-El-Haija et al., 2012). They noticed elevated activation of the apoptotic caspase-3 pathway in the CF pig pancreas whereas the α-smooth muscle actin, a myofibroblast marker and activator of early fibrosis pathways, was observed in both fetal and newborn pigs. Tissue remodeling with mucus accumulation and duct cell proliferation was observed in the neonatal but not in fetal CF pigs, indicating that these changes do not initiate disease pathogenesis but follow pancreatic damage over time (Abu-El-Haija et al., 2012). Compared to $Cftr^{-/-}$, $Cftr^{F508del/F508del}$ pigs exhibit slightly less severe exocrine pancreatic pathogenesis that may be attributed to the residual CFTR function as was described by Ostedgaard *et al.* (2011) (Abu-El-Haija et al., 2012; Ostedgaard et al., 2011).

2. Airway Physiology and Changes in CF

2.1 Airway Innate Defense

Airway defense consists of coughing, physical and anatomical barriers, turbulent airflow and innate immunity. The main lung innate defense mechanism is the mucociliary clearance (MCC) (Bustamante-Marin et al., 2017). Everyday, we inhale approximately 10,000 litres of air, which in big cities contains close to $5x10^{10}$ harmful substances (Widdicombe et al., 2015). The very tiny particles enter the alveoli and afterwards are

cleaned by macrophages of the lower airways, while the largest particles and pathogens are entrapped by mucus and propelled towards the mouth by the ciliary beating in the upper airways. Mucociliary clearance is the removal of the mucus, present at the surface of the airways surface liquid layer (ASL) by the movement of cilia on top of ciliated airway epithelial cells. The ASL coats the airway epithelium, and is composed of the mucus layer, and the periciliary layer (PCL). PCL hydrates the airways, enables ciliary beating for proper mucus clearance, and also has a crucial role in innate immunity and antimicrobial defense. The simultaneous coordination of all these components produce the effective mucociliary clearance in healthy airways for maintaining them sterile (Bustamante-Marin et al., 2017; Smith et al., 2008; Widdicombe et al., 2015).

The volume of the ASL depends on gland secretion and the hydration state of the produced mucus. Mucus secretion is a physical and pH barrier for the underlying tissues and protects them from inhaled pathogens found in the external environment. It is isotonic and composed of 98% of water, and the rest 2% of ions, mucins MUC5B and MUC5AC, peptides, proteins and other small molecules (Widdicombe et al., 2015; Wine, 2007).

2.2 Submucosal Glands Secretion (SMGs)

Most of the mucus secreted by the airways (95%) is produced by tracheal and bronchial submucosal glands located down to conducting airways of 1-2 mm diameter, and only 5% of the mucus is secreted by the goblet cells, found on the airways epithelium in the first 8-10 airway generations of the conducing zone (Widdicombe et al., 2015).

Submucosal glands (SMGs) consist of the ciliated duct where ciliated and goblet cells are located, the collecting duct that contains non-secretory non-ciliated cells, and the secretory duct that has mucus cells in mucus tubules and serous cells in acini (Widdicombe et al., 2015). Serous cells are the predominant defensive cells of the airway mucosa and need CFTR expression in order to regulate fluid secretion (BéruBé et al., 2010; May et al., 2015). Constituents of the fluid produced by serous cells are anti-inflammatory products such as lysozyme and lactoferrin, immunoglobulin A, surfactant protein A, leukocyte protease inhibitor and mucins MUC2 and MUC7. Instead, mucus cells produce a gel-like fluid that contains MUC2 and MUC5B while goblets cells have mainly MUC5AC (Widdicombe et al., 2015; Wine, 2004; Wine, 2007).

The submucosal glands secrete upon synergistic interaction of neurotransmitters, Acetylcholine (ACh) and Vasoactive Intestinal Peptide (VIP). As mentioned above, fluid secretion from serous cells is CFTR-dependent while from mucus cells it is CFTR-independent. Neurotransmitters that increase intracellular Ca^{2+}, for example ACh, trigger secretion from both serous and mucus cells, while pathways that increase intracellular cAMP such as VIP, trigger serous cells but not the mucus cell secretion. Glands secrete at low levels in response of VIP stimulation alone while the co-stimulation of VIP and acetylcholine that is observed in healthy glands, is lost in CF (Wine, 2007).

2.3 Innate Host Defense Defect in CF

When the submucosal glands are not functioning properly, it can result in mucus overproduction and/or defective mucociliary clearance, involved in the pathogenesis of four airway diseases: CF, chronic bronchitis (CB), chronic obstructive pulmonary disease (COPD) and asthma. In CF the synergistic interaction between VIP and ACh is lost. Studies in healthy single submucosal glands utilizing the bubble method, demonstrated synergy after stimulation of these glands with low levels of cAMP elevating agents (VIP, forskolin or isoproterenol) and intracellular Ca^{2+} agents (histamine, carbachol, SP). This synergistic reaction was absent upon stimulation with high concentration of one or both agents while glands respond to high synergistic transmitter action in emergency airway defense, as described above. In CF, glands do not secrete after being stimulated with low doses of combined VIP and carbachol, which shows that in CF glands are defective and lack the synergy observed in healthy glands (Jae et al., 2007; Widdicombe et al., 2015; Wine, 2007).

Furthermore, CF glands are enlarged and produce thick tenacious mucus even before signs of infection and inflammation (Widdicombe et al., 2015), and the concentration of mucins is highly increased in sputum from CF patients, causing an overall impaired mucociliary clearance due to changes in mucus viscosity and dehydration of the ASL (Salinas et al., 2005; Verkman et al., 2003). Recent studies in CF pigs revealed that mucus strands did not separate as under normal conditions but remained attached to submucosal gland opening (Ermund et al., 2018; Hoegger et al., 2014; Xie et al., 2018).

Due to CFTR defect, fluid secretion in presence of VIP, forskolin or isoproterenol is absent

while the CACC-dependent secretion is not altered. The CF gland fluid is characterized by increased acidity, consequently inducing ASL acidification and enabling bacterial dominance. Eventually, airways mucus plugging that leads to infection and inflammation of the airways, mainly by *P. aeruginosa* pathogen (Salinas et al., 2005; Widdicombe et al., 2015).

2.4 Neuronal Control of Submucosal Glands

The airways are mainly controlled by the peripheral nervous system and more specifically by the airway intrinsic neuronal network that innervates glands, muscles and blood vessels. There are two types of gland secretions, one during normal "housekeeping" control, where a low amount but continuous secretion is produced, and another one during emergency airway defense. In the housekeeping function, secretion is controlled by intrinsic airway neuronal signals that rely on non-cholinergic pathways that elevate cAMP, mainly mediated by VIP and is CFTR-dependent. The low amount of gland secretion is adequate to maintain proper mucociliary clearance. During emergency airway defense reaction such as in response to viruses, inhalation of large particles, toxic aerosols, etc. this "emergency" airway innate defense mechanism secrete in response to ACh, VIP, substance P (SP) and nitric oxide synthase (NOS) stimulation (Wine, 2004; Wine, 2007).

The emergency airway defense response is primarily mediated through a central reflex pathway of vagus nerve afferents and efferents. The intrinsic nerves are triggered mainly by vagal parasympathetic afferents. The neuronal signal, coming from the vagus nerve

through the cell bodies located in the jugular/nodose ganglia, dispatches its terminal nerve fibers into the nucleus of the solitary track in the dorsomedial medulla oblongata. Afterwards, the interneurons mediate signal transduction to the airway vagal preganglionic neurons (AVPNs). The descending projections of the latter stimulate neurons in the airway intrinsic nervous system, and therefore, gland secretion (Widdicombe et al., 2015; Wine, 2007). Hence, during the emergency defense reflex a strong descending cholinergic signal, mediated by the vagal nerve, produce high rates of gland secretion that involves pathways which elevate intracellular Ca^{2+} and are CACC-dependent (CFTR-independent) (Wine, 2007).

3. Enteric Nervous System and Neuronal Control of the GI in CF

The gastrointestinal track (GI) comprises a number of neuronal layers that are all connected to each other: the myenteric plexus layer, the longitudinal muscle layer, the mucosa layer, the circular muscle layer, the deep muscular plexus layer, the submucosal plexus layer and the submucosal artery and lastly the muscularis mucosae (Figure 1.2) (Furness, 2000). In the small intestine most of the neural cells are found in two ganglionated plexuses: the myenteric plexus and the submucosal plexus (Costa et al., 2000; Furness, 2007). Studies from the small intestine of guinea-pig demonstrated that the myenteric plexus has three components: the primary component that contains the ganglia and interganglionic connections, the secondary component has thin nerve strands that are in parallel to the circular muscle layer and the third component, called tertiary plexus, located in the between of the very thin longitudinal muscle layer (Furness,

2007). Primary function of the myenteric plexus is to control gut motility of the circular and longitudinal muscles while the submucosal plexus is responsible for fluid secretion and absorption as well as secretion of endocrine and paracrine mediators.

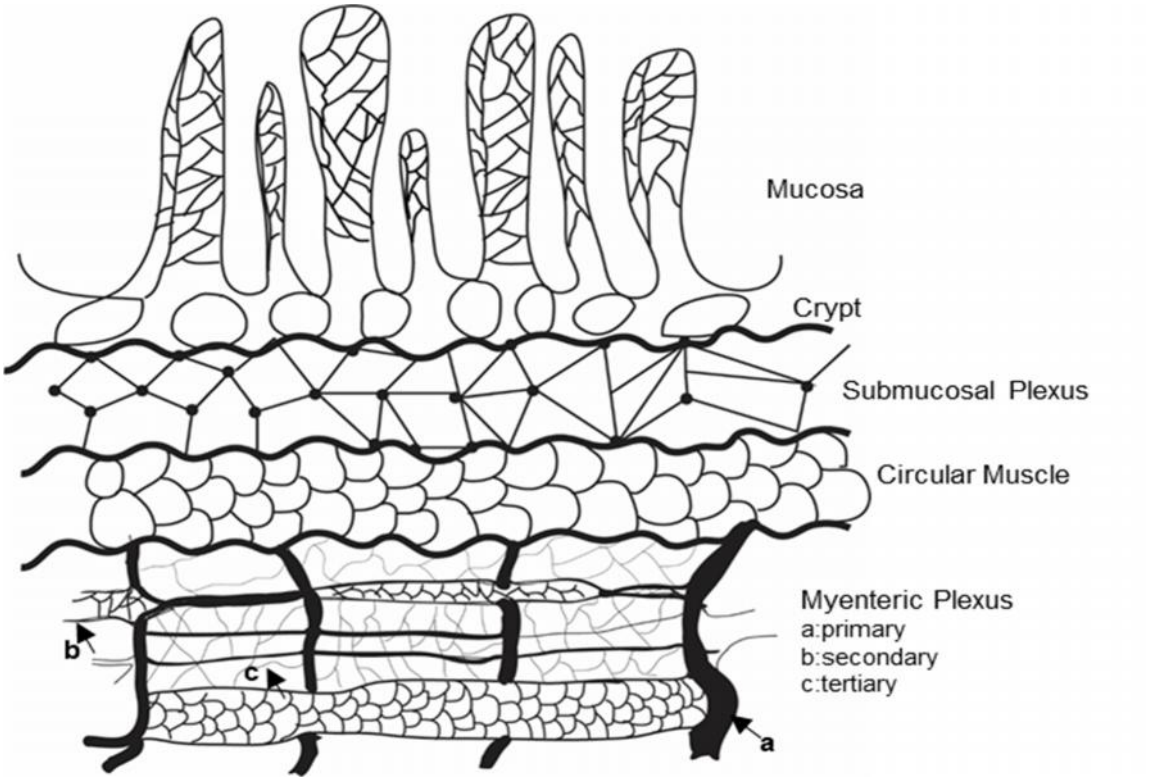

Figure 1.2: Schematic representation of intestinal tissue layers.

From the top to the bottom, villi are located at the mucosa layer followed by thy crypt layer. Next is the submucosal plexus layer and the circular muscle layer. The last intestinal tissue layer is the myenteric plexus that consists of three components: the primary (a), the secondary (b) and the tertiary (c) component (Semaniakou et al., 2020).

The nervous system of mammalian species has two parts, the central nervous system (CNS) and the peripheral nervous system (PNS). The CNS is formed by the brain

(cerebrum, cerebellum and brain stem) and the spinal cord, while the PNS has three subdivisions (the somatic, the autonomic and the enteric) and contains mainly bundles of neuronal cell bodies (ganglia) that conduct sensory stimulus in the head, neck and viscera. Nerves that send signal from the brain are named motor or efferent nerves, and the nerves that transport information from the body to the CNS are named sensory or afferent. The PNS links the CNS to the different tissues and organs of the body (Yoo et al., 2017). The autonomic nervous system, one of the PNS subtypes, is controlled by the sympathetic or parasympathetic innervation, and secrete mainly catecholamines (CChs) such as norepinephrine, epinephrine and dopamine, or ACh. The ENS nervous system is connected with the CNS through extrinsic innervation which consists of both sensory and sympathetic inputs, and vagal cholinergic parasympathetic neural fibers (Anlauf et al., 2003; Yoo et al., 2017). The intrinsic GI track innervation contains sets of ganglia and neurons found in the myenteric and submucosal plexus. The intrinsic enteric nervous system can communicate with the extrinsic enteric nervous system as well as the sympathetic and parasympathetic neuronal inputs (gut-brain axis) but it functions independently (Anlauf et al., 2003; Furness, 2012; Yoo et al., 2017). This elucidates why parasympathetic nerves stimulate motility and secretion during digestion while the sympathetic innervation inhibits gut motility and secretion (Furness, 2012; Furness et al., 2014).

Despite the interconnections of the CNS with the ENS, the enteric nervous system is the primary regulator of the GI activity. Both motility and secretion are coordinated mainly by intrinsic neuronal inputs. More specifically, studies in the guinea pig have revealed

fourteen neuronal types within the enteric nervous system of the small intestine that are divided into: sensory neurons, interneurons and motor neurons contributing all together to the peristaltic reflux that initiates gut motility (Furness, 2000). Sensory neurons are activated by mechanical and/or chemical stimuli that are accumulated in an interneuronal matrix. Sensory nerves, in turn, trigger excitatory motor neurons that innervate the upper part of the gut, and inhibitory motor neurons responsible for inhibitory innervation reflexes down the gut. Excitatory or inhibitory motor neurons, found in the myenteric plexus, promote and control motility and secretion. The main neurotransmitter of the excitatory ascending motor neurons is ACh, while inhibitory descending motor neurons exhibit inhibitory actions via NOS/VIP/ChAT. Thus, the excitatory cholinergic innervation enables muscle contraction through muscarinic receptor activation and ACh secretion, while muscle relaxation is enabled through a non-adrenergic, non-cholinergic (NANC) pathway via secretion of mainly nitric oxide and/or VIP. Moreover, the motor neurons mediates local reflexes through ascending or descending interneurons (Furness, 2000; Furness, 2012; Furness et al., 2014).

Fluid secretion and absorption processes need to be coordinated and maintained in a state of equilibrium locally and in the entire body. This local innervation is controlled by the sympathetic neural pathways. Accordingly, while the myenteric plexus contains motor neurons and interneurons, the submucosal gut plexus controls local secretion and absorption. It also consists of: non-cholinergic secretomotor vasodilator neurons that primarily release VIP, cholinergic secretomotor vasodilator neurons and cholinergic secretomotor non-vasodilator neurons that secrete mainly ACh (Furness, 2000).

4. Pancreatic Physiology in CF and CF-Related Diabetes (CFRD)

Pancreatic insufficiency was one of the very first hallmarks for diagnosis in CF. Depending on the percentage of pancreatic function and whether CF patients undergo pancreatic enzyme therapy (PERT) to preserve their nutrition health, they are either characterized as pancreatic sufficient (PS), ~15% of them, or pancreatic insufficient (PI) (Freeman et al., 2017; Singh et al., 2017). Almost 85% of CF newborns, are prone to PI. More specifically, children that have two of class I, II, III and VI mutations present a higher risk to develop PI early in life while children with two mutations of class IV and V, or a combination of one mild and one severe mutation are generally PS from birth. However, some of CF patients that are PS may become gradually PI during their life.

Similar findings were confirmed in pig and ferret models. Newborn $Cftr^{-/-}$ ferrets exhibit pancreatic insufficient pathology, similar to CF human infants, and are characterized by swollen acini and ducts with eosinophilic zymogen material, moderate alterations and pancreatic lesions observed in approximately 75% of $Cftr^{-/-}$ ferrets (Sun et al., 2014). Olivier *et al.* (2012) demonstrated that neonatal CF ferrets exhibited elevated apoptosis in exocrine ducts and acini suggesting that pancreatic inflammation starts very early in life. Within the first month of life and before adulthood, the pancreas undergoes rapid tissue deterioration with destruction of acini, duct dilatation and evidence of inflammatory cells (neutrophils, macrophages and lymphocytes) (Olivier et al., 2012). Interestingly, a small percentage of CF ferrets, are born PS with light pancreatic pathology while they have normal growth and fecal elastase-1 (EL1) levels (Sun et al., 2014). This finding demonstrates that, in ferrets, modifier genes could be responsible for this small

percentage of PS, indemnifying for the dysfunctional CFTR in the exocrine pancreas. Islets are disorganized in adult CF ferrets, characterized by large clusters that contain an abundance of β and α cells as occurs in the pancreas of CF patients (Olivier et al., 2012). The exocrine pancreas in newborn $Cftr^{-/-}$ pigs, as $Cftr^{-/-}$ ferrets, recapitulates the pancreatic pathogenesis as in human CF neonates. Consequently, pancreatic dysfunction starts *in utero* and deteriorates later on during adulthood, resulting in a complete acinar obstruction.

In contrast to exocrine pancreas, the endocrine pancreas remains intact during childhood. However, approximately 50% of CF patients develop CF-related diabetes (CFRD), which is the second co-morbidity in CF adults. Especially, as the life expectancy of CF patients has increased due to better therapeutic treatments, CFRD prevalence is getting higher. Most of CFRD patients are already PI while the average age of CFRD onset is about 20 years old (Mackie et al., 2003). CFRD is recognized as a third type of diabetes (type 3c, pancreatogenic) that shares characteristics of type I and type II diabetes (Rickels, 2015). Unlike type I diabetes, CFRD is not an autoimmune condition and is distinguished by partial insulin deficiency, reduced β-cell function and β-cell mass, as well as impaired glucagon suppression (Kayani et al., 2018). In addition to reduced insulin secretion and peripheral insulin resistance, CFRD patients express decreased amount of gastric inhibitory polypeptide (GIP) and glucagon-like peptide-1 (GLP-1), that play a significant role in the postprandial glucose regulation (Pozo et al., 2020). CFRD patients also present elevated random plasma glucose higher that 200mg/dl (11.1mmol/L).

Insulin is secreted by beta cells (islets of Langerhans) after glucose stimulation. Glucose

is the most effective stimulator of insulin release. Insulin secretion is biphasic: the first phase insulin secretion within the beta cells, that starts two minutes after the food intake and lasts for ~10 minutes, is followed by the second phase of insulin secretion, or postprandial insulin secretion, which reaches a plateau 2-3 hours later and is responsible for bringing blood glucose levels back to normal. Glucose enters the beta cell through GLUT2 transporter and the elevated glucose levels into the cell triggers glucose metabolism, and increases ATP/ADP ratio which in turn closes K_{ATP} channels. Closure of potassium channel leads to depolarization of the cell membrane and activation of voltage-gated Ca^{2+} channel in the plasma membrane which causes a rapid Ca^{2+} influx into the cell. This intracellular elevation of Ca^{2+} leads to exocytosis and insulin secretion into the blood. The amplification of postprandial glucose-induced insulin secretion in the bloodstream is determined by hormonal signals, gastrointestinal hormones and neuropeptides (e.g. GLP-1, GIP, VIP, peptide YY, estradiol, leptin etc.), nutrient signals such as amino acids and fatty acids, and, lastly, neural signals such as the neurotransmitter acetylcholine (Henquin, 2000). Neuropeptides and neurotransmitters stimulate insulin secretion through the vagal nerve activation, by binding to a receptor located at the cell membrane that will next provoke the activation of various signaling pathways that will eventually increase intracellular Ca^{2+} or cAMP. All the above mentioned signals collaborate with glucose to potentiate insulin release (Figure 1.3) (Henquin, 2000; Regazzi et al., 2016).

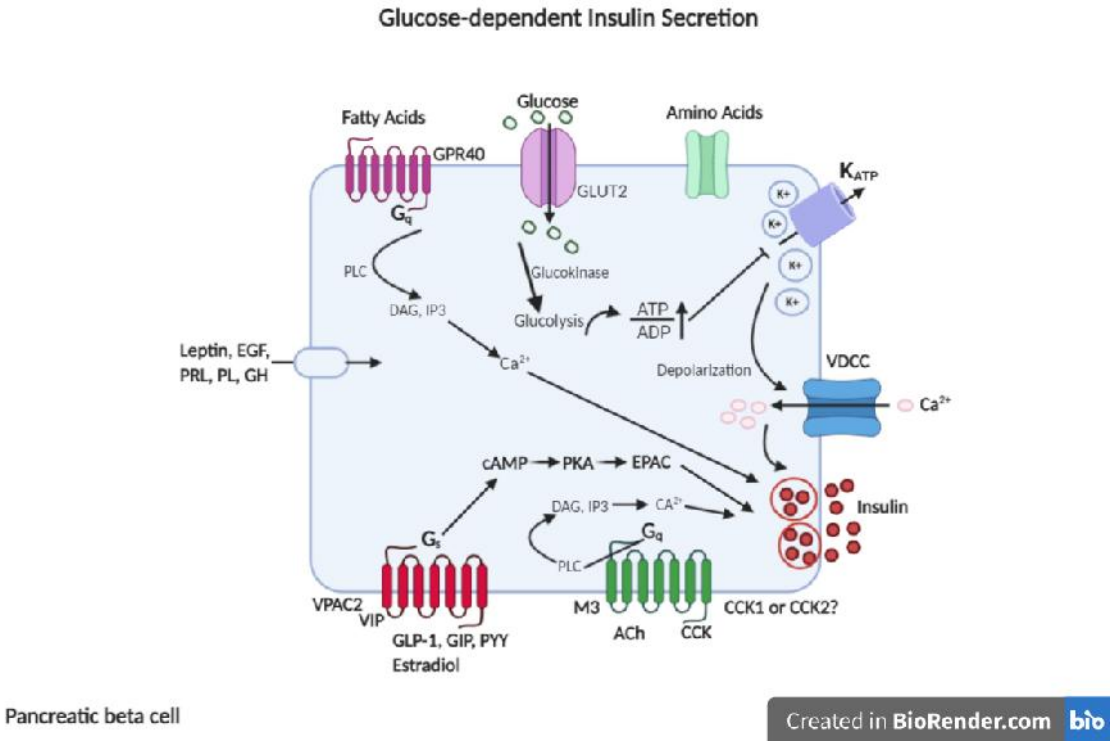

Figure 1.3: Glucose-dependent insulin secretion from a pancreatic beta cell and stimulus effectors.

Glucose is transported into the beta cell through the GLUT2 transporter and metabolized via glycolysis process facilitated by the glucokinase enzyme. Glucolysis elevates ATP/ADP ratio which in turn closes the ATP-dependent K^+ channels (K_{ATP}). Closure of the K_{ATP} channels leads to depolarization of the cell membrane and activation of the voltage-gated Ca^{2+} channels (VDCC) in the plasma membrane which cause a rapid Ca^{2+} influx into the cell and eventually insulin exocytosis. Glucose-induced insulin secretion is augmented by: fatty acids, amino acids, incretins glucagon-like peptide-1 (GLP-1) and glucose-dependent insulinotropic peptide (GIP), vasoactive intestinal peptide (VIP), peptide YY (PYY), estradiol, acetylcholine (ACh), cholecystokinin (CCK), leptin hormone, epidermal growth factor (EGF), prolactin (PRL), placental lactogen (PL) and growth hormone (GH). VIP augments insulin secretion via coupling to VPAC2 receptor which leads to cAMP accumulation, and consequently activation of the PKA signaling pathway and/or EPAC family inducing insulin secretion.

The CFRD etiology is complicated and yet controversial. Studies in human islets and animal models (rats/ferrets) support that dysfunctional CFTR contributes to β cell dysfunction through direct CFTR dependent mechanisms, or indirect non-β-cell CFTR defects on the pancreas (e.g., CFTR expression in other cells types located in the exocrine pancreas that indirectly affect insulin secretion) that, therefore, cause reduced insulin secretion and impaired glucagon suppression (Hart et al., 2018; Sun et al., 2017). Defective CFTR causes elevation of intracellular chloride in β cells which could hinder their depolarization after glucose stimulation and accordingly reduced insulin release. In α cells, elevation of intracellular chloride leads to hyperpolarization that in turn causes excessive glucagon secretion via triggering adenosine triphosphate-sensitive K^+ channels. Another hypothesis is that β cell dysfunction is a consequence of inflammation that leads to reduced β cell mass and islet loss. A recent study from Hart *et al.* (2019) demonstrated that CFRD results from intra-islet inflammation and not from intrinsic islet dysfunction due to CFTR mutations (Hart et al., 2018; Pozo et al., 2020).

Since 2010, insulin is the only effective available and approved treatment for CFRD, which contributes to the risk of hyperglycemia for patients, almost the same to that observed in type I diabetes subjects (Moran et al., 2010). Incretins have been used as a therapeutic option for diabetic patients, especially the dipeptidyl peptidase 4 inhibitors and GLP-1 agonists. The latter, highly improves the pathophysiology of type II diabetes by increasing insulin production, reducing glucagon and gastric emptying as well as increasing satiety (Kayani et al., 2018). However, their therapeutic potential has been poorly studied in the CFRD population. Geyer *et al.* (2019) demonstrated that Exenatide ameliorates

postprandial hyperglycaemia in young people with CFRD (Geyer et al., 2019). Nonetheless, this group of young patients is less affected and further studies in adult population are required.

5. VASOACTIVE INTESTINAL PEPTIDE (VIP)

5.1 Historical Background & VIP Discovery

In 1968, Dr. San I. Said observed that individuals with advanced lung injury or severe pulmonary embolism, experienced vasodilation and hypotension. Therefore, in 1970s and in collaboration with Viktor Mutt, he decided to isolate, from pig's lung, a vasodilator peptide. However, lung tissue inadequacy due to the collection difficulty, did not allow for the extraction of a pure peptide. They next tried to isolate it from duodenal extracts that were more easily accessible, and with the idea that both lungs and small intestine have the same embryonic origin, the foregut. Their second trial was successful and indeed the peptide isolated from the porcine duodenum had vasodilator activity as was further confirmed in anesthetised dogs (Said et al., 1975, 1970; Said et al., 1972). Dr. Said named this peptide after the intestinal organ it was isolated and sequenced from as Vasoactive Intestinal Peptide or VIP (Said et al., 1970; Said et al., 1972).

Later on, Said and Rosenberg in 1976, demonstrated that VIP is expressed in the central, peripheral and intrinsic nervous systems (Delgado et al., 2004; Said et al., 1976). Since then, VIP presence as a neurotransmitter and neuromodulator has been identified in many organs and tissues such as the heart, lung, pancreas, intestine, thyroid gland,

kidney, immune system, urinary tract, and genital organs (Chappe et al., 2012; Henning et al., 2001).

5.2 Synthesis of Vasoactive Intestinal Peptide

VIP is a 28-amino acid (3,326 Da molecular weight) peptide (Figure 1.4) which belongs to the superfamily of secretin/glucagon/pituitary adenylate cyclase-activating peptide (PACAP) that are closely structurally related. Its amino acid sequence in humans has high similarity (more than 85%) with that in fish, frogs and mammals, with the exclusion of guinea pigs and chickens that differ by four amino acids (Dickson et al., 2009; Iwasaki et al., 2019).

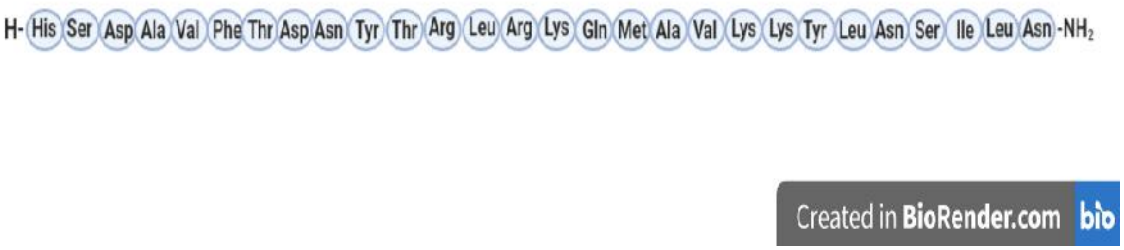

Figure 1.4: Amino acid sequence of the Vasoactive Intestinal Peptide

The structure of the peptide is related to secretin, glucagon, growth hormone releasing factor (GHFR), glucagon-like peptide-1 and -2 (GLP1, GLP2), helodermin, gastric inhibitor peptide (GIP, glucose-dependent insulinotropic peptide), and the mostly related to VIP

by 68% amino acid homology are PACAP27 and PACAP38 (Chappe et al., 2012; Delgado et al., 2013; Martínez et al., 2020).

VIP is synthesized from a 170-amino acid precursor molecule (Pro-VIP), its gene is mapped to chromosomal region 6q25 of chromosome 6 and contains 7 exons (Gozes et al., 1987; Tsukada et al., 1985). Post-translational modifications of the precursor yield the 28-amino acid peptide VIP and a 27-amino acid peptide histidine methionine (PHM, N-terminal histidine and C-terminal methionine amide) in humans, or peptide histidine isoleucine (PHI- N-terminal histidine and C-terminal isoleucine amide) in rodents. While PHM/PHI are structurally and biologically related to VIP, they are less potent than VIP (Delgado et al., 2013; Henning, 2013; Iwasaki et al., 2019). The three-dimensional VIP conformation alters on different environments. For example, in an anionic lipid bilayer or liposomes the long α-helix of VIP plays role for its receptor binding (Umetsu et al., 2011). VIP is degraded by neutral endopeptidase (NEP), an enzyme that is found throughout the body and cleaves multiple peptides, as well as by tryptases and mast cell proteases during immediate hypersensitivity conditions such as inflammation (Caughey et al., 1988; Henning, 2013).

5.3 General Biological Functions of VIP

VIP distribution in various organ systems affect them differently. In the circulatory system VIP controls heart contraction, increases cardiac output, elevates glycogenolysis and reduce arterial blood pressure. In the endocrine system, it augments glucose-dependent insulin secretion and glucagon. In the respiratory system, VIP plays an important role in

smooth muscle relaxation and causes bronchodilation, and most importantly, it contributes to local innate defense by stimulating the movement of water and chloride transport across intestinal and tracheobronchial epithelia. In the immune system, VIP has strong anti-inflammatory effects while in the digestive system it highly contributes to muscle motility, fluid secretion and regulation of pancreatic enzymes. Lastly, in the nervous system, VIP controls circadian rhythm, promotes growth hormone from the pituitary gland, the secretion of prolactin, luteinizing hormone, analgesia, hyperthermia, learning and memory, it has neurotrophic effects, and regulates bone metabolism, brain and embryonic development (Chappe et al., 2012; Delgado et al., 2013; Iwasaki et al., 2019).

5.4 VIP Receptors

The pleiotropic physiological effects of VIP are provided via binding to a class II G protein-coupled receptors (GPCRs) composed of seven-transmembrane domain interconnected with three extracellular (EC1, EC2, and EC3) and three intracellular (IC1, IC2, and IC3) loops, a long N-terminal extracellular domain and an intracellular C-terminal domain. There are three types of VIP receptors: VPAC1, VPAC2 and PAC1. These receptors are the same for both VIP and PACAP. VIP has the strongest affinity to VPAC1 (EC_{50} <0.1nM), next to VPAC2 (EC_{50} =10nM), and the lowest affinity to PAC1 (EC_{50} ~40nM). PACAP binds with strong affinity to PAC1 (EC_{50} ~0.2nM). Additional PACAP members, such as secretin, can bind to VPAC receptors, however VIP has the highest affinity. VPAC1 and VPAC2 activate mainly the adenylate cyclase (AC) pathway, increasing intracellular cAMP, while the PAC1

triggers both adenylate cyclase and phospholipase C (PLC). The α-helix in the N-terminus is critical for the VIP being able to recognize and bind to the receptors, as it connects firstly to the NH_2-terminus of its receptor and next to the additional domains, the N-terminal domain and a poorly described binding domain on the receptor core (Laburthe et al., 2007).

Distribution and expression of VIP receptors is higher in arteries than in veins, explaining the vasodilatory capacity of VIP in veins. More specifically, both VPAC1 and VPAC2 are found in endothelium and smooth muscle of arteries, arterioles and myocardium and cerebral while VPAC1 is highly expressed in brain (cerebral cortex and hippocampus), and in various organs such as lungs, intestine, GI track, liver, thyroid and reproductive organs, as well as immune cells (lymphocytes, macrophages, monocytes, dendritic cells etc.). VPAC2 is mostly identified in intrinsic cardiac neurons, in thalamus and suprachiasmic nucleus of the CNS, and in some exocrine tissues such as pancreas, stomach, kidneys, testis and in adipose tissue. Lastly, PAC1 is mainly identified in brain (olfactory bulb, thalamus, hypothalamus, dentate gyrus of the hippocampus and cerebellum) and in the adrenal medulla.

GPCRs have three subunits (α, β, γ). Class II GPCRs, usually, couple to $G_{\alpha s}$ and increase intracellular cAMP through AC activation, which in turn stimulates protein kinase A (PKA) that induces phosphorylation, and can, therefore, activate or inactivate different signaling pathways, depending on the cell type. This is the traditional signaling pathway of VIP receptors through which VIP moderates its functions. Nonetheless, additionally to the common $G_{\alpha s}$ and cAMP cascade, some studies have demonstrated that VIP receptors

can also bind to other G proteins and modify signaling pathway cross-talk through coupling to $G_{\alpha i/q}$ and activating the PLC signaling cascade (Chappe F. et al., 2008; Chappe et al., 2012; Dérand et al., 2004; Rafferty et al., 2009).

As mentioned on the fluid secretion section, VIP in collaboration with acetylcholine, promotes fluid secretion, maintaining airways sterile. VIP binding to the VPAC1 receptor, on the basolateral membrane of epithelial cells, regulates CFTR-dependent secretion in the airways. More specifically, in airway epithelial cells, CFTR channel function is regulated by VIP through PKA- and PKC-dependent signaling pathways (Alcolado et al., 2011). Research from the Chappe lab have demonstrated that VIP regulates CFTR membrane stability via the activation of the VPAC1 receptor and the $G_{\alpha i/q}$ signaling cascade through PKCε-dependent interaction of NHERF1 and P-ERM proteins with CFTR PDZ domain in a complex that helps stabilizing CFTR at the cell membrane and enhancing its function (Alshafie et al., 2014) (Figure 1.5). Moreover, in the human nasal epithelial cell line JME/CF15, derived from a CF patient homozygous for the F508del mutation, prolonged VIP exposure can rescue trafficking to the cell membrane and increases the function of F508del-channels (Alcolado et al., 2011) (Figure 1.5). In addition to the basolateral membrane of epithelial cells, it has been reported that the VPAC1, contrary to the VPAC2 receptor, is identified in the nucleus of tumor cells (e.g., breast cancer, human renal carcinoma and glioblastoma) (Barbarin et al., 2014; Vacas et al., 2013; Valdehita et al., 2010). A recent study from Villanueva-Romero *et al.* (2019) demonstrated the presence of VPAC1 on the surface and nuclear membrane of T helper (Th) cells. However, upon Th cell activation the receptor expression is only found in the

nucleus (Villanueva-Romero et al., 2019). This nuclear expression of the VPAC1 is due to a sequence in its C-terminal domain for nuclear translocation to occur via Cys37 which should be palmitoylated (a reversible, post-translational alteration of a protein with the insertion of 16-carbon fatty acid, palmitate, to a cysteine residue) (Barbarin et al., 2014; Yu et al., 2017).

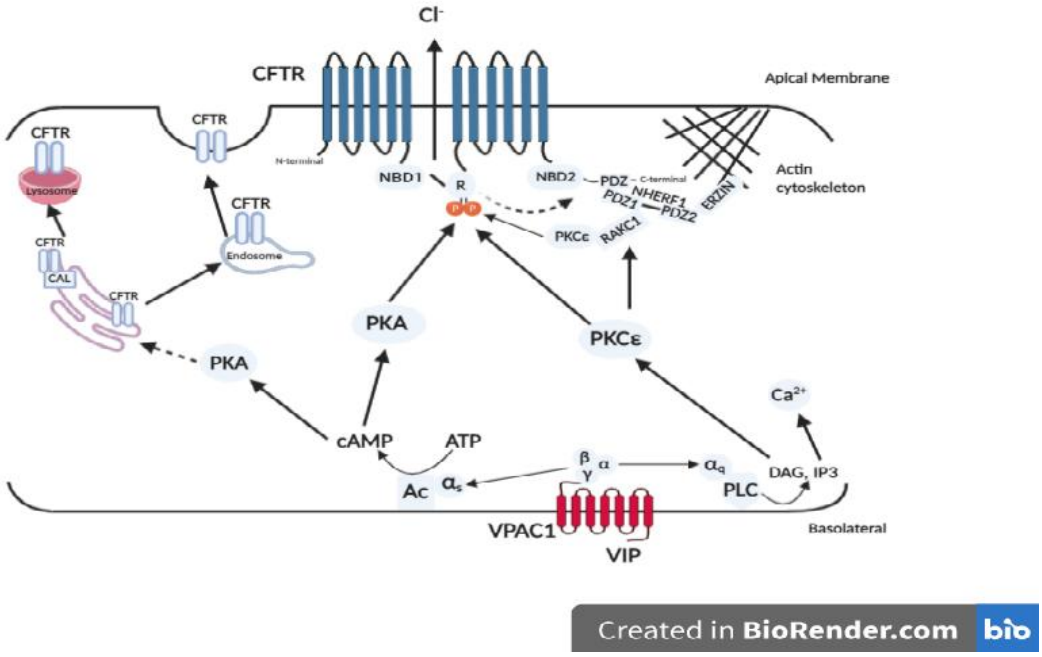

Figure 1.5: Regulation of CFTR by VIP peptide.

VIP regulates CFTR membrane stability via the activation of the VPAC1 receptor at the basolateral membrane, and the $G_{\alpha i/q}$ signaling cascade through PKCε-dependent interaction of NHERF1 and P-ERM proteins with CFTR PDZ domain stabilizing CFTR at the apical membrane and enhancing its function. CFTR function is further enhanced by PKC phosphorylation of the regulatory domain. In parallel, VPAC1 receptor upon coupling to the $G_{\alpha i/s}$, activates adenylyl cyclase (Ac) which in turn leads to cAMP production and consequently activation of PKA that directly phosphorylates the R domain of CFTR stimulating CFTR function. Also, activation of the PKA signaling pathway rescues CFTR from lysosomal degradation, via impeding CFTR and CAL connection. Based on Alshafie *et al.* (2014).

5.5 VIP Distribution as a Neurotransmitter

VIP is broadly distributed in the central and peripheral nervous systems as well as in the digestive, respiratory, reproductive, and cardiovascular systems as a neurotransmitter and neuroendocrine releasing factor. VIP is mainly expressed in cholinergic parasympathetic neurons and only a small percentage is expressed in sympathetic nerves. In the heart, intrinsic VIPergic nerves are localized in the sinoatrial node, cardiac glomeruli, in the nerve terminals of the atria arteries and upward aorta as well as in the intrinsic cardiac ganglia (Henning, 2013). In the cardiovascular system VIP coexists with acetylcholine in the parasympathetic nerves.

In the human gastrointestinal track VIPergic nerves are highly dense in the myenteric and submucosa plexus layers and less in the longitudinal muscle. In a quantitative analysis of the intrinsic neuronal distribution, Anlauf *et al.* (2003) reported that the submucosa layers of the stomach and large intestine contain the greatest amount of VIPergic ganglionic cells. In the myenteric layer, the stomach has a higher density of VIP-positive nerve fibers compared to the myenteric layer in the small and large intestine. In the parasympathetic nervous system, VIP is co-localized with acetylcholine, in order to promote maximal fluid secretion as was previously described (see section 2.2). This co-localization was further confirmed at the neuronal level by Anlauf *et al.* (2003). The expression of acetylcholine was revealed with the cholinergic VChAT (vesicular acetylcholine transporter involved in acetylcholine synthesis) antibody. Indeed, co-expression of VIP and VChAT was shown in both myenteric and submucosal plexuses throughout the human gut. Their co-existence was also shown in the smooth muscle,

mucosa and blood vessels (Anlauf et al., 2003). Only the submucosa layer of the colon was missing the co-localization of VIP and VChAT. Consequently, in the human gut VIP exerts its biological functions as a cholinergic co-transmitter of the intrinsic gut neuronal network, contrary to studies in the intestine of the guinea pig and other mammals where VIP functions as a non-adrenergic, non-cholinergic (NANC) neuropeptide (Anlauf et al., 2003; Costa et al., 1996). Additionally, VIP is expressed in inhibitory motor neurons and interneurons of the myenteric circular muscle, enabling intestinal smooth muscle relaxation, other than promoting fluid secretion (Anlauf et al., 2003; Furness, 2000; Porter et al., 1996; Porter et al., 1997). As both VIP and acetylcholine are released from the same intrinsic cholinergic neurons, VIP plays a critical role in the control of cholinergic neurotransmission. In addition to that, in peripheral ganglia of the mouse intestine, during embryonic development at stage E16, strong VIPergic innervation has been identified, suggesting that VIP has a significant role during the development of the nervous system (Waschek et al., 1996). VIP neuronal effects as a non-cholinergic transmitter are very minimal, and occur only when it is expressed in the secretomotor neurons of the intestine which are either cholinergic or non-cholinergic. Intrinsic secretomotor neurons maintain the balance of absorption and secretion locally, and are controlled by local reflex circuits which in turn are under the control of central sympathetic pathways. Some of these neurons are cholinergic secretomotor/non-vasodilator and utilize acetylcholine as their main transmitter and others are non-cholinergic secretomotor/vasodilator neurons using VIP (Furness, 2000).

In the respiratory track, VIP is a potent vasodilator and is distributed in the tracheobronchial smooth muscle layer of the airways, the inner walls of pulmonary and bronchial vessels. There is a dense VIPergic innervation around submucosal glands. The density of VIPergic nerves reduces towards the smaller airways, with only a few VIP neurones being localized in bronchioles and alveolar space (Barnes et al., 1991; Laifihen et al., 1985; Laitinen et al., 1985; Wu et al., 2011). Co-localization of VIP with acetylcholine has been revealed in all intrinsic nerves surrounding peribronchial ganglia and following the parasympathetic pathway (Anlauf et al., 2003). The parasympathetic innervation is of high significance for the development and coordination of ductal tubologenesis in the submucosal glands and salivary glands, enabling ductal growth, and lumen enlargement. Pregnant mice that were treated with a VPAC1 receptor antagonist during the gland developmental stage (E12-E16) showed smaller luminal cavities compared to control PBS treated embryos. The absence of VIP innervation contributed to abnormal submucosal gland tubulogenesis with decreased branching and alteration of lumen development (Nedvetsky et al., 2014).

In the exocrine pancreas, VIP-parasympathetic nerves are identified between acini, surrounding ducts and blood vessels. In the islets of Langerhans of the endocrine pancreas VIPergic nerve fibers are distributed in the form of a very dense matrix throughout the islets. This condensed VIPergic neuronal network of the endocrine pancreas indicates an important role for VIP in the control and release of pancreatic hormones such as somatostatin, glucagon, insulin and pancreatic polypeptide (Havel et al., 1997; Iwasaki et al., 2019; Sanlioglu et al., 2012).

Lastly, the eccrine sweat glands are principally controlled by cholinergic innervation in addition to adrenergic and peptidergic innervation. Human axillary skin, where the eccrine sweat glands are abundant, is characterized by a rich intrinsic VIPergic neuronal network around the secretory sweat gland acini and a less dense VIPegic network in the re-absorptive ducts (Heinz-Erian et al., 1985; Sato et al., 1984; Sato et al., 1988). Also, most of the VIP neurons were found to be closely related to glandular cells, duct cells and myoepithelial cells (Eedy et al., 1990).

5.6 VIP and Cystic Fibrosis

As mentioned above, a rich VIPergic neuronal network innervates all exocrine glands including the pancreas, sweat and salivary glands, lachrymal, bronchial and intestinal glands. The link between VIP and cystic fibrosis disease was first reported by Heinz-Erian *et al.* (1985) when they revealed sparse or absent VIP-containing nerve fibers around the eccrine glands of CF patients' skin compared to healthy subjects. VIP peptide is a potent vasodilator and bronchodilator, and the major physiological agonist of CFTR. In synergy with acetylcholine, it regulates exocrine gland secretions, contributing to local innate defense, by stimulating the movement of water and chloride across intestinal and tracheobronchial epithelium. A demonstration of VIPergic deficiency or neuronal discontinuation at that time (given that the CFTR gene was discovered four years later, in 1989) was a very significant finding for the understanding of CF disease development as it could explain the abnormal secretory activity and high chloride levels in the sweat (Heinz-Erian et al., 1985). Findings of Heinz-Erian *et al.* about sparse VIP-innervation in

CF was also confirmed by Savage *et al.* five years later, further showing reduced VIPergic innervation of cutaneous blood vessels (Savage et al., 1990). Moreover, VIPergic neuronal deficiency was shown in the nasal and intestinal mucosa of CF patients by Wattchow *et al.* (1988). The authors also demonstrated that neuropeptide Y (NPY) nerves were sparse in the CF mucosa layer of the intestine where VIP and NPY are co-expressed in some of the intestinal neurons.

Human CF SMGs only secrete minimally in response to agonists that increase intracellular cAMP alone (VIP and FSK) or slightly to agonists that elevate $[Ca^{2+}]_i$ (substance P and CCh). The combination of these two types of agents produce a synergetic response that is lost in CF (Ianowski et al., 2007; Jae et al., 2007).

The fundamental role of VIP in CF was also confirmed by our lab with VIP-KO mice where the VIP gene was genetically deleted. These mice, developed by the late Said group (Hamidi et al., 2006), were characterized by goblet cells hyperplasia and inflammatory cells infiltration in the intestine, alveolar and peribronchial thickening, edema and inflammation in the lungs while the pancreas presented ductal infiltration with the presence of inflammatory cells (Alcolado et al., 2014). VIP-KO mice were injected intraperitoneally with VIP for three weeks and after the treatment, the pathological signs in the lung and duodenum were corrected with tissue closely resembling the wild-type phenotype (Alcolado et al., 2014). As VIP regulates CFTR function through the activation of VPAC receptors, the authors examined the impact of VIP injections on the CFTR protein expression at the cell membrane. Before treatment, in contrast to wild-type, in VIP-KO mice, CFTR localization was lost from the apical membrane of lung and duodenum

epithelial cells. However, the intracellular localization of the CFTR protein was corrected after the VIP treatment and membrane localization was restored. An Ussing chamber study of VIP-KO mouse ileum confirmed the absence of a CFTR-dependent chloride current in VIP-KO mice tissues. This was corrected by the VIP treatment, confirming membrane expression of the channel. These results were further confirmed in primary tracheal epithelial cells of VIP-KO mice, where, indeed, the VIP treatment maintained CFTR at the apical membrane establishing the necessity for chronic VIP stimulation in the regulation of CFTR localization and function (Alcolado et al., 2014). Similar findings were also reported in preparations of rectal glands from the spiny dogfish shark that express a CFTR ortholog with 72% similarity to the human protein. Acute VIP treatment increased the CFTR apical trafficking (Lehrich et al., 1998). Also, in rat CFTR high expressor cells (CHE) that are found in the villi of the small intestine, CFTR was restored at the apical plasma membrane after stimulation of cAMP levels by VIP (Ameen et al., 1999).

VIP treatment can rescue ΔF508-CFTR trafficking and maintain the channel stable at the cell membrane, acting through the VPAC1 receptor in airway epithelial cells. In nasal epithelial cells (JME/CF15) from a ΔF508 homozygous patient, ΔF508-CFTR membrane insertion was stimulated by the PKA-dependent signaling pathway in response to VIP stimulation, while its stabilization at the cell surface was PKC-dependent and involved the interaction of CFTR with the RAKC1-NHERF1-pERM complex. Consequently, it is demonstrated *in vivo* and *in vitro* that VIP stimulation contributes to the channel function, corrects the trafficking of the mutated protein and increases its stability at the apical cell membrane (Alcolado et al., 2011; Rafferty et al., 2009).

6. Animal Models of CF – The Mouse Model in CF

The figures and text presented in this chapter are from a review manuscript published to the Journal *Frontiers in Pharmacology*. Anna Semaniakou, Roger P. Croll, and Valerie Chappe (2019). Animal models in the pathophysiology of cystic fibrosis. https://www.frontiersin.org/articles/10.3389/fphar.2018.01475/full.

As the first author on this article, I wrote the manuscript which was edited by Dr. Valerie Chappe and Dr. Roger P. Croll.

6.1 Overview

Our understanding of the multiorgan pathology of cystic fibrosis (CF) has improved impressively during the last decades, but we still lack a full comprehension of the disease progression. Animal models have greatly contributed to the elucidation of specific mechanisms involved in CF pathophysiology and the development of new therapies. Soon after the cloning of the CFTR gene in 1989, the first mouse model was generated and this model has dominated in vivo CF research ever since. To our knowledge, 14 more mouse models have been described in the literature to date with different characteristics, grouping them in two categories. The first category consists of those models in which the CFTR gene was disrupted using a "replacement strategy" or an "insertional strategy." A replacement strategy causes an interruption of the CFTR gene and generates complete nulls ("knockout": KO) with no normal CFTR protein production, while with the "insertional strategy" a low amount (~10%) of normal mouse CFTR mRNA is produced. Phenotypic differences are observed between the absolute nulls and the residual function models due to the low amount of normal CFTR expression in the latter. The second category contains mouse models that replicate known clinical mutations in CF, such as the Class II F508del ($Cftr^{tm1Eur}$, $Cftr^{tm1Kth}$, and $Cftr^{tm2Cam}$) and Class III, G551D ($Cftr^{tm1G551D}$) utilizing a replacement-gene targeting strategy or a double homologous recombination method, also known as a "hit and run" procedure. In this category, survival rates, disease severity and pathology vary from model to model. The variations are attributed to different types of mutations, levels of mRNA expression, environmental

factors and genetic backgrounds that can be responsible for various levels of activity of modifier genes in the mouse strains used (Semaniakou *et al*., 2019).

6.2 Mouse Model for Studying Lung Defects in CF

In 1997, Kent and colleagues designed a model from a single genetic background (congenic), C57BL/6JCftr^{tm1Unc}/Cftr^{tm1Unc}, that under specific pathogen-free conditions, developed spontaneous and progressive lung disease (Guilbault et al., 2005; Guilbault et al., 2006; Kent et al., 1997). Loss of mucociliary transport, postbronchiolar hyperinflation of alveoli, and parenchymal interstitial thickening with indication of fibrosis and inflammatory cell recruitment characterize the lung disease on this congenic model (Kent et al., 1997). It also showed reduced control of the *P. aeruginosa* infection. Acinar and alveolar over inflation, reflect small airway obstructions that are observed in the early stages of CF in humans (Guilbault et al. 2005). Later on, more studies boosted our knowledge with significant observations in CF pulmonary pathology using mice that were not exposed to pathogens. Thus, excessive inflammation was noticed in Cftr^{tmr1Hgu} mice, mucociliary clearance (MCC) dysfunction in Cftr^{tm1Hgu} and Cftr^{tm1Unc} mice, goblet cell hyperplasia with airway surface liquid (ASL) depletion in the nasal epithelium of Cftr^{tm1Unc} mice, and a distal extension of submucosal glands (SMGs) in Cftr^{tm1Hgu} and Cftr^{tm1G551D} mice (Cowley et al., 1997; Semaniakou et al., 2019; Tarran et al., 2001; Zahm et al., 1997). The Cftr^{tm1G551D} model demonstrated defective pulmonary clearance and a high sensitivity to *P. aeruginosa* (McMorran et al., 2001).

Durie *et al.* (2004) described a promising long-living congenic $Cftr^{-/-}$ model bred in the C57Bl/6 background that displays the human lung pathology with signs of inflammation, presence of macrophages, tissue damage, and acinar dilation (Durie et al., 2004). Moreover, $Cftr^{-/-}$ mice challenged with *P. aeruginosa* had increased IL-8, IL-6 and TNF-α levels and decreased IL-10 level, indicating that the absence of CFTR can cause excessive lung inflammation (Bruscia et al., 2016). Additionally, the number of both alveolar and peritoneal macrophages was high in F508del mice infected with lipopolysaccharides (LPS), illustrating their adaptability in the airway environment (Bruscia et al., 2016). CF mice may not be able to develop abrupt lung disease as patients with CF do, but they have been successfully used to demonstrate a defective autophagy mechanism which can lead to lung hyper-inflammation (Luciani et al., 2010). Lastly, in 2011, Zhou and colleagues generated a transgenic "β-ENaC" mouse model to recapitulate the pathophysiology of the CF lung. This model, which over-expresses the β subunit of ENaC with increased Na^+ absorption, presented with ASL depletion, reduced MCC with airway mucus obstruction, goblet cell hyperplasia, chronic lung inflammation, and high mortality related to lung disease (Zhou et al., 2011).

6.3 Mouse Model for Studying the Intestinal Pathology in CF

CF mice are characterized by severe intestinal obstructions, similar to CF patients. The severity of the disease and the survival rate differ among genotypes (Semaniakou et al., 2019). The neonatal death rate is ~60% for CF null mice and only 35% for F508del-CFTR. However, this percentage of MI is still high compare to only 10% in the human disease.

The $Cftr^{tm1Eur}$ and $Cftr^{tm2Hgu}$ models, carrying the F508del and G480C mutations, respectively, exhibit intestinal alterations that are not as severe as those in the CFTR-KO mice (De Lisle et al., 2013). The $Cftr^{tm1G551D}$ has an approximate 70% survival rate with less severe pathology than the null models. A murine F508del model was generated with a replacement-gene targeting method by Colledge *et al.* (1995) and was suggested to be an accurate model for testing therapeutic drugs. It demonstrated severe meconium obstruction, reduced cAMP-stimulated Cl^- secretion, and the temperature-dependent trafficking. defect that is described associated with this mutation in the human disease (Colledge et al., 1995). Tissue sections of the colon and duodenum revealed huge crypt dilation with increased mucus accumulation. As previously mentioned, the genetic background variation and low residual level of expression of normal CFTR have been proposed to explain dissimilarities between models (Semaniakou et al., 2019).

Studies have shown that the expression of modifier genes may also be responsible for this intestinal variability. A genetic modifier of MI was detected in chromosome 19 in humans and on mouse chromosome 7 and was shown to be involved in the disease progression in KO mice (Gyömörey et al., 2000; Rozmahel et al., 1996; Zielenski et al., 1999).

Norkima *et al.* (2004), using a DNA microarray, observed the presence of some gene expression associated with inflammation and presence of innate immune cells, such as mast cells and neutrophils, similar to those observed in the intestine of patients with CF (Norkina et al., 2004). Amelioration of the intestinal obstruction and an increase in the survival rate was achieved by the expression of human CFTR cDNA in the intestinal track

of $Cftr^{tm1Unc}$ mice, under the control of the rat intestinal fatty-acid-binding protein (iFABP) gene promoter. This $Cftr^{tm1Unc}$ –$TgN^{(FABPCFTR)}$ model enabled long-term studies in the intestine (De Lisle et al., 2013). Electrophysiological studies have confirmed the ion transport abnormalities in CF mice with a similar phenotype to that of the human CF intestine: low or absence of cAMP-mediated Cl^- transport (Grubb et al., 1997).

6.4 Mouse Model for Studying Pancreatic Disease in CF

In contrast to patients with CF in whom exocrine pancreatic insufficiency (PI) is a major condition, CF mice exhibit only moderate pancreatic changes (Snouwaert et al., 1992). Durie *et al.* (2004) demonstrated that a long-living CF-KO mouse bred into a congenic C57Bl/6 background develops pancreatic pathology similar to humans with presence of inflammatory cells and macrophages, and increased acinar volume at an older age (Durie et al., 2004). Surprisingly, mice with the F508del or G551D mutation, do not show any apparent pancreatic disease (Colledge et al., 1995; Delaney et al., 1996; van Doorninck et al., 1995). The milder pancreatic disease in mice is attributed first to the lower level of normal CFTR expression in the murine pancreas, while high CFTR expression level has been shown in humans (Gray et al. 1995), and second to differences in the CACC channel expression. The CACC is detected in both WT and CF mice alleviating the pancreatic disease progression, perhaps explaining the mild murine pancreatic pathology (Clarke et al., 1994; Gray et al., 1995; Keiser et al., 2011; Marino et al., 1991).

6.5 Murine Sweat Glands in CF

Murine sweat glands are an underestimated tissue in the field of CF. Sato *et al.* (1994) investigated changes in cholinergic and β-adrenergic responsiveness during the postnatal life and reported that the mouse sweat glands are mainly under cholinergic control and express CFTR. Sweat secretion can be monitored in response to cAMP elevating agonists with activation of either K^+ channels, Cl^- channels, or both. The secretion rates are higher in older animals (over 6-weeks old) but are independent from glandular enlargement (Sato et al., 1994). Sweat glands remain free of infection, do not exhibit morphological alterations and are easy to collect, as they are found under the mouse paw (Semaniakou et al., 2019).

7. Research Hypothesis and Objectives

VIP is distributed in the central and peripheral nervous systems richly innervating all exocrine glands. In CF patients it was shown that VIP-positive nerve fibers of the skin and intestinal mucosa are sparse compared to healthy individuals. Since VIP plays a very significant role in the local innate defense by stimulating the movement of water and chloride across intestinal and tracheobronchial epithelium it was hypothesized, that abnormal VIP innervation may contribute to the CF disease pathogenesis. Nonetheless, the mechanism behind this phenomenon remained unknown. Consequently, the main general question of this PhD research was to examine changes in VIP amount.

More specifically, we examined changes in the VIP content in the duodenum, lungs, sweat glands, endocrine and exocrine pancreas in the 8-week and 17-week-old C57Bl/6 CF mice, homozygous for the ΔF508 mutation, compared to same age wild-type littermates. These two different age groups reflect the early and late disease state. Next, we determined if these changes in VIP peptide were related to tissue inflammation and/or infection observed in the duodenum and lung tissues. Additionally, we further investigated the mechanism behind this reduced VIP amount, in neuronal level, studying the VIP innervation, the general innervation and the co-transmission of VIP with acetylcholine in CF. Innervation data were focused mainly in the mucosa and myenteric plexuses as these two layers express the highest density of nerve fibers.

As described above, CFRD is the second co-morbidity in CF, following respiratory failure, and affecting approximately more than 50% of adult CF patients. CFRD is characterized by partial insulin insufficiency, impaired glucagon suppression and elevated random

plasma glucose. Glucose-dependent insulin secretion and glucagon release are augmented and indirectly regulated by VIP. To ascertain if changes in VIP content can affect insulin and glucagon secretion as well as glucose levels, and possibly contributing to CFRD pathogenesis, we investigated the VIP content in the endocrine and exocrine pancreas as well as the secretion of insulin, glucagon and random plasma glucose concentration. Furthermore, we examined the general neuronal innervation in the pancreas and correlated it to the reduced VIP amount.

This study aims to shed light on three broad unanswered questions in the field regarding the defective VIP innervation: 1) Is this sparse VIP innervation related to disease progression or due to defective VIP peptide synthesis?, 2) when does VIP reduction start and what is the connection with the disease development?, 3) what is the impact of VIP reduction on the pancreas and on the development of CFRD disease?.

CHAPTER 2: MATERIALS AND METHODS

2.1 Chemicals and Antibodies

Antibodies are shown in Table 2.1; Normal mouse blocking serum was from Santa Cruz Biotechnology (ImmunoCruz goat ABC Staining System; sc-2023); Normal rabbit blocking serum was from Santa Cruz Biotechnology (ImmunoCruz goat ABC Staining System; sc-2018); Normal donkey serum (D9663) was from Sigma (St. Louis, MO); Normal goat blocking serum was from Vector Laboratories (Cat. No. NC9270494); Avidin-Biotin complex was from Santa Cruz (ImmunoCruz ABC kit; sc-516216); Triton X-100 (T8532) was from Sigma; 16% paraformaldehyde aqueous solution (15710) was from Electron Microscopy Sciences (Hatfield, PA); Collagenase Type IA was from Sigma (Collagenase from Clostridium histolyticum; C2674); Glycerol Mounting Medium was from Abcam (ab188804); DAB (3, 3 -diaminobenzidine) HRP Substrate Kit (ab64238) was from Abcam (Cambridge, MA); Enzyme-Linked-Immunosorbent Assay kit for VIP was from Cloud-Clone Corp. (Cat. No. CEA380Mu; Houston-TX); Enzyme-Linked-Immunosorbent Assay kit for murine Insulin was from Millipore (Cat. No. EZRMI-13K); Cayman's Glucose Colorimetric Assay kit was from Cayman Chemical (Cat. No. 10009582); Enzyme-Linked-Immunosorbent Assay kit for MIP-2 was from Mybiosource (Cat. No. MBS175915; San Diego-CA); Vectashield Mounting Media for Fluorescence was from Vector Laboratories (Cat. No. 101098-042); Alcian Blue 8GX solution (A5268) was from Sigma; Albumin Bovine (BSA) was from Sigma (A2153); Quick Start Bradford 1X Dye Reagent (Cat. No. 5000205) was from Bio-Rad (California, USA); Protease inhibitor cocktail tablets were from Roche (cOmplete, Mini; Cat. No. 11 836 153 001). Other chemicals were from Sigma.

Table 2.1: Summary of Antibodies and their Dilutions.

Polyclonal Primary Antibodies	Dilution & Application	Secondary Antibodies	Dilution
Anti-VIP (M-19; sc-7841), Santa Cruz Biotechnology (Santa Cruz, CA)	1:75 (IHC)	ImmunoCruz goat avidin/biotinylated complex Staining System (sc-2023), Santa Cruz Biotechnology	As per kit instructions
Anti-VIP (Cat. No. PA5-78224); Thermofisher (CA, USA)	1:100 (IHC)	ImmunoCruz rabbit avidin/biotynilated complex Staining System (sc-2018), Santa Cruz Biotechnology	As per kit instructions
Anti-Choline Acetyltransferase (ChAT; AB144P), EMD Millipore (Bellerica, MA)	1:100 (IHC)	ImmunoCruz goat avidin/biotinylated complex Staining System (sc-2023), Santa Cruz Biotechnology	As per kit instructions
Anti-PGP 9.5 *(*ab15503), Abcam (Cambridge, MA)	1:200 (IHC)	ImmunoCruz rabbit avidin/biotynilated complex Staining System (sc-2018), Santa Cruz Biotechnology	As per kit instructions
Anti-VIP (20077), ImmunoStar (Hudson, WI)	1:100 (whole mount immunostaining)	Donkey anti-Rabbit IgG (H+L) (Alexa Fluor 555; A-31572), Invitrogen (Carlsbad, CA)	1:500
Anti-PGP 9.5 *(*ab15503), Abcam (Cambridge, MA)	1:100 (whole mount immunostaining)		
Anti-Choline Acetyltransferase (ChAT; AB144P), EMD Millipore (Bellerica, MA)	1:50 (whole mount immunostaining)	Donkey anti-goat IgG (H+L) (Alexa Fluor 555; A-21432), Invitrogen (Carlsbad, CA)	
Anti-Insulin (ab7842) Abcam (Cambridge, MA)	1:50 (IHC)	Goat anti-guinea pig IgG, Fc fragment specific (Cat. No. 106-035-008); Jackson Laboratories (Pennsylvania, USA)	
Anti-Glucagon (sc-13091; FL-180; Lot No. K0304); Santa Cruz Biotechnology (Santa Cruz, CA)	1:50 (Immunofluorescence)	Donkey anti-rabbit IgG (H+L); Alexa Fluor 594 (Cat. No. 711-585-152); Jackson Laboratories (Pennsylvania, USA)	1:200

2.1.1 RIPA Buffer

For the preparation of 20ml of RIPA lysis buffer we mixed 16mg of 0.08% Deoxycholic Acid, 0.2ml of 1% Triton X-100, 20mg of 0.1% SDS, 0.175g of 0.15M NaCl, 7.45mg of 1Mm EDTA, 24.23mg of 10mM Tris and ½ tablet of the protease inhibitor cocktail from Roche. The pH was adjusted to 7.5 and the buffer was stored at -20^{o}C. The protease inhibitor cocktail protects proteins from early degradation as it inhibits serine and cysteine proteases.

2.2 Mice

Male, 8- and 17-week-old wild-type C57Bl/6 mice and C57Bl/6 homozygous for the F508del mutation (C57Bl/6 homozygous *Cftr*^{tm1Kth} ΔF508) were obtained from Dr. Craig Hodges at Case Western Reserve University (Ohio, USA). For the 8-weeks age group, wild-type and CF, we had 5 male mice, while for the 17-weeks we had 5 control mice for the wild-type category and 3 mice for the CF group. Mice were housed in an Allentown IVC rack with irradiated corncob bedding, Prolab autoclaved RMH 3500 feed and municipal (chlorinated tap) water with 3% Colyte. Mice were evaluated daily during routine health checks. If they showed signs of distress, they were weighed, given SC fluids if needed and monitored more frequently by lab personnel. If signs of distress did not resolve (e.g., obstruction passed), they were humanely euthanized. All experimental procedures were in accordance with the principles of the Canadian Council on Animal Care (CCAC) and according to the National Institute of Health *Guide to the Care and Use of Experimental*

Animals. Protocols were approved by Dalhousie University (Halifax, Canada) Animal Care and Use ethic committee.

2.3 Tissue Preparation

Mice were humanely euthanized by intraperitoneal overdose of sodium pentobarbital + lidocaine before tissue collection (50µl and 150µl). Mice were measured and weighted before necropsy. Salivary glands, trachea, lungs, stomach, pancreas, all small intestine (duodenum, jejunum, ileum) colon, rectum, sweat glands and heads (for brain and nasal cavities) were collected immediately upon euthanasia, rinsed with 70% ethanol or sterile ice-cold PBS (intestinal lumen) and fixed in 10% formalin buffer (0.2L 37% Formaldehyde, 1.8L dH_2O and 46.1g Na Acetate-$3H_2O$), or flash frozen in liquid nitrogen before storage at -80^oC for later use.

2.3.1 Mouse Tissue Homogenization

For protein extraction, tissues were homogenized. A piece of frozen tissue was cut, placed into a pre-weighted 2ml tube and carefully weighted to adjust the amount of lysis buffer. Typically, we used approximately 30mg of tissue. Next, we immersed the tissues in lysis RIPA buffer with 100µl of lysis buffer for every 10mg of tissue. Afterwards, tissue was homogenized with a rotor-stator homogenizer for 1.5-2 minutes followed by 30 seconds of vortexing. The tissue then underwent sonication at 30% output for 5 cycles of 20 seconds to break the cell membrane and allow the protein extraction. After the sonication step, the tissue was gently shaken at 4^oC for 30 minutes, with 30 seconds of

vortexing at 15 minutes. Next, the tissue lysate was sonicated again at 30% output for 3 cycles of 20 seconds and centrifuged at 8,000 rpm for 10 minutes at 4^{o}C to remove large debris. The supernatant was collected and went through another cycle of gentle shaking for 15 minutes at 4^{o}C, followed by 30 seconds of vortexing again. Finally, samples were centrifuged at 13,000 rpm for 20 minutes at 4^{o}C to remove any remaining debris before the supernatant was collected, aliquoted and stored at -80^{o}C. Protein concentration was determined with the Bradford protein assay method.

2.4 Plasma Collection

For collecting plasma, immediately after the mouse euthanasia, as described above, we used intra-cardiac puncture to collect blood by aspiration with a 26-30G needle filled with 2% EDTA to prevent coagulation and 1ml syringe. Blood collected was placed into a 1.5mL Eppendorf tube with 100µl of 2% EDTA and centrifuged in an 8G centrifuge for 10 minutes at 4°C. The supernatant (plasma) was collected into a new tube, aliquoted and stored it at -80^{o}C until further use.

2.5 Histology with Hematoxylin and Eosin (H&E) Staining

As described above, tissues were immediately fixed in 10% formalin buffer and incubated for at least 72hrs before fine dissection. Fixed tissues were then washed in ethanol and bring to the Dalhousie Histology Lab for embedding in paraffin blocks before longitudinal sectioning into 5-µm-thin microsections. Tissue embedding and sectioning were done at

the Histology and Research Services (HRS) Laboratory, Pathology Department, Faculty of Medicine, Dalhousie University.

H&E staining: 5µm thick mice tissue samples annealed to microscope slides were deparaffinised as follow: incubated three times in xylene (5 minutes each dip), two times in 100% ethanol (5 minutes each dip), three times in 95% ethanol (5 minutes every time), and lastly a 5-minute incubation in 70% ethanol. Slides were afterwards run under tap water for 2 minutes. After the deparaffinization step, slides were stained in Harris Hematoxylin for 50 seconds, run immediately under tap water for 2 minutes, next incubated in Scott's water for 2 minutes, followed by a washing step under tap water for 2 more minutes. Afterwards, slides were quickly dipped in 0.2% Nitric Acid and run under tap water for 2 minutes, dipped in Scott's water for 2 minutes, run again under tap water for 2 minutes, following 10 dips in Eosin Y, and lastly run under tap water for 1 minute. Before mounting, slides went through dehydration step in ethanol solution: 20 dips in 70% ethanol (three times), 20 dips in 95% ethanol (three times), 20 dips in 100% ethanol (two times), and lastly 20 dips in xylene (four times). Slides were then mounted with a mounting medium (Cytoseal 60; Cat. No. 23-244257; Fisher Scientific), stored at RT for a few hours and visualized under light microscopy (Zeiss Axioplan II microscope). Images were taken with a Zeiss Axiocam HRC Colour Camera utilizing 10X, 20X or 40X objectives.

2.6 Immunohistochemistry (IHC)

Thin tissue sections (5µm) annealed to microscopy slides were deparaffinised for 15 minutes (3 times for 5 minutes) in xylene, 15 minutes (3 times for 5 minutes) in 100% ethanol, 10 minutes (2 times for 5 minutes) in 95% ethanol and 10 minutes (2 times for 5 minutes) in 70% ethanol. Slides were then run under tap water for 5 minutes. Next, slides were placed in 200ml of 0.1M citrate buffer (pH 6.0) and then inside a pressure cooker for a 35 minutes' heat-induced antigen retrieval. After the antigen retrieval step, slides were allowed to cool down at room temperature (RT) for approximately 20 minutes inside the citrate buffer.

Next, slides were washed twice for 5 minutes each time in PBS and incubated in 1% peroxidase blocking solution for 5 minutes. After another 10-minute washing step with PBS, slides were incubated in normal mouse blocking serum for 1h at RT in a humidified chamber, then incubated overnight with the primary antibody for VIP (M-19, 1:75), choline acetyltransferase (ChAT; 1:100), Insulin (1:50) or Protein Gene Product 9.5 (PGP 9.5; 1:200). VIP (M-19; see table 2.1) was discontinued after three years, and we continued our experiments using VIP (PA5-78224, 1:100; see table 2.1). For the negative control, the primary antibody was omitted, and slides were incubated overnight at 4^{o}C on PBS (Figure 2.1). The next day tissue slides were washed three times for 5 minutes each with PBS and afterwards incubated with a biotinylated secondary antibody (1:200; ABC ImmunoCruz staining system, see table 2.1 for details on primary and secondary antibodies combinations) for 30 minutes at RT. After three washes with PBS for 5 minutes each, slides were incubated in avidin/biotinylated complex (ABC ImmunoCruz staining

system, see table 2.1) for 30 minutes at RT and then washed again three times in PBS for 5 minutes each. VIP, ChAT, Insulin or PGP 9.5 signal was revealed with a DAB HRP peroxidase substrate. DAB-stained slides were visualized under a light microscope every minute or so, in order to set the optimal signal intensity. For VIP (M-19) DAB incubation was set at 7.5 minutes for both WT and CF. For VIP (PA5-78224) DAB incubation was set at 4 minutes for both WT and CF, for the ChAT signal slides were incubated on DAB substrate for 7 minutes, for Insulin slides were incubated for 3 min and for PGP 9.5 slides were incubated only 45 seconds.

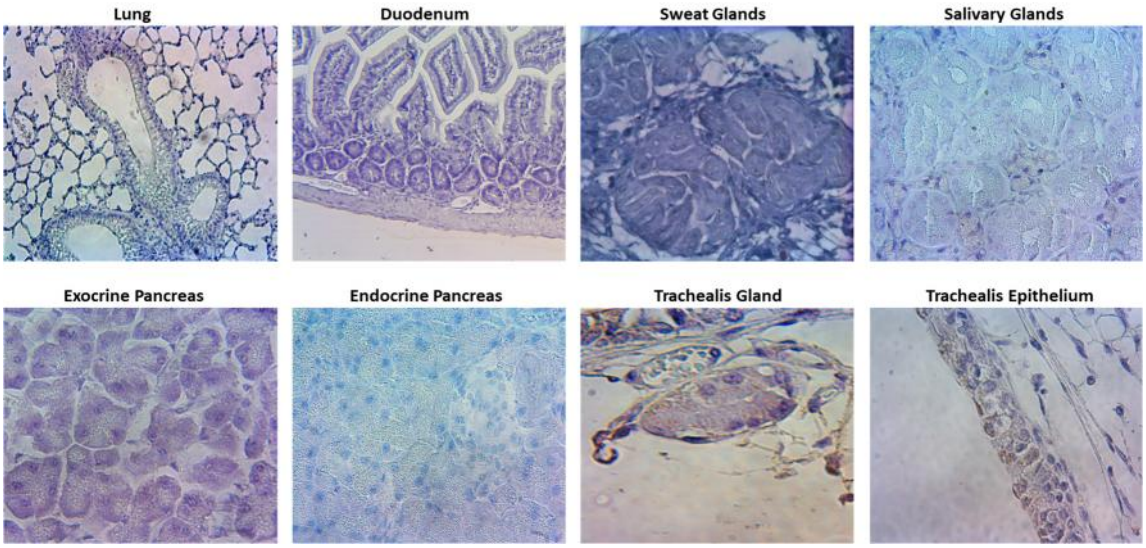

Figure 2.1: Negative controls of exocrine tissues.

Lung, duodenum, sweat glands, salivary glands, exocrine and endocrine pancreas, trachealis glands and epithelium, where the primary VIP antibody was omitted.

Next, slides were counterstained with hematoxylin and then dehydrated in 20 dips of 70% ethanol, 20 dips (three times) in 95% ethanol, 20 dips (two times) in 100% ethanol, in xylene 20 dips (three times) and finally incubated in xylene for 5 minutes. After dehydration, slides were mounted with a mounting medium (Cytoseal 60; Cat. No. 23-244257; Fisher Scientific), stored at RT for a few hours (under hood area) and visualized under light microscopy (Zeiss Aneaxioplan II microscope) with a 10X, 25X, 40X or 63X objective. Images were taken with a Zeiss Axiocam HRC Colour Camera.

2.7 Microscopy Imaging – Semi-quantification and Arbitrary Scale

Images were taken with a Zeiss Axiocam HRC Colour Camera mounted on an Axioplan II microscope. Scoring of images was used for semi-quantification of the IHC signal by two blinded investigators using an arbitrary scale (0 = none, 0.5 = minimal, 1 = low, 1.5 = some, 2 = moderate, 2.5 = strong and 3 = highest). Colour balance, contrast and brightness of whole images were adjusted for consistency within tissue sections. Experiments were repeated at least twice for each tissue sample and three to five mice in each age group were used. An average of 8 to 15 images from each mouse were used for the semi-quantification.

2.8 PGP 9.5 Immunohistochemistry of the Pancreas

For quantifying IHC PGP 9.5 signal intensity in both endocrine and exocrine islets, approximately 5-10 images containing 1 or 2 islets per image, for every mouse and in each age group (8- and 17-week-old), were used to measure the raw integrated PGP 9.5

signal intensity using Image J software. Raw integrated density is the sum of all the pixel intensities values within a selected region, providing a total signal value. Images were converted to 8-bit. Scale was set up in μm^2 and each islet area or PGP 9.5 innervated area of the exocrine pancreas was defined using ROI Manager option. Next, the selected area was thresholded in the blue channel and the raw integrated density of the PGP 9.5 signal was measured.

2.9 Immunofluorescence (IF) of the Pancreas

Glucagon in the pancreas was revealed with immunofluorescence experiments. Paraffin sections (5µm thick) of pancreatic tissues were deparaffinised as described above in 2.3. After the antigen retrieval step, slides were rinsed three times in tris-buffered saline (TBS), next incubated in TBS for 5 minutes and afterwards in blocking solution (1:20 dilution of normal goat serum in TBS with 5% milk powder) for 20 minutes at RT. The tissues were then covered with the Glucagon primary antibody (1:50) and stored overnight at 4^{o}C in humidity chamber. For the negative control, the primary antibody was omitted, and slides was incubated overnight at 4^{o}C in TBS. The next day, tissue slides were washed with TBS three times for 5 minutes to remove the primary antibody and then incubated with Alexa Fluor 594 secondary antibody overnight at 4^{o}C (1:200). Before tissue mounting with Vectashield Mounting Media for Fluorescence, slides were washed three times for 5 minutes with TBS in a dark room. Eventually, the slides were stored at -20^{o}C until viewed with a Zeiss LSM 710 confocal microscope. Glucagon signal, observed around the islets of Langerhans, were visualized with 10X and 20X objectives and no oil

immersion. Confocal microscopy settings were adjusted on the WT pancreas sections and were kept consistent for the CF tissues as well: detection pinhole (1 AU), gain settings (700-800), digital offset (17-19) and digital gain (1.00) and laser 561.

2.9.1 Quantification of Fluorescence Intensity of Glucagon Signal

For quantifying glucagon signal intensity in the islets, approximately 5-10 images containing 1 or 3 islets per image, for every mouse and in each age group (8- and 17-week-old), were used to measure the raw integrated glucagon signal intensity using Image J software. Scale was set up in μm^2 and each islet area was defined using ROI Manager option. Next the α-cell area was thresholded in the red channel and the raw integrated density of the glucagon signal of the selected islet area was measured.

2.10 Whole Mount Immunofluorescence

Sections of 0.5 cm of the duodenum tissue from 8-week-old C57Bl/6 males wild-type or F508del homozygotes (n=5) CF mice were immunostained for VIP, PGP9.5 (ubiquitin hydrolase) or ChAT (Choline Acetyltransferase).

Tissues used in whole mount experiments were immediately dissected at necropsy, and stretched thinly, carefully attached flat with micro pins, on a silicone plate under the microscope, and fixed in 4% paraformaldehyde (PFA) buffer overnight at 4°C. For long-term storage, tissues were stored in 2% PTA (0.1 M Phosphate-Triton Azide Buffer) at 4°C. Before use in IF experiments, tissues were washed twice with PBS for 15 minutes each, followed by 0.05% collagenase treatment for 2h. To find the optimal collagenase

treatment conditions that would enable the antibody penetration in all tissue layers, we tested different collagenase treatment times (30min, 60min, 90min and 120min). Our experimental incubation trials showed that the 2h collagenase treatment enabled the best penetration of the antibodies.

Next, tissues were washed 5 times with PBS for 15 minutes each and incubated overnight with 1% normal donkey serum in 2% TritonX-100. Afterwards, tissues were incubated with a primary antibody: VIP (Immunostar 20077; 1:100 dilution), PGP9.5 (1:100 dilution) or ChAT (1:50 dilution) for 10 days at 4^{o}C. After the ten days' incubation, tissues were washed five times in PBS for 15 minutes each. For the negative control, the primary antibody was omitted, and slides were incubated in blocking serum for ten days. After this washing step, tissues were incubated with a Donkey anti-Goat Alexa Fluor 555 (1:500 dilution) secondary antibody for 5 days at 4^{o}C. The secondary antibody was removed with a five-time washing step with PBS for 15 minutes each, in a light protected area. Tissues were incubated overnight, at 4^{o}C, in a Clear Unobstructed Brain/Body Imaging Cocktail (CUBIC). Cubic is a hydrophilic tissue-clearing medium that allows a clearer and deeper visualization of the tissue layers during imaging with confocal microscopy.

2.10.1 Confocal Microscopy Imaging

Innervation was observed for qualitative assessment using 3D confocal microscopy (Zeiss LSM 510 Meta Confocal Microscope; HeNe 543 nm laser) at the CMDI facility, Faculty of Medicine, Dalhousie University. Slides were visualized under 10X magnification (no oil immersion) and 25X magnification (under oil immersion), and excited with 543nm laser.

Approximately 30 slices of Z-Stack (0.96 interval and 0.96µm optimal) for the mucosa and myenteric plexuses were recorded using an upright laser confocal setting, screening the tissue from the very upper layer to the deeper layer, and eventually providing a final image with a greater depth of field than one single image. The detection pinhole (1 AU), gain settings (600-800), digital offset (0.05-0.08) and digital gain (1.00) were determined at the beginning of each experiment with a WT tissue section, and were kept consistent during the imaging for both WT and CF. Different magnification views were used to visualize distinct areas of both mucosa and myenteric layers. For every WT and CF mouse tissue section, multiple Z-Stacks and regular images were taken to precisely evaluate the innervation. For the 3D reconstruction movie, we used Imaris 3D reconstruction software and Image J software. All the images used for the creation of this 3D video had the same numerical aperture, pinhole and amplifier voltage.

2.11 Bradford Protein Assay

To measure total proteins in our tissues we used the Bradford protein assay. Firstly, we prepared the standard curve and made dilutions, in duplicates, of 0, 2, 5, 10, and 15µg of BSA in ddH_2O and adding 10ul of diluted RIPA buffer (Table 2.2). 10µl of lysate was mixed with 40µl of ddH_2O and vortexed. Afterwards, 10µl from the first diluted sample was mixed with 490µl ddH_2O. Samples were prepared in duplicates. Next, to both tissue samples and standard curve samples was added 500µl of Quick Start Bradford Dye Reagent, and immediately vortexed. All samples were incubated for 15 minutes at RT before reading the optical density (OD). Optical density was then measured with a

spectrophotometer at 595nm.

Table 2.2: Standard Curve Dilutions

Standard concentrations (ug)	ddH2O	Diluted Ripa	BSA 2ug/ul	Complete with ddH2O
0	490ul	10ul	0ul	0ul
2	480ul	10ul	1ul	9ul
5	480ul	10ul	2.5ul	7.5ul
10	480ul	10ul	5ul	5ul
15	480ul	10ul	7.5ul	2.5ul

2.12 ELISAs

2.12.1 ELISA for VIP

Flash frozen tissues from C57Bl/6 8-week-old males, wild-type and F508del homozygotes CF mice were homogenized in RIPA buffer containing proteases inhibitors and lysates were used in mouse ELISA kit with high sensitivity and high specificity (Cloud-Clone Corporation, competitive inhibition for VIP). For quantifying VIP, we followed the manufacture protocol as described below:

Reagent Preparation:

1. All the reagents were brought at RT before use
2. Stock standard was reconstituted with 1ml of the standard diluent and its final concentration was 500pg/ml. From the stock standard we made 5 consecutive dilutions: 166.67pg/mL, 55.56pg/mL, 18.52pg/mL, 6.17pg/mL, and 0 pg/ml (the blank with only standard diluent).

3. The 5 standard dilutions were prepared in duplicates while for the duodenum and pancreas samples we tested multiple dilutions to find the most suitable dilution. The pancreatic tissue was not diluted, while the duodenum tissue was diluted 10-fold with PBS (5µl of duodenum sample diluted in 45µl of 1X PBS).
4. Detection Reagent A and B was diluted 100-fold with the Assay Diluent A and B respectively.
5. Wash solution was diluted 30-fold using dH_2O.
6. TMB (3,3',5,5'-Tetramethylbenzidine) was protected from light.
7. The needed amount of the reagents was used based on the numbers of samples we had every time.
8. To prevent protein degradation fresh samples stored in -80^oC were used as fast as possible, and maintained on ice before the dilution and kit use.

After every washing step with the Wash buffer, the plate was gently tapped to remove the remaining liquid, without letting it dry.

Assay Procedure:

1. Standard (S1-S5) samples were prepared in duplicates, consequently 10 wells, one well was for blank and the rest for the samples. In each well was a total of 100µl. So, into S1-S5 wells we added 50µl of standard and 50µl of Reagent A, into the blank well we added 100µl of only standard diluent, and into the sample wells we added 50µl of duodenum (10-fold diluted in PBS as mentioned above) or pure pancreatic sample (50µl) and 50µl of Reagent A.
2. The plate was sealed with a plate sealer and incubated at 37^oC for 1h.

3. After the 1h incubation, the solution was aspirated and the plate was washed with 350µl Wash solution for 4 times with 1-2 minutes' incubation for every washing step.
4. Afterwards, to all the wells, we added 100µl Detection Reagent B, covered with plate sealer and incubated for 30 minutes at 37^{o}C.
5. After this 30-minute incubation, the wash process was repeated 5 more times as described above.
6. Next, to all the wells, we added 90µl of Substrate Solution, sealed and incubated for 10-20 minutes at 37^{o}C in a dark room. The plate solution turned blue by adding the Substrate.
7. Lastly, after the last incubation we added 50µl of Stop Solution to each well and the mixture turned yellow.
8. The plate was immediately read at a spectrophotometer plate reader, at 450nm, and absorbance was measured.
9. For calculating our results, we plotted the log of VIP concentration on the y-axis and absorbance on the x-axis (Figure 2.2). A logarithmic equation was used to calculate the log of VIP concentration of every mouse tissue sample and from that was calculated the sample concentration. This concentration was next adjusted and normalized to total protein content by dividing it to the latter. For the duodenum tissue this equation was multiplied with the dilution factor (times ten), and next divided by the total protein content. The pancreatic tissue was not diluted, so the concentration was just normalized to total protein as for the duodenum tissue.

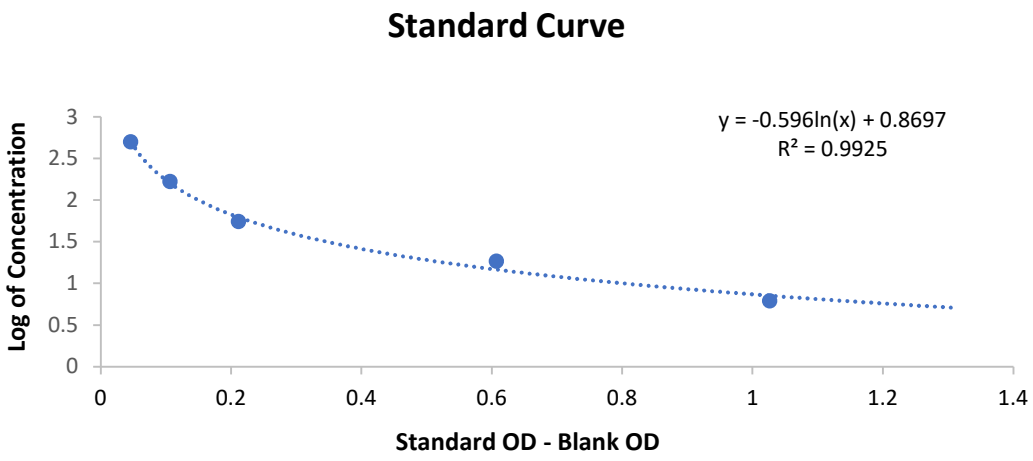

Figure 2.2: Typical Standard Curve for measuring VIP concentration in duodenum or pancreatic homogenized tissue samples.

An example of a logarithmic equation (y=-0.596ln(x) + 0.8697, R^2=0.9925) we got after plotting the standard OD minus the blank OD of standards 0ug to 15ug as described in section 2.11. This equation was used to calculate the log of VIP concentration of every mouse tissue sample and from the log of VIP concentration we calculated the VIP sample concentration.

2.12.2 ELISA for Insulin

For quantifying insulin concentration in the pancreatic tissue, a rat/mouse ELISA kit from Millipore was used. This assay was a Sandwich ELISA. The coated on the plate insulin is captured by a specific capture antibody, and to this detecting captured insulin binds (to an additional epitope) a biotinylated polyclonal antibody. Substrate 3,3',5,5'-tetramethylbenzidine is added and the produced signal, measured by a spectrophotometer, is proportional to the amount of insulin presents in the pancreatic tissue sample. Sandwich ELISA has the highest specificity and sensitivity. For measuring insulin, we followed the manufacture protocol as described below:

Reagent Preparation:

1. All reagents were brought at RT before use.
2. The Wash buffer was diluted 10-fold with deionized water.
3. Plate was washed 3 times with the diluted Wash buffer before use.
4. Standard dilutions were ready to use. There were 6 standards, 0.2ng/ml, 0.5ng/ml, 1ng/ml, 2ng/ml, 5ng/ml and 10ng/ml.
5. The pancreas WT samples were diluted 1:80, in 1X PBS, and the CF samples 1:40.
6. After every washing step with the Wash buffer, the plate was gently tapped to remove the remaining liquid, without letting it dry.
7. Assay Procedure:
8. All wells had in total 100µl of mixture. Into the blank well, was added 20µl of the assay buffer and 80µl of Detection Ab. Into the standard wells we added 10µl of each standard in each well respectively, and then 10µl of assay buffer and 80µl of Detection Ab. Into the sample wells we added 10µl of the already diluted sample, 10µl assay buffer and 80µl of Detection Ab. The plate was sealed with plate sealer and incubated at RT for 2h.
9. After this incubation time, the plate was washed 3 times with 300µl of diluted Wash buffer into each well.
10. Next, after the washing step, was added 100µl of Enzyme Solution. The plate was sealed and incubated at RT for 30 minutes.
11. After this second incubation, wells were washed 6 times with 300µl of the Wash buffer into each well.

12. Afterwards, to each well was added 100µl of Substrate Solution. The plate was protected from light, sealed and incubated for 15 minutes at RT in a plate shaker. Blue color was observed in each one of the wells and the blue intensity was proportional to the standard samples (starting from the lower to the higher concentration) and to insulin concentration.
13. Finally, we added 100µl of the Stop Solution and the blue color turned yellow.
14. The optical density was read with a spectrophotometer plate reader at 450nm and 590nm. The optical density measured at 590nm was a background, non-specific signal and it was subtracted from the optical density at 450nm which was the actual increased insulin concentration.
15. To quantify insulin, we plotted the concentration on the y-axis and the optical density (450nm-590nm) on the x-axis. A linear equation (Figure 2.3) was used to calculate insulin concentration. The found concentration was multiplied by the dilution factor which mas different between the WT and the CF, as mentioned above. Next, this concentration was adjusted to total protein content, dividing it by the latter.

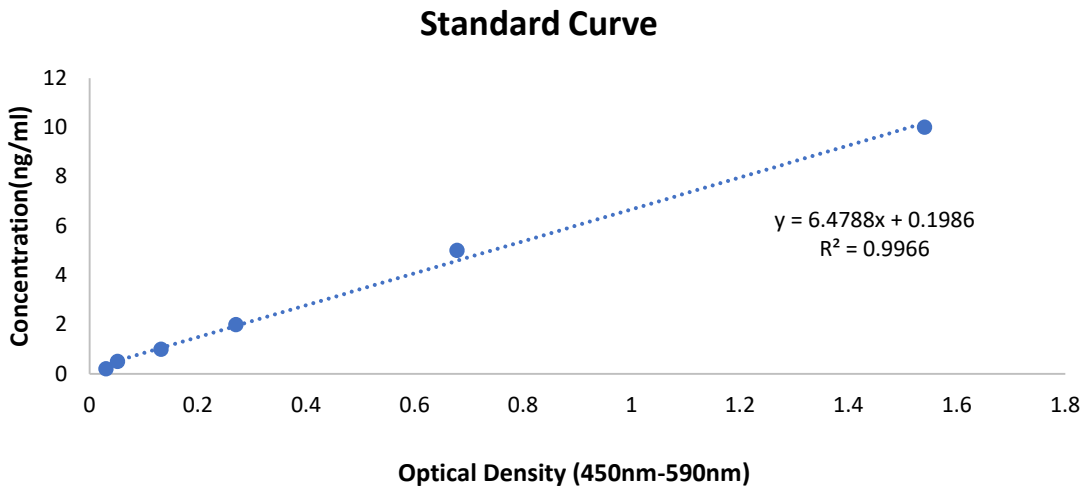

Figure 2.3: Typical Standard Curve for measuring Insulin concentration in pancreatic homogenates.

An example of a linear regression (y=6.4788x+0.1986, R^2=0.9966) obtained by plotting standards ODs (as described in section 2.11) as a function of the concentration from standard samples. The linear equation we got was used to calculate the insulin concentration.

2.12.3 ELISA for MIP-2

To measure the levels of Cxcl2 cytokine (manufacture name is MIP-2 in mice; IL-8 in humans) in murine lung, we purchased the MIP-2 ELISA Kit Picokine from MyBiosource (Cat. No. MBS175915). This ELISA is a Sandwich ELISA (described in Methods section 2.12.2) and has a high sensitivity. We followed the manufacture protocol as described below:

Reagent Preparation:

1. All reagents were brought at RT before the use.
2. The Wash buffer powder was diluted in 1000ml of ddH_2O to prepare a 1X concentration.

3. The Biotinylated antibody was prepared immediately prior to use and diluted 1:100 in the Antibody Diluent.
4. The Avidin-Biotin-Peroxidase Complex was prepared immediately prior to use and diluted 1:100 in Avidin-Biotin-Peroxidase Diluent.
5. The Stock Standard was reconstituted in 1ml of Sample diluent.
6. For the Standard Curve we prepared 8 standards (S1-S8) of concentrations: 1000pg/ml, 500pg/ml, 250pg/ml, 125pg/ml, 62.5pg/ml, 31.25pg/ml, 15.625pg/ml and 0pg/ml (blank). Standard were prepared in duplicates.
7. The lung samples were diluted 1:1 (50µl of sample diluted in 50µl of Sample Diluent).

Assay Procedure:

1. In each well there was a total of 100µl of standard sample, sample and the blank, where we only added 100µl of sample diluent buffer.
2. Plate was covered with plate sealer and incubated for 2h at RT.
3. Next the liquid was discarded, and without letting the plate dry, 100µl of prepared Biotinylated Antibody was added. Plate was sealed and incubated at RT for 90 minutes.
4. Next, we washed the plate 3 times with 300µl Wash buffer added on each well. In every washing step, the plate was incubated for about 1 minute in the Washing buffer. The liquid was gently discarded.
5. Afterwards, we added 100µl of prepared Avidin-Biotin-Peroxidase Complex into each well. Plated was sealed and incubated for 40 minutes at RT.
6. Next, the plate was washed again 5 times, with 1-minute incubation in the between,

with 300µl Wash buffer. The liquid was gently discarded.

7. Finally, we added 90µl of Color Developing Reagent. Plate was sealed and incubated in a dark area for 30 minutes at RT. The color started turning blue.
8. After this incubation, a 100µl of Stop Solution was added and the color turned yellow. The yellow intensity was proportional to MIP-2 concentration measured in the sample.
9. Optical Density absorbance was read with a spectrophotometer at 450nm. To calculate our results, we plotted on y-axis the OD and the x-axis the concentration (pg/ml), using an equation to calculate the MIP-concentration (Figure 2.4).

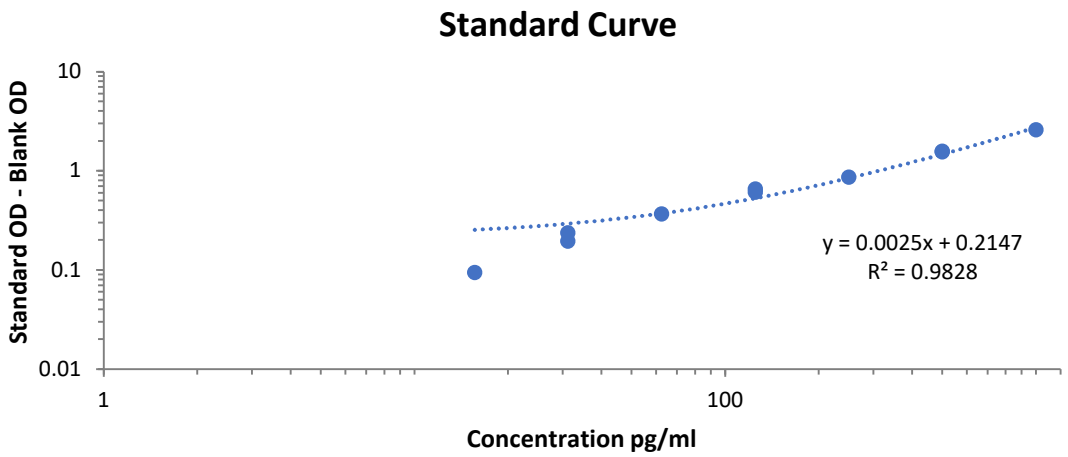

Figure 2.4: **An example of Standard Curve for measuring MIP-2 concentration on lung homogenates samples.**

A usual equation (y=0.0025x + 0.2147, R^2=0.9828) by plotting standards ODs minus the blank ODs (as described in section 2.11) as a function of the concentration from standard samples. The equation we got was solved for x calculator to calculate MIP-2 concentration.

2.13 Random Glucose Measurements

Plasma from 8- and 17-weeks old mice was used to estimate random glucose level using the Cayman's Glucose Colorimetric assay kit. All the mice were under the same regular diet (Prolab RMH 3500) and plasma was collected in the morning. Plasma was diluted 20-fold with assay buffer before use. The assay protocol was based on the manufacture instructions as described below:

Reagent Preparation:

1. To make the 100mg/dl Stock Glucose Standard we mixed 50µl of the 1,000mg/dl Glucose Standard with 450µl diluted Assay Buffer.
2. To dilute the Assay Buffer, the 10ml of the 250mM Sodium Phosphate Assay Buffer was mixed with 40ml HPLC-grade water.
3. The Glucose Colorimetric Enzyme Mixture was diluted in 6ml of diluted Assay buffer.
4. The prepared standard samples (S1-S7) and the plasma samples were in duplicates

Assay Procedure:

1. Initially, we prepared 7 standards (S1-S7) with glucose concentration: 2.5mg/dl, 5mg/dl, 7.5mg/dl, 10mg/dl, 15mg/dl, 20mg/dl and 25mg/dl. In the blank sample we only added assay buffer.
2. The total amount in every well was 200µl. For preparing the 7 standard wells we added 85µl of diluted Assay Buffer and 15µl of the S1-S7 standard to each well respectively. For the sample wells we added 85µl of the diluted Assay Buffer and 15µl of the diluted sample.
3. Afterwards, 100µl of the Enzyme Mixture was added to all the wells.

4. Plate was sealed with plate sealer and incubated at 37°C for 10 minutes. After the incubation time, the color turned pink and the intensity was proportional to glucose concentration measured in the sample.
5. Absorbance was read with a spectrophotometer at 500nm. To calculate our results, we plotted on the y-axis the standard OD minus the blank sample OD, and on the x-axis the glucose concentration (mg/dl) (Figure 2.5). The used equation was: [(Corrected absorbance) – (y-intecept)/slope] x dilution.

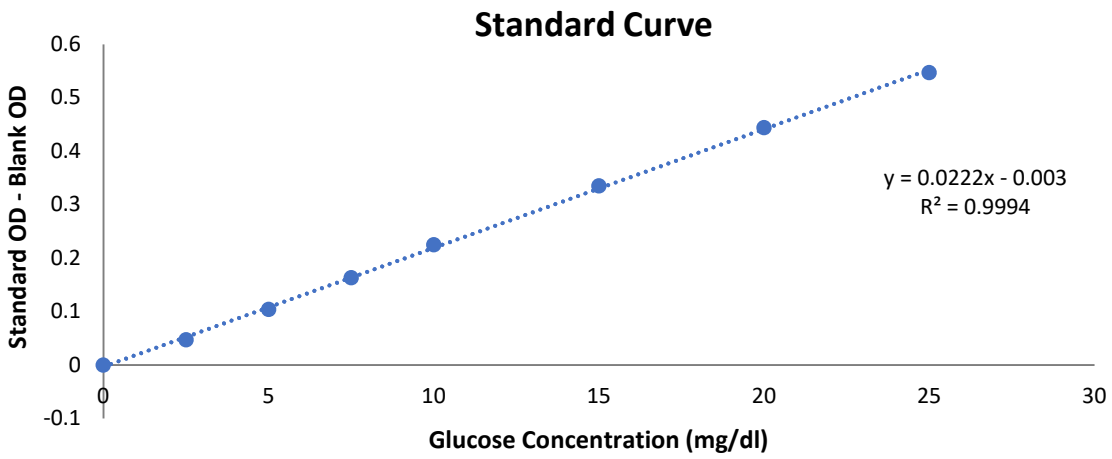

Figure 2.5: An example of Standard Curve for measuring glucose concentration on plasma murine samples.

An example of Standard Curve for measuring glucose concentration on plasma murine samples. A typical linear equation we got by the line of this standard curve: y=0.0222x - 0.003, R^2=0.9994

2.14 Duodenum Tissue Morphology Measurements

Tissue samples were well-oriented to allow for longitudinal cut of crypts and villi to precisely assess alterations in the overall intestinal tissue architecture. Undamaged areas where normal villi were present have been used to measure morphological parameters such as villi height, from base to villus tip, and villi width from the central part of the villus. Beneath each villus, we measured the total crypt area height from the muscle layer to the base of villi; the diameter of adjacent crypts to assess their dilation, and the muscle layer thickness. Before measuring the above-mentioned morphological parameters, a scale was set for every image. NIH Image J software (https://imagej.nih.gov/ij/download.html) was used to perform the measurements of height, villi width, crypt height, crypt dilation and smooth muscle layer thickness (Semaniakou et al., 2020).

For smooth muscle thickness, only the inner circular muscle layer was measured in ten randomly located regions throughout the section. All sections were scored by two observers blinded to the mouse strain. Image J software protocol was used to measure duodenum tissue alterations, and muscle thickness (Semaniakou et al., 2020)

2.15 Goblet Cells Quantification

Alcian blue 8GX solution (1% Alcian blue solution in 3% acetic acid) was used to stain and count the number of goblet cells in the villi and crypts of the duodenum. The tissues were deparaffinised in xylene as described above (see section 2.5). After the deparaffinization step, duodenum tissue slides were incubated in Alcian Blue staining solution for 35

minutes at room temperature, rinsed for 2 minutes under running tap water, followed by hematoxylin staining for 5 minutes. Slides were then dehydrated and mounted as described above (see section 2.5) before imaging under light microscopy. NIH Image J software was used to count the number of the goblet cells per villi and crypt area. For every mouse (n = 5) and in each age group (8- and 17-week-old) we used 10 different images along the whole tissue, each image containing 5 to 6 consecutive and well distended villi. For counting the number of the goblet cells on the crypt area, the crypt area beneath every villus was selected.

2.16 Lung Injury Score

Evaluation of the lung inflammation was based on a recent paper from Bayes *et al.* (2016) (Bayes et al., 2016). Histological lung tissue sections from both 8- and 17-weeks, wild-type and CF mice, were scored for alveolar thickening and peribronchial infiltration using a scoring system described in Figure 2.6. For every mouse we scored blindly approximately 10-15 images from various areas of the entire lung section, using the 10X magnification. Afterwards, to further confirm our results and avoid a biased scoring that would depend on every separate section, we did an overall scoring estimation of the whole tissue section using the 4X magnification. Our results were double validated by two independent blinded investigators (Semaniakou et al., 2020).

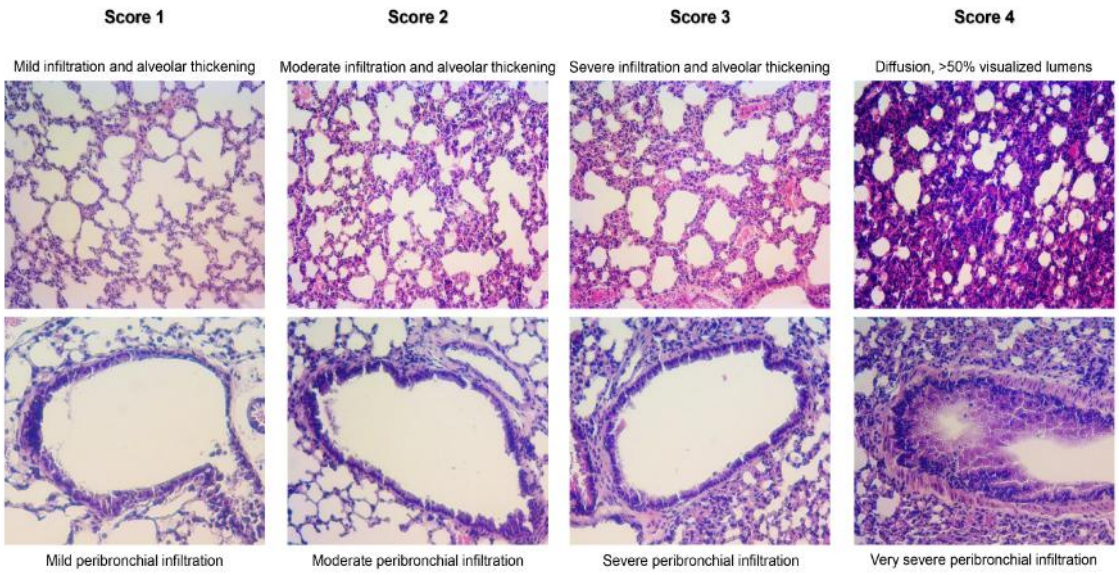

Figure 2.6: Histological scoring system for the evaluation of lung inflammation.

Presence of mild infiltration and alveolar thickening as well and mild peribronchial infiltration was score 1, moderate infiltration and alveolar thickening plus moderate peribronchial infiltration is used as score 2, severe infiltration and alveolar thickening plus severe peribronchial infiltration is characterized as score 3 and, lastly, diffusion in combination with very severe peribronchial infiltration is characterized as score 4 (Semaniakou et. al., 2020).

2.17 Statistics

Results are reported as means ± SE. Statistical differences between groups were calculated by the non-parametric ANOVA (Meyerholz et al., 2018). $p < 0.05$ was considered statistically significant. N represents the number of independent experiments.

CHAPTER 3: RESULTS SUMMARY

3.1 Changes in VIP Content in Exocrine CF Murine Tissues

VIP is distributed in the central and peripheral nervous systems richly innervating all exocrine glands. In CF patients it was shown that VIP-positive nerve fibers of the skin and intestinal mucosa are sparse compared to healthy individuals. Since VIP plays a critical role in the local innate defense by stimulating the movement of water and chloride across intestinal and tracheobronchial epithelium it was hypothesized, that abnormal VIP innervation may contribute to the CF disease pathogenesis. Nonetheless, the mechanism behind this phenomenon remained unknown. Consequently, the main general question of this PhD research was to examine changes in VIP amount in CF and shed light on three unanswered questions in the field regarding the defective VIP innervation: 1) Is sparse VIP innervation correlated to tissue damage due to disease progression or due to defective VIP peptide synthesis?; 2) When does VIP reduction starts and what is the connection with the tissue damage?; 3) What is the impact of VIP reduction on the development of CF disease in the intestine, lung and pancreas?.

As for the murine model, as a selected model for studying VIP changes in CF, instead of others such as rats or ferrets, we published a detailed review (Semaniakou et al., 2019) describing in depth the mouse model and its advantages for studying CF disease. Since the discovery of the CFTR gene, more than 14 mice models have been genotyped and extensively used until nowadays (Semaniakou et al., 2019). CF murine models recapitulate some aspects of the human pathophysiology of CF lung, demonstrating airway inflammation/infiltration, tissue damage, mucus obstruction, while in the

intestine they present goblet cell hyperplasia, meconium obstruction and tissue remodeling. Also, electrophysiological studies have confirmed the ion transport abnormalities in CF mice with a similar phenotype to that of the human CF intestine: low or absence of cAMP-mediated Cl^- transport. The murine nasal mucosa exhibits two important characteristics of human CF airways: Na^+ hyper-absorption and a defect in cAMP-mediated Cl^- secretion. Consequently, it offers an excellent model for investigating the abnormal electrophysiological profile of CF epithelial cells and testing potential corrector drugs. Moreover, tracheal SMGs are widely used to examine MCC abnormalities and airway inflammation in CF disease. Lastly, in contrast to patients with CF for whom PI is a major condition, CF mice exhibit only moderate pancreatic changes mainly due to the Ca^{2+}-activated chloride channel (CACC) expression (Semaniakou et al., 2019).

More specifically, for the first question (Is the sparse VIP content correlated to tissue damage due to disease progression or to defective VIP peptide synthesis?) using IHC and ELISA, we examined changes in the VIP content in the duodenum, lungs, sweat glands, endocrine and exocrine pancreas, salivary glands and trachea in 8-week, 12-week and 17-week-old C57Bl/6 CF mice, homozygous for the F508del mutation, compared to same age wild-type littermates. Results are presented in Figures 4.3, 4.4, 4.5 and 5.1, and were published in the *Journal of Cystic Fibrosis* (See Chapter 4 of this thesis).

Our data showed a strong reduction of VIP in the duodenum of CF mice. Immunohistochemistry (IHC) signal for VIP was revealed in wild-type mice around the epithelium of villi, into the lamina propria area, around the crypt and in muscle layers of

duodenum longitudinal tissue sections following immunostaining for VIP with a specific polyclonal antibody. VIP signal intensity in CF and wild-type tissues from 8- and 17-week-old mice was semi-quantified from scanned microscopy images using an arbitrary scale from 0 to 3 (see Methods). Results reveal that the signal for VIP was reduced by 49.01% ±0.11 ($p < 0.001$) in 8-week-old CF mice and by 32.48% ±0.01 ($p < 0.001$) in 17-week-old CF mice in comparison to the same age WT animals. Reduction in the amount of VIP present in the duodenum was further confirmed by ELISA. VIP content was 0.63 ±0.05 pg/µl in wild-type and 0.19 ±0.045 pg/µl in CF tissue lysates ($p < 0.001$), confirming a strong reduction of VIP in CF compared to wild-type tissues.

Furthermore, VIP amount was decreased in the lung and sweat glands of CF mice. VIP-containing nerve fibres have been described in tracheobronchial smooth muscle, around submucosal glands and in the walls of pulmonary and bronchial vessels (Barnes et al., 1991). In the lung, we examined the presence of VIP around the epithelium of the bronchioles in both 8- and 17-week-old WT and CF mice. IHC signal for VIP was reduced by 52.63% ±0.26 ($p < 0.001$) in the 8-week-old CF mice. The difference in VIP signal observed in the older mice, was not statistically significant. Moreover, we conducted experiments on salivary glands and trachea. In the salivary glands VIP expression, as detected by IHC, was reduced in both 8-weeks (57.25%) and 17-weeks CF mice (54.8%, $p < 0.05$) compared to wild-type (Figure 3.1).

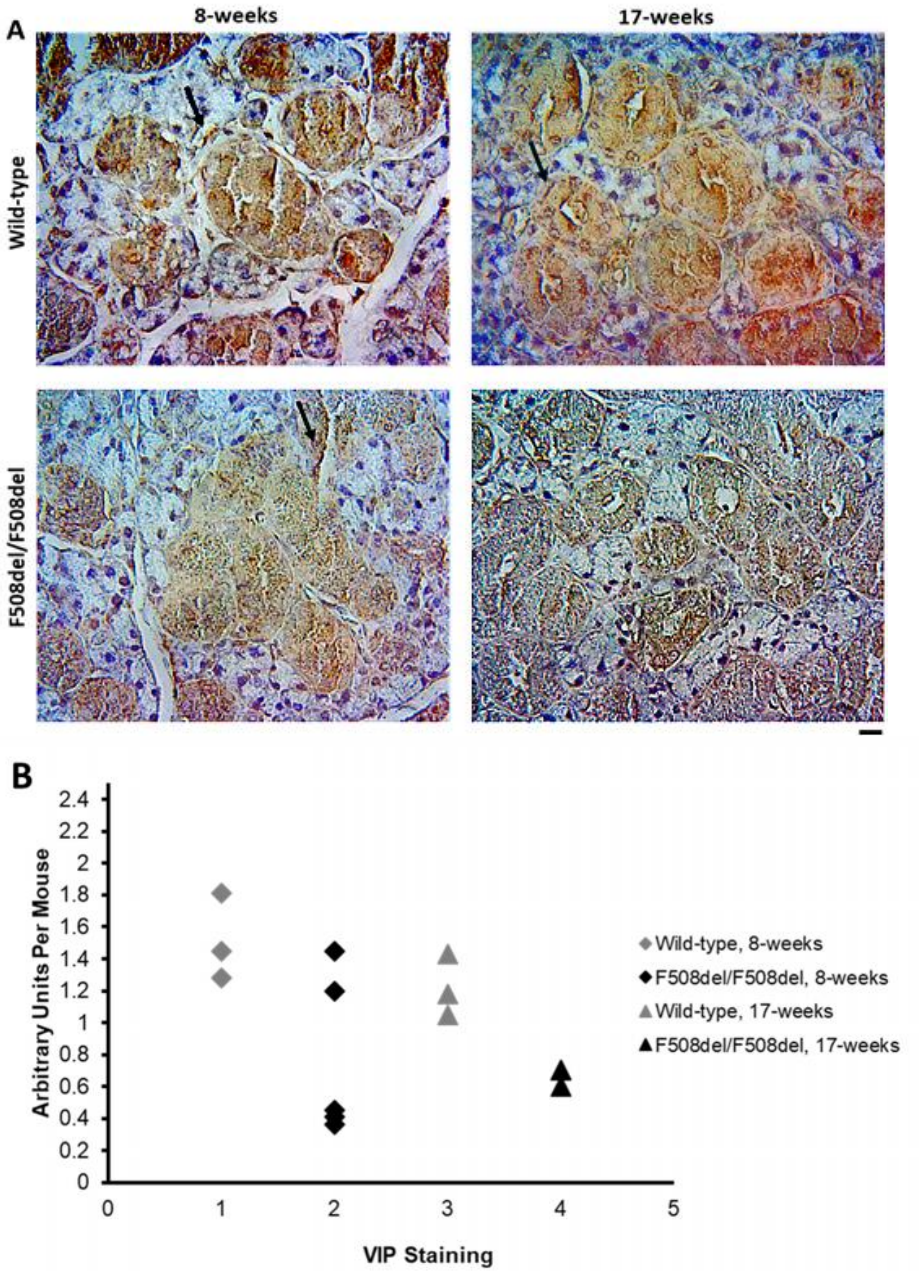

Figure 3.1: VIP signal in the salivary glands.

A, Representative images (40X objective) of salivary glands showing VIP signal (brown, black arrows) around the salivary gland and gland area revealed by IHC, in wild-type (top panels) and CF (F508del/F508del) mice (bottom panels) at 8- and 17-week-old as indicated. ***B,*** Semi-quantification of VIP signal for each mouse. Each dot represents the average score of 8 to 15 images from each mouse (N = 3). Arbitrary scale from 0 to 3 indicates: 0 = none, 0.5 = minimal, 1 = low, 1.5 = some, 2 = moderate, 2.5 = strong and 3 = highest. Scale 50 µm.

In the trachea, VIP was found in the airway epithelium and around the tracheal glands. Surprisingly, our data indicated no statistical differences between the wild-type and CF tissues with a trend toward more VIP in CF tissues (Figure 3.2A & B). These data are not consistent with what we found in all other tissues. Although our data showed no considerable difference in VIP between the wild-type and CF mice (Figure 3.2C), there are no human data on those tissues and further research is needed.

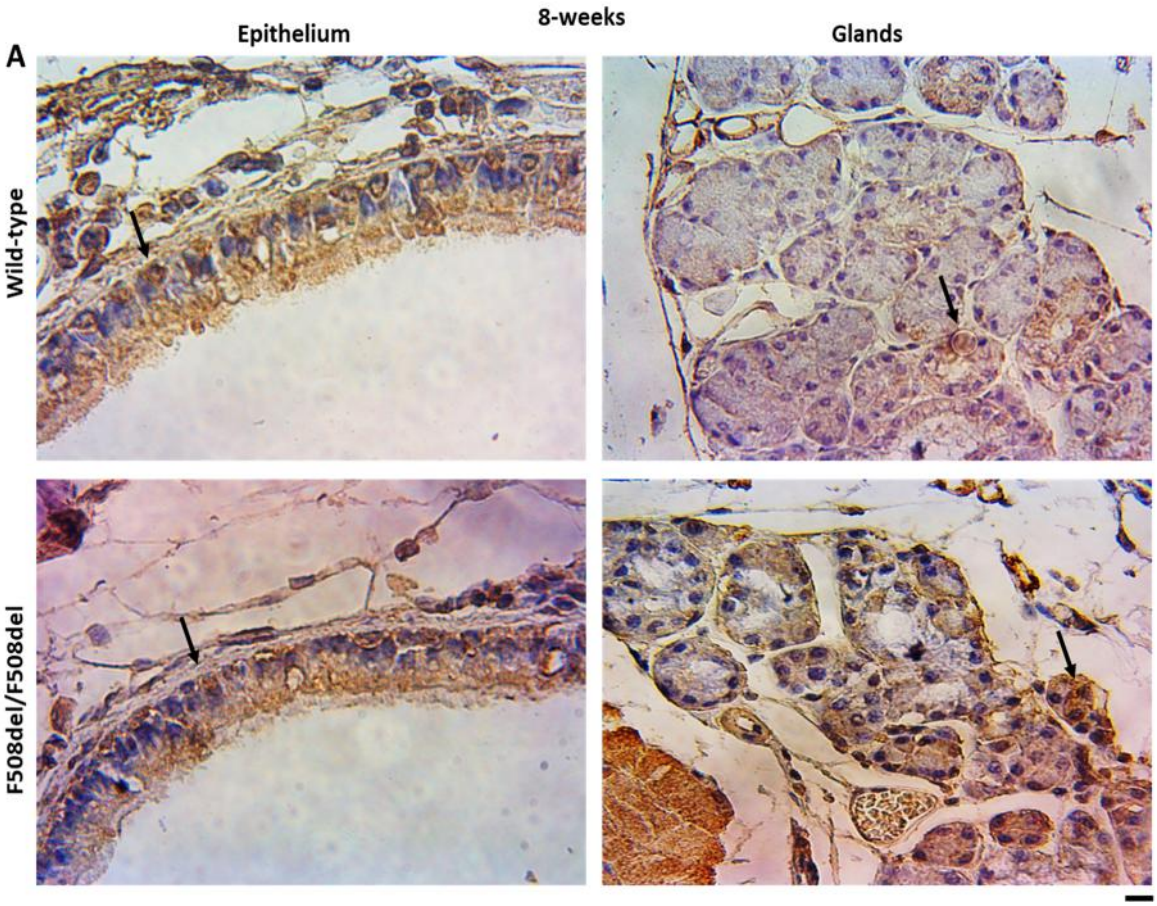

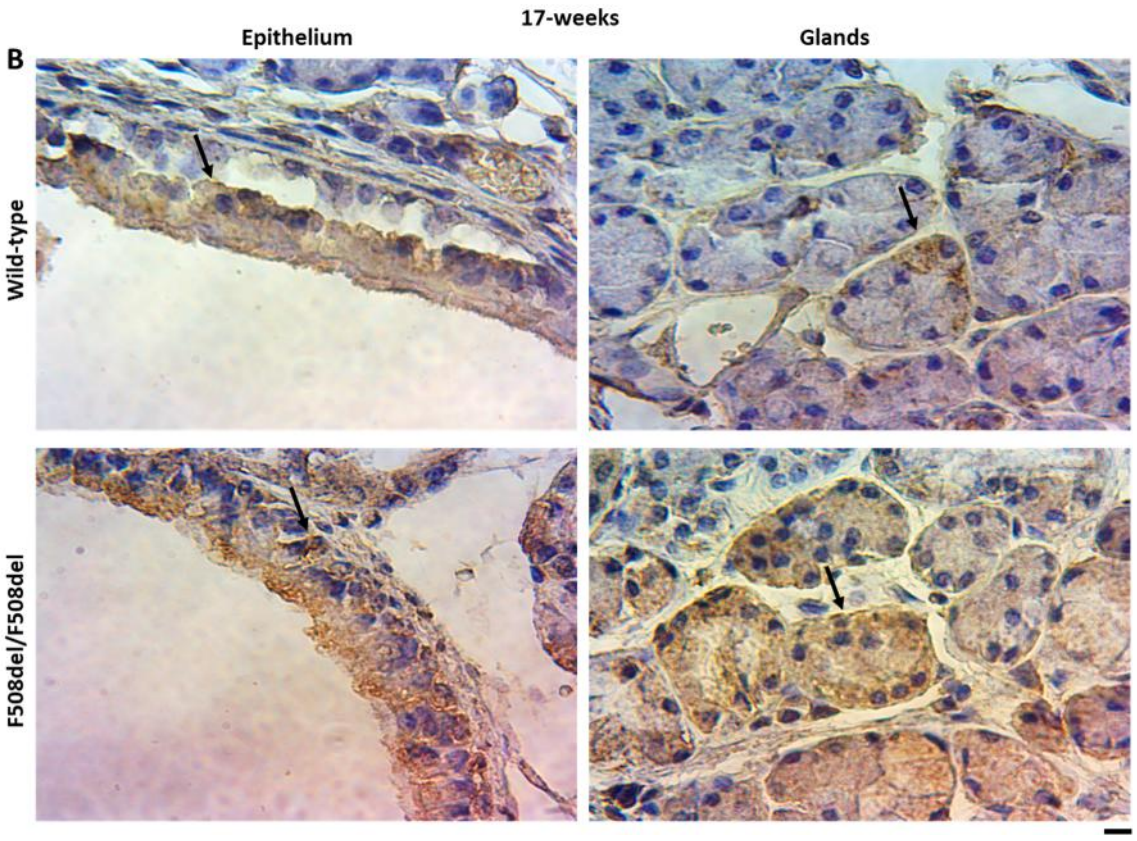
17-weeks
Epithelium
Glands
B
Wild-type
F508del/F508del

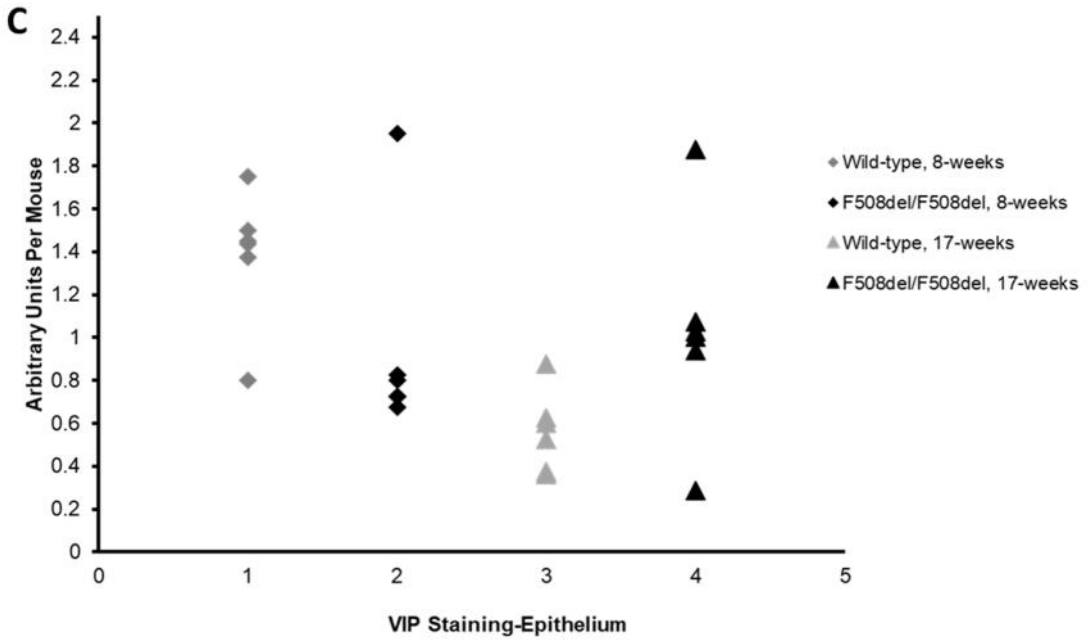
C
Arbitrary Units Per Mouse
VIP Staining-Epithelium
Wild-type, 8-weeks
F508del/F508del, 8-weeks
Wild-type, 17-weeks
F508del/F508del, 17-weeks

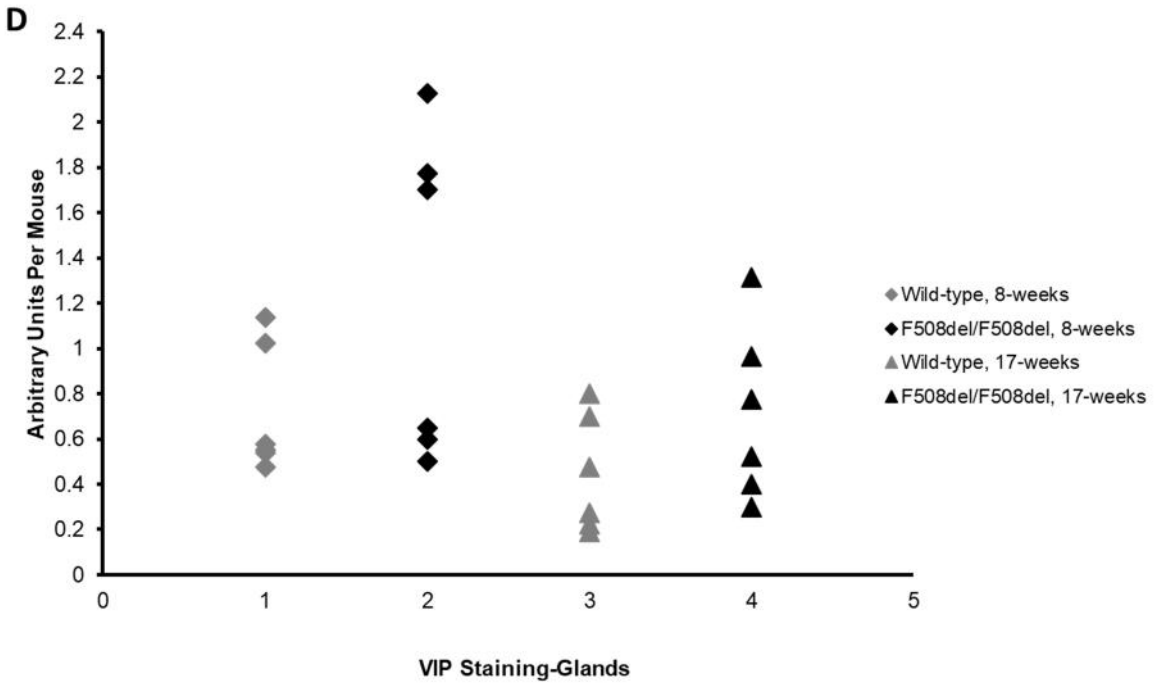

Figure 3.2: VIP signal in the tracheal epithelium and glands.

A & B, Representative images (60X objective) of trachea cross sections showing VIP signal (dark brown, black arrows) around the tracheal epithelium and glands revealed by IHC, in wild-type (top panels) and CF (F508del/F508del) (bottom panels) mice at 8- and 17-week-old. ***C & D,*** Semi-quantification of VIP signal in the epithelium and submucosal glands of the trachea for each mouse. Individual dots represent the average score of 8 to 15 images from each mouse (N = 3). Arbitrary scale from 0 to 3 indicates: 0 = none, 0.5 = minimal, 1 = low, 1.5 = some, 2 = moderate, 2.5 = strong and 3 = highest. Scale 100 µm.

3.2 VIP Reduction and Correlation with Tissue Damage

To determine if changes in VIP content were related to tissue damage from the disease progression, we assessed disease development in the duodenum by examining morphological alterations in the villi height, the villi width, crypt height, crypt dilation, muscle layer thickness and the number of the goblet cells which are responsible for mucus production. In the lungs, we measured the murine IL-8 homologue KC, MIP-2

(macrophage-inflammatory protein 2) levels, and inflammation with an arbitrary scoring system for alveolar thickening and peribronchial infiltration (See Figure 4.1 & 4.2, Chapter 4 of this thesis). In the sweat glands, which are free of inflammation, we assessed gland enlargement and duct opening as an indication of disease modification (Semaniakou et al., 2020) (See Figure 4.5; Chapter 4 of this thesis).

At the beginning of this study, we started investigating the VIP amount in most of the exocrine tissues affected in CF, in the three different age groups mentioned above (8-, 12- and 17-weeks). Each age group represented different disease stages: beginning of the disease (6-8-weeks), moderate disease stage (10-12-weeks) and advanced disease stage (15-17-weeks). However, we decided to limit our study to the duodenum, lungs, sweat glands and pancreas, in 8- and 17-week-old CF mice. The 12-weeks old age group was found to have inconsistent results in all the above-mentioned exocrine tissues, presumably due to maturational hormonal changes as this age is a puberty period peak age of the mouse (Brownstein, 2003; Falconer, 2020; Prevot, 2015). Therefore, we decided to exclude the 12-weeks old group from the study and focused our research on 8- and 17-weeks old groups that reflect the early and late disease stage (Figure 3.3).

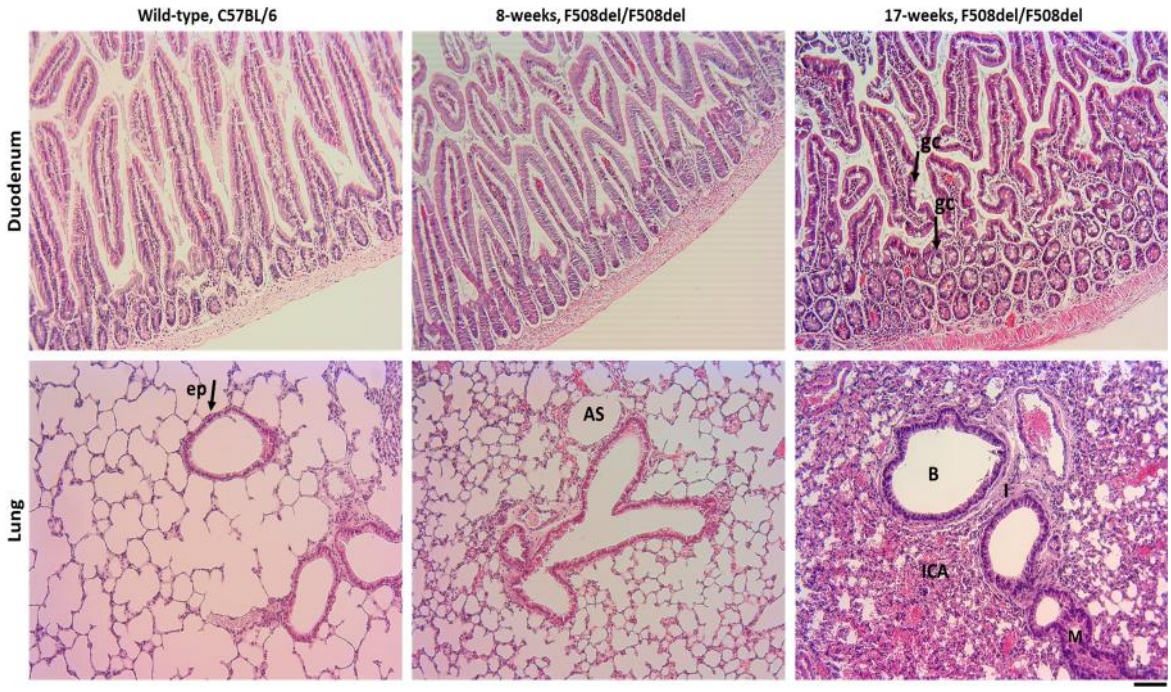

Figure 3.3: Histology images of duodenum and lung tissues from 8- and 17-week-old wild-type C57BL/6 and CF (F508del/F508del) mice.

5 µm thick sections were H&E stained before light microscopy imaging at 10X magnification. Compared to wild-type, duodenum and lung tissues from 8-week-old CF mice showed minimal signs of disease, whereas tissues from 17-week-old CF mice showed goblet cell hyperplasia in both villus and crypt area as well as morphological alterations in the duodenum tissue. In the lung tissue of 17-week-old CF mice disease had also progressed, and characterized by high levels of inflammation, inflammatory cells aggregation (ICA), thickening of alveolar walls, tissue damage and mucus presence. B: bronchiole, AS: alveolar space, ep: epithelium, I: inflammation, M: mucus. Scale: 100µm.

Briefly, we showed that the VIP amount is significantly lessened in the duodenum, lung, sweat glands, endocrine and exocrine pancreas of CF mice, in both ages (8- and 17-weeks) compared to wild-type tissues. Most importantly, this VIP reduction was found to be very high in 8-weeks CF mice. That was an important finding as those young CF mice

presented close to wild-type tissue morphology, with minimal inflammation and no signs of tissue damage. However, in the 17-weeks old group, the disease had progressed significantly, with changes to villi and crypt in the duodenum and high levels of inflammation in the lung. Moreover, the strongest decrease in VIP was found in the sweat glands (almost 70% reduction) of young CF mice that are free of inflammation.

Interestingly, the amount of the VIP present in the duodenum of wild-type mice was higher in younger mice and declined progressively with age (Figure 3.4). In CF tissues however, a consistent low amount of VIP was found independently of the age or pathological signs. Studies have shown age-related peptide concentrations in different parts of the gastrointestinal track (El-Salhy et al., 1999) but the reason for these age-related peptide changes to our knowledge remains unknown.

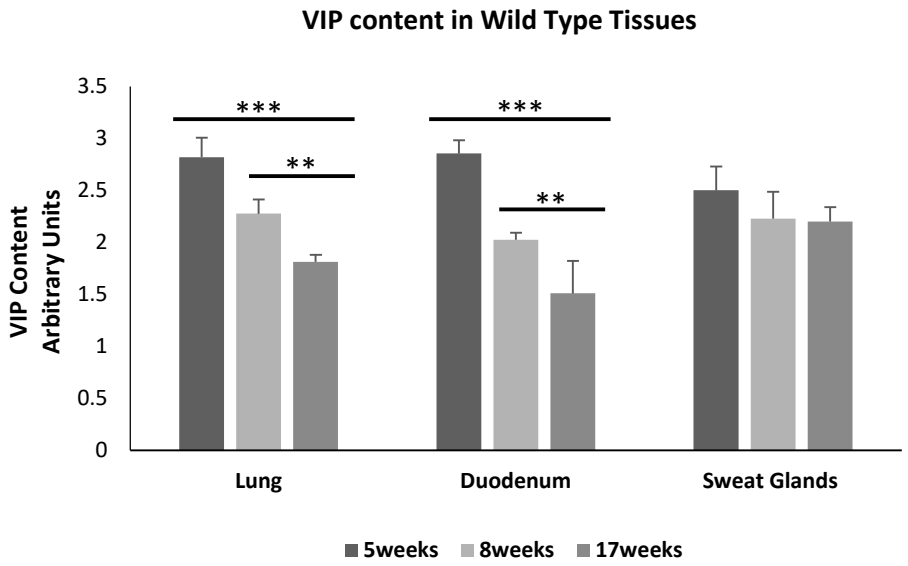

Figure 3.4: Semi-quantification of VIP signal in 5- to 17-week-old wild-type lung, duodenum and sweat glands.

Histogram bars represent averages of 8 to 15 images from each mouse (3 to 5 mice per age group). Arbitrary scale from 0 to 3 indicates: 0 = none, 0.5 = minimal, 1 = low, 1.5 = some, 2 = moderate, 2.5 = strong and 3 = highest. **$p < 0.01$, ***$p < 0.001$.

Altogether, these data demonstrated that VIP depletion is a primary defect in CF, starting at a very young age, where the disease has not progressed yet and before tissue damages are observed. Therefore, tissue damage does not account for this VIP reduction (Semaniakou et al., 2020) (See Chapter 4 of this thesis).

3.3 Mechanism of VIP Depletion – Alterations in the Nervous System

We further investigated the mechanism behind this diminished VIP amount, at the neuronal level, by studying VIP-specific innervation, the general parasympathetic innervation and the co-localization of VIP with acetylcholine (Semaniakou et al., 2020), (See Chapter 4 of this thesis). While the synergistic action of VIP and acetylcholine was already known to be lost in CF (Ianowski et al., 2007; Jae et al., 2007), our study was the first to demonstrate in depth neuronal alterations and sparse innervation for both VIP and acetylcholine in CF tissues.

To examine VIP innervation, we conducted whole mount experiments in various tissues: ileum, duodenum, jejunum, rectum, colon, salivary glands, sweat glands, trachea, lungs and pancreas. We were only successful with this technique in the ileum, jejunum, rectum and duodenum tissues. Our data on innervation were mainly obtained from the mucosa and myenteric plexuses of the duodenum, as these two layers express the highest density of nerve fibers. Ileum, jejunum and rectum provided results on innervation in the myenteric plexus layer, as was revealed by the PGP 9.5, ChAT and VIP immunofluorescence signal. However, we were not able to visualize the mucosa layer as in the duodenum tissue (Figure 3.5).

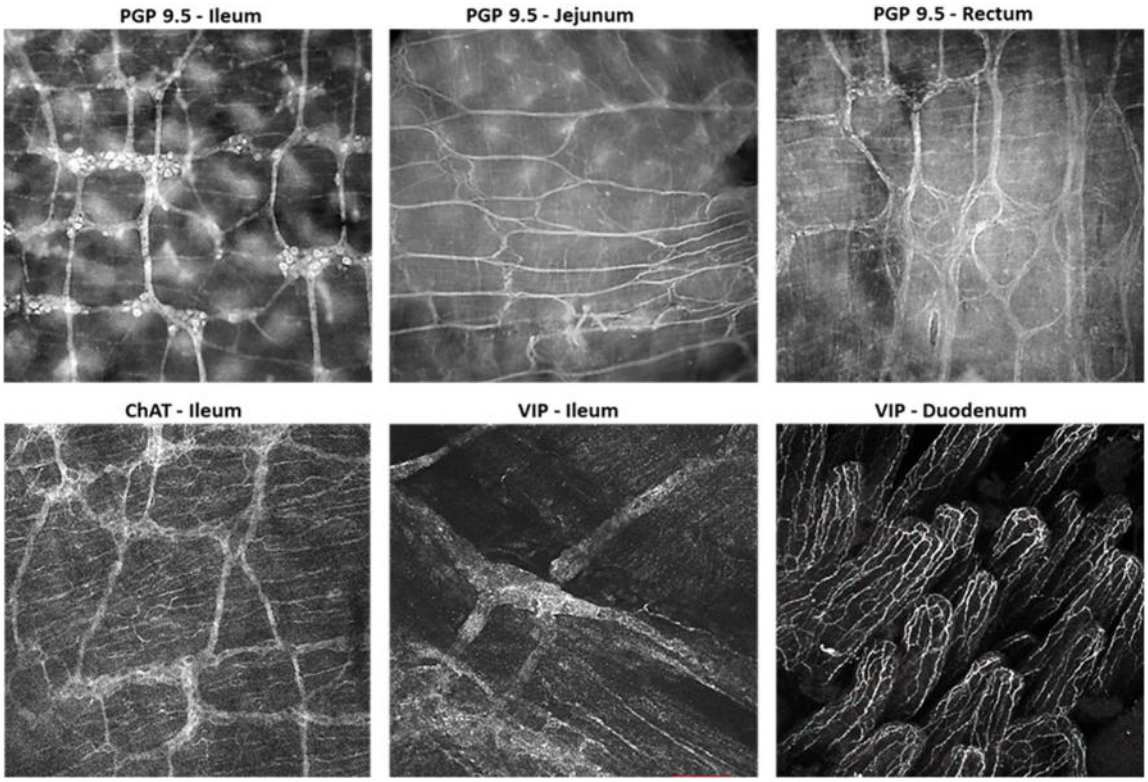

Figure 3.5: Representative whole mount confocal microscopy images showing PGP 9.5, ChAT and VIP innervation.

Myenteric plexus layer innervation of ileum, jejunum and rectum tissues from 8-week-old C57Bl/6 homozygote mouse, while innervation at the mucosa layer was identified only at the duodenum tissue immunostained for VIP. Fresh tissues were prepared for whole mount immunofluorescence as described in the method section and immunostained with a monoclonal anti-PGP 9.5 antibody, a monoclonal anti-ChAT antibody or a monoclonal anti-VIP antibody, all followed by secondary antibody conjugated with Alexa Fluor 555. All images were taken with 20X magnification, except for VIP innervation in the ileum that was taken with 40X.

Duodenum is an excellent tissue to study innervation as it also expresses high levels of CFTR. We selected the young age of mice (8-weeks) that had minimal signs of disease to examine the innervation in an attempt to understand if the VIP deficiency was due to a

neural defect or changes in VIP peptide biosynthesis. Our results indicated a sparse, disorganised, discontinued in some areas, and an overall disrupted VIP innervation in the duodenum of CF mice at the mucosa and circular muscle layer, with fewer fine axons in the villi (Semaniakou et al., 2020). Results are presented in Figure 4.6 (See Chapter 4 of this thesis).

To examine the general innervation, we used the PGP 9.5 antibody as a general neuronal marker. PGP 9.5 signal showed a significant alteration of the myenteric plexus layer, where two out of three components of the myenteric plexus in the CF duodenum tissue were lost, but no significant changes were observed in the mucosal part. Hence, there was a disorganization of the intrinsic neuronal network in the CF mice intestine that could not fully be justified by the sparse VIP innervation but rather involves the intrinsic parasympathetic innervation as a whole (Semaniakou et al., 2020).

The synergistic action of VIP and acetylcholine is lost in CF (Ianowski et al., 2007; Jae et al., 2007), and both VIP and acetylcholine are released from either the same or from distinct neurons (Anlauf et al., 2003). Accordingly, we examined the cholinergic neuronal network with the ChAT antibody. Anti-Choline Acetyltransferase (ChAT) is an enzyme responsible for the synthesis of acetylcholine. Interestingly, ChAT signal was very low in the duodenum of CF mice, especially in the crypt area, while in the lamina propria area of the villi the cholinergic innervation was not as severely disrupted as for the VIPergic nerves. Consequently, cholinergic neurons are affected in CF but not to the same extent as VIPergic neurons suggesting that some specific cholinergic innervation is still intact. Importantly, this part of the study illustrated that disruption of the intrinsic innervation

network (VIPergic and cholinergic) causes reduced distribution of the VIP peptide in exocrine tissues (Semaniakou et al., 2020).

3.4 VIP Deficiency in the Pancreas and CF-Related Diabetes (CFRD)

The last tissue that was investigated for VIP deficiency, was the pancreas. We evaluated the VIP content in the endocrine and exocrine pancreas of CF mice. Our IHC data showed a strong decrease of VIP amount in the exocrine pancreas around the ducts and acinar cells that was further confirmed by ELISA. Most importantly, the reduction in VIP was higher in the endocrine pancreas that expresses the highest number of VIPergic neuronal fibers (Semaniakou et al., 2020). Results are presented in Figure 5.1 (See Chapter 5 of this thesis).

Furthermore, we examined the general innervation in both exocrine and endocrine (islets of Langerhans) pancreas. We found a significant alteration of the general innervation which had started at an early disease stage in the islets and deteriorated in an older age. Additionally, the continuous general neuronal innervation observed in the exocrine pancreas in both ages, was discontinued and lower density of nerve fibers was observed in the pancreas of CF mice (Semaniakou et al., 2020). Results are presented in Figure 5.2 (See Chapter 5 of this thesis). CF-related diabetes is the second co-morbidity in CF, following respiratory failure, and affecting more than 50% of adult CF patients. CFRD is characterized by partial insulin insufficiency, impaired glucagon suppression and elevated random plasma glucose >200mg/dl. VIP is known to have insulinotropic effects on pancreatic beta cells as glucose-dependent insulin secretion and glucagon release

respectively are augmented and indirectly regulated by VIP. Hence, we asked if changes in VIP content, because of sparse innervation of the pancreas, could have an implication on CFRD pathogenesis, affecting insulin and glucagon secretion as well as glucose levels. Accordingly, we measured basal insulin amount, in non-fasting animals, glucagon and random plasma glucose concentration. Our results showed that a low level of VIP, which starts at an early stage of CF disease, leads to insulin reduction in both ages of CF mice. Glucagon changes in CFRD are poorly studied in both human and animal models. Most of the research is focused on the impact of the CFTR dysfunction in insulin secretion and whether CFTR is expressed in α-cells. To our knowledge, only two studies until now, using F508del/F508del mice (12-14 weeks) and CF pigs (newborn and older CF pigs) demonstrated high glucagon levels in CF (Huang et al., 2017; Uc et al., 2015). Our research data showed a significant increase in glucagon levels in both 8-weeks and 17-weeks of CF mice, accompanied with high random glucose levels. While VIP, indirectly, elevates glucose-dependent insulin secretion and glucagon expression, we suggest that early loss of VIP in the pancreas of CF mice, before tissue damage develops, may contribute to CFRD pathophysiology (Semaniakou et al., 2020). Results are presented in Figure 5.4 (See Chapter 5 of this thesis).

CHAPTER 4: DISRUPTED LOCAL INNERVATION RESULTS IN LESS VIP EXPRESSION IN CF MICE TISSUES

The figures and text presented in this chapter are from a manuscript published i the Journal of Cystic Fibrosis: Anna Semaniakou, Sarah Brothers, Grayson Gould, Mehrsa Zahiremani, Jamie Paton, Frederic Chappe, Audrey Li, Younes Anini, Roger P. Croll and Valerie Chappe (2020). Disrupted local innervation results in less VIP expression in CF mice tissues. https://www.sciencedirect.com/science/article/pii/S1569199320307773 *Journal of Cystic Fibrosis*.

As the first author on this article, I performed most of the experiments, analysis, data interpretation, statistics and wrote the manuscript. The manuscript was edited by Dr. Valerie Chappe, Dr. Younes Anini and Dr. Roger P. Croll.

4.1 Abstract

Vasoactive Intestinal Peptide (VIP) is the major physiological agonist of the Cystic Fibrosis Transmembrane conductance Regulator (CFTR) chloride channel activity. VIP functions as a neuromodulator and neurotransmitter secreted by neurons innervating all exocrine glands. VIP is also a potent vasodilator and bronchodilator that regulates exocrine gland secretions, contributing to local innate defense by stimulating the movement of water and chloride transport across intestinal and tracheobronchial epithelia. Previous human studies have shown that the rich intrinsic neuronal networks for VIP secretion around exocrine glands could be lost in tissues from patients with cystic fibrosis. Our research has since confirmed, *in vitro* and *in vivo*, the need for chronic VIP exposure to maintain functional CFTR chloride channels at the cell surface of airways and intestinal epithelium, as well as normal exocrine tissues morphology (Alcolado et al., 2014). The goal of the present study was to examine changes in VIP in the lung, duodenum and sweat glands of 8- and 17-weeks old F508del/F508del mice and to investigate VIPergic innervation in the small intestine of CF mice, before important signs of the disease development. Our data show that a low amount of VIP is found in CF tissues prior to tissue damage. Moreover, we found a specific reduction in VIPergic and cholinergic innervation of the small intestine. The general innervation of the primary and secondary myenteric plexus was lost in CF tissues, with the presence of enlarged ganglionic cells in the tertiary layer. We propose that low amount of VIP in CF tissues is due to a reduction in VIPergic and cholinergic innervation and represents an early defect that constitutes an aggravating factor for CF disease progression.

4.2 Introduction

Vasoactive Intestinal Peptide (VIP), which was discovered in the 1970s by Said and Mutt, is a 28-amino-acid neuropeptide that belongs to a superfamily of brain-gut peptide hormones which are structurally related (Ishihara et al., 1992). This family includes significant neuropeptides such as the secretin, glucagon and pituitary adenylyl cyclase-activating peptide (PACAP) (Said et al., 1975, 1970). VIP immunoreactive nerve fibers originate from the central, peripheral, and intrinsic nervous systems innervating all exocrine glands and blood vessels throughout the body.

VIP has strong anti-inflammatory, bronchodilatory and immunomodulatory properties (Said, 1991; Said, 1991; Said, 2008). As a neuromodulator and neurotransmitter, in the lung VIP plays a crucial role in maintaining airways innate immunity through mucociliary clearance, mostly by regulating CFTR-dependent secretions (Chappe et al., 2012; Widdicombe et al., 2015). Intrinsic neurons that contain VIP can be found around the walls of pulmonary and bronchial arteries, submucosal and serous glands as well as blood vessels (Said, 1991).

In the gut, VIP originates mainly from intrinsic VIP-positive neurons in the myenteric and submucosal plexuses and extrinsic parasympathetic autonomic nerves (de Jonge, 2013). In the upper intestine, VIP controls many physiological processes such as smooth muscle relaxation for peristaltic movement and sphincter use (Biancani et al., 1984), and inhibitory control of the circular muscle layer. Also, in both ileum and duodenum it stimulates ion transport and mucus secretion (Crist et al., 1992; Fox-Threlkeld et al., 1991; Kato et al., 2011; Plaisancié et al., 1998; Racusen et al., 1977).

The expression of VIP in the intrinsic neuronal network of the gut of mammals has been widely demonstrated (Brookes et al., 1991; Costa et al., 1996; Crowe et al., 1992; Furness et al., 1984, 1979; Jessen et al., 1980; Porter et al., 1996; Porter et al., 1997; Schafer et al., 1995; Schäfer et al., 1998; Schemann et al., 1993, 1995; Steele et al., 1991). In the upper small intestine, mucosa and circular muscle layer are characterized by high density of VIP-positive nerve fibers as well as smooth muscles layers across all GI regions (Anlauf et al., 2003). More specifically, in the duodenum 53% of VIP positive neurons are found in the submucosal layer and only 14% are present in the myenteric plexus (Anlauf et al., 2003).

Previous data from Chappe and colleagues have demonstrated, *in vivo* and *in vitro*, that chronic VIP exposure is needed to maintain functional CFTR chloride channels at the cell surface of airways and intestinal epithelium, as well as normal exocrine tissue morphology (Rafferty et al., 2009). In airways epithelial cells, CFTR channel function is regulated by VIP through PKA- and PKC-dependent signaling pathways (Alcolado et al., 2011). Our group have demonstrated that VIP regulates CFTR membrane stability via the activation of the VPAC1 receptor and the $G_{\alpha i/q}$ signaling cascade through PKCε-dependent interaction of NHERF1 and P-ERM proteins with CFTR PDZ domain in a complex that helps stabilizing CFTR at the cell membrane and enhancing its function (Alshafie et al., 2014). In the human nasal epithelial cell line JME/CF15, derived from a CF patient homozygous for the F508del mutation, we found that prolonged VIP exposure can rescue trafficking to the cell membrane and increases the function of F508del-channels (Alcolado et al., 2011). Lastly, our *in vivo* studies, with VIP knock-out (KO) mice, demonstrate that the

absence of VIP induces a CF-like phenotype, with CFTR intra-cellular retention in epithelial cells of the lung and small intestine (Alcolado et al., 2011). Chronic VIP treatment corrected exocrine tissue pathology and CFTR membrane expression and function, providing a molecular link between the absence of VIP stimulation and CFTR dysfunction.

Early studies have demonstrated that VIPergic innervation of the sweat glands is sparse or absent in tissues from patients with CF, suggesting that a reduction or lack of VIP secretion could significantly contribute to CF disease progression (Heinz-Erian et al., 1985; Savage et al., 1990; Sharma et al., 1995; Wattchow et al., 1988). Until now, the etiology of this phenomenon remains unknown.

In the present study, we have investigated changes in VIP content as well as the morphological pattern of nerves surrounding exocrine tissues in CF mice homozygotes for the F508del-CFTR mutation, the most common mutation found in patients with cystic fibrosis (Fajac et al., 2017). We used mice at different ages, reflecting early and late disease progression. Our data suggest that the low amount of VIP found in CF tissues starts before tissue damage is visible and corresponds to a strong reduction in VIPergic and cholinergic innervation, as well as a significant disruption of the intrinsic neuronal network in CF duodenum tissues.

4.3 Materials and Methods

4.3.1 Chemicals. Antibodies are shown in Table 3; Normal mouse blocking serum was from Santa Cruz Biotechnology (ImmunoCruz goat ABC Staining System; sc-2023); Normal donkey serum (D9663) was from Sigma (St. Louis, MO); Triton X-100 (T8532) was from Sigma; 16% paraformaldehyde aqueous solution (15710) was from Electron Microscopy Sciences (Hatfield, PA); DAB (3, 3 -diaminobenzidine) HRP Substrate Kit (ab64238) was from Abcam; Enzyme-Linked-Immunosorbent Assay kit for VIP was from Cloud-Clone Corp. (Cat. No. CEA380Mu; Houston-TX); Alcian Blue 8GX solution (A5268) was from Sigma; Protease inhibitor cocktail tablets were from Roche (cOmplete, Mini; Cat. No. 11 836 153 001). Other chemicals were from Sigma and of the highest grade available.

Table 3: Summary of Antibodies and their Dilutions Used in Chapter 4.

<table>
<tr><th>Polyclonal Primary Antibodies</th><th>Dilution & application</th><th>Secondary Antibodies</th><th>Dilution</th></tr>
<tr><td>Anti-VIP (M-19; sc-7841), Santa Cruz Biotechnology (Santa Cruz, CA)</td><td>1:75 (IHC)</td><td>ImmunoCruz goat avidin/biotinylated complex Staining System (sc-2023), Santa Cruz Biotechnology</td><td>As per kit instructions</td></tr>
<tr><td>Anti-VIP (20077), ImmunoStar (Hudson, WI)</td><td>1:100 (whole mount immunostaining)</td><td rowspan="2">Donkey anti-Rabbit IgG (H+L) (Alexa Fluor 555; A-31572), Invitrogen (Carlsbad, CA)</td><td rowspan="3">1:500</td></tr>
<tr><td>Anti-PGP 9.5 (ab15503), Abcam (Cambridge, MA)</td><td>1:100</td></tr>
<tr><td>Anti-Choline Acetyltransferase (ChAT; AB144P), EMD Millipore (Bellerica, MA)</td><td>1:50 (whole mount immunostaining)

1:100 (IHC)</td><td>Donkey anti-goat IgG (H+L) (Alexa Fluor 555; A-21432), Invitrogen (Carlsbad, CA)</td></tr>
</table>

4.3.2 Mice. Male, 8- and 17-week-old wild-type C57Bl/6 mice and C57Bl/6 homozygous for the F508del mutation (C57Bl/6 homozygous *Cftr*^{tm1Kth} ΔF508) were obtained from Dr. Craig Hodges at Case Western Reserve University (Ohio, USA). Mice were housed in an Allentown IVC rack with irradiated corncob bedding, Prolab autoclaved RMH 3500 feed and municipal (chlorinated tap) water with 3% Colyte. Mice were evaluated daily during routine health checks. If they showed signs of distress, they were weighed, given SC fluids if needed and monitored more frequently by lab personnel. If signs of distress did not resolve (i.e. obstruction passed), they were humanely euthanized. All experimental procedures were in accordance with the principles of the Canadian Council on Animal Care (CCAC) and according to the National Institute of Health *Guide to the Care and Use of Experimental Animals*. Protocols were approved by Dalhousie University (Halifax, Canada) Animal Care and Use ethic committee.

4.3.3 Tissue preparation. Mice were humanely euthanized by intraperitoneal overdose of sodium pentobarbital before tissue collection. For sectioning, tissues of 8- and 17-week-old males, C57Bl/6 F508del homozygotes (ΔF508) CF mice and same age C57Bl/6 wild-types (WT) were flash frozen in liquid nitrogen before storage at -80^{o}C for later use or immediately fixed in 10% formalin buffer. Tissues were then embedded in paraffin blocks before longitudinal sectioning into 5-µm-thin sections for histology using hematoxylin and eosin (H and E) staining (Feldman et al., 2014) or immunohistochemistry experiments as described below. Tissues used in whole mount experiments were immediately fixed in 4% paraformaldehyde (PFA) following dissection and incubated overnight at 4˚C, followed by 2% PTA (0.1 M Phosphate-Triton Azide Buffer) for long-term storage. Tissue

embedding and sectioning were done at the Histology and Research Services (HRS) Laboratory, Pathology Department, Faculty of Medicine, Dalhousie University.

4.3.4 Immunohistochemistry (IHC) and microscopy imaging. Thin tissue sections (5µm) annealed to microscopy slides were deparaffinized in xylene and rehydrated prior to a 35 min heat-induced antigen retrieval. Next, the slides were washed twice for 5 minutes each time in PBS and incubated in 1% peroxidase blocking solution for 5 minutes. After another 10-minute washing step with PBS, the slides were incubated in normal mouse blocking serum for 1h at RT in a humidified chamber, then overnight with the primary antibody for VIP (1:75) or choline acetyltransferase (ChAT; 1:100). The next day tissue slides were washed three times for 5 minutes each with PBS and then incubated with a biotinylated secondary antibody (1:200; ABC ImmunoCruz staining system) for 30 minutes at RT. After three washes with PBS for 5 minutes each, the slides were incubated in avidin/biotinylated complex for 30 minutes at RT and then washed again three times in PBS for 5 minutes each. VIP or ChAT signal was revealed with a DAB HRP peroxidase substrate and slides were counterstained with hematoxylin. After dehydration, a xylene based Permount was used to mount a coverslip, and slides were observed under light microscopy with 10X, 25X, 40X and 63X objectives. Images were taken with a Zeiss Axiocam HRC Colour Camera mounted on an Axioplan II microscope. Scoring of images was used for semi-quantification of the IHC signal by two blinded investigators using an arbitrary scale (0 = none, 0.5 = minimal, 1 = low, 1.5 = some, 2 = moderate, 2.5 = strong and 3 = highest). Colour balance, contrast and brightness of whole images were adjusted for consistency within tissue sections. Experiments were repeated at least twice for each

tissue sample and three to five mice in each age group were used. An average of 8 to 15 images from each mouse were used for the semi-quantification.

4.3.5 Goblet cells quantification and tissue morphology measurements. Tissue samples were well-oriented with longitudinally cut crypts and villi to precisely assess alterations in the overall intestinal tissue architecture. Undamaged areas where villi were present have been used to measure morphological parameters such as villi height, from base to tip, and villi width from the central part of the villi. Beneath each villus, we measured the total crypt area height from the muscle layer to the base of villi; the diameter of adjacent crypts to assess their dilation, and the muscle layer thickness. Alcian blue 8GX solution (1% Alcian blue solution in 3% acetic acid) was used to stain and quantify the number of goblet cells in the villi and crypts of the duodenum (Wardi et al., 1972). After the deparaffinization step, duodenum tissue slides were incubated in Alcian Blue staining solution for 35 minutes at room temperature, rinsed for 2 minutes under running tap water, followed by hematoxylin staining for 5 minutes. Slides were then dehydrated and mounted with xylene before imaging under light microscopy. NIH Image J software (https://imagej.nih.gov/ij/download.html) was used to count the number of the goblet cells per villi, as well as for morphological parameters measurement. For every mouse (n = 5) and in each age group (8- and 17-week-old) we used 10 different images along the whole tissue, each image containing 5 to 6 consecutive and well distended villi.

4.3.6 Smooth muscle identification: For smooth muscle thickness, only the inner circular muscle layers were measured in ten randomly located regions throughout the section. All sections were scored by two observers blinded to mouse strain. Image J software

protocol, was used to measure duodenum tissue alterations, was used for muscle measuring and scoring.

4.3.7 Lung injury score: Evaluation of the lung inflammation was based on a recent paper from Bayes *et al.* (2016). Histological lung tissue sections from both 8-and 17-weeks, wild-type and CF mice, were scored for alveolar thickening and peribronchial infiltration using a scoring system described in Figure 4.1 (Bayes et al., 2016). For every mouse we scored blindly approximately 10-15 images that would cover the entire mouse section, using the 10X magnification. Afterwards, to further confirm our results and avoid a biased scoring that would depend on every separate section, we did an overall scoring estimation of the whole tissue section using the 4X magnification. Our results were double validated by two independent blinded investigators.

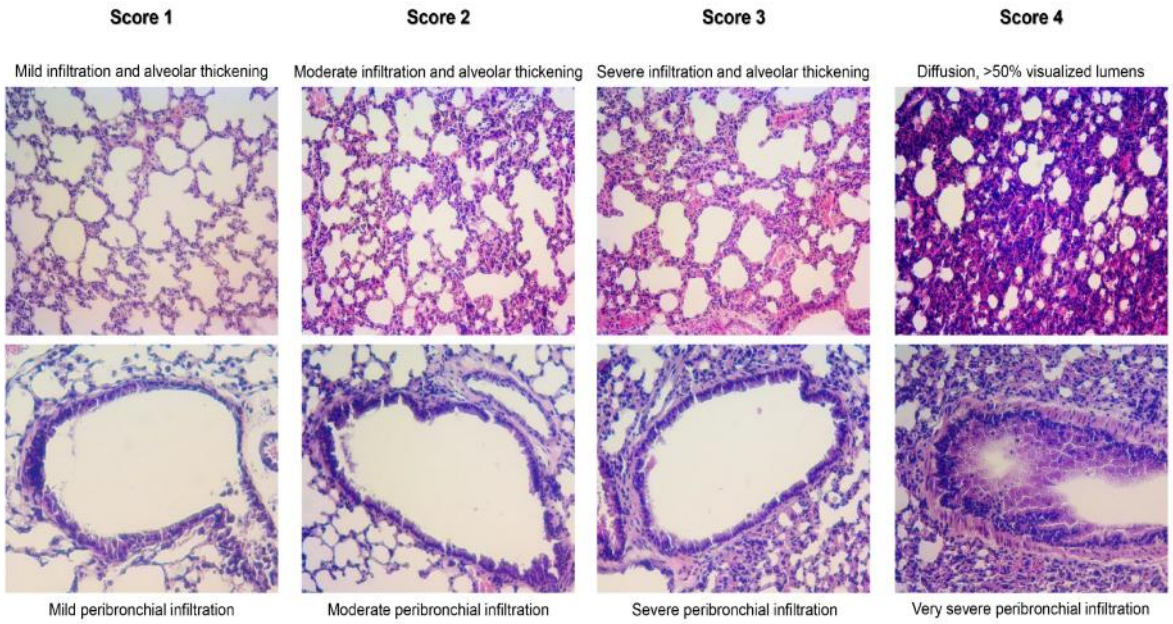

Figure 4.1: Histological scoring system for the evaluation of lung inflammation.

Presence of mild infiltration and alveolar thickening as well and mild peribronchial infiltration was score 1, moderate infiltration and alveolar thickening plus moderate peribronchial infiltration is used as score 2, severe infiltration and alveolar thickening plus severe peribronchial infiltration is characterized as score 3 and, lastly, diffusion in combination with very severe peribronchial infiltration is characterized as score 4.

4.3.8 Whole mount immunofluorescence and confocal images. Fresh sections of 0.5 cm of the duodenum tissue from 8-week-old males C57Bl/6 wild-type or F508del homozygotes (n=5) CF mice were immunostained for VIP, PGP 9.5 (ubiquitin hydrolase) or ChAT (Choline Acetyltransferase) (Newton et al., 2014). Tissues were fixed in 4% paraformaldehyde (PFA) overnight at 4^{o}C. Two washing steps of PBS for 15 minutes each, were followed by 0.05% collagenase treatment for 2h. Next, the tissues were washed 5 times with PBS for 15 minutes each and incubated overnight with 1% Normal donkey

serum in 2% TritonX-100. Next, the tissues were incubated with a primary antibody: VIP (Immunostar 20077; 1:100 dilution), PGP 9.5 (1:100 dilution) or ChAT (1:50 dilution) for 10 days and washed five times in PBS for 15 minutes each. After this washing step, tissues were incubated with a Donkey anti-Goat –Alexa Fluor 555 (1:500 dilution) secondary antibody for 5 days. A final five times washing step with PBS for 15 minutes each was followed by overnight incubation in Clear Unobstructed Brain/Body Imaging Cocktails (CUBIC), a hydrophilic tissue-clearing medium before imaging. Innervation was observed for qualitative assessment using 3D confocal microscopy under 10X and 25X magnification (Zeiss LSM 510 Meta Confocal Microscope; HeNe 543 nm laser) at the CMDI facility, Faculty of Medicine, Dalhousie University. Z-stacks of the mucosa and myenteric plexuses were recorded using an upright laser confocal setting. The detection pinhole and gain settings were determined at the beginning of each experiment and were kept consistent. Different magnification views were captured to visualize distinct areas of both the mucosa and myenteric plexus.

4.3.9 ELISA. Flash frozen duodenum tissues from C57Bl/6 8-week-old males, wild-type and F508del homozygotes CF mice were homogenized in RIPA buffer containing proteases inhibitors and lysates were used in mouse ELISA kit with high sensitivity and high specificity for VIP (Cloud-Clone Corporation, competitive inhibition). The kit was used according to the manufacturer's instructions. Optical density was measured with a spectrophotometer at 450nm. VIP concentration was afterwards normalized to total proteins measured by protein assay using a Standard Bradford Assay with a standard BSA curve from 0 to 15µg in RIPA buffer.

4.3.10 Statistics.

Results are reported as means ± SE. Statistical differences between groups were calculated by the non-parametric ANOVA (Meyerholz et al., 2018). $p < 0.05$ was considered statistically significant. N represent the number of independent experiments.

4.4 Results

4.4.1 Disease progression in the duodenum of CF mice.

In the small intestine, and more specifically in the duodenum, CFTR is highly expressed along the crypt-villus axis, regulating fluid secretion. In CF animal models, absent or reduced CFTR expression leads to a dehydrated and acidic luminal environment causing intestinal obstruction with morphological changes of the small intestine such as wider villi, more goblet cells and crypt dilation (Semaniakou et al., 2019). Previous studies have shown small intestinal differences of those parameters between ΔF508 and wild-type 12 weeks mice (Bazett et al., 2015). Accordingly, we performed a pathological assessment of the duodenum tissue of mice used in the present study by measuring the villi height, the villi width, crypt height, crypt dilation, muscle layer thickness and the number of the goblet cells in 8- and 17-week-old WT and CF mice to assess disease progression in these two age groups (Fig. 4.2A). In younger CF mice (8-week-old), the morphological tissue parameters were not statistically significantly altered compared to same age WT tissues (Fig. 4.2B), indicating that the disease progression is minimal at this age group. In older mice (17-week-old) however, significant differences were found, with villi and crypt being remarkably longer than in WT tissues (+67.92 %, $p < 0.001$; +36.66 %, $p < 0.001$,

respectively) (Fig. 4.2C). Our results for villi width, crypt dilation and muscle layer did not show a significant difference between WT and CF.

Another important disease marker that we considered was the number of the goblet cells in the villi and crypt area. A major consequence of the altered luminal environment in CF is the accumulation of mucus that is partially produced by goblet cells. The presence of goblet cells was revealed by Alcian Blue staining (Fig. 4.2D). Interestingly, duodenum tissue sections from 8-week-old CF mice presented a higher number of goblet cells in both villi (+22.82%, $p < 0.001$) and crypts (+30.55 %, $p < 0.001$) compared to same age WT. In the 17-week-old CF mice group, an increased number of goblet cells in the CF tissues was also observed in both crypts and villi ($p < 0.01$) (Fig. 4.2E). Larger group of older CF animals may be needed to further confirm the goblet cell hyperplasia.

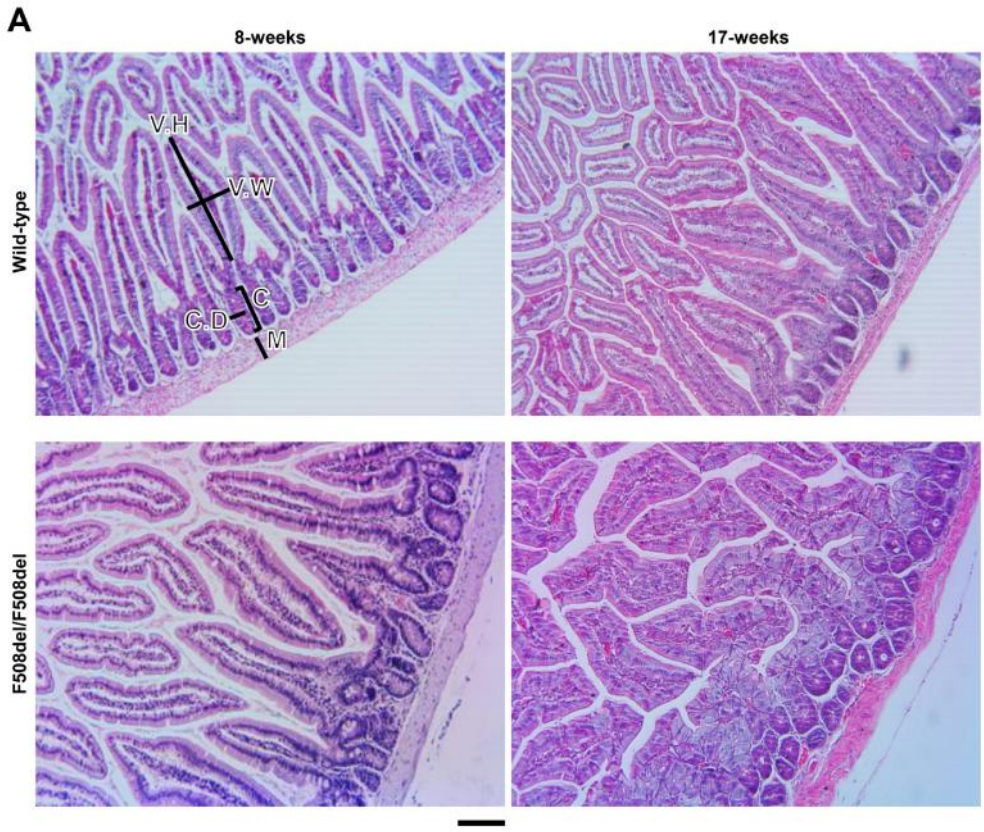

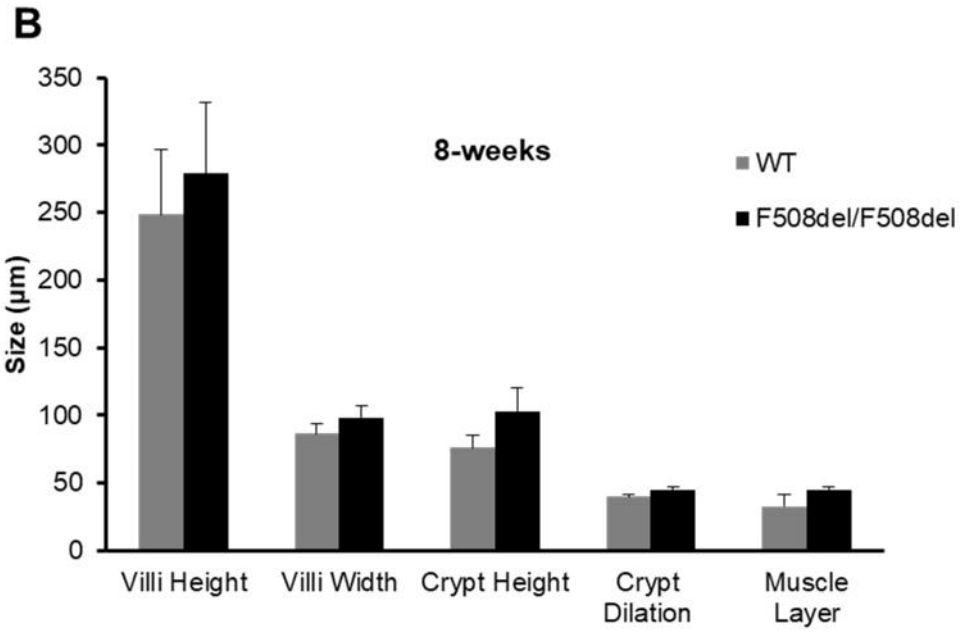
B
8-weeks
WT
F508del/F508del
Size (µm)
350
300
250
200
150
100
50
0
Villi Height
Villi Width
Crypt Height
Crypt Dilation
Muscle Layer

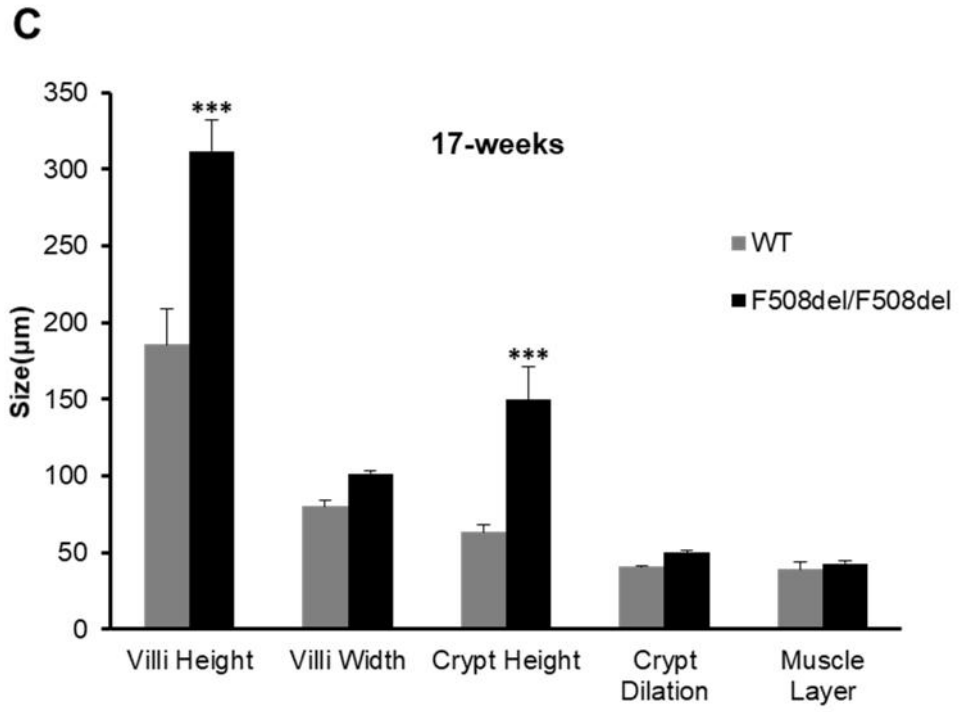
C
17-weeks
WT
F508del/F508del
Size(µm)
***
***
350
300
250
200
150
100
50
0
Villi Height
Villi Width
Crypt Height
Crypt Dilation
Muscle Layer

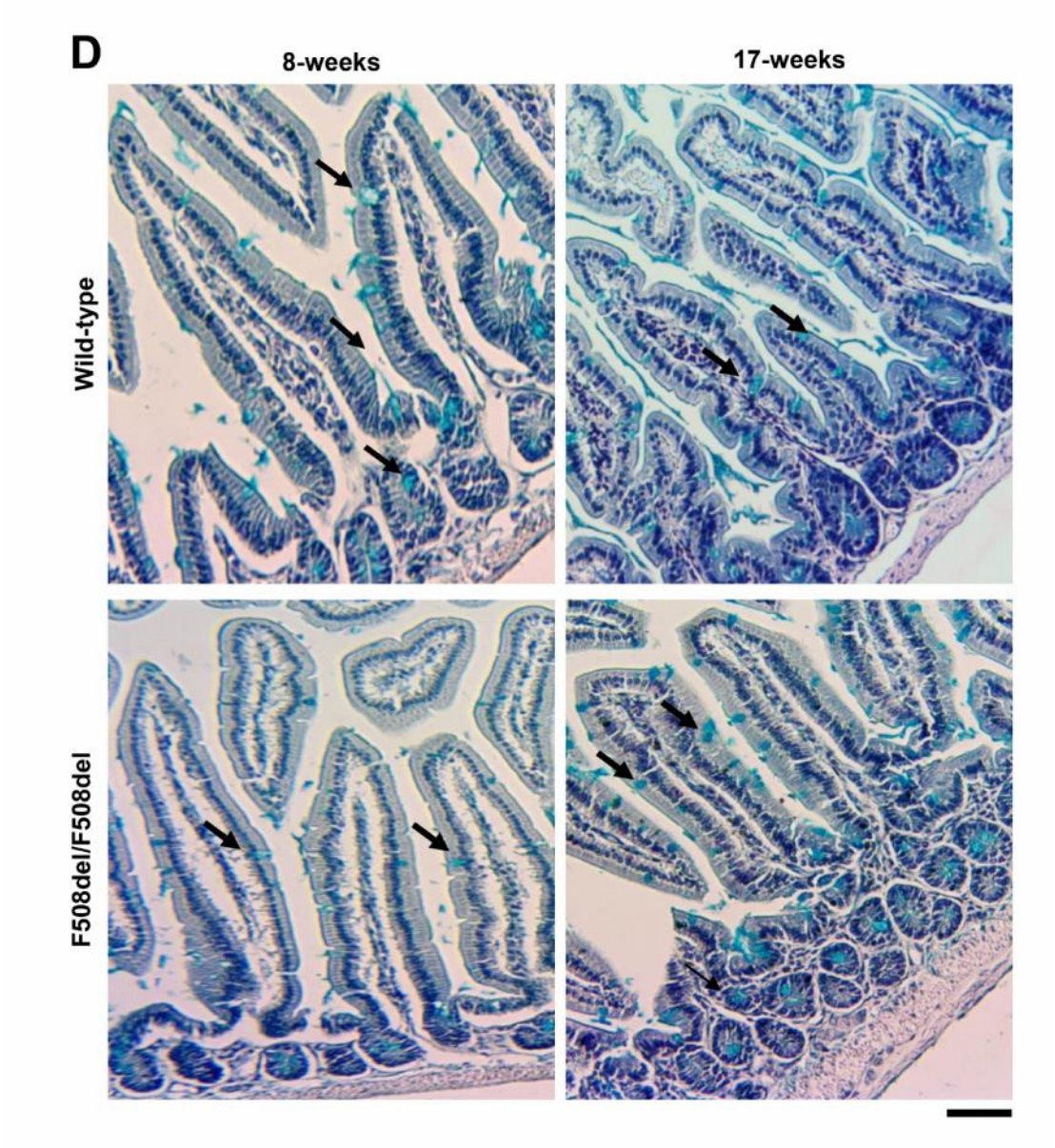
D
8-weeks
17-weeks
Wild-type
F508del/F508del

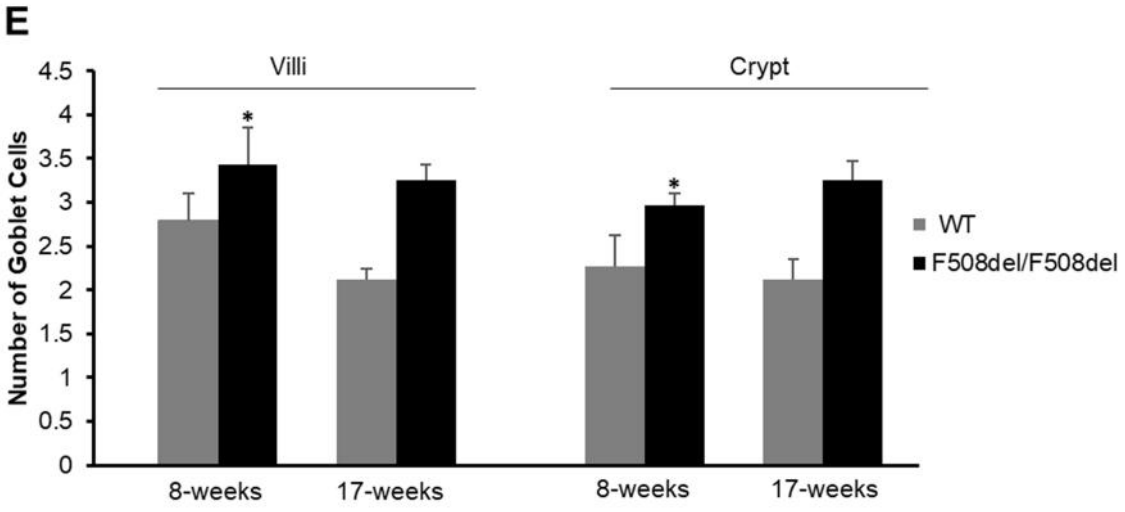

Figure 4.2: Pathological assessment of duodenum.

A, Histology images of duodenum tissues from 8- and 17-week-old wild-type and F508del homozygous (F508del/F508del), CF mice. Samples were embedded in paraffin before sectioning (longitudinal). 5µm thick sections were mounted onto microscopy slides and H&E stained before being imaged for pathological assessments. Images from sections encompassing the whole tissue were taken with a light microscope at 20X magnification. ***B & C,*** Measurement of villi height, villi width, crypt height, crypt dilation and muscle layer thickness in 8-week-old (B) and 17-week-old (C) wild-type (WT) and CF (F508del/F508del) mice duodenum. Histogram bars represent averages from 3 to 5 mice (5 to 6 images for each tissue were used). ***D,*** Histology images after Alcian Blue staining for the quantification of goblet cells (black arrows) in 8-week-old and 17-week-old wild-type and CF (F508del/F508del) mice duodenum. ***E,*** Histogram bars represent the average amount of goblet cells per villi or crypt that have been counted in 8 to 10 images per mouse. V.H = villi height, V.W = villi width, C = crypt height, C. D = crypt dilation, M = muscle layer. Scale:100 µm, **$p < 0.01$, ***$p < 0.001$. 3-5 mice, N=3.

Altogether, these data indicate that we can discriminate between very early disease stage (8-week-old) and well-developed disease stage with these two age groups of CF mice. In the 17-week-old CF mice, the disease has clearly progressed with changes to longer villi and longer crypts as expected while in the younger age the intestinal histology was close to wild-type.

4.4.2 Changes in VIP around the lung, sweat glands and duodenum of CF mice.

4.4.2.1 Strong reduction of VIP in the duodenum of CF mice. Immunohistochemistry (IHC) signal for VIP was revealed in wild-type mice around the epithelium of villi, into the lamina propria area, around the crypt and in muscle layers of duodenum longitudinal tissue sections following immunostaining for VIP with a specific polyclonal antibody (Fig. 4.3A-4.3D top). VIP signal intensity in CF and wild-type tissues from 8- and 17-week-old mice was semi-quantified from scanned microscopy images using an arbitrary scale from 0 to 3 (see Methods). Results show that the signal for VIP was reduced by 49.01 % ± 0.11 ($p < 0.001$) in 8-week-old CF mice and by 32.48 % ± 0.01 ($p < 0.001$) in 17-week-old CF mice in comparison to the same age WT animals (Fig. 4.3F).

Reduction in the amount of VIP present in the duodenum was further confirmed by ELISA. VIP content was 0.63 ± 0.05 pg/µl in wild-type and 0.19 ±0.045 pg/µl in CF tissue lysates ($p < 0.001$), confirming a strong reduction of VIP in CF compared to wild-type tissues (Fig. 4.3G).

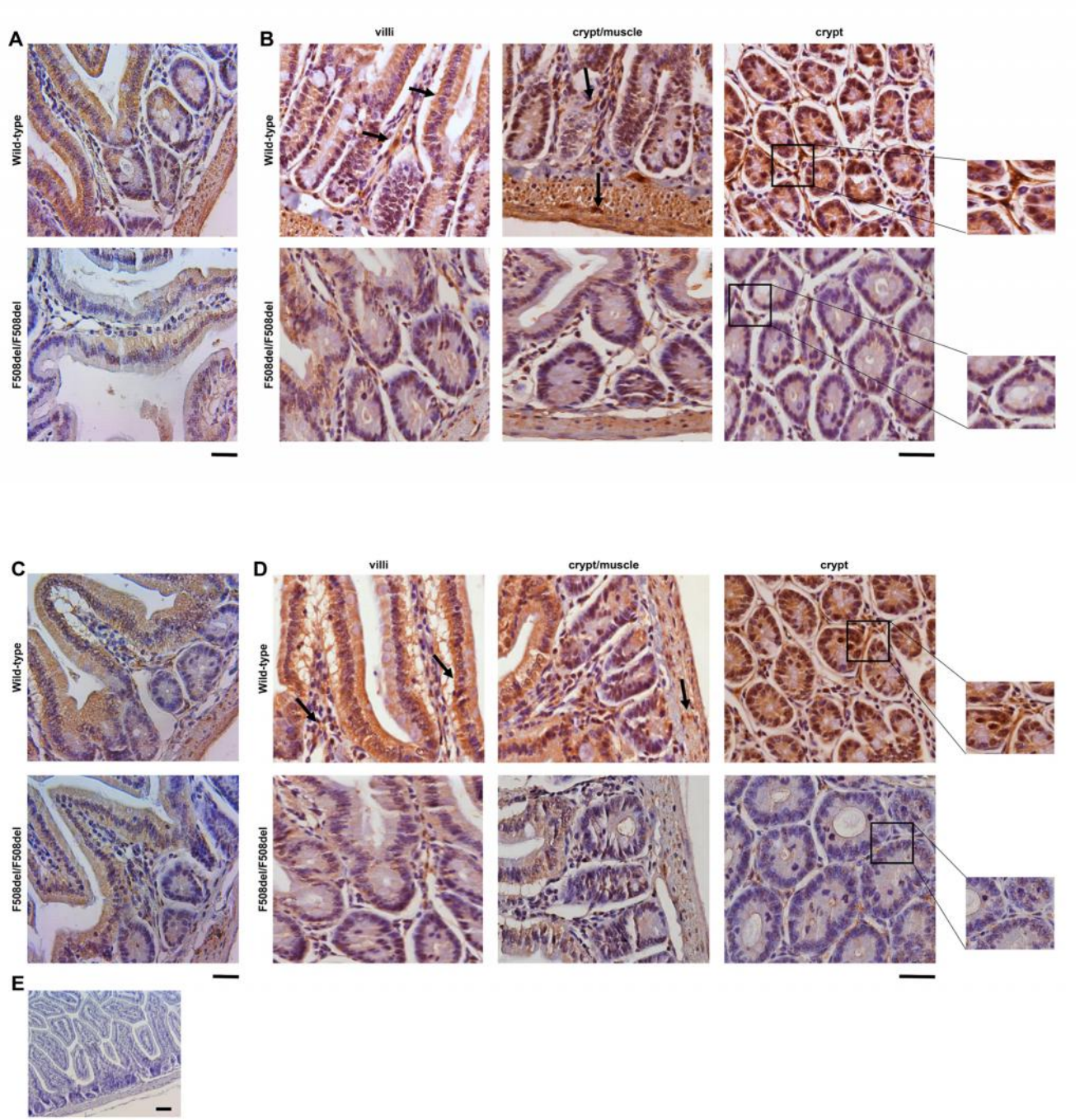
A
B
villi
crypt/muscle
crypt
Wild-type
F508del/F508del
C
D
E

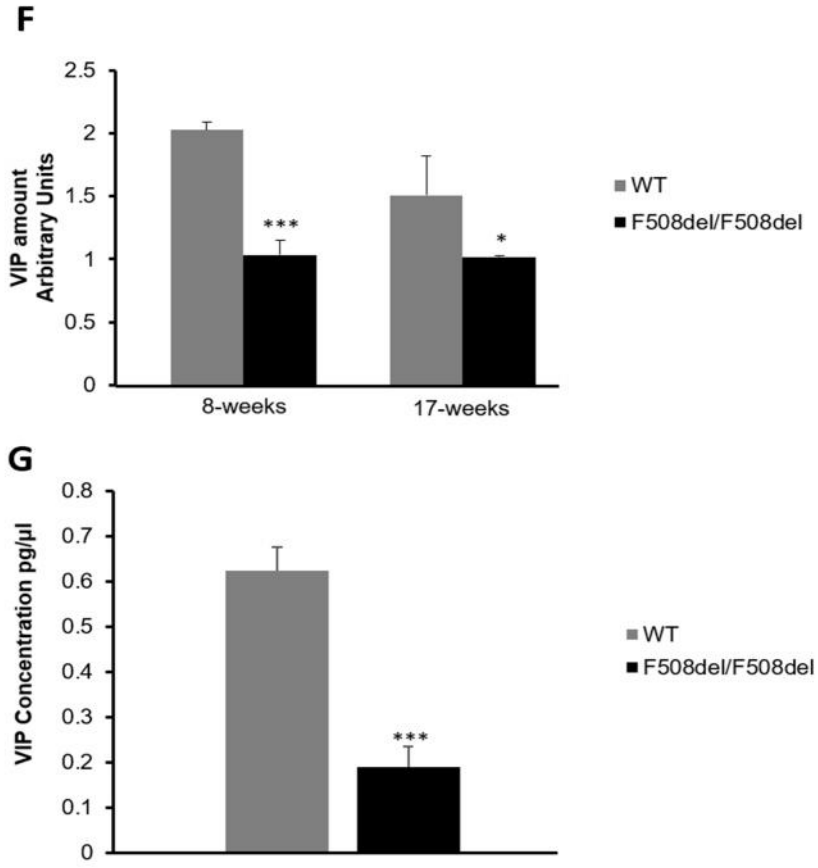

Figure 4.3: VIP signal in the duodenum tissues

A - D, Representative IHC images of duodenum tissues stained for VIP (dark brown) in 8- and 17-week-old wild-type and F508del homozygous CF (F508del/F508del) mice showing VIP signal around the villi, lamina propria, crypt and muscle layer. ***A & C***: 40X objective, scale: 20µm. ***B & D,*** High magnification images with 63X objective, scale: 200µm. ***E,*** Negative control where the VIP antibody was omitted. ***F,*** Semi-quantification of VIP signal in 8- and 17-week-old wild-type and CF duodenum. Histogram bars represent averages of 8 to 15 images from each mouse (3 to 5 mice per age group) Arbitrary scale from 0 to 3 indicates: 0 = none, 0.5 = minimal, 1 = low, 1.5 = some, 2 = moderate, 2.5 = strong and 3 = highest. ***G,*** VIP concentration measured by ELISA in 8-week-old wild-type and CF mice duodenum tissue homogenates, normalized to total proteins (5 mice), N = 2. ***$p < 0.001$.

4.4.2.2 Decreased VIP in the lung and sweat glands of CF mice. VIP-containing nerve fibres have been described in tracheobronchial smooth muscle, around submucosal glands and in the walls of pulmonary and bronchial vessels (Barnes et al., 1991). In the lung, we examined the presence of VIP around the epithelium of the bronchioles in both 8- and 17-week-old WT and CF mice (Fig. 4.4A & 4.4B top *vs.* 4.4A & 4.4B bottom). IHC signal for VIP was reduced by 52.63 % ± 0.26 ($p < 0.001$) in the 8-week-old CF mice. The difference in VIP signal observed in the older mice (Fig. 4.4D), was not statistically significant. Histology of lung sections with hematoxylin and eosin staining showed close to normal lung structure in the 8-week-old CF mice compared to wild-type, in contrast to 17-week-old CF mice where we observed inflammation and infiltration of immune cells in the bronchi and alveoli, mucus obstruction and tissue damage (Fig. 4.4E). Additionally, our lung injury score demonstrated very high levels of alveolar thickening and peribronchial infiltration in the 17-weeks CF mice compared to 8-weeks diseased mice (Fig.4.4F). In the young CF mice, where the VIP amount was highly reduced, the quantitative histological score did not reveal any tissue remodelling. These data are in agreement with a previous study from Guilbault *et al*. (2006), supporting that CF mice only start to develop spontaneous lung disease between 12- and 16-week-old and gradually deteriorate (Guilbault et al., 2006).

We measured the murine IL-8 homologue KC, MIP-2 (macrophage-inflammatory protein 2) levels in both ages. Our data did not show any significant difference in MIP-2 concentration between the wild-type and CF mice for both 8- and 17-week-old (Fig. 4.4G). This is in agreement with a study from Wu *et al.* (2010) which showed that MIP-2

levels were not altered in 8-9 week-old CFTR $^{-/-}$ mice even when challenged with LPS compared to CFTR $^{+/+}$ (Wu et al., 2010). While MIP-2 is a chemokine that attracts neutrophils (Ohtsuka et al., 2001), it may not be highly expressed in the intestine of the C57Bl/6 homozygous *Cftr*^{tm1Kth} ΔF508 mice used in the present study.

In wild-type sweat glands we examined the VIP signal inside the glands as well as around the glands (innervation). Interestingly, sweat glands which are free of inflammation, also showed a strong reduction in IHC signal for VIP with 68.46 % ± 0.13 reduction in the 8-week-old CF compared to wild-type ($p < 0.001$) and 48.36 % ± 0.19 reduction in the 17-week-old CF tissue compared to same age wild-type ($p < 0.001$) (Fig. 4.5A & 4.5B top *vs.* 4.5A & 4.5B bottom). Hematoxylin and eosin staining did reveal histopathological tissue alterations between the two ages of CF mice when compared to control littermates. More specifically, sweat glands of 17-weeks CF mice had wider duct opening, but no signs of inflammation as expected (Fig. 4.5E).

Altogether those data show that even in tissues with minimal manifestations of the disease (8-week-old, sweat glands), much less VIP is present, suggesting that it is not a consequence of advanced disease manifestation but an early defect.

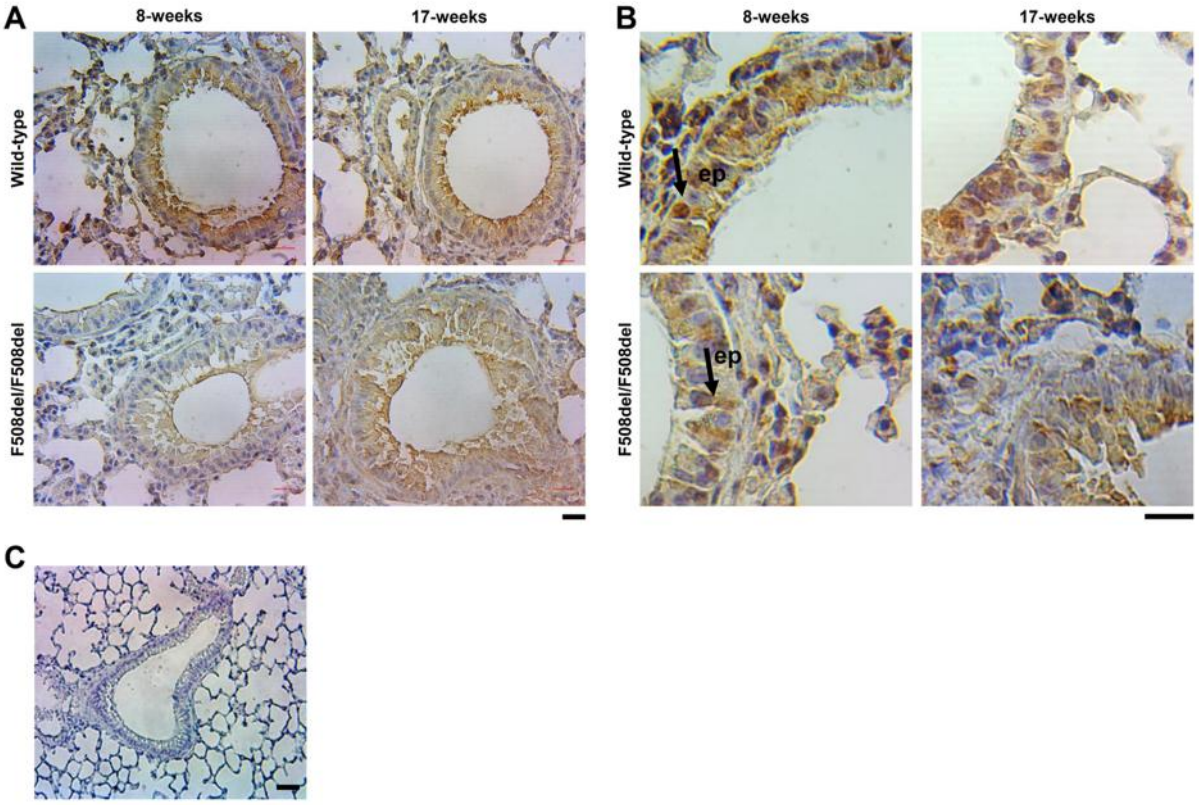
A
8-weeks
17-weeks
Wild-type
F508del/F508del
B
8-weeks
17-weeks
Wild-type
F508del/F508del
ep
ep
C
D
VIP amount
Arbitrary Units
3
2.5
2
1.5
1
0.5
0
***
8-weeks
17-weeks
WT
F508del/F508del

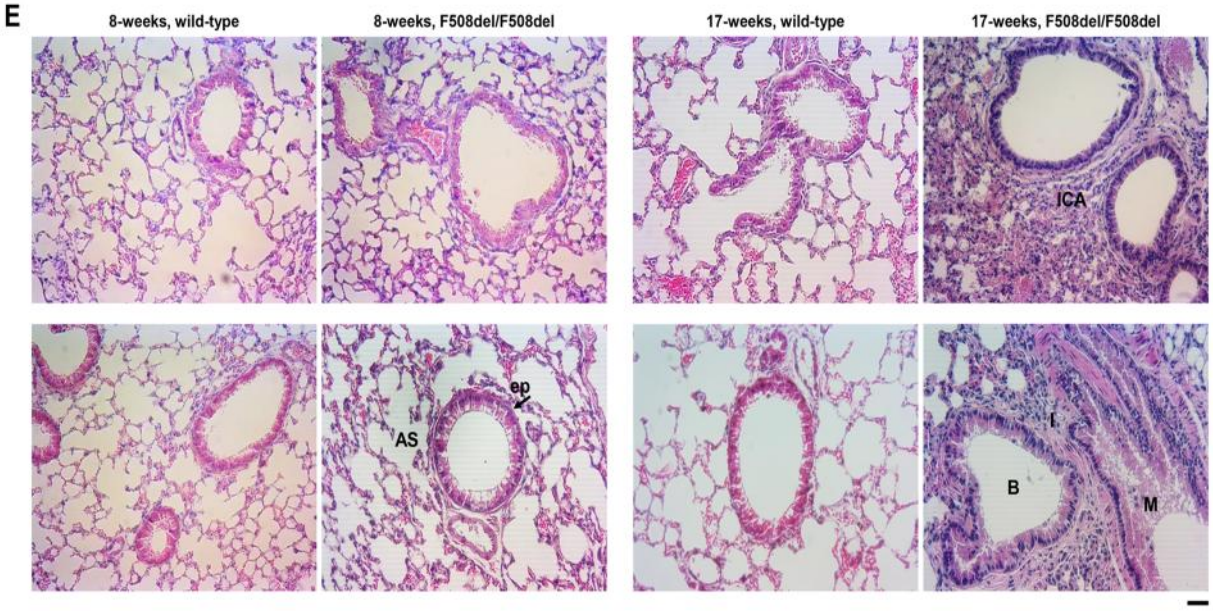
E
8-weeks, wild-type
8-weeks, F508del/F508del
17-weeks, wild-type
17-weeks, F508del/F508del
ICA
ep
AS
I
B
M

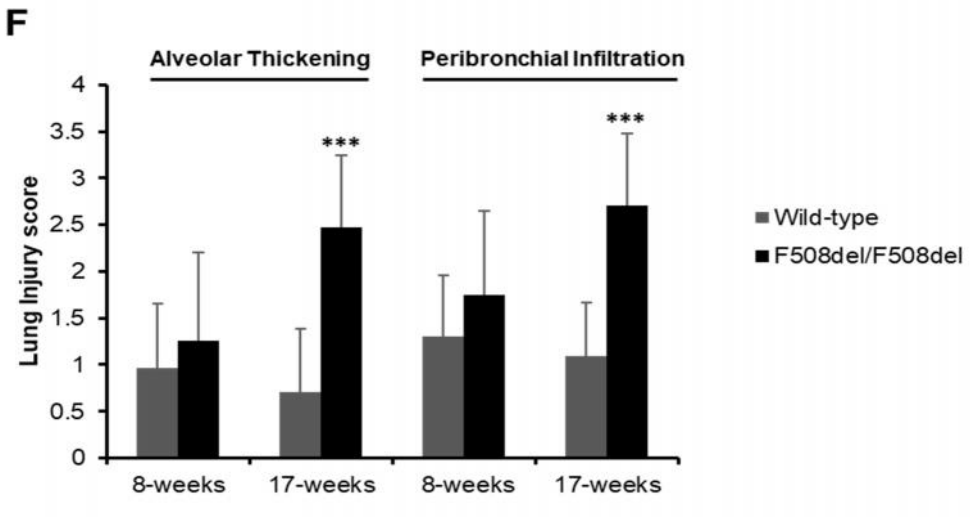
F
Alveolar Thickening
Peribronchial Infiltration
Lung Injury score
4
3.5
3
2.5
2
1.5
1
0.5
0
***
***
8-weeks
17-weeks
8-weeks
17-weeks
Wild-type
F508del/F508del

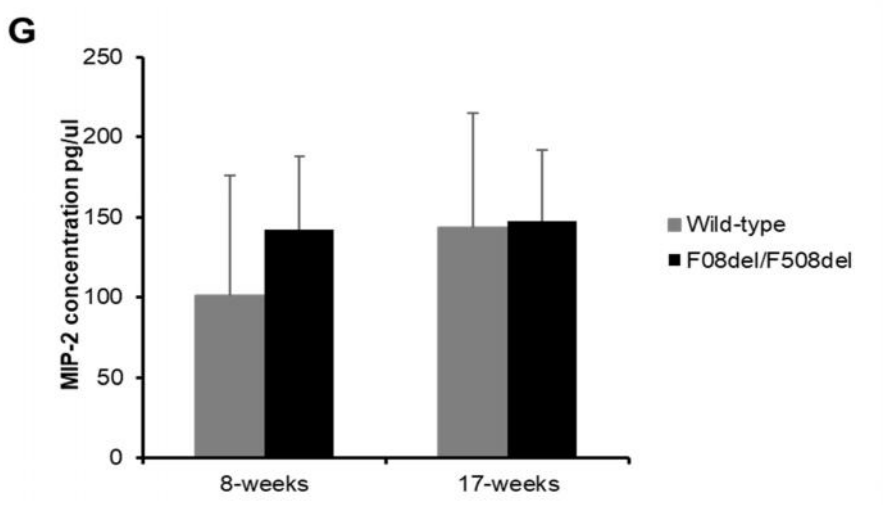

Figure 4.4: VIP signal in the lungs.

A & B, Representative images (A, 40X objective) of lung tissues showing VIP signal (dark brown, black arrows) revealed by IHC, in wild-type and CF (F508del/F508del) mice at 8- and 17-week-old. ***B,*** High magnification images (60X objective) of representative images of the same groups. ***C,*** Negative control where the VIP antibody was omitted. ***D,*** Semi-quantification of VIP signal. Histogram bars represent averages of 8 to 15 images from each mouse (3 to 5 mice per age group, N = 3). Arbitrary scale from 0 to 3 indicates: 0 = none, 0.5 = minimal, 1 = low, 1.5 = some, 2 = moderate, 2.5 = strong and 3 = highest. Ep = epithelium. Scale 20µm. ***p < 0.001. ***E,*** Histology images of lung tissues from 8- and 17-week-old wild-type and CF (F508del/F508del) mice. 5µm thick sections were H&E stained before light microscopy imaging at 20X magnification. Compared to wild-type, tissues from 8-week-old CF mice showed minimal signs of disease, whereas tissues from 17-week-old CF mice showed some inflammation, inflammatory cells aggregation (ICA), thickening of alveolar walls, moderate tissue damage and mucus presence. B: bronchiole, AS: alveolar space, ep: epithelium, I: inflammation, M: mucus. Scale:100µm. (3 to 5 mice per age group, N = 3). ***F,*** Histological lung scoring for alveolar thickening and peribronchial infiltration in wild-type and CF (F508del/F508del) mice at 8- and 17-week-old (3 to 5 mice in each group. N = 2). ***p < 0.001. ***G,*** MIP-2 concentration measured by ELISA in 8- and 17-week-old wild-type and CF mice lung tissue homogenates, normalized to total proteins (5 mice, N = 2 performed in duplicates).

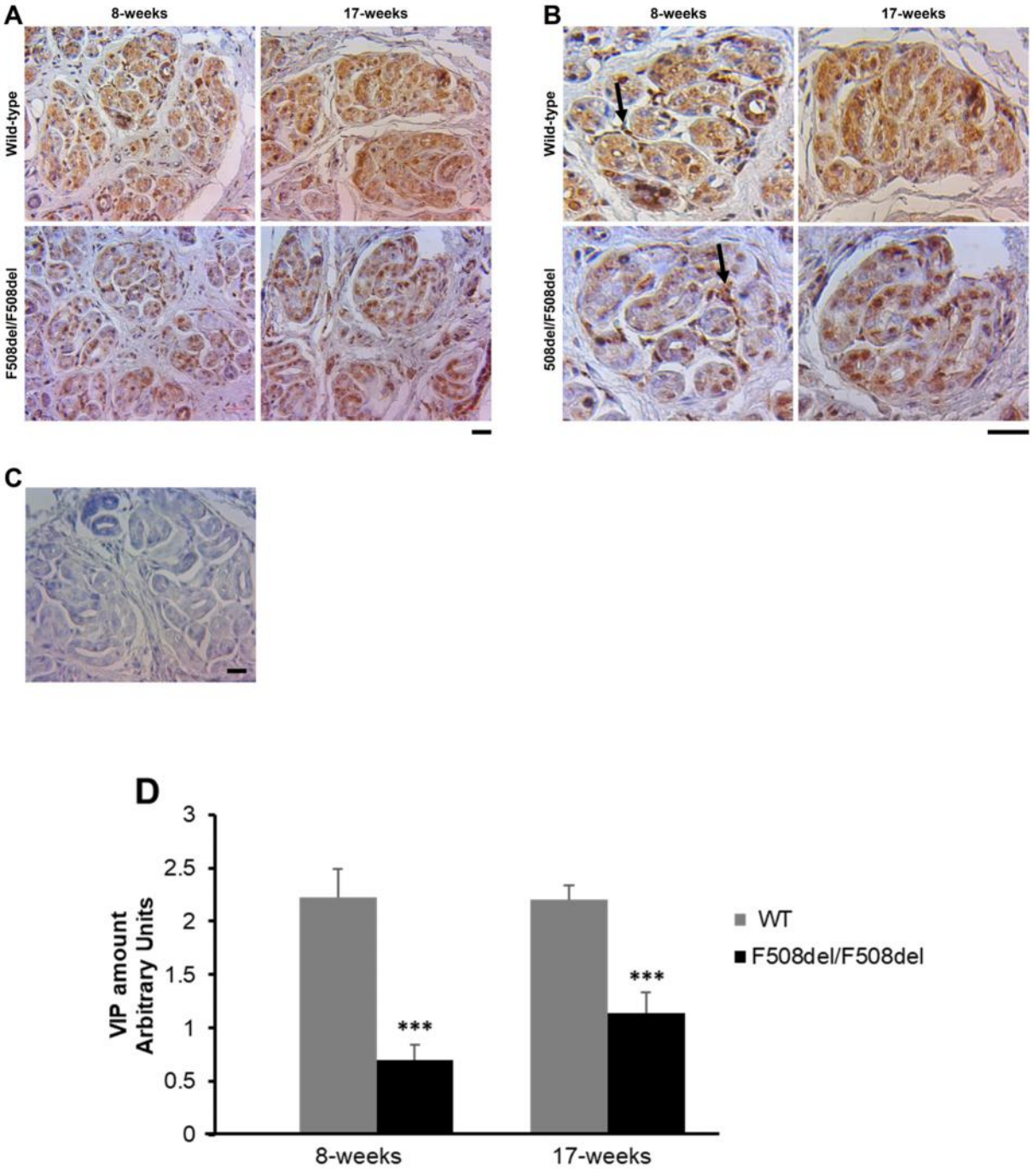
A
8-weeks
17-weeks
Wild-type
F508del/F508del
B
8-weeks
17-weeks
Wild-type
508del/F508del
C
D
VIP amount
Arbitrary Units
3
2.5
2
1.5
1
0.5
0
***
***
8-weeks
17-weeks
WT
F508del/F508del

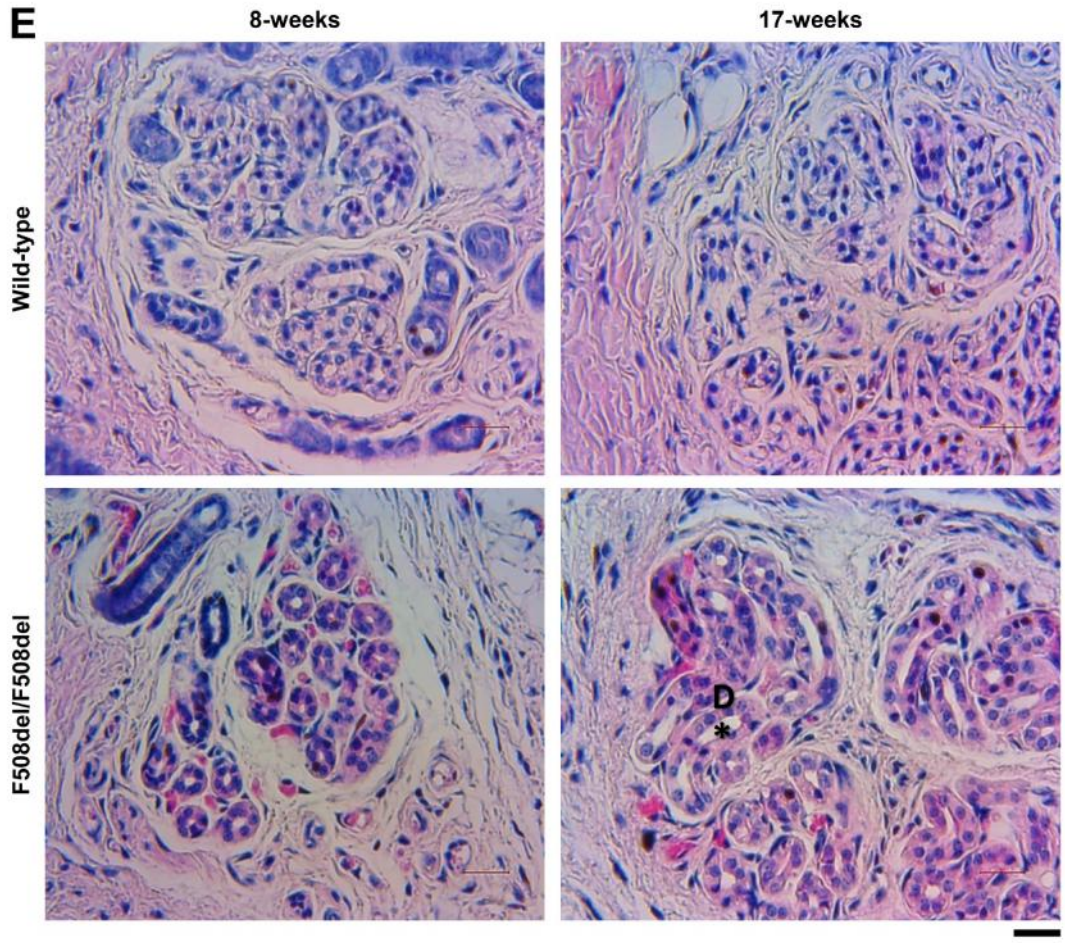

Figure 4.5: **VIP signal in the sweat glands**.

A & B, Representative images (*A*, 40X objective) of sweat glands showing VIP signal (dark brown, black arrows) revealed by IHC, in wild-type and CF (F508del/F508del) mice at 8- and 17-week-old. ***B,*** High magnification images (60X objective). ***C,*** Negative control where the VIP antibody was omitted. ***D,*** Semi-quantification of VIP signal. Histogram bars represent averages of 8 to 15 images from each mouse (3 to 5 mice per age group, N = 3). Arbitrary scale from 0 to 3 indicates: 0 = none, 0.5 = minimal, 1 = low, 1.5 = some, 2 = moderate, 2.5 = strong and 3 = highest. Scale 20 µm (A & C) and 50 µm (B). ***p < 0.001. ***E,*** Histology images of sweat glands from 8- and 17-week-old wild-type and CF (F508del/F508del) mice. 5µm thick sections were H&E stained before imaging with a light microscope at 40X magnification. D = sweat gland duct. Scale: 100 µm.

4.4.3 VIP innervation is strongly reduced at the mucosa and myenteric plexus of CF duodenum tissues.

VIPergic innervation was previously found to be sparse or absent from the skin of humans with CF. In the present study, we examined VIP innervation in the duodenum of 8-week-old CF mice to determine if a similar finding can be made and to correlate the reduction in VIP content with a change of innervation. The duodenum contains several layers including the myenteric plexus, circular muscle, submucosal plexus and mucosal layer (Fig. 4.6F) (Furness, 2006). We used the whole-mount immunofluorescence method with a specific VIP antibody to stain the VIPergic neuronal network. Confocal microscopy images and 3D reconstitution of the immunofluorescence signal demonstrated a lower level of aggregation of VIP-positive nerve fibers at the mucosa and myenteric plexus layers of CF duodenum (Fig. 4.6). More specifically, in CF tissues, VIP innervation in the primary layer of the myenteric plexus was lost as well as in the deeper circular muscle layer (Fig. 4.6D bottom). Also, at the CF mucosa layer, the dense continuous network of VIP nerve fibers that is normally visible in the lamina propria region with WT tissues, seemed to have lower density and in some areas was sparse (Fig. 4.6B bottom, Supplementary movie at https://www.cysticfibrosisjournal.com/article/S1569-1993(20)30777-3/fulltext#supplementaryMaterial). At the mucosa layer, the VIP neuronal network was severely damaged in CF tissues compared to the myenteric plexus layer (Fig. 4.6B bottom). This is an interesting finding since the mucosa layer was reported to contain the highest density of VIP nerve fibers in humans (Anlauf et al., 2003).

Figure 4.6: VIP innervation at the mucosa and myenteric plexus of duodenum tissues.

Representative confocal microscopy images (right panels: high power magnification; left panels: low power magnification) showing VIP innervation at the mucosa and myenteric plexus layers of duodenum tissues from 8-week-old F508del homozygote CF mice ***(B, D)*** compared to same age wild-type mice ***(A, C)***. Fresh tissues were prepared for whole mount immunofluorescence as described in the method section and immunostained with a monoclonal anti-VIP antibody followed by secondary antibody conjugated with Alexa Fluor 555. Experiments were performed on tissues from 5 mice and repeated three times (N = 3). ***E,*** Negative control where the VIP antibody was omitted. ***F,*** Schematic representation of intestinal tissue layers. Scale:100 µm.

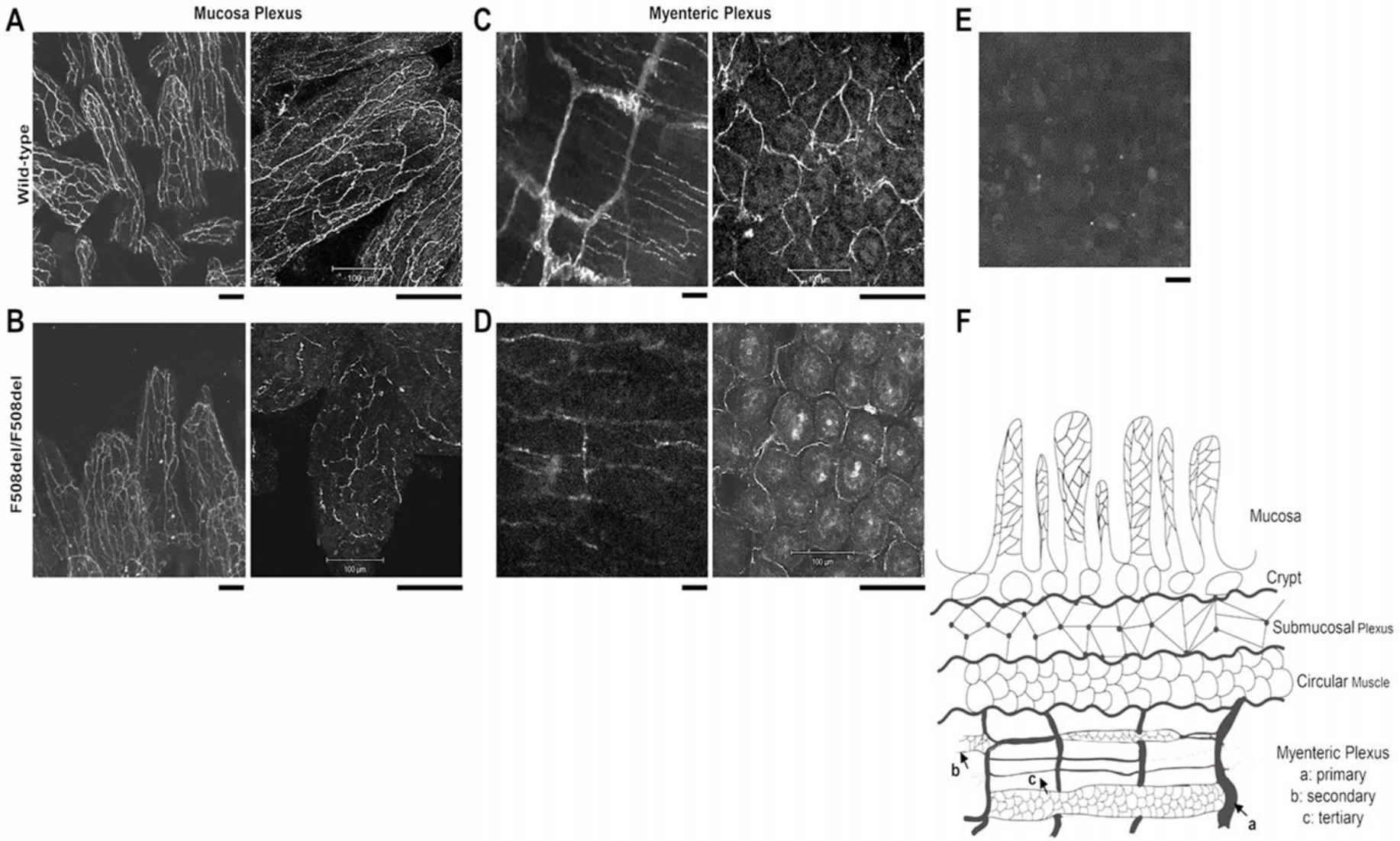
A
Mucosa Plexus
C
Myenteric Plexus
E
Wild-type
B
D
F
F508del/F508del
100 µm
Mucosa
Crypt
Submucosal Plexus
Circular Muscle
Myenteric Plexus
a: primary
b: secondary
c: tertiary
a
b
c

4.4.3.1 The general innervation is disrupted in the myenteric plexus of the CF duodenum.

To further investigate changes in innervation of CF mice intestinal tissues, we examined the morphological integrity of the nervous system using a general neuronal marker, PGP 9.5 (Schofield et al., 1995). PGP 9.5 is a member of the ubiquitin C terminal carboxyl hydrolase isozymes family (UCHL1). It is a cytoplasmic protein that is involved in the regulation of the ubiquitin pathway which is widely expressed in neuronal tissues, making up 1-2% of soluble brain proteins. Studies have shown that PGP 9.5 antibody stain neuronal cell bodies and axons in the CNS and periphery, small nerve fibers in peripheral tissues as well as neuroendocrine cells in the pituitary, thyroid, lungs and the gastrointestinal track (Schofield et al., 1995). In our experiments, the whole-mount immunofluorescence signal for PGP 9.5 showed well-shaped villi with strong general innervation of mucosa and myenteric plexus in WT duodenum tissues (Fig. 4.7A) while in CF duodenum tissues two out of three components of the myenteric plexus were lost (primary and secondary plexus) with the presence of enlarged ganglionic cells in the tertiary layer (Fig. 4.7B). Interestingly, in all our experiments, in both WT and CF, we were not able to visualize any PGP 9.5 or VIP staining in the inner circular muscle layer of the myenteric plexus. Also, in the CF mucosal layer we observed an increased number of cell bodies in the lamina propria area compared to WT (Fig. 4.7B). This finding suggests a potential accumulation of VIP in enlarged ganglionic cells that we observed at the myenteric plexus. Our data suggest a disorganization of the intrinsic neuronal network as a whole in CF mice intestine that could justify the sparse VIP innervation.

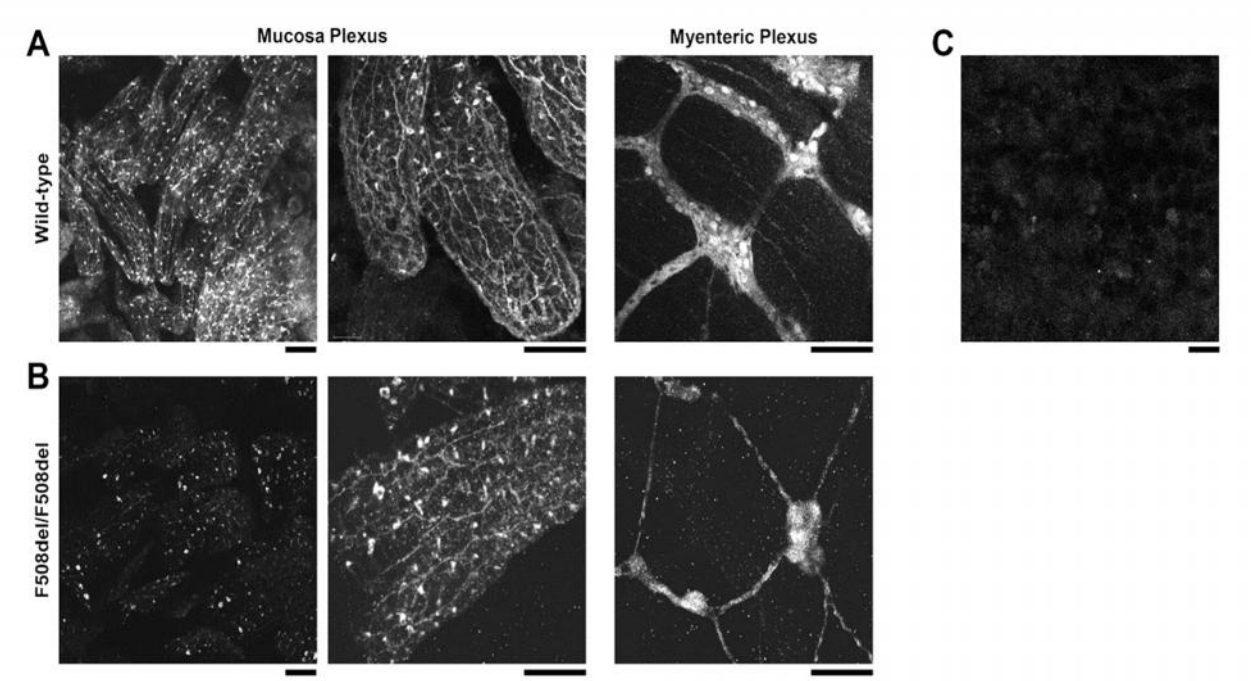

Figure 4.7: General innervation at the mucosa layer of duodenum tissues.

Representative confocal microscopy images showing general innervation at the mucosa (left panel: low power magnification; middle and right panels: high power magnification) and myenteric plexus of duodenum tissues from 8-week-old CF (F508del/F508del) mice ***(B)*** compared to same age wild-type mice ***(A).*** Fresh tissues were prepared for whole mount immunofluorescence experiments as described in the method section and immunostained with a monoclonal anti-PGP 9.5 antibody followed by secondary antibody conjugated with Alexa Fluor 555. Experiments were performed on tissues from 5 mice and repeated three times (N = 3). ***C,*** Negative control where the PGP 9.5 antibody was omitted. Scale: 100µm.

4.4.3.2 The cholinergic neuronal network is damaged in CF duodenum. Co-localization of VIP with acetylcholine has been previously demonstrated (Anlauf et al., 2003). In addition, there is a small number of enteric neurons that can be mainly cholinergic or mainly VIPergic (Anlauf et al., 2003). In CF, the functional synergy between VIP and Acetylcholine is lost (Jae et al., 2007). We further examined the acetylcholine innervation of wild-type and CF duodenum and compared the results with the observed alteration in the VIPergic innervation. The presence of cholinergic neurons was revealed with an antibody raised against choline acetyltransferase (ChAT), an enzyme involved in the formation of acetylcholine. In whole mount fluorescence experiments, the data reveal that CF duodenum tissues have highly disrupted cholinergic innervation of the mucosal layer and myenteric plexus layer with major loss of cell bodies in contrast to the longitudinal and latitudinal ChAT signal in the mucosa with the presence of many cell bodies and densely innervated myenteric plexus that were observed in the duodenum of WT tissues (Fig. 4.8A & 4.8C top *vs.* 4.8B & 4.8D bottom).

These results indicate that cholinergic neurons are affected in CF, however not to the same extent as VIPergic neurons, suggesting that some cholinergic specific innervation is still intact. We also performed a qualitative assessment of ChAT signal by immunohistochemistry in paraffin embedded sections of duodenum from 8-week-old CF mice and compared it with the same age WT tissue sections. We found that the cholinergic innervation was well visible around the crypt area (submucosa) that leads to the nerve supply of the lamina propria area (mucosa plexus) in WT mice, but was minimal in CF mice tissue sections, confirming whole mount immunofluorescence data (Fig. 4.9).

Furness (2000) has shown that cholinergic secretomotor/vasodilator axons give rise to the mucosal innervation and in our study those axons are missing or are sparse in CF tissues (Furness, 2000). We observed an unexpected ChAT staining around the epithelium of the villi similar to a recent study from Takahashi *et al.* (2014) that demonstrated a non-neuronal ACh synthesis in mouse gut sections and crypt-villus axis organoids that do not have neurons and immune cells (Takahashi et al., 2014). Our data show that the distribution of the intrinsic VIPergic and cholinergic neuronal network is affected in the small intestine of CF mice.

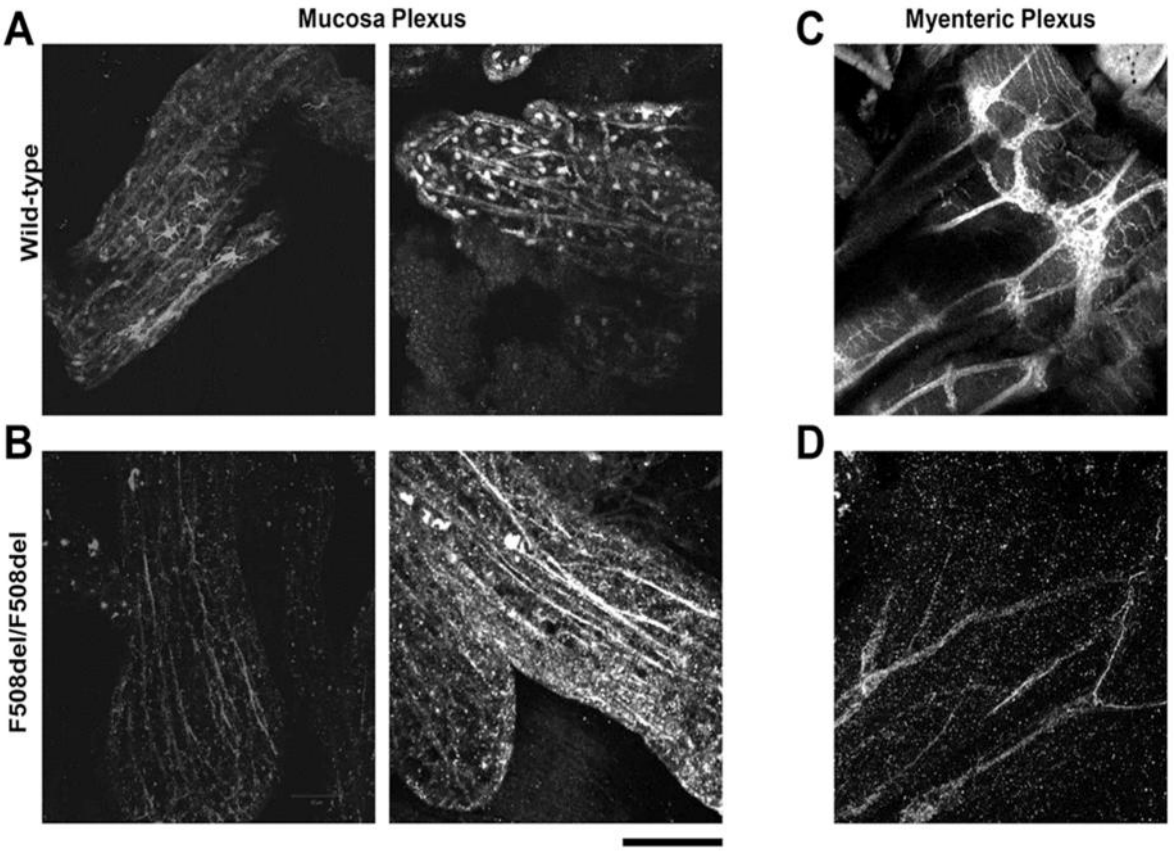

Figure 4.8: Significant disruption of cholinergic neuronal network in CF duodenum tissues.

Representative confocal microscopy images showing cholinergic innervation at the mucosa and myenteric plexus of duodenum tissue from 8-week-old CF mice (F508del/F508del) **(*B, D*)** compared to same age wild-type mice **(*A, C*)**. Fresh tissues were prepared for whole mount immunofluorescence as described in the method section and immunostained with a monoclonal anti-ChAT antibody followed by secondary antibody conjugated with Alexa Fluor 555. Experiments were performed on tissues from 5 mice and repeated three times (N = 3). Scale 100µm.

Figure 4.9: Significant loss of cholinergic innervation in the 8-week-old CF mice duodenum.

Significant loss of cholinergic innervation in the 8-week-old CF mice duodenum. ***A & B,*** Representative images of duodenum tissues showing cholinergic innervation (ChAT: dark brown, black arrows) revealed by IHC, in wild-type and CF (F508del/F508del) mice (5 mice), N= 3. Scale 50 µm.

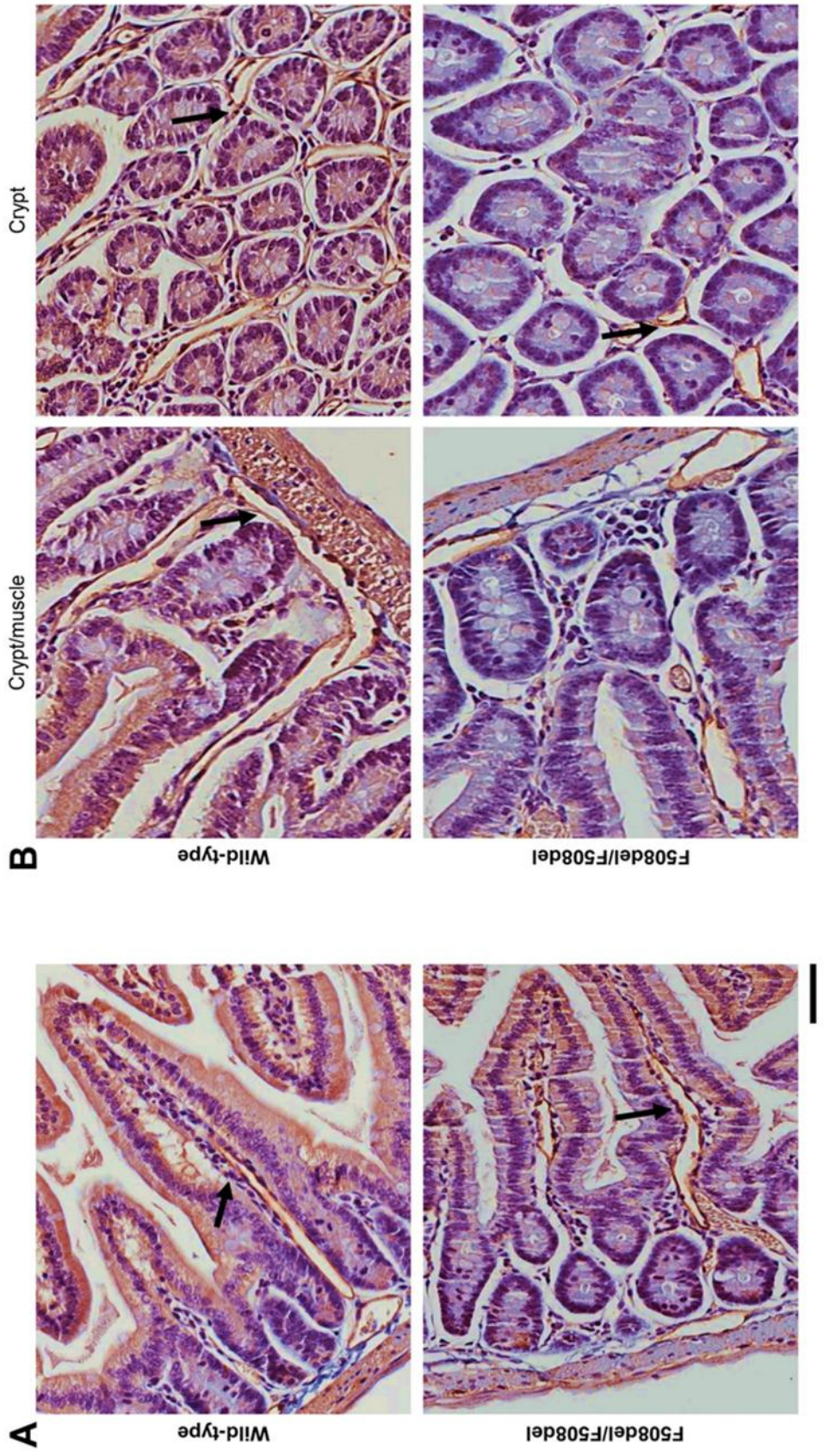
B
Crypt
Crypt/muscle
Wild-type
F508del/F508del
A
Wild-type
F508del/F508del

4.5 Discussion

The significance of VIP in CFTR regulation is well studied at the cellular level (Alcolado et al., 2011; Alcolado et al., 2014; Alshafie et al., 2014; Chappe F. et al., 2008; Chappe et al., 2012). Moreover, a study from Alcolado *et al.* (2014) demonstrated that VIP knockout mice (VIP-KO) display a CF-like phenotype characterized by lymphocyte aggregation, increased airway secretion, alveolar thickening and edema in the lung, as well as by goblet cell hyperplasia and tissue alterations in the duodenum (Alcolado et al., 2014). VIP treatment reversed those pathological signs close to a wild-type phenotype and regulated CFTR membrane stability.

Here, we have examined the presence of VIP in the lungs, duodenum and sweat glands of F508del-CFTR mice at a young age (8-week-old) where the disease was very minimal and tissue morphology was close to wild-type. We also used older age mice (17-week-old) with multiple signs of well-developed pathology. In both age groups, the amount of VIP was strongly reduced compared to wild-type. Interestingly, the amount of the VIP present in wild-type mice was higher in younger mice and declined progressively with age (data not shown). In CF tissues however, a consistent low amount of VIP was found independently of the age or pathological signs. A study from El-Salhy *et al.* (1999) using NMRI/Bom mice has demonstrated age-related changes in various peptide concentrations in different parts of the gastrointestinal track (El-Salhy et al., 1999). The reason for those age-related peptide changes to our knowledge remain unknown. We found a strong reduction of the amount of VIP in the duodenum as well as in the lung and sweat glands of CF mice presenting minimal signs of spontaneous disease at 8 weeks

of age. A study from van Doorninck *et al.* (1995) similarly reported that young homozygous ΔF508 mice (5-7 weeks) do not present severe pathological signs in the small intestine compared to Cftr null mice that showed severe goblet cell hyperplasia, mucus overproduction and luminal obstruction in the ileum (van Doorninck et al., 1995). Spontaneous disease manifestations seem to appear later on during development. 12-week-old mice with the ΔF508 mutation have been shown to present intestinal morphological alterations including goblet cell hyperproliferation, increased crypt to villus axis as well as thicker circular muscle layer compared to their wild-type littermates (Bazett et al., 2015). This is similar to what we have observed in the 17-weeks old mice used in the present study. As mice were kept in clean and sterile environment, we did not expect any spontaneous lung pathology, at least in the young mice. However, we observed significant signs of spontaneous lung disease in the 17-week-old animals. Similarly, a study from Guilbault *et al*. (2006) using 16-20 weeks uninfected Cftr null mice, showed cell infiltration in the bronchi and alveoli, fibrosis and hyperplasia of the epithelium compared to wild-type littermates (Guilbault et al., 2006). Altogether these data confirm disease progression in the lung of aging CF mice, in absence of induced bacterial infection.

The intrinsic nervous system around sites of importance in cystic fibrosis has not yet been broadly studied. Heinz-Erian *et al.* (1985) were the first to describe a reduced VIPergic innervation of the sweat glands in humans with CF (Heinz-Erian et al., 1985), linking the loss of fluid secretion in CF to abnormality in the intrinsic nervous system regulating exocrine glands. Jie Pan *et al.* (2006) have shown a reduced density of the intrinsic

innervation of airways smooth muscles which started *in utero* and continued post-natal in Cftr knockout mice (Pan et al., 2006). The present study confirms those data and expand it to other tissues in both young and older CF mice carrying the ΔF508 mutation. CFTR dysfunction is not only linked to pulmonary and gastrointestinal pathology but is also associated with extra-pulmonary diseases such as cystic fibrosis related diabetes (CFRD), end-stage liver disease, chronic sinusitis, changes in circadian clock, decreased olfaction, retinal epithelia dysfunction, changes in homeostasis and energy metabolism (Liou, 2019). Although CFTR is mainly expressed in epithelial cells, some studies suggest that it could also be present in the peripheral and central nervous system (CNS). In the CNS, CFTR mRNA was found in the hypothalamus, thalamus, arcuate and amygdaloid nuclei areas. In newborn CFTR-KO pigs, Reznikov *et al.* (2013) found that Schawnn cells are an important site of CFTR expression (Reznikov et al., 2013). The authors suggested that altered neuronal function might contribute to mucus secretion and intestinal obstruction in older patients with CF. Although it is well known that neuronal activity regulates submucosal glands secretion and intestinal motility, whether the neuronal abnormalities observed in CF tissues are coming as primary or secondary disease manifestations is not clear yet. Free of inflammation tissues such as the sweat glands had highly decreased content in the VIP peptide, both in human and mice with CF. Our data argue in favor of a primary disease manifestation, prior to tissue inflammation and damage.

VIP-immunoreactive fibers innervate all exocrine glands, including sweat gland acini, respiratory epithelium, pancreas and intestine. VIP relaxes smooth muscles, increases

mucus and enzyme secretions and works in synergy with acetylcholine to promote electrolyte secretion through the activation of CFTR (Chappe et al., 2012). In the gastrointestinal track, motility and secretion are controlled by both intrinsic and extrinsic nervous system. Colonic strictures in patients with cystic fibrosis who received high-dose pancreatic enzyme supplements where shown to contain ganglion cell abnormalities and increased mucosal cholinergic and adrenergic activity. A case report by Johannes Wildhaber *et al.* (1996) in a newborn girl with cystic fibrosis and neuronal intestinal dysplasia type B (NID-B), had shown intestinal malformation characterized by hyperplasia of the myenteric plexus with an increased number of cholinergic nerves in the circular muscle layer while in the submucosa there were detected cholinergic nerve bundles branching into the lamina propria area (Wildhaber et al., 1996). In the present study, we did not include the colon, but we found that the VIP-positive as well as ChAT-positive network of nerve fibers is significantly disrupted in the small intestine. In the duodenum of CF mice with minimal disease progression, we found that VIPergic fibers are sparse in both the mucosa and myenteric plexus, compared to the dense continuous neuronal network of the duodenum layers in wild-type mice. We also found that the signal from a general neuronal marker, PGP 9.5, was altered in CF. Duodenum tissues presented major neuronal changes in the myenteric plexus which displayed enlarged clusters of ganglionic cells and loss of two of the three components of the myenteric plexus, the primary and the secondary plexus (Furness, 2008). The general innervation of the mucosa plexus layer in CF mice showed more cell bodies in the connective tissue (lamina propria) of the mucosa in comparison to wild-type mice. Given that the co-localization of acetylcholine

and VIP in the intrinsic innervation of the intestine of mammals is well studied and their synergistic action is lost in CF, we also asked if the cholinergic neuronal network shows the same disruption as the VIP nerve fibers in CF mice tissues. Interestingly, our data revealed that there is a significant decrease in the density of the cholinergic neurons in the myenteric plexus while the mucosa layer is characterized by less cell bodies compared to the wild-type and loss of latitudinal cholinergic neuronal network.

A recent study suggests that CFTR is expressed in both peripheral and central nervous systems. Xue *et al.* (2016) demonstrated CFTR mRNA and protein expression in the ganglia of the human gastrointestinal track (Xue et al., 2016). Accordingly, neuronal alterations of the nervous system could be responsible for some of the CF disease manifestations. Changes in neuronal innervation could, therefore, be expected in CF compared to healthy tissues and could be linked to the findings from the present study where VIPergic and cholinergic neurons are affected, thus reducing the production and distribution of these two neurotransmitters to important sites of CF manifestation. This would also explain, at least in part, functional data with a lost VIP/acetylcholine synergy in fluid secretion by CF glands.

Dysfunction of the VIPergic system has been proposed to be involved in the pathophysiology of several diseases in the gut, such as intestinal ileus, inflammatory bowel disease, but also of Type II diabetes, bronchial asthma, COPD and more due to the loss of VIP peptide, suggesting that the absence of VIP could play a role in aggravating those pathologies (Atanasova et al., 2018; Chappe et al., 2012; Sanlioglu et al., 2012). In cystic fibrosis, old data suggested that VIP-positive fibers of the skin of CF patients are

sparse compared to healthy tissues (Heinz-Erian et al., 1985), but this has never been thoroughly investigated. Our data suggest that the strong reduction in VIP is an early defect in CF, which starts before important disease manifestation. We also found a pronounced reduction in both VIP-specific and cholinergic innervation at the mucosa and myenteric plexus of CF mice duodenum. The general intrinsic innervation of the tissue was discontinued in the mucosal layer with major disruption of the myenteric plexus layers. We propose that the deficiency in VIP is not attributed to disease progression, but rather results from a disruption of the intrinsic innervation network. Our data represent a significant progress in the understanding of CF pathology at the tissue level and explain, at least in part, the lost of functional synergy between VIP and acetylcholine in the regulation of secretions in CF glands, a hallmark of CF disease.

4.6 Acknowledgments

This work was supported by Cystic Fibrosis Canada and the Cystic Fibrosis Foundation (USA) research grants. A.S. was supported by a Faculty of Medicine Excellence in Research Award and by CFF grant. The authors thank Stephen Whitefield (Dalhousie CMDI) and Arnaud Gaudin for expert advice with confocal microscopy and digital imaging, Dr. X. Zhu for expert pathological opinion, Patricia Colp for technical expertise with histology as well as Konstantina Semaniakou for designing the intestinal layers in figure 4.6F.

4.7 Conflict of Interest Statement.

There are no conflicts of interest to declare.

CHAPTER 5: VIP REDUCTION IN THE PANCREAS OF F508-DEL HOMOZYGOUS CF MICE AND EARLY SIGNS OF CYSTIC FIBROSIS RELATED DIABETES (CFRD)

The figures and text presented in this chapter are from a manuscript submitted to the Journal of Cystic Fibrosis: Anna Semaniakou, Frederic Chappe, Younes Anini, and Valerie Chappe (2020). VIP reduction in the pancreas of F508del homozygous CF mice and early signs of Cystic Fibrosis Related Diabetes (CFRD). *Journal of Cystic Fibrosis*.

As the first author on this article, I performed most of the experiments, analysis, data interpretation, statistics and wrote the manuscript. The manuscript was edited by Dr. Valerie Chappe and Dr. Younes Anini.

5.1 Abstract

Vasoactive Intestinal Peptide (VIP), a 28-amino acid neuropeptide with potent anti-inflammatory, bronchodilatory and immunomodulatory functions, is secreted by intrinsic neurons innervating all exocrine glands, including the pancreas in which it exerts regulatory function for the secretion of insulin and glucagon. Cystic Fibrosis-Related Diabetes (CFRD) is the most common co-morbidity associated with cystic fibrosis (CF) impacting approximately 50% of adult patients. CF is caused by the deficiency or absence of the cystic fibrosis transmembrane conductance regulator (CFTR) chloride channel from the apical membrane of epithelial cells due to mutations in the CFTR gene. The CFTR protein is mainly regulated by VIP. We recently demonstrated a 50 % reduction of VIP abundance in the lungs, duodenum and sweat glands of C57Bl/6 CF mice homozygotes for the F508del-CFTR mutation. This VIP deficiency resulted from a reduction in VIPergic and cholinergic innervation, starting before signs of CF disease were observed. As VIP functions as a neuromodulator with strong anti-inflammatory properties and insulinotropic effects on pancreatic beta cells, we sought to study changes in VIP in the pancreas of CF mice. Our goal was to examine VIP content and VIPergic innervation in the pancreas of 8- and 17-week-old F508del-CFTR homozygous mice, to determine if changes would contribute to CFRD development. Our data show that a low amount of VIP and reduced innervation are found in CF mice pancreas correlated with reduced insulin secretion, up-regulation of glucagon production, and high random blood glucose levels, compared to same age WT mice. We propose that low amount of VIP, due to reduced innervation of the CF pancreas, and starting at an early disease stage,

contributes to changes in insulin and glucagon secretion that can lead to CFRD disease development.

5.2 Introduction

Vasoactive Intestinal Peptide (VIP), which was discovered in the 1970s by Said and Mutt, is a 28-residue amino acid polypeptide, first isolated from porcine small intestine as a vasodilatory peptide (Said et al., 1970; Said et al., 1972). It belongs to a superfamily of brain-gut peptide hormones structurally related to secretin, glucagon and pituitary adenylyl cyclase-activating peptide (PACAP) superfamily (Said et al., 1970; Said, 1991). VIP mediates its functions through VPAC1 or VPAC2 receptors that are G protein-coupled receptors (Iwasaki et al., 2019). VIP is expressed in the central and peripheral nervous systems as well as in the digestive, respiratory, reproductive, and cardiovascular systems as a neurotransmitter or neuromodulator (Iwasaki et al., 2019; Umetsu et al., 2011). Additionally, it has potent anti-inflammatory, bronchodilatory and immunomodulatory functions and plays a crucial role in maintaining airways clean through mucociliary clearance, contributing to local innate defense by stimulating the movement of water and chloride across intestinal and tracheobronchial epithelium (Heinz-Erian et al., 1985; Said, 1991; Said, 1991; Said, 2008). Previous data from Chappe and colleagues have demonstrated that chronic VIP exposure is needed to maintain functional CFTR chloride channels at the cell surface of airways and intestinal epithelium, as well as normal exocrine tissue morphology (Alcolado et al., 2011; Alcolado et al., 2014; Alshafie et al., 2014; Chappe et al., 2012; Rafferty et al., 2009). Mutations in the CFTR gene cause CF

disease, the most common, fatal, chronic, autosomal and recessive disease in European and north American populations. Worldwide, one in 2,500 children are born with CF and approximately 100,000 people are affected with the disease (Kelly, 2017). While the primary cause of morbidity and mortality is progressive obstructive lung disease, CF is a multifactorial disorder due to the CFTR expression in multiple organs. In addition to the lungs, it affects the gastrointestinal track, the liver, the pancreas and the reproductive systems (Kelsey et al., 2019).

As the life expectancy of patients with CF is improving, cystic fibrosis-related diabetes (CFRD) is becoming the most prevalent CF co-morbidity, increasing the mortality rate by 6-fold in comparison to CF patients without diabetes (Brennan et al., 2004). CFRD impacts approximately 2% of children, 19% of adolescents, and 50% of adults over the age of 30 with CF and appears to affect females slightly more than males (Gibson-Corley et al., 2016; Laguna et al., 2010). Usually, CFRD is not detected before the age of 10 as the disease onset is thought to produce an asymptomatic phenotype (Barrio, 2015; Gibson-Corley et al., 2016; Konrad, et al., 2013). CFRD is a complex disease, also identified as pancreatogenic (type 3c) diabetes, and does not fall into either type 1 or 2 diabetes categories (Rickels, 2015). It constitutes a special, separate category that has features of type 1 diabetes (T1D) and type 2 diabetes (T2D) with specific pathophysiological differences to apart its own distinct classification (Hart et al., 2018). CFRD is characterized by decreased insulin secretion from the loss of beta cell mass and progressive increase in inflammation (Gibson-Corley et al., 2016). Some of the most common risk factors that could predispose patients to CFRD are severe CFTR genotypes (class *I*, *II* and *III* CFTR gene

mutations), modifier genes, family background of T2D and pancreatic insufficiency (Barrio, 2015; Blackman et al., 2013; Granados et al., 2019; Hart et al., 2018; Konrad, Scheuing, et al., 2013; Moran et al., 2010).

VIP is known to augment insulin secretion in the presence of glucose (Iwasaki et al., 2019; Sanlioglu et al., 2012). Through VPAC2, that is highly expressed in the pancreatic islets, VIP activates adenylate cyclase (AC) to increase intracellular cAMP levels that triggers protein kinase A (PKA) activation and EPAC sensors resulting in membrane depolarization from the closure of ATP-dependent K^+ channels, and calcium (Ca^{2+}) entry into cells. Influx of calcium into the cells initiates insulin secretion after glucose stimulation (Winzell et al., 2007). While numerous studies, utilizing genetically altered mice models, have examined the therapeutic ability of VIP and VPAC receptor agonists to modulate glucose-induced insulin secretion on T2D, to our knowledge, none of them have investigated their role in CFRD (Henquin, 2000; Persson-Sjögren et al., 2006; Sanlioglu et al., 2012; Tsutsumi et al., 2002). In a recent study, we have demonstrated that VIP content is 50% lower in the lung, sweat glands and small intestine of C57Bl/6 mice homozygotes for the F508del-CFTR, compared to WT. This deficiency resulted from a reduction in VIPergic and cholinergic innervation, starting at a young age, before signs of CF disease were observed (Semaniakou et al., 2020). In the present study, we asked if there were changes in VIP abundance and innervation of the pancreas, at different stages of CF disease progression, that could affect insulin and glucagon secretion and contribute to CFRD development. We used 8- and 17-week-old CF mice homozygotes for the F508del-CFTR mutation, the most common disease-causing mutation found in patients with CF and associated with

higher risk for CFRD pathogenesis. Our data show that VIP reduction, due to reduced innervation of the pancreas, affects insulin and glucagon secretion, potentially leading to the development of CFRD.

5.3 Materials and Methods

5.3.1 Chemicals. Antibodies are shown in Table 4; Normal mouse blocking serum was from Santa Cruz Biotechnology (ImmunoCruz goat ABC Staining System; sc-2023); Normal rabbit blocking serum was from Santa Cruz Biotechnology (ImmunoCruz goat ABC Staining System; sc-2018); Normal donkey serum (D9663) was from Sigma (St. Louis, MO); Normal goat blocking serum was from Vector Laboratories (Cat. No. NC9270494); Avidin-Biotin complex was from Santa Cruz (ImmunoCruz ABC kit; sc-516216); DAB (3, 3 -diaminobenzidine) HRP Substrate Kit (ab64238) was from Abcam; Enzyme-Linked-Immunosorbent Assay kit for murine VIP was from Cloud-Clone Corp. (Cat. No. CEA380Mu; Houston-TX); Enzyme-Linked-Immunosorbent Assay kit for murine Insulin was from Millipore (Cat. No. EZRMI-13K); Cayman's Glucose Colorimetric assay kit was from Cayman Chemical (Cat. No. 10009582); Vectashield Mounting Media for Fluorescence was from Vector Laboratories (Cat. No. 101098-042). Protease inhibitor cocktail tablets were from Roche (complete, Mini; Cat. No. 11 836 153 001). Other chemicals were from Sigma and of the highest grade available.

Table 4: Summary of Antibodies and their Dilutions Used in Chapter 5.

Polyclonal Primary Antibodies	Dilution & Application	Secondary Antibodies	Dilution
Anti-VIP (Cat. No. PA5-78224); Thermofisher (CA, USA)	1:100 (IHC)	ImmunoCruz rabbit avidin/biotynilated complex Staining System (sc-2018), Santa Cruz Biotechnology	As per kit instructions
Anti-PGP 9.5 *(*ab15503), Abcam (Cambridge, MA)	1:200 (IHC)	ImmunoCruz rabbit avidin/biotynilated complex Staining System (sc-2018), Santa Cruz Biotechnology	As per kit instructions
Anti-Insulin (ab7842) Abcam (Cambridge, MA)	1:50 (IHC)	Goat anti-guinea pig IgG, Fc fragment specific (Cat. No. 106-035-008); Jackson Laboratories (Pennsylvania, USA)	1:500
Anti-Glucagon (sc-13091; FL-180; Lot No. K0304); Santa Cruz Biotechnology (Santa Cruz, CA)	1:50 (Immunofluo-rescence)	Donkey anti-rabbit IgG (H+L); Alexa Fluor 594 (Cat. No. 711-585-152); Jackson Laboratories (Pennsylvania, USA)	1:200

5.3.2 Mice. Male, 8- and 17-week-old wild-type C57Bl/6 mice and C57Bl/6 homozygous for the F508del mutation (C57Bl/6 homozygous *Cftr*^{tm1Kth} ΔF508) were obtained from Dr. Craig Hodges at Case Western Reserve University (Ohio, USA). Mice were housed in an Allentown IVC rack with irradiated corncob bedding, Prolab autoclaved RMH 3500 feed and municipal (chlorinated tap) water with Colyte added. Mice were evaluated daily during routine health checks. If they showed signs of distress/GI complications, they were weighed, given subcutaneous fluids if needed and monitored more frequently by lab personnel. If signs of distress did not resolve (i.e. obstruction passed), they were euthanized. All experimental procedures were in accordance with the principles of the Canadian Council on Animal Care (CCAC) and according to the National Institute of

Health *Guide to the Care and Use of Experimental Animals*. Protocols were approved by Dalhousie University Animal Care and Use ethic committee.

5.3.3 Tissue preparation. Mice were humanely euthanized by intraperitoneal overdose of sodium pentobarbital before tissue collection. For sectioning, tissues were immediately fixed in 10% formalin buffer. Tissues were then embedded in paraffin blocks before longitudinal sectioning into 5-µm-thin sections for histology using hematoxylin and eosin (H and E) staining (Feldman et al., 2014) or immunohistochemistry experiments as described below. Tissue embedding and sectioning were done at the Histology and Research Services (HRS) Laboratory, Pathology Department, Faculty of Medicine, Dalhousie University. For protein analysis, tissues were flash frozen in liquid nitrogen before storage at -80^{o}C for later use.

5.3.4 Immunohistochemistry (IHC) and Microscopy imaging. Thin tissue sections (5µm) annealed to microscopy slides were deparaffinised in xylene and rehydrated prior to a 35 min heat-induced antigen retrieval. Next, the slides were washed twice for 5 minutes each time in PBS and incubated in 1% peroxidase blocking solution for 5 minutes. After another 10-minute washing step with PBS, the slides were incubated in normal mouse blocking serum for 1h at RT in a humidified chamber, then overnight with the primary antibody for VIP (1:100), Insulin (1:50), or *Ubiquitin* C-terminal *hydrolase* 1 (PGP 9.5; 1:200). The next day, tissue slides were washed three times for 5 minutes each with PBS and then incubated for 30 minutes at RT with a biotinylated anti-rabbit secondary antibody for VIP and PGP 9.5 (1:200; ABC ImmunoCruz staining system), for 1-hour at anti-guinea pig secondary antibody for Insulin (1:500; *Jackson* ImmunoResearch*).* VIP,

Insulin and PGP 9.5 signal were revealed with a DAB HRP peroxidase substrate and slides were counterstained with hematoxylin. After dehydration, a xylene based Permount was used to mount a coverslip. Slides were observed under light microscopy with 10X, 25X, 40X and 63X objectives. Images were taken with a Zeiss Axiocam HRC Colour Camera mounted on an Axioplan II microscope.

Scoring of images was used for semi-quantification of the IHC signal by two blinded investigators using an arbitrary scale (0 = none, 0.5 = minimal, 1 = low, 1.5 = some, 2 = moderate, 2.5 = strong and 3 = highest). Colour balance, contrast and brightness of whole images were adjusted for consistency within tissue sections. Experiments were repeated at least twice for each tissue sample and three to five mice were used in each age group. An average of 8 to 15 images from each tissue were used for the DAB signal semi-quantification. For quantification of protein gene product 9.5 (PGP 9.5) we measured immunohistochemistry signal intensity in both endocrine and exocrine pancreas using Image J software.

5.3.5 Immunofluorescent (IF) staining and signal quantification. Paraffin sections of pancreatic tissues after the deparaffinization and rehydration step as mentioned above, were rinsed three times in TBS, next incubated in TBS for 5 minutes and afterwards in blocking solution for 20 minutes at RT. The tissues were then covered with the Glucagon primary antibody (1:50) and stored overnight at 4^{o}C in humidity chamber. The next day the tissue slides were washed with TBS three times for 5 minutes to remove the primary antibody and then incubated with Alexa Fluor 594 secondary antibody overnight (1:200). Before mounting the tissue with Vectashield Mounting Media for Fluorescence, slides

were washed three times for 5 minutes with TBS to remove the secondary antibody in the dark. Afterwards, the slides were stored at -20^{o}C until viewed with a Zeiss LSM 710 confocal microscope. Quantification of fluorescence signal intensity of glucagon was done using Image J software.

5.3.6 Random glucose measurements. Plasma from 8- and 17-weeks old mice was used to estimate random glucose level using the Cayman's Glucose Colorimetric assay kit. This is a high sensitivity enzymatic assay specific for precise glucose quantification. All the mice were under the same regular diet (*Prolab RMH 3500*) and plasma was collected in the morning. For collecting plasma, immediately after the mouse euthanasia, we used intra-cardiac puncture to collect blood by aspiration with a fine needle filled with 2% EDTA to prevent coagulation and 1ml syringe. Blood collected was placed into a 1.5mL Eppendorf tube with 100µl of 2% EDTA and centrifuged for 10 minutes at 2,200 - 2,500rpm (8G centrifuge) at 4°C. The supernatant (plasma) was collected into a new tube, aliquoted and stored it at -80^{o}C until further use. Plasma was diluted 20-fold with assay buffer before use. Absorbance was read with a spectrophotometer at 514nm.

5.3.7 ELISA. Flash frozen pancreatic tissues samples from C57Bl/6 8- and 17-weeks old males, wild-type and F508del homozygotes CF mice were homogenized in RIPA buffer containing proteases inhibitors and lysates were used in mouse ELISA kit with high sensitivity and high specificity for VIP (Cloud-Clone Corporation, competitive inhibition) and Insulin (Millipore Mouse Insulin ELISA kit; EZRMI-13K). Both kits were used according to the manufacturer's instructions. Optical density was measured with a spectrophotometer at 450nm. VIP and Insulin concentration were afterwards normalized

to total proteins measured by protein assay using a Standard Bradford Assay with a standard BSA curve from 0 to 15µg in RIPA buffer.

5.3.8 Statistics. Results are reported as means ± SE. Statistical differences between groups were calculated by the one-way ANOVA. $p < 0.05$ was considered statistically significant. N represent the number of independent experiments.

5.4 Results

5.4.1 VIP is present in reduced amount in both endocrine and exocrine pancreas of CF mice.

Based on our previous study, the 17-week-old CF mice represent a well-developed CF disease, while in the 8-week-old mice the disease was minimal. In wild-type tissues, VIP amount was revealed by IHC with a polyclonal anti-VIP antibody and the signal was found around the ducts and acinar cells in the exocrine pancreas and in the islets of Langerhans (D1 cells) of the endocrine pancreas (Fig. 5.1A). The majority of the signal detected was found in the islets of Langerhans (Fig. 5.1B). DAB signal intensity was semi-quantified from scanned microscopy images using an arbitrary scale from 0 to 3 (see Methods). Results show that the signal for VIP in the exocrine pancreas was reduced by 44.5% ± 0.3 ($p < 0.05$) in 8-week-old CF mice and by 55.1% ± 0.1 ($p < 0.05$) in 17-week-old CF mice in comparison to the same age WT tissues (Fig. 5.1C). In the endocrine pancreas, VIP signal was decreased by 51.2% ± 0.2 in 8-week-old CF mice tissues and 51.3% ± 0.2 in 17-week-old CF mice compared to the same age WT (Fig. 5.1C).

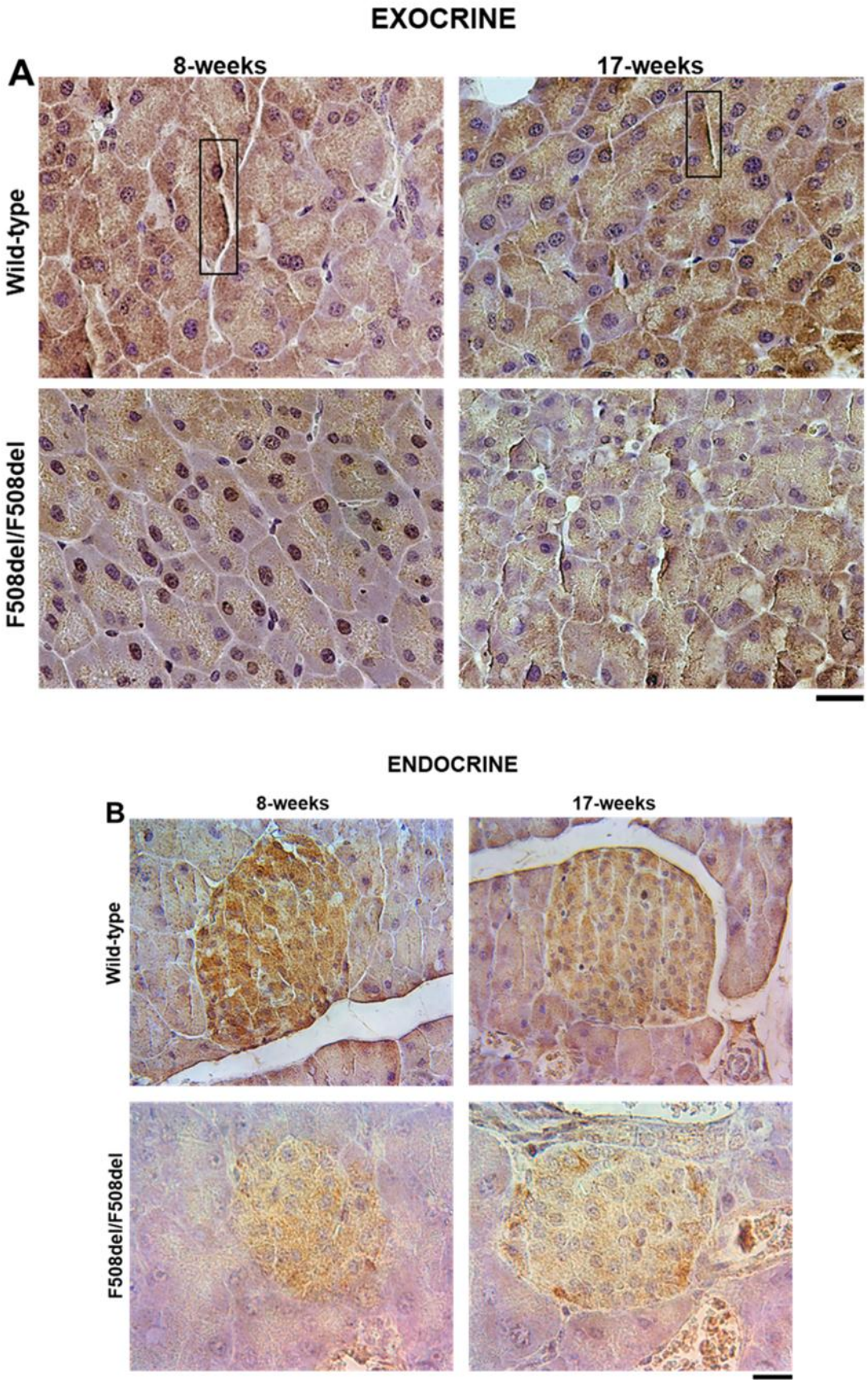
EXOCRINE
A
8-weeks
17-weeks
Wild-type
F508del/F508del
ENDOCRINE
B
8-weeks
17-weeks
Wild-type
F508del/F508del

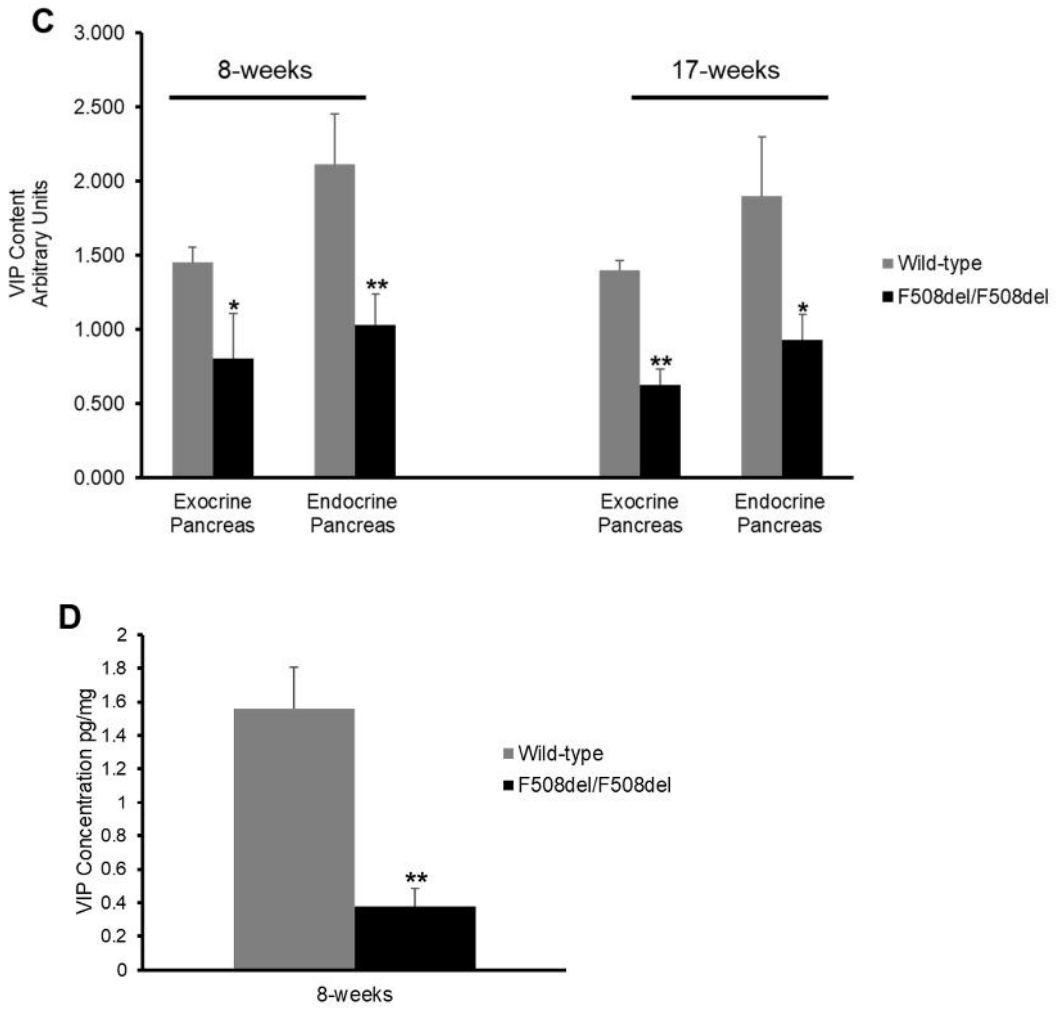

Figure 5.1: VIP signal in the exocrine and endocrine pancreatic tissues.

A & B, Representative IHC images of exocrine ***(A)*** and endocrine ***(B)*** pancreatic tissues stained for VIP (dark brown) in 8- and 17-week-old wild-type and F508del homozygous CF (F508del/F508del) mice showing VIP signal around the ducts (arrows) and acinar cells (arrow) in the exocrine pancreas and in the islets of Langerhans (D1 cells); 40X objective and scale: 20µm. Small images are captured on 63X magnification and scale 10µm. ***C,*** Semi-quantification of VIP signal in 8- and 17-week-old wild-type and CF endocrine and exocrine pancreas. Histogram bars represent averages of 8 to 15 images from each mouse (3 to 5 mice per age group). Arbitrary scale from 0 to 3 indicates: 0 = none, 0.5 = minimal, 1 = low, 1.5 = some, 2 = moderate, 2.5 = strong and 3 = highest. ***D,*** VIP concentration measured by ELISA in 8-week-old wild-type and CF mice pancreatic tissue homogenates, normalized to total proteins (5 mice), N = 2. *$p < 0.05$, **$p < 0.01$.

Total VIP content (normalized to total protein) in the pancreas was measured by ELISA. Results show that it was reduced by 75.8% in 8-weeks old CF mice, (1.55 ± 0.24 pg/mg in wild-type and 0.37 ±0.11 pg/mg in CF tissue lysates respectively, $p < 0.01$) (Fig. 5.1D). For the older mice (17-weeks old) VIP concentration was below the detection limit for both wild-type and CF. Altogether these data show that the amount of VIP is strongly reduced in the pancreas of CF mice, both at early and late stages of disease progression.

5.4.2 General innervation of the pancreas is reduced in CF mice.

In our previous study we showed that reduced amount of VIP in the lungs, duodenum and sweat glands of homozygous ΔF508 mice was due to sparse VIP-ergic neuronal fibers, and disrupted general neural network.

In the present study, we found reduced amount of VIP in both endocrine and exocrine pancreas and we decided to further test the general innervation using a PGP 9.5 antibody. Islets are known to express the highest amount of hormonal neuronal fibers, especially for VIP (Bishop et al., 1980; Havel et al., 1997). The PGP 9.5 signal measured by immunohistochemistry, in islets and exocrine pancreas, was quantified by Image J software. In wild type tissues, the PGP 9.5 signal was strong at the periphery of the islets and long fibers were visible in the exocrine pancreas (Fig. 5.2A - 5.2D, top). Our data showed a reduced PGP 9.5 signal in the islets of CF mice by 58.8% ±4.18 in the 8-weeks ($p < 0.001$) and 49.4% ±1.96 ($p < 0.05$) in the 17-weeks old CF mice compared to same age wild-type mice. Interestingly, in the exocrine pancreas we also observed decreased innervation at both ages of CF mice (Fig. 5.2B and 5.2D bottom) with only sparse short

fibers. The reduction in PGP 9.5 signal was found to be statistically significant for the 17-weeks old CF mice (73.2%±0.27, $p < 0.001$) (Fig. 5.2F).

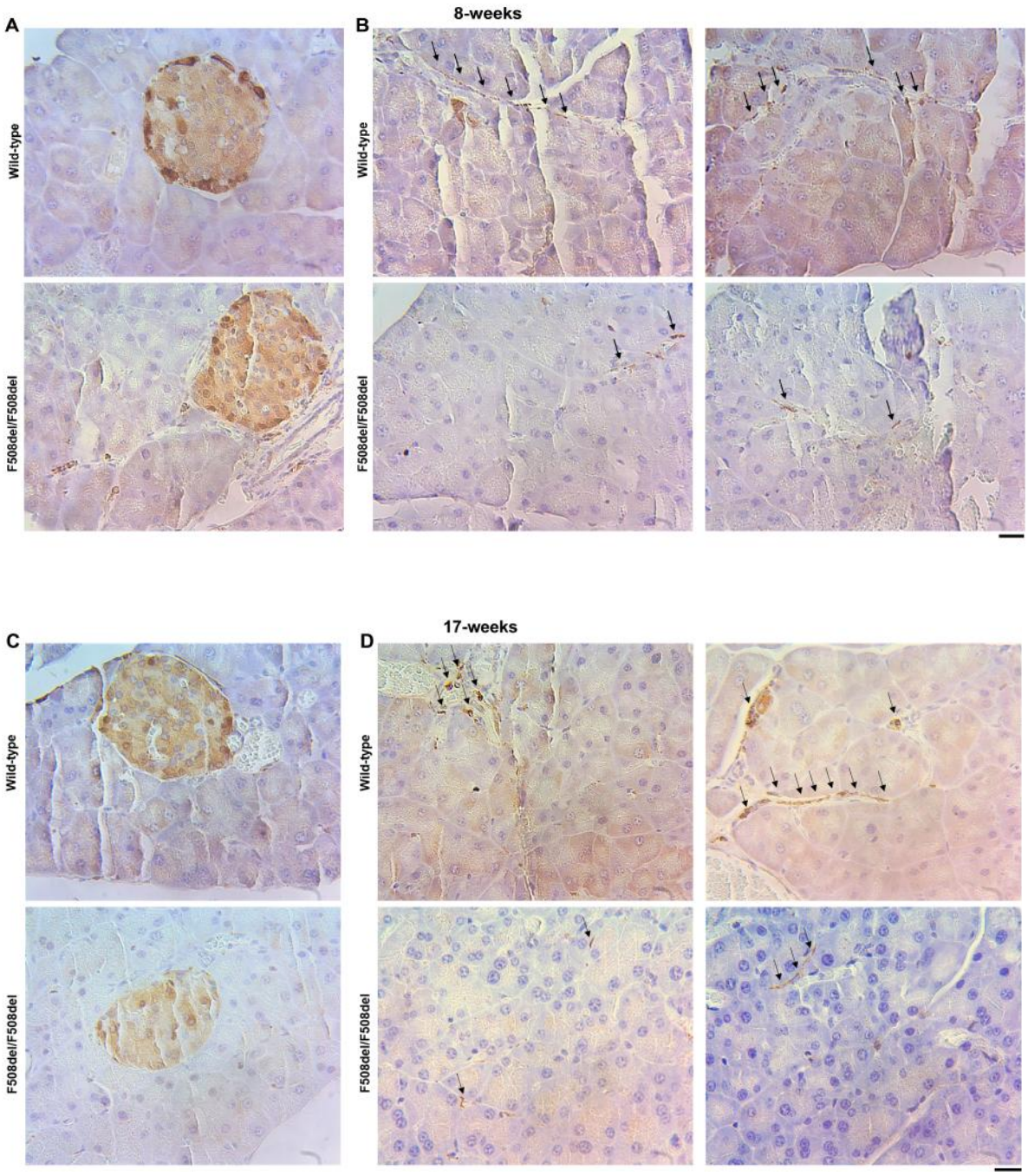

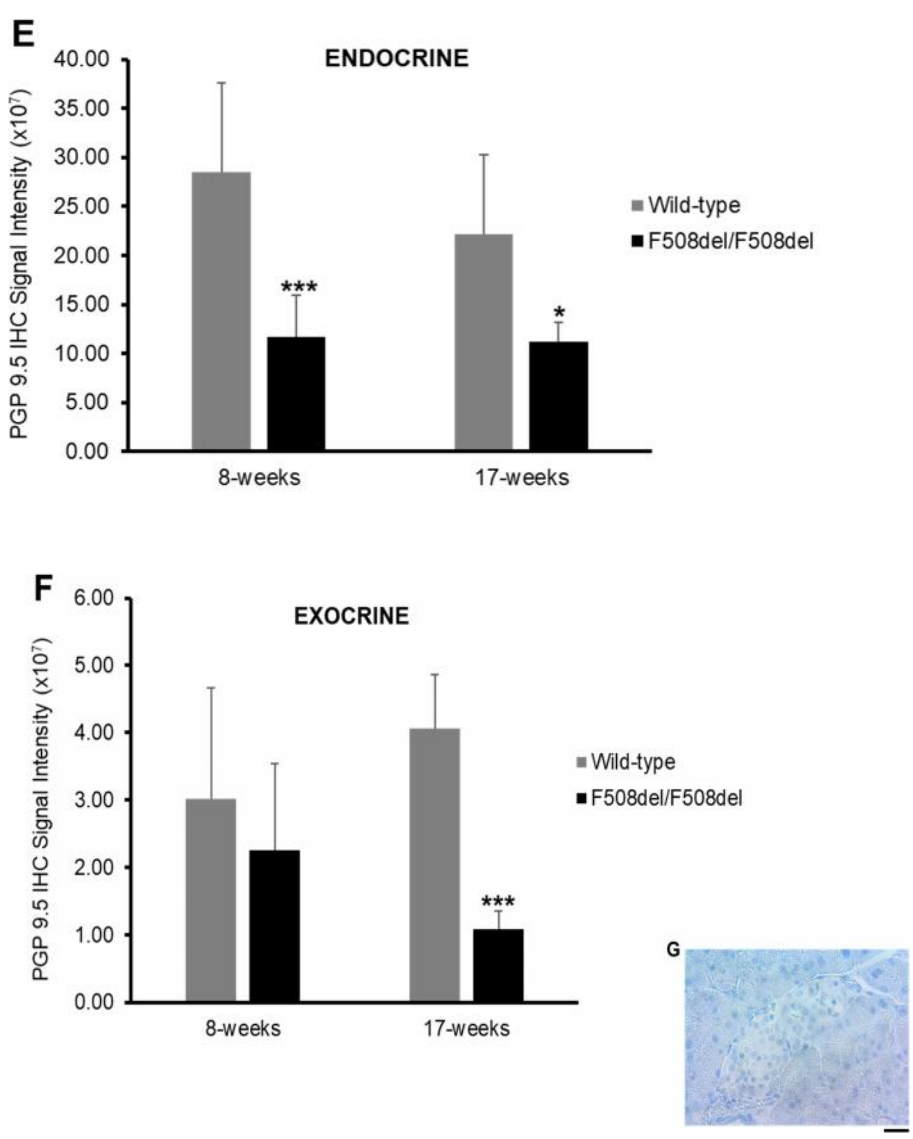

Figure 5.2: PGP 9.5 innervation is disrupted in both endocrine and exocrine pancreatic tissue. Representative images of endocrine **(*A*)** and exocrine 8-weeks (***B,*** arrows) and 17-weeks respectively (***C & D,*** arrows) pancreatic tissues showing the general innervation as represented by the PGP 9.5 antibody (dark brown, black arrows), and revealed by IHC, in wild-type and CF (F508del/F508del) mice (5 mice), N= 3. Scale 20 µm. ***E & F***, Quantification of IHC PGP 9.5 signal intensity (x10^7) in the islets (***E***) and in the exocrine pancreas respectively **(*F*)**. ***G,*** Negative control where the PGP 9.5 antibody was omitted. *$p < 0.05$, ***$p<0.001$

5.4.3 Reduced Insulin and elevated Glucagon in the endocrine pancreas of CF mice.

Insulin is produced by the pancreatic beta cells, located in the islets of Langerhans, after glucose stimulation. The glucose-induced amount of insulin release is further modulated by amino and fatty acids, gastrointestinal hormones and neurotransmitters secreted from the autonomous nervous system, including VIP (Ahrén et al., 2005; Henquin, 2009; Henquin, 2000). Given the low levels of VIP expression in both endocrine and exocrine pancreas of CF mice, we asked whether basal insulin level, in non-fasting animals, could be reduced in CF mice (Fabricius et al., 2011; Jamen et al., 2000; Kato et al., 1994; Kato et al., 2006; Persson-Sjögren et al., 2006; Sanlioglu et al., 2012; Tsutsumi et al., 2002; Winzell et al., 2007). IHC staining for insulin (DAB, dark brown color) in the beta cells of pancreatic islets was performed with a specific polyclonal antibody (Fig. 5.3A) and semi-quantified as described above for VIP. Our data show that basal insulin was significantly lower in both young (8-weeks) and older (17-weeks) CF mice compared to same-age wild-type. We found that the amount of insulin detected was reduced by 35% ± 0.2 ($p < 0.05$) in 8-week-old CF mice and by 38.7% ± 0.18 ($p < 0.05$) in 17-week-old CF mice in comparison to the same age WT (Fig. 5.3B). To confirm the low amount of basal insulin level in CF pancreas, we also measured total insulin content (normalized to total protein) by ELISA and found that it was reduced by 69.7% in 8-weeks old CF mice (41.46 ± 7.2 ng/mg in wild-type and 12.54 ±3.89 ng/mg in CF tissue lysates; $p < 0.05$) and reduced by 33.6% in the advanced disease mice (17-week-old) compared to WT (22.82 ± 8.22 ng/mg in wild-type and 15.15 ±13.24 ng/mg in CF tissue lysates respectively) (Fig. 5.3C). In normal individuals, insulin produced by β cells, and glucagon produced by α cells work together

to maintain glucose homeostasis where insulin secretion is elevated and glucagon production is decreased after every meal (Haedersdal et al., 2018). However, in T2D there is an imbalance between the glucagon and insulin release ratio with higher glucagon levels produced (Lee et al., 2019). Edlund et al. (2017) demonstrated disrupted glucagon levels in CFRD (Edlund et al., 2017). Since we wanted to investigate the pancreatic profile of CF mice, we next asked if glucagon secretion was affected.

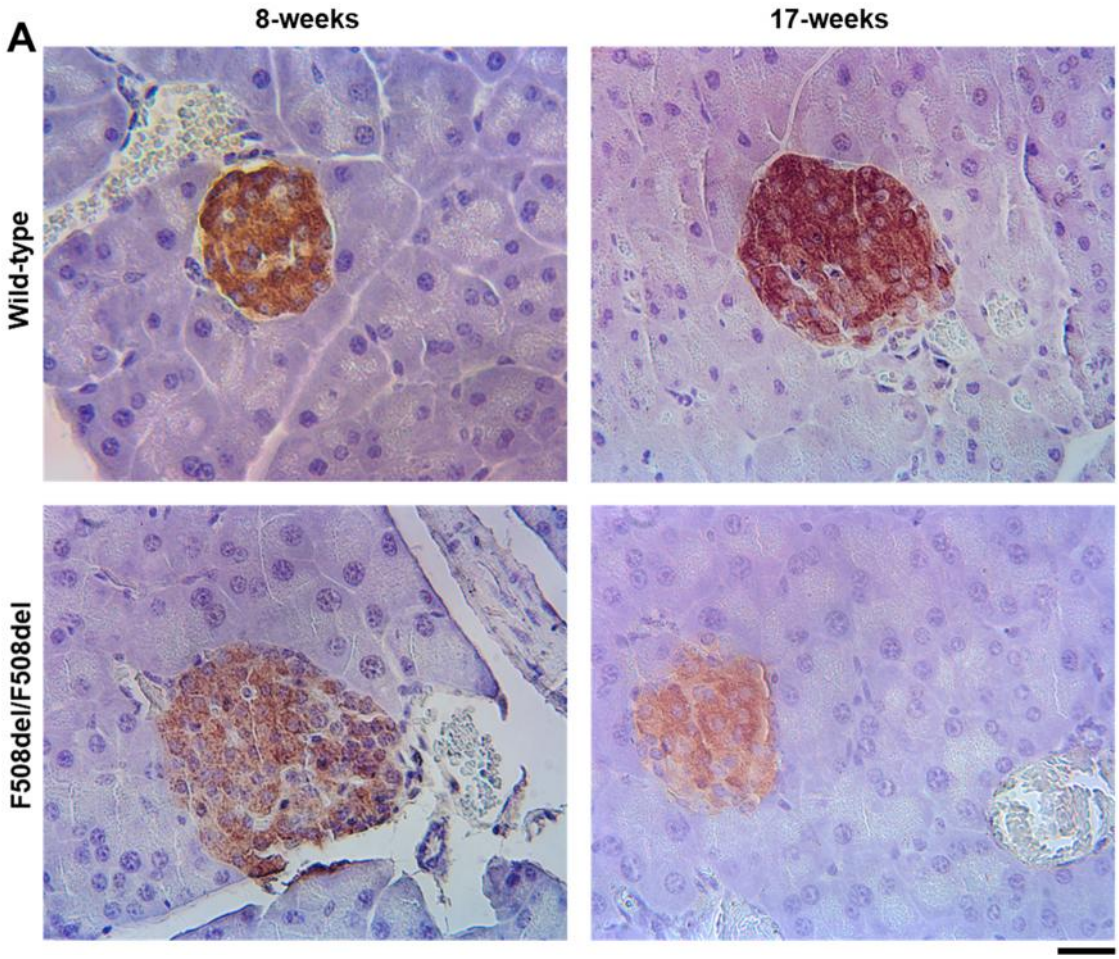

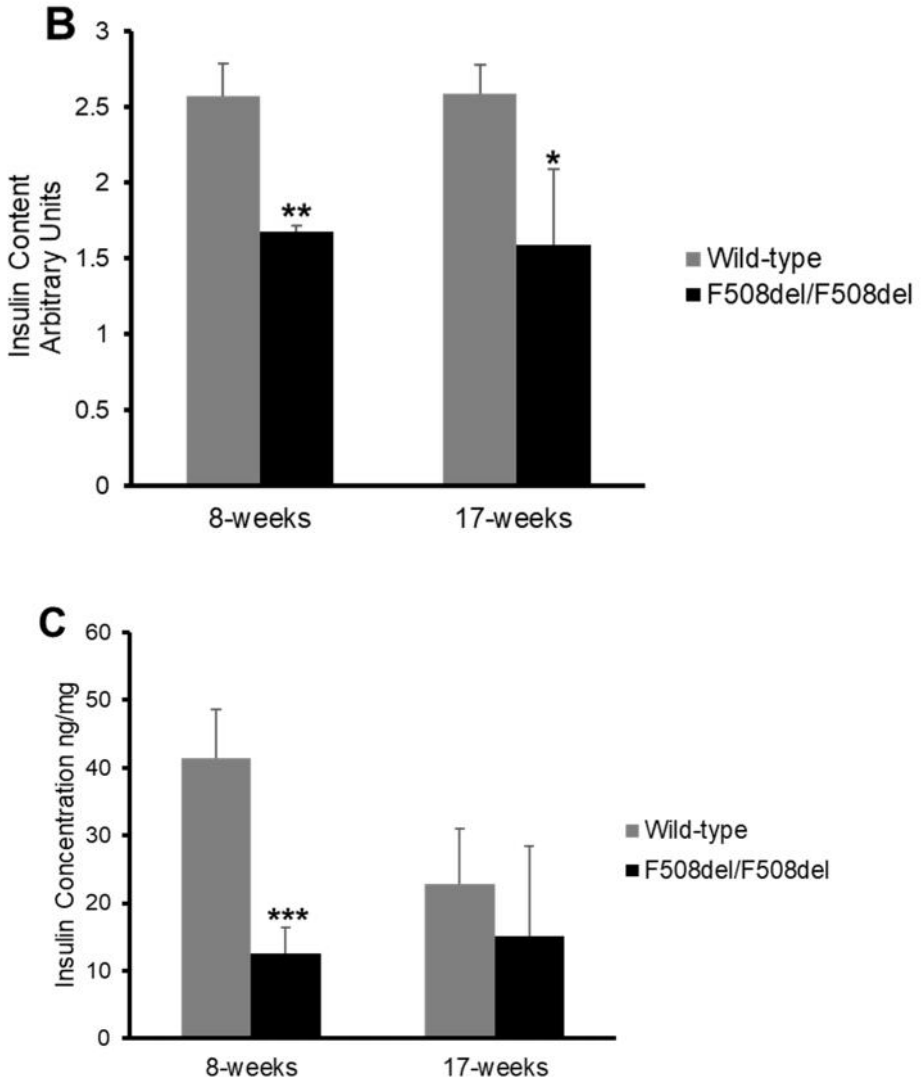

Figure 5.3: Insulin signal is highly reduced in the endocrine pancreas of CF mice.

Representative IHC images of endocrine pancreatic tissues ***(A)*** stained for Insulin (dark brown) in 8- and 17-week-old wild-type and F508del homozygous CF (F508del/F508del) mice showing VIP signal in the islets of Langerhans; 40X objective and scale: 20µm. ***B,*** Semi-quantification of Insulin signal in 8- and 17-week-old wild-type and CF endocrine pancreas. Histogram bars represent averages of 8 to 15 images from each mouse (3 to 5 mice per age group). Arbitrary scale from 0 to 3 indicates: 0 = none, 0.5 = minimal, 1 = low, 1.5 = some, 2 = moderate, 2.5 = strong and 3 = highest. ***C,*** Insulin concentration measured by ELISA in 8-week and 17-week-old wild-type and CF mice pancreatic tissue homogenates, normalized to total proteins (3-5 mice), N = 2. *$p < 0.05$, **$p < 0.01$, ***$p<0.001$

We performed immunofluorescence experiments and glucagon fluorescence intensity was quantified using Image J software following confocal microscopy. Our immunofluorescence data show that glucagon is present in the α cells of the islets and the strongest expression levels were found in tissues from 8-weeks old CF mice (Fig. 5.4A). Our results demonstrate that there is an upregulation of glucagon in both 8-weeks and 17-weeks CF mice pancreas as expected from the low level of insulin (Fig. 5.4C).

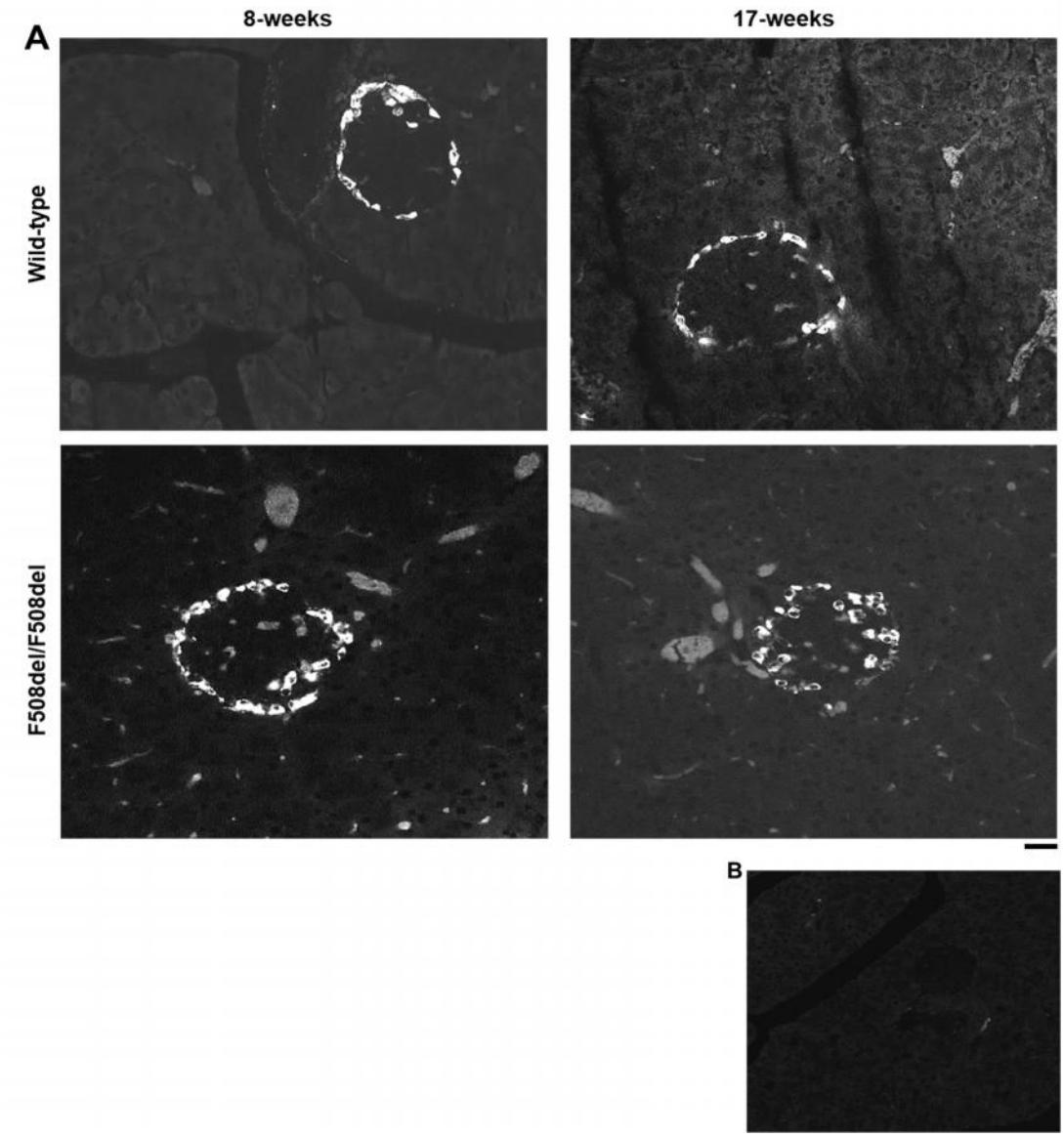

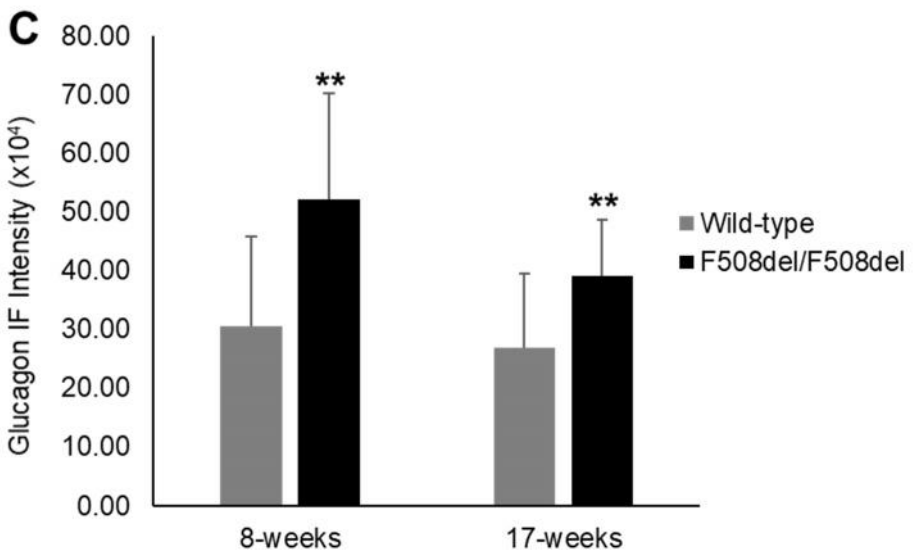

Figure 5.4: Glucagon IF signal intensity is elevated in both young and older CF mice.

Representative confocal microscopy images from 8- and 17-week-old (***A***) wild-type (top) and F508del homozygous CF (F508del/F508del) mice (bottom) showing Glucagon immunofluorescence signal intensity. ***B,*** Negative control where the Glucagon antibody was omitted. ***C,*** Quantification of Glucagon immunofluorescence signal intensity ($x10^4$) in 3-5 mice per age group. N = 2. **$p < 0.01$.

We then performed random glucose measurements with serum samples collected before sacrificing the animals for tissue collection. Our data reveal a high level of random glucose of 206 mg of glucose/dl of serum ± 63.8, while the normal range for random glucose level in C57Bl/6 mice is 70-110mg/dl.

Altogether, our results show a reduction in insulin and an upregulation of glucagon in CF mice pancreas, which is an indication that a CFRD phenotype can develop at an early stage of disease progression.

5.5 Discussion

The role of VIP in human diseases such as cystic fibrosis, asthma, chronic obstructive pulmonary disease and diabetes is a matter of investigation (Alcolado et al., 2014; Asnicar et al., 2002; Szema et al., 2017, 2014).

A study from Alcolado *et al*. (2014) in VIP-KO mice that developed a CF-like phenotype, demonstrated that VIP treatment corrected close to wild-type phenotype the lymphocyte aggregation, increased airway secretion, alveolar thickening and edema in the lung, as well as goblet cell hyperplasia and tissue alterations in the duodenum tissue found in absence of VIP. *In vitro,* addition of VIP to the cell media regulated defective CFTR internalization rate and increased membrane stabilization in the apical membrane of bronchial serous cells Calu-3 (Alcolado et al., 2011; Alshafie et al., 2014; Chappe F. et al., 2008). In the immune system, the critical role of VIP is illustrated in autoimmune diseases where VIP can skew the pro-inflammatory immune response to an anti-inflammatory response, downregulating the expression of TNFα, IL-6, IL-12, IL-1β and enhancing IL-10 production, blocking Th1 cells and consequently preventing Th2 production as well as mediating the functions of Th1/Th17 cells (Ganea et al., 2015).

As VIP can twist the pro-inflammatory cytokine profile to an anti-inflammatory response, its therapeutic actions has been tested in many chronic inflammatory and autoimmune diseases such as diabetes (Jimeno et al., 2010; Rosignoli et al., 2006), sepsis (Delgado et al., 2000), Crohn's disease (Gonzalez-Rey et al., 2006) and multiple sclerosis (Cobo et al., 2013). More specifically, VIP treatment in non-obese diabetic (NOD) mice rescued them from developing T1D through the activation of the T cell, suppression of Th1 cytokines

and upregulation of IL10 synthesis (Rosignoli et al., 2006). Moreover, VIP was found to augment insulin production from young obese (ob/ob) mice (Winzell et al., 2007).

Our most recent study, with the same CF mice as used in this paper, showed that VIP content is significantly reduced in the lungs, duodenum and sweat glands of young homozygous ΔF508 mice with minimal disease progression. Also, we found that these mice present highly discontinued or sparse VIPergic network in the small intestine and this VIPergic deficiency was not attributed to disease progression but to a disruption of the intrinsic innervation network.

In diabetes, VIP stimulates postprandial glucose-induced insulin secretion from pancreatic islets through VPAC2 receptors, and in collaboration with PACAP, VIP triggers glucagon release, increasing insulin secretion without leading to hyperglycemia (Sanlioglu et al., 2012). Studies in rats and mice have shown that VPAC2 receptor is the primary receptor expressed in beta cells through which VIP exerts most of its actions in the pancreas while VPAC1 is mainly localized around the islets.

VIP-containing fibers are distributed between acini, around ducts and blood vessels in the exocrine pancreas. Contrary to the exocrine, the endocrine pancreas has a very dense network of VIPergic fibers that entangle the islets, creating insular neuronal nexuses (Bishop et al., 1980; Winzell et al., 2007).

In the present study, given that VIP is a neuropeptide with pleiotropic abilities, we decided to examine the distribution and abundance of VIP in the pancreas of C57Bl/6 mice that express the most common mutation in CF, F508del/F508del, and further evaluate if changes in VIP would correlate with changes in insulin and glucagon secretion

that could potentially lead to the development of CFRD disease. We have measured the VIP amount in both young (8-weeks) and older (17-weeks) CF mice that reflect very early and late CF disease progression respectively (Semaniakou et al., 2020). Our results show that VIP abundance and localization, semi-quantified by immunohistochemistry and ELISA, was significantly reduced (~ 51% reduction) in the pancreas of CF mice at both 8- and 17-weeks of age. However, the strongest reduction was observed in the endocrine pancreas, that accounts for most of the peptide localization.

Numerous studies have reported the significance of VIP peptide in the pancreas, acting as a neurotransmitter and released upon activation of the vagus nerve (Ahrén, 2000). Already in 1980, a study from Bishop *et al.* demonstrated that VIPergic nerve fibers innervate acinar cells, ducts and blood vessels in the exocrine pancreas of rats while the islets of Langerhans have richer VIP neuronal network (Bishop et al., 1980). Additionally, research data on pig pancreas showed that VIP plays a critical role in fluid and bicarbonate release innervating the pancreatic nerves (Chandra et al., 2015; Holst et al., 1984). The insulinotropic potential of VIP to stimulate insulin secretion in presence of glucose has also been described in cells and animal models (Fabricius et al., 2011; Jamen et al., 2000; Kato et al., 1994; Kato et al., 2006; Persson-Sjögren et al., 2006; Sanlioglu et al., 2012; Tsutsumi et al., 2002; Winzell et al., 2007). In the present study, we demonstrate that the general neuronal network that innervates both the endocrine and exocrine pancreas of young and older CF mice is highly disrupted, with decreased signal in the islet and sparse nerve fibers in the exocrine pancreas. The current data is complementing our previous study showing that VIP is highly decreased in exocrine tissues of CF mice, even at a young

age with minimal disease (8-week-old) and continues to be low when the disease is well developed (17-week-old). A recent study from Hart *et al*. (2018) demonstrated that CFRD is primarily caused by islet loss and intra-islet inflammation showing elevated levels of IL-6, IL-1β, TNFa, IFN-γ, and CXCL10. In the present study, we found reduced insulin and elevated glucagon in young CF mice with no signs of disease. We can thus exclude the role of inflammation or tissue damage in this dysregulation.

Given the fact that VIP stimulates glucose-dependent insulin secretion and contributes to the regulation of glucagon release, we hypothesized that down-regulation of VIP secretion due to VIPergic neuronal disruption may result in a decrease in insulin and increase in glucagon expression levels, contributing to CFRD development. Consequently, we next measured insulin secretion and interestingly we found that insulin was significantly reduced at both ages tested. These results validate our hypothesis that changes in VIP amount and innervation in the endocrine pancreas may have an impact in postprandial insulin secretion.

VIP-induced glucagon production, which in turn maintains glycaemia, was described by Havel *et al.* (1997) (Havel et al., 1997). While most of the attention is on insulin, the role of glucagon is also essential in understating the pathophysiology of T2D. Drugs such as GLP-1 receptor agonists that improve glycaemia by regulating glucagon levels are considered a new treatment option of T2D (Haedersdal et al., 2018). Investigating in more detail glucagon secretion in CF mice and its relationship to VIP secretion in the endocrine pancreas would provide important knowledge on the etiology of CFRD. Our present data revealed that glucagon secretion is high in CF mice and this increase starts

early in the disease development (8-weeks). This observation is in agreement with what is reported in diabetic patients who have elevated post-prandial glucagon levels while under normal circumstances it should be downregulated (Lee et al., 2019). In the CFRD research field, only a few studies in F508del/F508del mice (12-14 weeks) and CF pigs have examined the role of glucagon, reporting elevated levels (Huang et al., 2017; Uc et al., 2015). Nonetheless, glucagon action in the pathophysiology of CFRD remains unclear and further research is needed to determine its role.

In addition to insulin and glucagon, another significant indicator of CFRD development is blood glucose levels. When we measured random blood glucose levels in the serum, we found an elevated average of 206 mg/dl. Typically, normal plasma has glucose concentrations in the range of 70-110mg/dl for C57Bl/6 mice. That was a significant result in addition to the previous data, further indicating that a decrease in VIP amount in the pancreas contributes to the development of physiological changes that will lead to CFRD disease. The main etiology of CFRD is islet dysfunction. However, the mechanisms behind β-cell impairment leading to disease development is a matter of debates. To our knowledge, three hypotheses have been described in the literature, until now: (1) islets are lost as a consequence of severe pancreatic fibrosis/inflammation, (2) if CFTR is expressed in the islets, its mutations (mainly class I-III CFTR) are responsible for the CFRD pathology due to islet ducts obstruction, therefore, affecting insulin secretion via a β-cell intrinsic CFTR dependent mechanism, and (3) CFTR is not expressed in β-cells and islet dysfunction is due to a non-β-cell extrinsic mechanism (Hart et al., 2018; Kelsey et al., 2019; Sun et al., 2017). Several studies have reported the significance of CFTR in glucagon

production in humans, rats and mice (Edlund et al., 2017; Huang et al., 2017). Nonetheless, the aim of this study was not to investigate the consequence of the dysfunctional CFTR in CFRD but rather to investigate the suitability of F508del/F508del mice as a valuable model to study CFRD development.

5.6 Acknowledgments

This work was supported by Cystic Fibrosis Canada and the Cystic Fibrosis Foundation (USA) research grants. A.S. was supported by a Faculty of Medicine Excellence Award and by CFF grant. The authors thank Stephen Whitefield (Dalhousie CMDI) for the expert advice with confocal microscopy and digital imaging, and Patricia Colp for technical expertise with histology.

5.7 Conflict of Interest Statement.

There are no conflicts of interest to declare.

CHAPTER 6: DISCUSSION

VIP is the major physiological agonist of the CFTR chloride channel. It functions as a neuromodulator and neurotransmitter secreted by intrinsic neurons innervating all exocrine glands. VIP-containing nerve fibers innervate tracheobronchial smooth muscle, submucosal glands and the walls of pulmonary and bronchial vessels (Barnes et al., 1991). In CF disease, VIP-dependent gland secretion, through CFTR activation, is defective. Glands cannot secrete in response to VIP alone and the co-localization of VIP and acetylcholine that is observed in healthy tissues is lost in CF (Jae et al., 2007; Widdicombe et al., 2015; Wine, 2007).

The significance of VIP in CF disease was first described in 1985 by Heinz-Erian and colleagues, showing reduced VIPergic innervation in the sweat glands of CF patients (Heinz-Erian et al., 1985). Given that CFTR gene was discovered in 1989, a demonstration of VIPergic deficiency or neuronal discontinuation at that time was a very significant finding for the understanding of CF disease and that could explain the abnormal secretory activity and high salt sweat levels in this condition (Heinz-Erian et al., 1985). Findings of Heinz-Erian *et al*. about sparse VIP-innervation in CF was further confirmed by Wattchow *et al.*, who demonstrated less VIP nerve fibers in intestinal and nasal mucosa, and Sharma *et al.*, who revealed reduced VIP innervation around the epithelium and alveolar wall of CF patients (Sharma et al., 1995; Wattchow et al., 1988). However, none of these studies investigated if VIP neural deficiency was related or not to a progressed disease stage and what was the impact of reduced VIP release in CF disease progression.

Unfortunately, despite the tremendous progress in diagnosis and therapeutic options during the last two decades, that have significantly improved the management of CF patients and consequently increased survival rate, nervous system defects are poorly studied in the CF literature. Most of the knowledge we have today is from the early 1980s, before the discovery of the CFTR gene, when scientists trying to better understand the CF disease pathophysiology had highlighted a connection between defects in the nervous system and the disease (Heinz-Erian et al., 1985; O'riordan et al., 1995.; Savage et al., 1990). Nowadays, most of the research attention is drawn to modern biological and pharmacological strategies, gene engineering methods and new drugs while the nervous system defects remain a challenge to delineate (Rey et al., 2019). Consequently, this study shed light on questions that had remained unanswered for more than thirty years. We demonstrated that the reduced VIP amount observed in CF exocrine tissues is an early onset of CF disease, present before the disease has progressed and not related to tissue damage. Our study demonstrated reduced VIP content in exocrine tissues, yet examining VIP receptor expression would add more knowledge regarding the impact of VIP reduction. VIP receptor expression were not evaluated in our studies. As the therapeutic potential of VIP for other diseases has already been reported, determining VIP receptors expression in CF tissue should be further considered in future studies, aiming to a tissue specific treatment with VIP receptor agonist molecules. Previous data from the Chappe lab demonstrated that pathological signs of disease in lungs (inflammation/infiltration) and duodenum of VIP-KO mice (morphological intestinal alterations and goblet cell hyperplasia) that presented CF-like disease symptoms, were

corrected after VIP treatment, demonstrating the critical role of VIP to maintain tissue morphology and CFTR function. VPAC1 and VPAC2 receptors were found to be over-expressed in VIP-KO mice (Alcolado et al., 2014).

To explore if this VIP deficiency was due to neuronal defect or VIP peptide biosynthesis, we further examined intrinsic VIPergic innervation in the duodenum of young homozygous F508del mice that had minimal pathological signs of disease. Most importantly, we investigated for the first time whether the general intrinsic nervous system of the small intestine remained intact in CF or if only neurons co-expressing VIP and acetylcholine were affected.

The small intestine is innervated by the enteric and central nervous systems containing motor neurons, interneurons, intrinsic primary afferent neurons and secretomotor/vasomotor neurons (Furness, 2000). VIP and ACh descending interneurons play a significant role in the intestinal motility along with having secretomotor effects moderating most of the local reflex reactions (Furness, 2000). We demonstrated that the dense VIPergic continuous network of the duodenum was highly disrupted in CF mice tissues, compared to wild-type. VIP-containing nerve fibers of the mucosa and myenteric plexus layers of the duodenum of CF mice had a lower level of aggregation, lower density and in some areas, VIPergic innervation was sparse. It is worth mentioning that the mucosa and myenteric layers are characterized by a high density of VIPergic neurons in healthy intestinal tissues. Additionally, we showed that the cholinergic network, on the same animals, was significantly reduced at both mucosal and myenteric plexus layers. This finding supported previous data in the field indicating that the functional synergy of

VIP and ACh for gland secretion is lost in CF (Ianowski et al., 2007; Jae et al., 2007). Moreover, given that the small intestine, and especially the duodenum, expresses the highest density of CFTR proteins. Lastly, we revealed that general intrinsic neuronal innervation of the duodenum was altered in CF, and this alteration cannot be attributed to tissue damage induced by disease progression.

Altogether, these data add valuable knowledge to the field, elucidating the question of early neuronal changes as a primary defect, while neuronal abnormalities are observed when disease has not progressed yet. It would be interesting to examine if neural network restoration in these tissues is achieved after prolonged treatment with exogenous VIP when added very early, eventually during embryonic development.

Defective fluid secretion which is a primary defect in CF, is mainly controlled by the parasympathetic nervous system, while the sympathetic innervation has only a minor input (Widdicombe et al., 2015; Wine, 2007). A study from Nedvetsky *et al.* (2014) described the critical role of parasympathetic nerves in the tubulogenesis of the developing salivary glands and the role of VIP innervation and CFTR in lumen expansion, in mice (Nedvetsky et al., 2014). Salivary glands are well studied in CF for their secretory components and defects (Dhooghe et al., 2015; Gonçalves et al., 2013). Future investigation of the VIP innervation of salivary glands either in CF patients or animal models would add valuable information about gland neural defects in the CF disease. A study from Pan *et al.* (2006) demonstrated that the dense intrinsic innervation network of airway smooth muscle and nerve endings were highly reduced in CFTR knockout mice (Pan et al., 2006). Importantly, the authors reported that this deficient innervation starts

in utero during lung development and continues postnatally, proposing that neural abnormalities in absence of CFTR could impact the airway structure, function and innervation.

CFTR expression has been described in immature cells during embryonic development of human brain, lungs, intestine and male reproductive track (Harris et al., 1991; Marcorelles et al., 2007, 2012, 2014; Tizzano et al., 1993). Marcorelles *et al.* (2014) examined CFTR expression in the human brain during developmental stage in specimen from individuals with wildtype CFTR and from individuals with CF. In wildtype specimens they found a widespread CFTR distribution that had a specific expression pattern, initially observed in infratenporial brain areas and lastly in the cerebral cortex (Marcorelles et al., 2014). In CF specimens however, the CFTR distribution was different based on the brain structure or the stage of the cell maturity (Marcorelles et al., 2014). A study from Reznikov *et al*. (2013), which to our knowledge is the only one that examined the innervation in CF pig models, reported CFTR expression in Schwann cells that have a significant role in the survival and neuronal function, producing the myelin sheath around neuronal axons. CFTR null piglets showed structural myelin sheath alterations and increased expression of myelin gene which in turn caused decrease of axonal myelin density (Reznikov et al., 2013). These findings clarified the significance of CFTR absence in peripheral nervous system and that, indeed, neural changes happen before disease progression as our research demonstrated in homozygous F508del mice.

It is important to understand the altered neuronal activity that could contribute to the main CF disease manifestations: airways and intestinal obstruction. Also, what is the

effect of CFTR potentiators and correctors in the nervous system, do the neural abnormalities in CF start *in utero* and what is the impact of these treatments during pregnancy to the fetus and its nervous system etc. are some intriguing questions that remain unanswered.

During our study, we found that VIP content was highly reduced in both endocrine and exocrine pancreas of young (8-weeks) and older (17-weeks) homozygous F508del mice. CF-related diabetes is a common complication in CF affecting nearly 50% of adult CF patients. While having a complex etiology, its pathophysiology remains unclear. This emphasizes the necessity for a deeper and better understanding of this condition. CFRD shares characteristics of both T1D and T2D diabetes but it is considered as a distinct entity. Patients with severe CFTR mutations, especially the F508del, are more prone to develop CFRD. Beta cell dysfunction contributes to CFRD which then leads to reduced insulin secretion, elevated glucagon levels and abnormal glucose tolerance. Additional characteristics of CFRD are islets inflammation, islets amyloid deposition, reduced islet mass and exocrine pancreatic dysfunction (Edlund et al., 2017; Huang et al., 2017; Kelsey et al., 2019; Norris et al., 2019). Nonetheless, the beta cell failure in CFRD is not considered sufficient to directly cause CFRD, as approximately 50% of the beta cell mass is preserved in CFRD patients (Norris et al., 2019; Sun et al., 2017). Interestingly, research indicates that this remaining beta cell number should be able to prevent CFRD (Norris, 2019; Norris et al., 2019). Accordingly, there has been a lot of debate regarding the main reasons of the beta cell dysfunction, and if there is an additional beta cell defect involved in the impaired insulin secretion. Three different hypotheses have been discussed and

described in the literature in regard to CFRD pathogenesis: (1) CFRD may results from islet loss and inflammation leading to reduced beta cell growth, (2) expression of dysfunctional CFTR in the beta cells may lead to beta cell failure through intrinsic mechanisms that are CFTR-dependent, (3) loss of the CFTR from the exocrine pancreas, which is the main site for CFTR expression, causes cystic dilation and exocrine pancreas inflammation that may influence all the parts of the pancreas and therefore, cause beta cell loss through a paracrine mechanism (Bogdani et al., 2017; Hart et al., 2018; Norris et al., 2019; Sun et al., 2017).

The goal of our study was not to decipher these hypotheses, but rather determine if the homozygous F508del mouse model used in our study developed signs of CFRD in reduced expression of VIP. We hypothesized that since glucose-induced insulin secretion and glucagon, two key hormones in CFRD pathogenesis, are elevated by VIP, with reduced VIP secretion these mice may develop signs of CFRD. VIP is known to amplify glucose-dependent insulin secretion through parasympathetic activation of the vagal nerve, and coupling to VPAC2 receptor, highly expressed in the pancreatic islets (Sanlioglu et al., 2012). Together with low VIP expression in the pancreas of 8- and 17-week-old CF mice, our data showed reduced insulin secretion in both ages. Also, immunofluorescence quantification demonstrated statistically significant increased glucagon expression in the younger and older age of CF mice. The mechanism of glucagon release from pancreatic alpha cells in CFRD remains unclear as it is an understudied area. There is some intense controversy in the field about the role of CFTR in glucagon secretion. A few publications support that CFTR is expressed in alpha cells and in presence of glucose it hyperpolarizes

the membrane potential by potentiating adenosine triphosphate–sensitive K^+ (K_{ATP}) channel activity. CFTR inhibition would thus result in depolarization of alpha cells, contributing to elevated glucagon release in both human and rodent islets (Boom et al., 2007; Edlund et al., 2017; Huang et al., 2017). However, the mechanism of how CFTR potentiates the K_{ATP} channel is not known yet. This is in contrast to a study by Sun *et al.* (2017) in newborn ferret pancreas revealing the presence of CFTR mRNA in the exocrine ductal cells but not in the β- cells, α-cells, PP cells and δ-cells of the endocrine pancreas (Sun et al., 2017). Similarly, Hart *et al.* (2018) reasserted that CFTR mRNA is too low in CFRD human islets and that CFTR protein is not detectable in endocrine cells, suggesting that CFRD is mainly caused by inflammation. Despite the significance of this study, one of its limitations, as reported by the authors, was that they used CF human islets from severely diseased patients that had been under many medications for a long period of time (Hart et al., 2018).

In our study, we demonstrated elevated glucagon levels in young homozygous F508del mice (8 – 9 weeks), as was previously shown by Huang *et al*. (2017) (Huang et al., 2017;), in older CF mice (17-weeks) and in CF pigs (Uc et al., 2015). While the knowledge about glucagon secretion is very controversial, future quantitative methods (e.g. western blot method or mRNA levels) would further establish our results and resolve some dissension in the CFRD field.

Another significant parameter to consider for future experiments is the role of incretins (C-peptide, GLP-1, GIP) and their correlation with insulin deficiency and glucagon increase in presence of low VIP expression. GLP-1 is the most potent stimulator of

glucose-dependent insulin augmentation and glucagon inhibitor secretion (Ahrén et al., 2003; Sanlioglu et al., 2012). Also, GLP-1 receptor agonists (e.g. Exenatide) have recently been approved for the treatment of T2D (Hinnen, 2017). However, for the CFRD pathophysiology, the incretin-based potential therapy remains unclear. A recent small study from Geyer *et at*. (2019) reported that Exenatide improved postprandial hyperglycaemia in young CF patients with abnormal glucose levels. Nonetheless, Exenatide effects on gastric emptying were slower (Geyer et al., 2019). Given these uncertainties, more research is needed to elucidate if insulin reduction is due to reduced VIP secretion or due to abnormal incretin hormones, before we propose with confidence that VIP deficiency account for CFRD development. Measuring the GLP-1 levels in CF mouse model treated with the long-lasting VIP molecules that binds to the VPAC2 receptor, highly expressed on the islets, would allow us to investigate insulin levels after the treatment. To compare the levels of insulin restoration, we could also treat CF mice with GLP-1 receptor agonists (e.g. Exenatide) and compare insulin secretion after VIP and Exenatide treatment.

One of the hypotheses for CFRD pathogenesis is the important role of inflammation, either in the exocrine pancreas, affecting the pancreatic duct branches interconnected with the endocrine pancreas and indirectly leading to reduced beta cell growth and insulin deficiency, or the islet inflammation directly. As VIP has strong anti-inflammatory potentials, VIP treatment would reduce both exocrine and endocrine inflammation. Therefore, treatment with VIP and measurement of inflammatory factors (IL-1β, IL-6, TNFα etc.), as well as insulin, glucose and glucagon levels, would contribute to a better

evaluation of the role of VIP in CFRD condition.

VIPergic nerve fibers control fluid and bicarbonate secretion, as was shown in pig pancreas (Holst et al., 1984). Strong reduction of the VIP amount was shown to be due to neuronal damage in the duodenum of CF mice. In the pancreas, VIPergic intrinsic nerves and fibers are widely distributed in the endocrine pancreas, playing a significant role in the regulation of the islet hormonal secretion. Consequently, reduced VIPergic innervation explains the reduced VIP amount measured in the pancreas of both young and older CF mice, accounting for, at least in part, the insulin reduction. PGP 9.5 staining, a general neuronal marker, identified neuronal fibers inside the islets and mostly surrounding the islet area. In the exocrine pancreas PGP 9.5 signal was identified in between ducts and within the walls of blood vessels. In the CF pancreas the innervation around the islets was significantly reduced in both 8- and 17-weeks CF mice, and the exocrine pancreas was characterized with lower density of neural fibers that appeared discontinued in areas compared to wild-type tissues. These data are in agreement with the disrupted general innervation that we demonstrated in the small intestine of CF mice. Lastly, in our study we found elevated random plasma glucose levels in the 8-weeks CF mice. Despite the fact that random blood glucose concentrations >11mmol/L can be used to diagnose CFRD initiation, the recommended standard screening method is the 2-hour oral glucose tolerance test (OGTT >11mmol/L) (Boudreau et al., 2016). Future measurement of OGTT would affirm our results.

CONCLUSION

Almost 30 years after the discovery of CFTR gene, despite the important progress at the molecular and cellular level, there are still under studied topics, and one of them is the nervous system. Neural abnormalities in CF patients have been reported through the years and CFTR has been described in central and peripheral nervous systems. While most of the research is center on how to cure the basic CFTR defects in CF disease with restoration of the CFTR chloride channel function, the dysfunctional nervous system and how it affects the disease progression is yet a thirst for knowledge.

In our research, we demonstrated that the VIP deficiency and sparse VIPergic innervation around the exocrine organs is not attributed to disease development and to tissue damage but to a general disruption of the intrinsic innervation network. Moreover, this study was the first to show that nerves co-expressing VIP and acetylcholine are reduced in density, explaining partially the loss of functional synergy in the regulation of fluid secretion, which is the main hallmark of CF disease. Furthermore, we investigated the role of VIP in the CF pancreas. Our data indicated low levels of VIP due to reduced innervation of the CF pancreas, starting at an early disease stage, which in consequence contributes to changes in insulin and glucagon secretion that can lead to CFRD disease development. Since CF is a multifactorial disorder, the autonomic nervous system should be considered as an additional system affected in CF, which should be further assessed and examined in depth in future research.

THESIS LIMITATIONS

Despite the high contribution of this study to the CF field, there were a few limitations that are worth mentioning. Different mouse models and background strains are used in CF research, accounting for the various techniques by which they were generated. Pathogen exposure compared to pathogen-free studies, and the husbandry conditions before evaluating the disease progression can have a significant impact on the research results. Moreover, the presence of a non-CFTR calcium-activated Cl^- channel (CACC) in parallel with CFTR in both the lungs and pancreas of mice can account for differences in resistance to bacteria, and perhaps explaining the mild-phenotype reported in studies of murine pancreatic pathology (Semaniakou et al., 2019). In the CF mouse model used in this study, the lungs, intestine and pancreas of the 17-week-old animals exhibited many pathophysiological signs that are characteristic of CF in humans. Eventhough we could only successfully maintain 3 mice up to that age, this is very significant

In the CF literature, 3 to5 CF mice are considered a reasonable number for conducting experiments due to the complexity of maintaining them healthy long enough, and our success with 17-week-old animals is very unique. Nevertheless, additional mice in this age group would make these findings even stronger.

VIP expression based on IHC is a semi-quantitative method which uses an arbitrary scoring system of DAB signal intensity, evaluated by two independent and blinded investigators. As this scoring system is based on visual observations it is an estimation of

the VIP expression level. Data were confirmed by quantitative ELISA and could be further evaluated by qt-RT-PCR or other more elaborated molecular methods if needed.

Extensive tissue damage was observed in the duodenum of 17-week-old CF mice. Our measurements of pathological signs are thus an underestimation of the disease progression as only semi-intact areas could be used to measure villi.

Multiple scoring systems and scales exist for lung disease evaluation. The scoring method used in this thesis was based on a publication by Bayes *et al.* (2016). This scoring was thought to be well representative of chronic lung diseases such as CF.

APPENDIX I: COPYRIGHT AND LICENSE AGREEMENT

1. This article: “Disrupted local innervation results in less VIP expression in CF mice tissues." *Journal of Cystic Fibrosis* (2020) https://www.sciencedirect.com/science/article/pii/S1569199320307773

Is under a **Creative Commons Non-Commercial No-Derivatives license** https://creativecommons.org/licenses/by-nc-nd/4.0/ which allows me to reuse this article for thesis dissertation, provided that I do not make a new derivative copy of the article or use it for commercial purposes. As a first author of this article, there is no need to seek permission from the publisher and from the Faculty of Graduate Studies as well.

2. This article: "Animal models in the pathophysiology of cystic fibrosis." *Frontiers in Pharmacology* (2019) https://www.frontiersin.org/articles/10.3389/fphar.2018.01475/full is an open-access article distributed under the terms of the **Creative Commons Attribution License (CC BY)**. This means that the use, distribution or reproduction in other forums is permitted, provided the original author(s) and the copyright owner(s) are credited and that the original publication in this journal is cited, in accordance with accepted academic practice. As the first author of this article, I owe the copyright permission for reuse in thesis dissertation.

REFERENCES

1. Abu-El-Haija, M., Ramachandran, S., Meyerholz, D. K., Abu-El-Haija, M., Griffin, M., Giriyappa, R. L., Stoltz, D. A., Welsh, M. J., McCray, P. B., & Uc, A. (2012). Pancreatic damage in fetal and newborn cystic fibrosis pigs involves the activation of inflammatory and remodeling pathways. American Journal of Pathology, 181(2), 499–507. https://doi.org/10.1016/j.ajpath.2012.04.024
2. Ahrén, B. (2000). Autonomic regulation of islet hormone secretion - Implications for health and disease. In Diabetologia (Vol. 43, Issue 4, pp. 393–410). Springer Verlag. https://doi.org/10.1007/s001250051322
3. Ahrén, B., & Pacini, G. (2005). Islet adaptation to insulin resistance: mechanisms and implications for intervention. https://doi.org/10.1111/j.1463-1326.2004.00361.x
4. Ahrén, B., Holst, J. J., & Mari, A. (2003). Characterization of GLP-1 effects on β-cell function after meal ingestion in humans. Diabetes Care, 26(10), 2860–2864. https://doi.org/10.2337/diacare.26.10.2860
5. Alcolado, N. , Conrad, D. J., Poroca, D., Li, M., Alshafie, W., Chappe, F. G., Pelis, R. M., Anini, Y., Xu, Z., Hamidi, S., Said, S. I., & Chappe, V. M. (2014). Cystic fibrosis transmembrane conductance regulator dysfunction in VIP knockout mice. American Journal of Physiology - Cell Physiology, 307(2). https://doi.org/10.1152/ajpcell.00293.2013
6. Alcolado, N., Conrad, D. J., Rafferty, S., Chappe, F. G., & Chappe, V. M. (2011). VIP-dependent increase in F508del-CFTR membrane localization is mediated by PKCε. Am J Physiol Cell Physiol, 301, 53–65. https://doi.org/10.1152/ajpcell.00568.2009
7. Allali, J., Chauve, C., Denise, A., Drevet, C., Ferraro, P., Gautheret, D., Herrbach, C., Leclerc, F., Ouangraoua, A., Sagot, M.-F., Termier, M., & Thermes, C. (2012). BRASERO: A resource for benchmarking RNA secondary structure comparison algorithms. Advances in Bioinformatics, 2012(893048), 5. https://doi.org/10.1155/2012

8. Alshafie, W., Chappe, F. G., Li, M., Anini, Y., & Chappe, V. M. (2014). VIP regulates CFTR membrane expression and function in Calu-3 cells by increasing its interaction with NHERF1 and P-ERM in a VPAC1- and PKCε-dependent manner. American Journal of Physiology - Cell Physiology, 307(1). https://doi.org/10.1152/ajpcell.00296.2013

9. Ameen, N. A., Martensson, B., Bourguinon, L., Marino, C., Isenberg, J., & McLaughlin, G. E. (1999). CFTR channel insertion to the apical surface in rat duodenal villus epithelial cells is upregulated by VIP in vivo. Journal of Cell Science, 112(6)

10. Andersen, (1938). Cystic Fibrosis of the Pancreas and its Relation to Celiac Disease. American Journal of Diseases of Children, 56(2), 344. https://doi.org/10.1001/archpedi.1938.01980140114013

11. Anlauf, M., Schäfer, M. K. H., Eiden, L., & Weihe, E. (2003). Chemical coding of the human gastrointestinal nervous system: Cholinergic, VIPergic, and catecholaminergic phenotypes. Journal of Comparative Neurology, 459(1), 90–111. https://doi.org/10.1002/cne.10599

12. Asnicar, M. A., Köster, A., Heiman, M. L., Tinsley, F., Smith, D. P., Galbreath, E., Fox, N., Ma, Y. L., Blum, W. F., & Hsiung, H. M. (2002). Vasoactive Intestinal Polypeptide/Pituitary Adenylate Cyclase-Activating Peptide Receptor 2 Deficiency in Mice Results in Growth Retardation and Increased Basal Metabolic Rate. Endocrinology, 143(10), 3994–4006. https://doi.org/10.1210/en.2002-220354

13. Atanasova, K. R., & Reznikov, L. R. (2018). Neuropeptides in asthma, chronic obstructive pulmonary disease and cystic fibrosis. In Respiratory Research (Vol. 19, Issue 1). BioMed Central Ltd. https://doi.org/10.1186/s12931-018-0846-4

14. Baker, L. B. (2019). Physiology of sweat gland function: The roles of sweating and sweat composition in human health. In Temperature (Vol. 6, Issue 3, pp. 211–259). Routledge. https://doi.org/10.1080/23328940.2019.1632145

15. Balázs, A., & Mall, M. A. (2019). Mucus obstruction and inflammation in early cystic fibrosis lung disease: Emerging role of the IL-1 signaling pathway. Pediatric Pulmonology, 54(S3), S5–S12. https://doi.org/10.1002/ppul.24462

16. Barbarin, A., Séité, P., Godet, J., Bensalma, S., Muller, J. M., & Chadéneau, C. (2014). Atypical nuclear localization of VIP receptors in glioma cell lines and patients. Biochemical and Biophysical Research Communications, 454(4), 524–530. https://doi.org/10.1016/j.bbrc.2014.10.113

17. Barnes, P. J., Baraniuk, J. N., & Belvisi, M. G. (1991). Neuropeptides in the respiratory tract: Part I. In American Review of Respiratory Disease (Vol. 144, Issue 5, pp. 1187–1198). https://doi.org/10.1164/ajrccm/144.5.1187

18. Barrio, R. (2015). Management of endocrine disease: Cystic fibrosis-related diabetes: Novel pathogenic insights opening new therapeutic avenues. In European Journal of Endocrinology (Vol. 172, Issue 4, pp. R131–R141). BioScientifica Ltd. https://doi.org/10.1530/EJE-14-0644

19. Bayes, H. K., Ritchie, N., Irvine, S., & Evans, T. J. (2016). A murine model of early Pseudomonas aeruginosa lung disease with transition to chronic infection. Scientific Reports, 6, 35838. https://doi.org/10.1038/srep35838

20. Bazett, M., Honeyman, L., Stefanov, A. N., Pope, C. E., Hoffman, L. R., & Haston, C. K. (2015). Cystic fibrosis mouse model-dependent intestinal structure and gut microbiome. Mammalian Genome, 26(5–6), 222–234. https://doi.org/10.1007/s00335-015-9560-4

21. BéruBé, K., Prytherch, Z., Job, C., & Hughes, T. (2010). Human primary bronchial lung cell constructs: The new respiratory models. In Toxicology (Vol. 278, Issue 3, pp. 311–318). Toxicology. https://doi.org/10.1016/j.tox.2010.04.004

22. Biancani, P., Walsh, J. H., & Behar, J. (1984). Vasoactive intestinal polypeptide. A neurotransmitter for lower esophageal sphincter relaxation. Journal of Clinical Investigation, 73(4), 963–967. https://doi.org/10.1172/JCI111320

23. Bishop, A. E., Polak, J. M., Green, I. C., Bryant, M. G., & Bloom, S. R. (1980). The Location of VIP in the Pancreas of Man and Rat. In Diabetologia (Vol. 18).

24. Blackman, S. M., Commander, C. W., Watson, C., Arcara, K. M., Strug, L. J., Stonebraker, J. R., Wright, F. A., Rommens, J. M., Sun, L., Pace, R. G., Norris, S. A., Durie, P. R., Drumm, M. L., Knowles, M. R., & Cutting, G. R. (2013). Genetic modifiers of cystic fibrosis-related diabetes. Diabetes, 62(10), 3627–3635. https://doi.org/10.2337/db13-0510

25. Bogdani, M., Blackman, S. M., Ridaura, C., Bellocq, J. P., Powers, A. C., & Aguilar-Bryan, L. (2017). Structural abnormalities in islets from very young children with cystic fibrosis may contribute to cystic fibrosis-related diabetes. Scientific Reports, 7(1). https://doi.org/10.1038/s41598-017-17404-z

26. Boom, A., Lybaert, P., Pollet, J. F., Jacobs, P., Jijakli, H., Golstein, P. E., Sener, A., Malaisse, W. J., & Beauwens, R. (2007). Expression and localization of cystic fibrosis transmembrane conductance regulator in the rat endocrine pancreas. Endocrine, 32(2), 197–205. https://doi.org/10.1007/s12020-007-9026-x

27. Borowitz, D. (2015). CFTR, bicarbonate, and the pathophysiology of cystic fibrosis. Pediatric Pulmonology, 50(S40), 2S4-S30. https://doi.org/10.1002/ppul.23247

28. Boudreau, V., Reynaud, Q., Dubois, C. L., Coriati, A., Desjardins, K., Durieu, I., & Rabasa-Lhoret, R. (2016). Screening for Cystic Fibrosis-Related Diabetes: Matching Pathophysiology and Addressing Current Challenges. In Canadian Journal of Diabetes (Vol. 40, Issue 5, pp. 466–470). Elsevier B.V. https://doi.org/10.1016/j.jcjd.2016.08.221

29. Brennan, A. L., Geddes, D. M., Gyi, K. M., & Baker, E. H. (2004). Clinical importance of cystic fibrosis-related diabetes. In Journal of Cystic Fibrosis (Vol. 3, Issue 4, pp. 209–222). Elsevier. https://doi.org/10.1016/j.jcf.2004.08.001

30. Brookes, S. J. H., Steele, P. A., & Costa, M. (1991). Identification and immunohistochemistry of cholinergic and non-cholinergic circular muscle motor neurons in the guinea-pig small intestine. Neuroscience, 42(3), 863–878. https://doi.org/10.1016/0306-4522(91)90050-X

31. Brownstein, D. G. (2003). Manipulating the Mouse Embryo: A Laboratory Manual. Third Edition. By Andras Nagy, Marina Gertsenstein, Kristina Vintersten, and Richard Behringer. Cold Spring Harbor (New York): Cold Spring Harbor Laboratory Press. $195.00 (hardcover); $115.00 (paper). x + 764 p; ill.; index. ISBN: 0-87969-574-9 (hc); 0-87969-591-9 (pb). 2003. The Quarterly Review of Biology, 78(3), 365–365. https://doi.org/10.1086/380032

32. Bruscia, E. M., & Bonfield, T. L. (2016). Cystic Fibrosis Lung Immunity: The Role of the Macrophage. In Journal of Innate Immunity (Vol. 8, Issue 6, pp. 550–563). S. Karger AG. https://doi.org/10.1159/000446825

33. Burns, J. L., & Rolain, J. M. (2014). Culture-based diagnostic microbiology in cystic fibrosis: Can we simplify the complexity? In Journal of Cystic Fibrosis (Vol. 13, Issue 1, pp. 1–9). Elsevier. https://doi.org/10.1016/j.jcf.2013.09.004

34. Bustamante-Marin, X. M., & Ostrowski, L. E. (2017). Cilia and mucociliary clearance. Cold Spring Harbor Perspectives in Biology, 9(4). https://doi.org/10.1101/cshperspect.a028241

35. Cai, Z. W., Liu, J., Li, H. Y., & Sheppard, D. N. (2011). Targeting F508del-CFTR to develop rational new therapies for cystic fibrosis. Acta Pharmacologica Sinica, 32(6), 693–701. https://doi.org/10.1038/aps.2011.71

36. Caughey, G. H., Leidig, F., Viro, N. F., & Nadel, J. A. (1988). Substance P and vasoactive intestinal peptide degradation by mast cell tryptase and chymase. Journal of Pharmacology and Experimental Therapeutics, 244(1).

37. Caverly, L. J., Zhao, J., & LiPuma, J. J. (2015). Cystic fibrosis lung microbiome: Opportunities to reconsider management of airway infection. In Pediatric Pulmonology (Vol. 50, pp. S31–S38). John Wiley and Sons Inc. https://doi.org/10.1002/ppul.23243

38. Chandra, R., & Liddle, R. A. (2015). Regulation of Pancreatic Secretion. https://doi.org/10.3998/panc.2015.38

39. Chappe, F., Loewen, M. E., Hanrahan, J. W., & Chappe, V. (2008). Vasoactive intestinal peptide increases cystic fibrosis transmembrane conductance regulator levels in the apical membrane of Calu-3 cells through a protein kinase C-dependent mechanism. The Journal of Pharmacology and Experimental Therapeutics, 327(1), 226–238. https://doi.org/10.1124/jpet.108.141143

40. Chappe, V., & I., S. (2012). VIP as a Corrector of CFTR Trafficking and Membrane Stability. In Cystic Fibrosis - Renewed Hopes Through Research. InTech. https://doi.org/10.5772/30840

41. Clarke, L. L., Grubb, B. R., Yankaskas, J. R., Cotton, C. U., McKenzie, A., & Boucher, R. C. (1994). Relationship of a non-cystic fibrosis transmembrane conductance regulator- mediated chloride conductance to organ-level disease in Cftr (-/-) mice. Proceedings of the National Academy of Sciences of the United States of America, 91(2), 479–483. https://doi.org/10.1073/pnas.91.2.479

42. Cobo, M., Anderson, P., Benabdellah, K., Toscano, M. G., Muñoz, P., García-Pérez, A., Gutierrez, I., Delgado, M., & Martin, F. (2013). Mesenchymal stem cells expressing vasoactive intestinal peptide ameliorate symptoms in a model of chronic multiple sclerosis. Cell Transplantation, 22(5), 839–854. https://doi.org/10.3727/096368912X657404

43. Colledge, W. H., Abella, B. S., Southern, K. W., Ratcliff, R., Jiang, C., Cheng, S. H., MacVinish, L. J., Anderson, J. R., Cuthbert, A. W., & Evans, M. J. (1995). Generation and characterization of a ΔF508 cystic fibrosis mouse model. Nature Genetics, 10(4), 445–452. https://doi.org/10.1038/ng0895-445

44. Costa, M., Brookes, S. J. H., & Hennig, G. W. (2000). Anatomy and physiology of the enteric nervous system. Gut, 47(SUPPL. 4), iv15–iv19. https://doi.org/10.1136/gut.47.suppl_4.iv15

45. Costa, M., Brookes, S. J., Steele, P. A., Gibbins, I., Burcher, E., & Kandiah, C. J. (1996). Neurochemical classification of myenteric neurons in the guinea-pig ileum. Neuroscience, 75(3), 949–967. https://doi.org/10.1016/0306-4522(96)00275-8

46. Cowley, E. A., Wang, C. G., Gosselin, D., Radzioch, D., & Eidelman, D. H. (1997). Mucociliary clearance in cystic fibrosis knockout mice infected with Pseudomonas aeruginosa. European Respiratory Journal, 10(10), 2312–2318. https://doi.org/10.1183/09031936.97.10102312

47. Crist, J. R., He, X. D., & Goyal, R. K. (1992). Both ATP and the peptide VIP are inhibitory neurotransmitters in guinea-pig ileum circular muscle. The Journal of Physiology, 447, 119–131. https://doi.org/10.1113/jphysiol.1992.sp018994

48. Crowe, R., Kamm, M. A., Burnstock, G., & Lennard-Jones, J. E. (1992). Peptide-containing neurons in different regions of the submucous plexus of human sigmoid colon. Gastroenterology, 102(2), 461–467. https://doi.org/10.5555/URI:PII:001650859290091C

49. Cui, C. Y., & Schlessinger, D. (2015). Eccrine sweat gland development and sweat secretion. In Experimental Dermatology (Vol. 24, Issue 9, pp. 644–650). Blackwell Publishing Ltd. https://doi.org/10.1111/exd.12773

50. Cuthbertson, L., Walker, A. W., Oliver, A. E., Rogers, G. B., Rivett, D. W., Hampton, T. H., Ashare, A., Elborn, J. S., De Soyza, A., Carroll, M. P., Hoffman, L. R., Lanyon, C., Moskowitz, S. M., O'Toole, G. A., Parkhill, J., Planet, P. J., Teneback, C. C., Tunney, M. M., Zuckerman, J. B., Bruce, K. D., & Van Der Gast, C. J. (2020). Lung function and microbiota diversity in cystic fibrosis. Microbiome, 8(1), 45. https://doi.org/10.1186/s40168-020-00810-3

51. Cystic Fibrosis Canada. (2020). Retrieved June 22, 2020, from https://www.cysticfibrosis.ca/our-programs/cf-registry

52. Danahay, H., & Gosling, M. (2020). TMEM16A: An alternative approach to restoring airway anion secretion in cystic fibrosis? In International Journal of

Molecular Sciences (Vol. 21, Issue 7). MDPI AG. https://doi.org/10.3390/ijms21072386

53. Davis, P. B. (2006). Cystic fibrosis since 1938. American Journal of Respiratory and Critical Care Medicine, 173(5), 475–482. https://doi.org/10.1164/rccm.200505-840OE

54. De Boeck, K. (2020). Cystic fibrosis in the year 2020: A disease with a new face. Acta Paediatrica, 109(5), 893–899. https://doi.org/10.1111/apa.15155

55. de Jonge, W. J. (2013). The Gut's Little Brain in Control of Intestinal Immunity. ISRN Gastroenterology, 2013, 1–17. https://doi.org/10.1155/2013/630159

56. De Lisle, R. C., & Borowitz, D. (2013). The cystic fibrosis intestine. Cold Spring Harbor Perspectives in Medicine, 3(9), a009753. https://doi.org/10.1101/cshperspect.a009753

57. Delaney, S. J., Alton, E. W. F. W., Smith, S. N., Lunn, D. P., Farley, R., Lovelock, P. K., Thomson, S. A., Hume, D. A., Lamb, D., Porteous, D. J., Dorin, J. R., & Wainwright, B. J. (1996). Cystic fibrosis mice carrying the missense mutation G551D replicate human genotype-phenotype correlations. EMBO Journal, 15(5), 955–963. https://doi.org/10.1002/j.1460-2075.1996.tb00432.x

58. Delgado, M., & Ganea, D. (2013). Vasoactive intestinal peptide: A neuropeptide with pleiotropic immune functions. In Amino Acids (Vol. 45, Issue 1, pp. 25–39). NIH Public Access. https://doi.org/10.1007/s00726-011-1184-8

59. Delgado, M., Gomariz, R. P., Martinez, C., Abad, C., & Leceta, J. (2000). Anti-inflammatory properties of the type 1 and type 2 vasoactive intestinal peptide receptors: role in lethal endotoxic shock. European Journal of Immunology, 30(11), 3236–3246. https://doi.org/10.1002/1521-4141(200011)30:11<3236::AID-IMMU3236>3.0.CO;2-L

60. Delgado, M., Pozo, D., & Ganea, D. (2004). The significance of vasoactive intestinal peptide in immunomodulation. In Pharmacological Reviews (Vol. 56,

Issue 2, pp. 249–290). American Society for Pharmacology and Experimental Therapeutics. https://doi.org/10.1124/pr.56.2.7

61. Denning, G. M., Anderson, M. P., Amara, J. F., Marshall, J., Smith, A. E., & Welsh, M. J. (1992). Processing of mutant cystic fibrosis transmembrane conductance regulator is temperature-sensitive. Nature, 358(6389), 761–764. https://doi.org/10.1038/358761a0

62. Dérand, R., Montoni, A., Bulteau-Pignoux, L., Janet, T., Moreau, B., Muller, J. M., & Becq, F. (2004). Activation of VPAC 1 receptors by VIP and PACAP-27 in human bronchial epithelial cells induces CFTR-dependent chloride secretion. British Journal of Pharmacology, 141(4), 698–708. https://doi.org/10.1038/sj.bjp.0705597

63. Dhooghe, B., Bouckaert, C., Capron, A., Wallemacq, P., Leal, T., & Noel, S. (2015). Resveratrol increases F508del-CFTR dependent salivary secretion in cystic fibrosis mice. Biology Open, 4(7), 929–936. https://doi.org/10.1242/bio.010967

64. Dickson, L., & Finlayson, K. (2009). VPAC and PAC receptors: From ligands to function. In Pharmacology and Therapeutics (Vol. 121, Issue 3, pp. 294–316). Pergamon. https://doi.org/10.1016/j.pharmthera.2008.11.006

65. Donaldson, S. H., Pilewski, J. M., Griese, M., Cooke, J., Viswanathan, L., Tullis, E., Davies, J. C., Lekstrom-Himes, J. A., & Wang, L. T. (2018). Tezacaftor/ivacaftor in subjects with cystic fibrosis and F508del/F508del-CFTR or F508del/G551D-CFTR. American Journal of Respiratory and Critical Care Medicine, 197(2), 214–224. https://doi.org/10.1164/rccm.201704-0717OC

66. Durie, P. R., Kent, G., Phillips, M. J., & Ackerley, C. A. (2004). Characteristic Multiorgan Pathology of Cystic Fibrosis in a Long-Living Cystic Fibrosis Transmembrane Regulator Knockout Murine Model. American Journal of Pathology, 164(4), 1481–1493. https://doi.org/10.1016/S0002-9440(10)63234-8

67. Edlund, A., Pedersen, M. G., Lindqvist, A., Wierup, N., Flodström-Tullberg, M., & Eliasson, L. (2017). CFTR is involved in the regulation of glucagon secretion in human and rodent alpha cells. Scientific Reports, 7(1), 90. https://doi.org/10.1038/s41598-017-00098-8

68. Edlund, A., Pedersen, M. G., Lindqvist, A., Wierup, N., Flodström-Tullberg, M., & Eliasson, L. (2017). CFTR is involved in the regulation of glucagon secretion in human and rodent alpha cells. Scientific Reports, 7(1). https://doi.org/10.1038/s41598-017-00098-8

69. Eedy, D. J., Shaw, C., Armstrong, E. P., Johnston, C. F., & Buchanan, K. D. (1990). Vasoactive intestinal peptide (VIP) and peptide histidine methionine (PHM) in human eccrine sweat glands: demonstration of innervation, specific binding sites and presence in secretions. British Journal of Dermatology, 123(1), 65–76. https://doi.org/10.1111/j.1365-2133.1990.tb01825.x

70. Elborn, J. S. (2016). Cystic fibrosis. In The Lancet (Vol. 388, Issue 10059, pp. 2519–2531). Lancet Publishing Group. https://doi.org/10.1016/S0140-6736(16)00576-6

71. El-Salhy, M., & Sandström, O. (1999). How age changes the content of neuroendocrine peptides in the murine gastrointestinal tract. Gerontology, 45(1), 17–22. https://doi.org/10.1159/000022050

72. Enaud, R., Hooks, K. B., Barre, A., Barnetche, T., Hubert, C., Massot, M., Bazin, T., Clouzeau, H., Bui, S., Fayon, M., Berger, P., Lehours, P., Bébéar, C., Nikolski, M., Lamireau, T., Delhaes, L., & Schaeverbeke, T. (2019). Intestinal Inflammation in Children with Cystic Fibrosis Is Associated with Crohn's-Like Microbiota Disturbances. Journal of Clinical Medicine, 8(5), 645. https://doi.org/10.3390/jcm8050645

73. Ermund, A., Meiss, L. N., Dolan, B., Bähr, A., Klymiuk, N., & Hansson, G. C. (2018). The mucus bundles responsible for airway cleaning are retained in cystic fibrosis and by cholinergic stimulation. Eur Respir J, 52, 1800457. https://doi.org/10.1183/13993003.00457-2018

74. Ertongur-Fauth, T., Hochheimer, A., Buescher, J. M., Rapprich, S., & Krohn, M. (2014). A novel TMEM16A splice variant lacking the dimerization domain contributes to calcium-activated chloride secretion in human sweat gland epithelial cells. Experimental Dermatology, 23(11), 825–831. https://doi.org/10.1111/exd.12543

75. Esposito, S., Pennoni, G., Mencarini, V., Palladino, N., Peccini, L., & Principi, N. (2019). Antimicrobial Treatment of Staphylococcus aureus in Patients with Cystic Fibrosis. In Frontiers in Pharmacology (Vol. 10, Issue JULY, p. 849). Frontiers Media S.A. https://doi.org/10.3389/fphar.2019.00849

76. Fabricius, D., Karacay, B., Shutt, D., Leverich, W., Schafer, B., Takle, E., Thedens, D., Khanna, G., Raikwar, S., Yang, B., Desmond, M. E., & O'Dorisio, M. S. (2011). Characterization of intestinal and pancreatic dysfunction in VPAC1-Null mutant mouse. Pancreas, 40(6), 861–871. https://doi.org/10.1097/MPA.0b013e318214c783

77. Fajac, I., & De Boeck, K. (2017). New horizons for cystic fibrosis treatment. Pharmacology & Therapeutics, 170, 205–211. https://doi.org/10.1016/j.pharmthera.2016.11.009

78. Falconer, D. S. (2020). Weight and age at puberty in female and male mice of strains selected for large and small body size. Genet. Res., Camb, 44, 47–72. https://doi.org/10.1017/S0016672300026240

79. Feldman, A. T., & Wolfe, D. (2014). Tissue processing and hematoxylin and eosin staining. Methods in Molecular Biology (Clifton, N.J.), 1180, 31–43. https://doi.org/10.1007/978-1-4939-1050-2_3

80. Festini, F., Buzzetti, R., Bassi, C., Braggion, C., Salvatore, D., Taccetti, G., & Mastella, G. (2006). Isolation measures for prevention of infection with respiratory pathogens in cystic fibrosis: a systematic review. In Journal of Hospital Infection (Vol. 64, Issue 1, pp. 1–6). J Hosp Infect. https://doi.org/10.1016/j.jhin.2006.02.021

81. Filkins, L. M., & O'Toole, G. A. (2015). Cystic Fibrosis Lung Infections: Polymicrobial, Complex, and Hard to Treat. PLOS Pathogens, 11(12), e1005258. https://doi.org/10.1371/journal.ppat.1005258

82. Fox-Threlkeld, J. E., Manaka, H., Manaka, Y., Cipris, S., & Daniel, E. E. (1991). Stimulation of circular muscle motility of the isolated perfused canine ileum: relationship to VIP output. Peptides, 12(5), 1039–1045. https://doi.org/10.1016/0196-9781(91)90057-v

83. Frizzell, R. A., & Hanrahan, J. W. (2012). Physiology of epithelial chloride and fluid secretion. Cold Spring Harbor Perspectives in Medicine, 2(6). https://doi.org/10.1101/cshperspect.a009563

84. Furness, J. B., & Costa, M. (1979). Projections of intestinal neurons showing immunoreactivity for vasoactive intestinal polypeptide are consistent with these neurons being the enteric inhibitory neurons. Neuroscience Letters, 15(2–3), 199–204. https://doi.org/10.1016/0304-3940(79)96113-5

85. Furness, J. B., Costa, M., & Keast, J. R. (1984). Choline acetyltransferase- and peptide immunoreactivity of submucous neurons in the small intestine of the guinea-pig. Cell and Tissue Research, 237(2), 329–336. https://doi.org/10.1007/bf00217152

86. Furness, J. B. (2000). Types of neurons in the enteric nervous system. Journal of the Autonomic Nervous System, 81(1–3), 87–96. https://doi.org/10.1016/s0165-1838(00)00127-2

87. Furness, J. B. (2008). The enteric nervous system: Normal functions and enteric neuropathies. In Neurogastroenterology and Motility (Vol. 20, Issue SUPPL. 1, pp. 32–38). https://doi.org/10.1111/j.1365-2982.2008.01094.x

88. Furness, J.B. (2012). The enteric nervous system and neurogastroenterology. In Nature Reviews Gastroenterology and Hepatology (Vol. 9, Issue 5, pp. 286–294). Nature Publishing Group. https://doi.org/10.1038/nrgastro.2012.32

89. Furness, J.B., Callaghan, B. P., Rivera, L. R., & Cho, H. J. (2014). The enteric nervous system and gastrointestinal innervation: Integrated local and central control. Advances in Experimental Medicine and Biology, 817, 39–71. https://doi.org/10.1007/978-1-4939-0897-4_3

90. Furness, J.B. (2007). The Enteric Nervous System. In John Barton Furness (Ed.), The Enteric Nervous System. Blackwell Publishing. https://doi.org/10.1002/9780470988756

91. Furness, J.B. (2008). The Enteric Nervous System.

92. Ganea, D., Hooper, K. M., & Kong, W. (2015). The neuropeptide vasoactive intestinal peptide: Direct effects on immune cells and involvement in inflammatory and autoimmune diseases. In Acta Physiologica (Vol. 213, Issue 2, pp. 442–452). Blackwell Publishing Ltd. https://doi.org/10.1111/apha.12427

93. Geyer, M. C., Sullivan, T., Tai, A., Morton, J. M., Edwards, S., Martin, A. J., Perano, S. J., Gagliardi, L., Rayner, C. K., Horowitz, M., & Couper, J. J. (2019). Exenatide corrects postprandial hyperglycaemia in young people with cystic fibrosis and impaired glucose tolerance: A randomized crossover trial. Diabetes, Obesity and Metabolism, 21(3), 700–704. https://doi.org/10.1111/dom.13544

94. Geyer, M. C., Sullivan, T., Tai, A., Morton, J. M., Edwards, S., Martin, A. J., Perano, S. J., Gagliardi, L., Rayner, C. K., Horowitz, M., & Couper, J. J. (2019). Exenatide corrects postprandial hyperglycaemia in young people with cystic fibrosis and impaired glucose tolerance: A randomized crossover trial. Diabetes, Obesity and Metabolism, 21(3), 700–704. https://doi.org/10.1111/dom.13544

95. Ghelani, D. P., & Schneider-Futschik, E. K. (2020). Emerging Cystic Fibrosis Transmembrane Conductance Regulator Modulators as New Drugs for Cystic Fibrosis: A Portrait of in Vitro Pharmacology and Clinical Translation. In ACS Pharmacology and Translational Science (Vol. 3, Issue 1, pp. 4–10). American Chemical Society. https://doi.org/10.1021/acsptsci.9b00060

96. Gibson, L. E., & Cooke, R. E. (1959). A test for concentration of electrolytes in sweat in cystic fibrosis of the pancreas utilizing pilocarpine by iontophoresis.

97. Gibson-Corley, K. N., Meyerholz, D. K., & Engelhardt, J. F. (2016). Pancreatic pathophysiology in cystic fibrosis. In Journal of Pathology (Vol. 238, Issue 2, pp. 311–320). John Wiley and Sons Ltd. https://doi.org/10.1002/path.4634

98. Gonçalves, A. C., Marson, F. A. de L., Mendonça, R. M. de H., Ribeiro, J. D., Ribeiro, A. F., Paschoal, I. A., & Levy, C. E. (2013). Saliva as a potential tool for cystic fibrosis diagnosis. Diagnostic Pathology, 8(1), 46. https://doi.org/10.1186/1746-1596-8-46

99. Gonzalez-Rey, E., & Delgado, M. (2006). Therapeutic Treatment of Experimental Colitis With Regulatory Dendritic Cells Generated With Vasoactive Intestinal Peptide. Gastroenterology, 131(6), 1799–1811. https://doi.org/10.1053/j.gastro.2006.10.023

100. Gozes, I., Avidor, R., Yahav, Y., Katznelson, D., Croce, C. M., & Huebner, K. (1987). The gene encoding vasoactive intestinal peptide is located on human chromosome 6p21→6qter. Human Genetics, 75(1), 41–44. https://doi.org/10.1007/BF00273836

101. Granados, A., Chan, C. L., Ode, K. L., Moheet, A., Moran, A., & Holl, R. (2019). Cystic fibrosis related diabetes: Pathophysiology, screening and diagnosis. Journal of Cystic Fibrosis. https://doi.org/10.1016/j.jcf.2019.08.016

102. Gray, M. A., Winpenny, J. P., Verdon, B., McAlroy, H., & Argent, B. E. (1995). Chloride channels and cystic fibrosis of the pancreas. Bioscience Reports, 15(6), 531–541. https://doi.org/10.1007/BF01204355

103. Grubb, B. R., & Gabriel, S. E. (1997). Intestinal physiology and pathology in gene-targeted mouse models of cystic fibrosis. American Journal of Physiology - Gastrointestinal and Liver Physiology, 273(2 36-2). https://doi.org/10.1152/ajpgi.1997.273.2.g258

104. Guilbault, C., Martin, P., Houle, D., Boghdady, M. L., Guiot, M. C., Marion, D., & Radzioch, D. (2005). Cystic fibrosis lung disease following infection with Pseudomonas aeruginosa in Cftr knockout mice using novel non-invasive direct pulmonary infection technique. Laboratory Animals, 39(3), 336–352. https://doi.org/10.1258/0023677054306944

105. Guilbault, C., Novak, J. P., Martin, P., Boghdady, M. L., Saeed, Z., Guiot, M. C., Hudson, T. J., & Radzioch, D. (2006). Distinct pattern of lung gene expression in the Cftr-KO mice developing spontaneous lung disease compared with their littermate controls. Physiological Genomics, 25(2), 179–193. https://doi.org/10.1152/physiolgenomics.00206.2005

106. Gyömörey, K., Rozmahel, R., & Bear, C. E. (2000). Amelioration of intestinal disease severity in cystic fibrosis mice is associated with improved chloride secretory capacity. Pediatric Research, 48(6), 731–734. https://doi.org/10.1203/00006450-200012000-00005

107. Haedersdal, S., Lund; Asger, Knop, F. K., & Vilsbøll, T. (2018). The Role of Glucagon in the Pathophysiology and Treatment of Type 2 Diabetes. https://doi.org/10.1016/j.mayocp.2017.12.003

108. Hamidi, S. A., Szema, A. M., Lyubsky, S., Dickman, K. G., Degene, A., Mathew, S. M., Waschek, J. A., & Said, S. I. (2006). Clues to VIP function from knockout mice. Annals of the New York Academy of Sciences, 1070, 5–9. https://doi.org/10.1196/annals.1317.035

109. Harris, A., Chalkley, G., Goodman, S., & Coleman, L. (1991). Expression of the cystic fibrosis gene in human development. Development (Cambridge, England), 113(1), 305–310. http://www.ncbi.nlm.nih.gov/pubmed/1765002

110. Hart, N. J., Aramandla, R., Poffenberger, G., Fayolle, C., Thames, A. H., Bautista, A., Spigelman, A. F., Babon, J. A. B., DeNicola, M. E., Dadi, P. K., Bush, W. S., Balamurugan, A. N., Brissova, M., Dai, C., Prasad, N., Bottino, R., Jacobson, D. A., Drumm, M. L., Kent, S. C., MacDonald, P. E., & Powers, A. C. (2018). Cystic

fibrosis-related diabetes is caused by islet loss and inflammation. JCI Insight, 3(8). https://doi.org/10.1172/jci.insight.98240

111. Havel, P. J., Dunning, B. E., Verchere, C. B., Baskin, D. G., O'Dorisio, T., & Taborsky, G. J. (1997). Evidence that vasoactive intestinal polypeptide is a parasympathetic neurotransmitter in the endocrine pancreas in dogs. Regulatory Peptides, 71(3), 163–170. https://doi.org/10.1016/S0167-0115(97)01014-8

112. Heinz-Erian P., Dey, R. D., Flux, M., & Said, S. I. (1985). Deficient vasoactive intestinal peptide innervation in the sweat glands of cystic fibrosis patients. Science (New York, N.Y.), 229(4720), 1407–1408. https://doi.org/10.1126/science.4035357

113. Henning, R. J. (2013). Handbook of Biologically Active Peptides. In Handbook of Biologically Active Peptides. Elsevier. https://doi.org/10.1016/B978-0-12-385095-9.00196-2

114. Henning, R. J., & Sawmiller, D. R. (2001). Vasoactive intestinal peptide: Cardiovascular effects. In Cardiovascular Research (Vol. 49, Issue 1, pp. 27–37). Oxford Academic. https://doi.org/10.1016/S0008-6363(00)00229-7

115. Henquin, J. C. (2000). Triggering and amplifying pathways of regulation of insulin secretion by glucose. In Diabetes (Vol. 49, Issue 11, pp. 1751–1760). American Diabetes Association Inc. https://doi.org/10.2337/diabetes.49.11.1751

116. Henquin, J. C. (2009). Regulation of insulin secretion: A matter of phase control and amplitude modulation. In Diabetologia (Vol. 52, Issue 5, pp. 739–751). https://doi.org/10.1007/s00125-009-1314-y

117. Henquin, J.C. (2000). Triggering and amplifying pathways of regulation of insulin secretion by glucose. In Diabetes (Vol. 49, Issue 11, pp. 1751–1760). American Diabetes Association Inc. https://doi.org/10.2337/diabetes.49.11.1751

118. Hinnen, D. (2017). Glucagon-like peptide 1 receptor agonists for type 2 diabetes. Diabetes Spectrum, 30(3), 202–210. https://doi.org/10.2337/ds16-0026

119. Hodge, B. D., & Brodell, R. T. (2018). Anatomy, Skin, Sweat Glands. In StatPearls. StatPearls Publishing. http://www.ncbi.nlm.nih.gov/pubmed/29489179

120. Hoegger, M. J., Fischer, A. J., McMenimen, J. D., Ostedgaard, L. S., Tucker, A. J., Awadalla, M. A., Moninger, T. O., Michalski, A. S., Hoffman, E. A., Zabner, J., Stoltz, D. A., & Welsh, M. J. (2014). Impaired mucus detachment disrupts mucociliary transport in a piglet model of cystic fibrosis. Science, 345(6198), 818–822. https://doi.org/10.1126/science.1255825

121. Holst, J. J., Fahrenkrug, J., Knuhtsen, S., Jensen, S. L., Seier Poulsen, S., & Vagn Nielsen, O. (1984). Vasoactive intestinal polypeptide (VIP) in the pig pancreas: role of VIPergic nerves in control of fluid and bicarbonate secretion. Regulatory Peptides, 8(3), 245–259. https://doi.org/10.1016/0167-0115(84)90066-1

122. Holst, J. J., Fahrenkrug, J., Knuhtsen, S., Jensen, S. L., Seier Poulsen, S., & Vagn Nielsen, O. (1984). Vasoactive intestinal polypeptide (VIP) in the pig pancreas: role of VIPergic nerves in control of fluid and bicarbonate secretion. Regulatory Peptides, 8(3), 245–259. https://doi.org/10.1016/0167-0115(84)90066-1

123. Huang, W. Q., Guo, J. H., Yuan, C., Cui, Y. G., Diao, F. Y., Yu, M. K., Liu, J. Y., Ruan, Y. C., & Chan, H. C. (2017). Abnormal CFTR affects glucagon production by islet a cells in cystic fibrosis and polycystic ovarian syndrome. Frontiers in Physiology, 8(NOV), 835. https://doi.org/10.3389/fphys.2017.00835

124. Huang, W. Q., Guo, J. H., Zhang, X. H., Yu, M. K., Chung, Y. W., Ruan, Y. C., & Chan, H. C. (2017). Glucose-Sensitive CFTR Suppresses Glucagon Secretion by Potentiating KATP Channels in Pancreatic Islet α Cells. Endocrinology, 158(10), 3188–3199. https://doi.org/10.1210/en.2017-00282

125. Ianowski, J. P., Choi, J. Y., Wine, J. J., & Hanrahan, J. W. (2007). Mucus secretion by single tracheal submucosal glands from normal and cystic fibrosis transmembrane conductance regulator knockout mice. The Journal of Physiology, 580(1), 301–314. https://doi.org/10.1113/jphysiol.2006.123653

126. Ishihara, T., Shigemoto, R., Mori, K., Takahashi, K., & Nagata, S. (1992). Functional expression and tissue distribution of a novel receptor for vasoactive intestinal polypeptide. Neuron, 8(4), 811–819. https://doi.org/10.1016/0896-6273(92)90101-I

127. Iwasaki, M., Akiba, Y., & Kaunitz, J. D. (2019). Recent advances in vasoactive intestinal peptide physiology and pathophysiology: Focus on the gastrointestinal system [version 1; peer review: 4 approved]. In F1000Research (Vol. 8). F1000 Research Ltd. https://doi.org/10.12688/f1000research.18039.1

128. Jae, Y. C., Nam, S. J., Krouse, M. E., Wu, J. V., Robbins, R. C., Ianowski, J. P., Hanrahan, J. W., & Wine, J. J. (2007). Synergistic airway gland mucus secretion in response to vasoactive intestinal peptide and carbachol is lost in cystic fibrosis. Journal of Clinical Investigation, 117(10), 3118–3127. https://doi.org/10.1172/JCI31992

129. Jamen, F., Persson, K., Bertrand, G., Rodriguez-Henche, N., Puech, R., Bockaert, J., Ahrén, B., & Brabet, P. (2000). PAC1 receptor-deficient mice display impaired insulinotropic response to glucose and reduced glucose tolerance. Journal of Clinical Investigation, 105(9), 1307–1315. https://doi.org/10.1172/JCI9387

130. Jay Freeman, A., & Ooi, C. Y. (2017). Pancreatitis and pancreatic cystosis in Cystic Fibrosis. Journal of Cystic Fibrosis, 16, S79–S86. https://doi.org/10.1016/j.jcf.2017.07.004

131. Jessen, K. R., Saffrey, M. J., Van Noorden, S., Blooms, S. R., Polak, J. M., & Burnstock, G. (1980). Immunohistochemical studies of the enteric nervous system in tissue culture and in situ: Localization of vascoactive intestinal polypeptide (VIP), Substance-P and enkephalin immunoreactive nerves in the

guinea-pig gut. Neuroscience, 5(10), 1717–1735. https://doi.org/10.1016/0306-4522(80)90091-3

132. Jimeno, R., Gomariz, R. P., Gutiérrez-Cañas, I., Martínez, C., Juarranz, Y., & Leceta, J. (2010). New insights into the role of VIP on the ratio of T-cell subsets during the development of autoimmune diabetes. Immunology and Cell Biology, 88(7), 734–745. https://doi.org/10.1038/icb.2010.29

133. Kato, A., & Romero, M. F. (2011). Regulation of electroneutral NaCl absorption by the small intestine. Annual Review of Physiology, 73, 261–281. https://doi.org/10.1146/annurev-physiol-012110-142244

134. Kato, I., Suzuki, Y., Akabane, A., Yonekura, H., Tanaka, O., Kondo, H., Takasawa, S., Yoshimoto, T., & Okamoto, H. (1994). Transgenic mice overexpressing human vasoactive intestinal peptide (VIP) gene in pancreatic β cells. Evidence for improved glucose tolerance and enhanced insulin secretion by VIP and PHM-27 in vivo. Journal of Biological Chemistry, 269(33), 21223–21228.

135. Kato, I., Suzuki, Y., Akabane, A., Yonekura, H., Tanaka, O., Kondo, H., Takasawa, S., Yoshimoto, T., & Okamoto, H. (2006). Enhancement of Glucose-induced Insulin Secretion in Transgenic Mice Overexpressing Human VIP Gene in Pancreatic β Cells1. Annals of the New York Academy of Sciences, 805(1), 232–243. https://doi.org/10.1111/j.1749-6632.1996.tb17486.x

136. Kayani, K., Mohammed, R., & Mohiaddin, H. (2018). Cystic fibrosis-related diabetes. In Frontiers in Endocrinology (Vol. 9, Issue FEB). Frontiers Media S.A. https://doi.org/10.3389/fendo.2018.00020

137. Keiser, N. W., & Engelhardt, J. F. (2011). New animal models of cystic fibrosis: What are they teaching us? In Current Opinion in Pulmonary Medicine (Vol. 17, Issue 6, pp. 478–483). NIH Public Access. https://doi.org/10.1097/MCP.0b013e32834b14c9

138. Kelly, J. (2017). Environmental scan of cystic fibrosis research worldwide. Journal of Cystic Fibrosis, 16(3), 367–370. https://doi.org/10.1016/j.jcf.2016.11.002

139. Kelsey, R., Manderson Koivula, F. N., McClenaghan, N. H., & Kelly, C. (2019). Cystic Fibrosis–Related Diabetes: Pathophysiology and Therapeutic Challenges. In Clinical Medicine Insights: Endocrinology and Diabetes (Vol. 12). SAGE Publications Ltd. https://doi.org/10.1177/1179551419851770

140. Kent, G., Iles, R., Bear, C. E., Huan, L. J., Griesenbach, U., McKerlie, C., Frndova, H., Ackerley, C., Gosselin, D., Radzioch, D., O'Brodovich, H., Tsui, L. C., Buchwald, M., & Tanswell, A. K. (1997). Lung disease in mice with cystic fibrosis. Journal of Clinical Investigation, 100(12), 3060–3069. https://doi.org/10.1172/JCI119861

141. Khan, M. A., Ali, Z. S., Sweezey, N., Grasemann, H., & Palaniyar, N. (2019). Progression of cystic fibrosis lung disease from childhood to adulthood: Neutrophils, neutrophil extracellular trap (NET) formation, and NET degradation. In Genes (Vol. 10, Issue 3). MDPI AG. https://doi.org/10.3390/genes10030183

142. Kim, J., Farahmand, M., Dunn, C., Davies, Z., Frisbee, E., Milla, C., & Wine, J. J. (2016). Evaporimeter and Bubble-Imaging Measures of Sweat Gland Secretion Rates. https://doi.org/10.1371/journal.pone.0165254

143. Konrad, K., Scheuing, N., Badenhoop, K., Borkenstein, M. H., Gohlke, B., Schöfl, C., Seufert, J., Thon, A., & Holl, R. W. (2013). Cystic fibrosis-related diabetes compared with type 1 and type 2 diabetes in adults. Diabetes/Metabolism Research and Reviews, 29(7), 568–575. https://doi.org/10.1002/dmrr.2429

144. Konrad, K., Thon, A., Fritsch, M., Fröhlich-Reiterer, E., Lilienthal, E., Wudy, S. A., & Holl, R. W. (2013). Comparison of cystic fibrosis-related diabetes with type 1 diabetes based on a German/Austrian pediatric diabetes registry. Diabetes Care, 36(4), 879–886. https://doi.org/10.2337/dc12-0807

145. Kopito, R. R. (1999). Biosynthesis and degradation of CFTR. In Physiological Reviews (Vol. 79, Issue 1 SUPPL. 1). American Physiological Society. https://doi.org/10.1152/physrev.1999.79.1.S167

146. Laburthe, M., Couvineau, A., & Tan, V. (2007). Class II G protein-coupled receptors for VIP and PACAP: Structure, models of activation and pharmacology. In Peptides (Vol. 28, Issue 9, pp. 1631–1639). Elsevier. https://doi.org/10.1016/j.peptides.2007.04.026

147. Laguna, T. A., Nathan, B. M., & Moran, A. (2010). Managing diabetes in cystic fibrosis. Diabetes, Obesity and Metabolism, 12(10), 858–864. https://doi.org/10.1111/j.1463-1326.2010.01250.x

148. Laifihen, A., Partanen, M., Hervonen, A., Pelto-Huikko, M., & Laitinen, L. A. (1985). Histochemistry VIP like immunoreactive nerves in human respiratory tract Light and electron microscopic study. In Histochemistry (Vol. 82). https://idp.springer.com/authorize/casa?redirect_uri=https://link.springer.com/article/10.1007/BF00494059&casa_token=Zbh2XO3wWU4AAAAA:r8MbP3Sa8nhqdbCmaqdWd1xgBqFpn8iRzxGK1QZjpC1Ybwk0twyN0gURwjso3QejPZGZqktEuPvp7BNVIA

149. Laitinen, A., Partanen, M., Hervonen, A., Pelto-Huikko, M., & Laitinen, L. A. (1985). VIP like immunoreactive nerves in human respiratory tract - Light and electron microscopic study. Histochemistry, 82(4), 313–319. https://doi.org/10.1007/BF00494059

150. Lee, M., Kim, M., Park, J. S., Lee, S., You, J., Ahn, C. W., Kim, K. R., & Kang, S. (2019). Higher glucagon-to-insulin ratio is associated with elevated glycated hemoglobin levels in type 2 diabetes patients. Korean Journal of Internal Medicine, 34(5), 1068–1077. https://doi.org/10.3904/kjim.2016.233

151. Lehrich, R. W., Aller, S. G., Webster, P., Marino, C. R., & Forrest, J. N. (1998). Vasoactive intestinal peptide, forskolin, and genistein increase apical CFTR trafficking in the rectal gland of the spiny dogfish, Squalus acanthias: Acute

regulation of CFTR trafficking in an intact epithelium. Journal of Clinical Investigation, 101(4), 737–745. https://doi.org/10.1172/JCI803

152. Lévêque, M., Le Trionnaire, S., Del Porto, P., & Martin-Chouly, C. (2017). The impact of impaired macrophage functions in cystic fibrosis disease progression. In Journal of Cystic Fibrosis (Vol. 16, Issue 4, pp. 443–453). Elsevier B.V. https://doi.org/10.1016/j.jcf.2016.10.011

153. Li, C., Wu, Y., Riehle, A., Ma, J., Kamler, M., Gulbins, E., & Grassmé, H. (2017). Staphylococcus aureus survives in cystic fibrosis macrophages, forming a reservoir for chronic pneumonia. Infection and Immunity, 85(5). https://doi.org/10.1128/IAI.00883-16

154. Liegeois, M., Legrand, C., Desmet, C. J., Marichal, T., & Bureau, F. (2018). The interstitial macrophage: A long-neglected piece in the puzzle of lung immunity. In Cellular Immunology (Vol. 330, pp. 91–96). Academic Press Inc. https://doi.org/10.1016/j.cellimm.2018.02.001

155. Liou, T. G. (2019). The Clinical Biology of Cystic Fibrosis Transmembrane Regulator Protein: Its Role and Function in Extrapulmonary Disease. In Chest (Vol. 155, Issue 3, pp. 605–616). Elsevier Inc. https://doi.org/10.1016/j.chest.2018.10.006

156. Lopes-Pacheco, M. (2020). CFTR Modulators: The Changing Face of Cystic Fibrosis in the Era of Precision Medicine. In Frontiers in Pharmacology (Vol. 10, p. 1662). Frontiers Media S.A. https://doi.org/10.3389/fphar.2019.01662

157. Luciani, A., Villella, V. R., Esposito, S., Brunetti-Pierri, N., Medina, D., Settembre, C., Gavina, M., Pulze, L., Giardino, I., Pettoello-Mantovani, M., D'Apolito, M., Guido, S., Masliah, E., Spencer, B., Quaratino, S., Raia, V., Ballabio, A., & Maiuri, L. (2010). Defective CFTR induces aggresome formation and lung inflammation in cystic fibrosis through ROS-mediated autophagy inhibition. Nature Cell Biology, 12(9), 863–875. https://doi.org/10.1038/ncb2090

158. Lukacs, G. L., & Verkman, A. S. (2011). CFTR: folding, misfolding and correcting the ΔF508 conformational defect. https://doi.org/10.1016/j.molmed.2011.10.003

159. Mackie, A. D. R., Thornton, S. J., & Edenborough, F. P. (2003). Cystic fibrosis-related diabetes. Diabetic Medicine, 20(6), 425–436. https://doi.org/10.1046/j.1464-5491.2003.00924.x

160. Marcorelles, P., Friocourt, G., Uguen, A., Ledé, F., Férec, C., & Laquerrière, A. (2014). Cystic Fibrosis Transmembrane Conductance Regulator Protein (CFTR) Expression in the Developing Human Brain: Comparative Immunohistochemical Study between Patients with Normal and Mutated CFTR. Journal of Histochemistry and Cytochemistry, 62(11), 791–801. https://doi.org/10.1369/0022155414546190

161. Marcorelles, P., Gillet, D., Friocourt, G., Ledé, F., Samaison, L., Huguen, G., & Ferec, C. (2012). Cystic fibrosis transmembrane conductance regulator protein expression in the male excretory duct system during development. Human Pathology, 43(3), 390–397. https://doi.org/10.1016/j.humpath.2011.04.031

162. Marcorelles, P., Montier, T., Gillet, D., Lagarde, N., & Ferec, C. (2007). Evolution of CFTR protein distribution in lung tissue from normal and CF human fetuses. Pediatric Pulmonology, 42(11), 1032–1040. https://doi.org/10.1002/ppul.20690

163. Marino, C. R., Matovcik, L. M., Gorelick, F. S., & Cohn, J. A. (1991). Localization of the cystic fibrosis transmembrane conductance regulator in pancreas. Journal of Clinical Investigation, 88(2), 712–716. https://doi.org/10.1172/JCI115358

164. Martínez, C., Juarranz, Y., Gutiérrez-Cañas, I., Carrión, M., Pérez-García, S., Villanueva-Romero, R., Castro, D., Lamana, A., Mellado, M., González-álvaro, I., & Gomariz, R. P. (2020). A clinical approach for the use of VIP axis in inflammatory and autoimmune diseases. In International Journal of Molecular

Sciences (Vol. 21, Issue 1, p. 65). MDPI AG. https://doi.org/10.3390/ijms21010065

165. May, A., & Tucker, A. (2015). Understanding the development of the respiratory glands. Developmental Dynamics, 244(4), 525–539. https://doi.org/10.1002/dvdy.24250

166. McMorran, B. J., Palmer, J. S., Lunn, D. P., Oceandy, D., Costelloe, E. O., Thomas, G. R., Hume, D. A., & Wainwright, B. J. (2001). G551d cf mice display an abnormal host response and have impaired clearance of Pseudomonas lung disease. American Journal of Physiology - Lung Cellular and Molecular Physiology, 281(3 25-3). https://doi.org/10.1152/ajplung.2001.281.3.l740

167. Meyerholz, D. K., & Beck, A. P. (2018). Fundamental Concepts for Semiquantitative Tissue Scoring in Translational Research. In ILAR Journal (Vol. 59, Issue 1, pp. 13–17). Oxford University Press. https://doi.org/10.1093/ilar/ily025

168. Middleton, P. G., Mall, M. A., Dřevínek, P., Lands, L. C., McKone, E. F., Polineni, D., Ramsey, B. W., Taylor-Cousar, J. L., Tullis, E., Vermeulen, F., Marigowda, G., McKee, C. M., Moskowitz, S. M., Nair, N., Savage, J., Simard, C., Tian, S., Waltz, D., Xuan, F., Rowe, S. M., & Jain, R. (2019). Elexacaftor–Tezacaftor–Ivacaftor for Cystic Fibrosis with a Single Phe508del Allele. New England Journal of Medicine, 381(19), 1809–1819. https://doi.org/10.1056/NEJMoa1908639

169. Morales, M. M., Capella, M. A. M., & Lopes, A. G. (1999). CFTR structure and function. In Brazilian Journal of Medical and Biological Research (Vol. 32, Issue 8).

170. Moran, A., Becker, D., Casella, S. J., Gottlieb, P. A., Kirkman, M. S., Marshall, B. C., Slovis, B., Alexander, P., Beall, R. J., Brunzell, C., Campbell, P. W., Chin, M., Cohen, R. C., Brooks, J. F., George, C., Hazle, L., Katz, M., McKeon, C., Onady, G., Robinson, K. A., Rodgers, T., Sabadosa, K. A., Schindler, T., Stecenko, A., Wood, M. E., & Young, D. (2010). Epidemiology, pathophysiology, and

prognostic implications of cystic fibrosis-related diabetes: A technical review. In Diabetes Care (Vol. 33, Issue 12, pp. 2677–2683). https://doi.org/10.2337/dc10-1279

171. Moran, A., Brunzell, C., Cohen, R. C., Katz, M., Marshall, B. C., Onady, G., Robinson, K. A., Sabadosa, K. A., Stecenko, A., Slovis, B., Alexander, P., Beall, R. J., Becker, D., Campbell, P. W., Casella, S. J., Chin, M., Brooks, J. F., George, C., Gottlieb, P. A., Hazle, L., Kirkman, M. S., McKeon, C., Rodgers, T., Schindler, T., Wood, M. E., & Young, D. (2010). Clinical care guidelines for cystic fibrosis-related diabetes: A position statement of the American Diabetes Association and a clinical practice guideline of the Cystic Fibrosis Foundation, endorsed by the Pediatric Endocrine Society. In Diabetes Care (Vol. 33, Issue 12, pp. 2697–2708). Diabetes Care. https://doi.org/10.2337/dc10-1768

172. Nedvetsky, P. I., Emmerson, E., Finley, J. K., Ettinger, A., Cruz-Pacheco, N., Prochazka, J., Haddox, C. L., Northrup, E., Hodges, C., Mostov, K. E., Hoffman, M. P., & Knox, S. M. (2014). Parasympathetic Innervation Regulates Tubulogenesis in the Developing Salivary Gland. Developmental Cell, 30(4), 449–462. https://doi.org/10.1016/j.devcel.2014.06.012

173. Newton, C. M., Stoyek, M. R., Croll, R. P., & Smith, F. M. (2014). Regional innervation of the heart in the goldfish, Carassius auratus: A confocal microscopy study. Journal of Comparative Neurology, 522(2), 456–478. https://doi.org/10.1002/cne.23421

174. Norkina, O., Kaur, S., Ziemer, D., & De Lisle, R. C. (2004). Inflammation of the cystic fibrosis mouse small intestine. American Journal of Physiology - Gastrointestinal and Liver Physiology, 286(6 49-6). https://doi.org/10.1152/ajpgi.00473.2003

175. Norris, A. W. (2019). Is cystic fibrosis–related diabetes reversible? New data on CFTR potentiation and insulin secretion. In American Journal of Respiratory and Critical Care Medicine (Vol. 199, Issue 3, pp. 261–263). American Thoracic Society. https://doi.org/10.1164/rccm.201808-1501ED

176. Norris, A. W., Ode, K. L., Merjaneh, L., Sanda, S., Yi, Y., Sun, X., Engelhardt, J. F., & Hull, R. L. (2019). Survival in a bad neighborhood: Pancreatic islets in cystic fibrosis. In Journal of Endocrinology (Vol. 241, Issue 1, pp. R35–R50). BioScientifica Ltd. https://doi.org/10.1530/JOE-18-0468

177. O'riordan, J. I., Hayes, J., Fitzgerald, M. X., & Redmond, J. (1995). Peripheral Nerve Dysfunction in Adult Patients with Cystic Fibrosis (Vol. 164, Issue 3).

178. O'Toole, G. A. (2018). Cystic fibrosis airway microbiome: Overturning the old, opening the way for the new. Journal of Bacteriology, 200(4). https://doi.org/10.1128/JB.00561-17

179. Ohtsuka, Y., Lee, J., Stamm, D. S., & Sanderson, I. R. (2001). MIP-2 secreted by epithelial cells increases neutrophil and lymphocyte recruitment in the mouse intestine. Gut, 49(4), 526–533. https://doi.org/10.1136/gut.49.4.526

180. Okiyoneda, T., Barrière, H., Bagdány, M., Raben, W. M., Du, K., Höhfeld, J., Young, J., & Lukacs, G. L. (2010). Peripheral Protein Quality Control Removes Unfolded CFTR from the Plasma Membrane. In Source: Science, New Series (Vol. 329, Issue 5993).

181. Olivier, A. K., Yi, Y., Sun, X., Sui, H., Liang, B., Hu, S., Xie, W., Fisher, J. T., Keiser, N. W., Lei, D., Zhou, W., Yan, Z., Li, G., Evans, T. I. A., Meyerholz, D. K., Wang, K., Stewart, Z. A., Norris, A. W., & Engelhardt, J. F. (2012). Abnormal endocrine pancreas function at birth in cystic fibrosis ferrets. Journal of Clinical Investigation, 122(10), 3755–3768. https://doi.org/10.1172/JCI60610

182. Ostedgaard, L. S., Meyerholz, D. K., Chen, J.-H., Pezzulo, A. A., Karp, P. H., Rokhlina, T., Ernst, S. E., Hanfland, R. A., Reznikov, L. R., Ludwig, P. S., Rogan, M. P., Davis, G. J., Dohrn, C. L., Wohlford-Lenane, C., Taft, P. J., Rector, M. V, Hornick, E., Nassar, B. S., Samuel, M., Zhang, Y., Richter, S. S., Uc, A., Shilyansky, J., Prather, R. S., McCray Jr, P. B., Zabner, J., Welsh, M. J., Stoltz, D. A., Hughes Medical Institute, H., & Carver, L. A. (2011). The ΔF508 Mutation Causes CFTR

Misprocessing and Cystic Fibrosis-Like Disease in Pigs. Sci Transl Med, 3(74), 74–98. https://doi.org/10.1126/scitranslmed.3001868

183. Pan, J., Luk, C., Kent, G., Cutz, E., & Yeger, H. (2006). Pulmonary neuroendocrine cells, airway innervation, and smooth muscle are altered in Cftr null mice. American Journal of Respiratory Cell and Molecular Biology, 35(3), 320–326. https://doi.org/10.1165/rcmb.2005-0468OC

184. Peckham, D., & Whitaker, P. (2018). Cystic fibrosis. In Foundations of Respiratory Medicine (pp. 195–213). Springer International Publishing. https://doi.org/10.1007/978-3-319-94127-1_12

185. Penque, D., Mendes, F., Beck, S., Farinha, C., Pacheco, P., Nogueira, P., Lavinha, J., Malhó, R., & Amaral, M. D. (2000). Cystic fibrosis F508del patients have apically localized CFTR in a reduced number of airway cells. Laboratory Investigation, 80(6), 857–868. https://doi.org/10.1038/labinvest.3780090

186. Persson-Sjögren, S., Forsgren, S., & Lindström, P. (2006). Vasoactive intestinal polypeptide and pituitary adenylate cyclase activating polypeptide: Effects on insulin release in isolated mouse islets in relation to metabolic status and age. Neuropeptides, 40(4), 283–290. https://doi.org/10.1016/j.npep.2006.04.001

187. Pittman, J. E., & Ferkol, T. W. (2015). The evolution of cystic fibrosis care. Chest, 148(2), 533–542. https://doi.org/10.1378/chest.14-1997

188. Plaisancié, P., Barcelo, A., Moro, F., Claustre, J., Chayvialle, J. A., & Cuber, J. C. (1998). Effects of neurotransmitters, gut hormones, and inflammatory mediators on mucus discharge in rat colon. The American Journal of Physiology, 275(5), G1073-84. https://doi.org/10.1152/ajpgi.1998.275.5.G1073

189. Porter, A. J., Wattchow, D. A., Brookes, S. J., Schemann, M., & Costa, M. (1996). Choline acetyltransferase immunoreactivity in the human small and large intestine. Gastroenterology, 111(2), 401–408. https://doi.org/10.1053/gast.1996.v111.pm8690205

190. Porter, A.J., Wattchow, D. A., Brookes, S. J. H., & Costa, M. (1997). The Neurochemical Coding and Projections of Circular Muscle Motor Neurons in the Human Colon. In GASTROENTEROLOGY (Vol. 113).

191. Pozo, L., Bello, F., Mendez, Y., & Surani, S. (2020). Cystic fibrosis-related diabetes: The unmet need. World Journal of Diabetes, 11(6), 213–217. https://doi.org/10.4239/wjd.v11.i6.213

192. Prevot, V. (2015). Puberty in Mice and Rats. In Knobil and Neill's Physiology of Reproduction: Two-Volume Set (Vol. 2, pp. 1395–1439). Elsevier Inc. https://doi.org/10.1016/B978-0-12-397175-3.00030-2

193. Quinton, P. M. (2007). Cystic fibrosis: Lessons from the sweat gland. In Physiology (Vol. 22, Issue 3, pp. 212–225). Physiology (Bethesda). https://doi.org/10.1152/physiol.00041.2006

194. Racusen, L. C., & Binder, H. J. (1977). Alteration of Large Intestinal Electrolyte Transport by Vasoactive Intestinal Polypeptide in the Rat. Gastroenterology, 73(4), 790–796. https://doi.org/10.1016/S0016-5085(19)31786-X

195. Rafferty, S., Alcolado, N., Norez, C., Chappe, F., Pelzer, S., Becq, F., & Chappe, V. (2009). Rescue of functional F508del cystic fibrosis transmembrane conductance regulator by vasoactive intestinal peptide in the human nasal epithelial cell line JME/CF15. Journal of Pharmacology and Experimental Therapeutics, 331(1), 2–13. https://doi.org/10.1124/jpet.109.155341

196. Rafferty, S., Alcolado, N., Norez, C., Chappe, F., Pelzer, S., Becq, F., & Chappe, V. (2009). Rescue of functional F508del cystic fibrosis transmembrane conductance regulator by vasoactive intestinal peptide in the human nasal epithelial cell line JME/CF15. Journal of Pharmacology and Experimental Therapeutics, 331(1), 2–13. https://doi.org/10.1124/jpet.109.155341

197. Raia, V., Maiuri, L., De Ritis, G., De Vizia, B., Vacca, L., Conte, R., Auricchio, S., & Londei, M. (2000). Evidence of chronic inflammation in

morphologically normal small intestine of cystic fibrosis patients. Pediatric Research, 47(3), 344–350. https://doi.org/10.1203/00006450-200003000-00010

198. Regazzi, R., Rodriguez-Trejo, A., & Jacovetti, C. (2016). Insulin secretion in health and disease: Nutrients dictate the pace. Proceedings of the Nutrition Society, 75(1), 19–29. https://doi.org/10.1017/S0029665115004152

199. Rey, M. M., Bonk, M. P., & Hadjiliadis, D. (2019). Cystic Fibrosis: Emerging Understanding and Therapies. Annual Review of Medicine, 70(1), 197–210. https://doi.org/10.1146/annurev-med-112717-094536

200. Rey, M. M., Bonk, M. P., & Hadjiliadis, D. (2019). Cystic Fibrosis: Emerging Understanding and Therapies. Annual Review of Medicine, 70(1), 197–210. https://doi.org/10.1146/annurev-med-112717-094536

201. Reznikov, L. R., Dong, Q., Chen, J. H., Moninger, T. O., Park, J. M., Zhang, Y., Du, J., Hildebrand, M. S., Smith, R. J. H., Randak, C. O., Stoltz, D. A., & Welsh, M. J. (2013). CFTR-deficient pigs display peripheral nervous system defects at birth. Proceedings of the National Academy of Sciences of the United States of America, 110(8), 3083–3088. https://doi.org/10.1073/pnas.1222729110

202. Rickels, L. G. and M. R. (2015). Pancreatogenic (Type 3c) Diabetes. Pancreapedia: The Exocrine Pancreas Knowledge Base. https://doi.org/10.3998/PANC.2015.35

203. Riordan, J. R., Rommens, J. M., Kerem, B. S., Alon, N. O. A., Rozmahel, R., Grzelczak, Z., Zielenski, J., Lok, S. I., Plavsic, N., Chou, J. L., Drumm, M. L., Iannuzzi, M. C., Collins, F. S., & Tsui, L. C. (1989). Identification of the cystic fibrosis gene: Cloning and characterization of complementary DNA. Science, 245(4922), 1066–1073. https://doi.org/10.1126/science.2475911

204. Rommens, J. M., Iannuzzi, M. C., Kerem, B. S., Drumm, M. L., Melmer, G., Dean, M., Rozmahel, R., Cole, J. L., Kennedy, D., Hidaka, N., Zsiga, M., Buchwald, M., Riordan, J. R., Tsui, L. C., & Collins, F. S. (1989). Identification of the cystic fibrosis gene: Chromosome walking and jumping. Science, 245(4922), 1059–1065. https://doi.org/10.1126/science.2772657

205. Rosignoli, F., Torroba, M., Juarranz, Y., García-Gómez, M., Martinez, C., Gomariz, R. P., Pérez-Leirós, C., & Leceta, J. (2006). VIP and tolerance induction in autoimmunity. Annals of the New York Academy of Sciences, 1070, 525–530. https://doi.org/10.1196/annals.1317.073

206. Rozmahel, R., Wilschanski, M., Matin, A., Plyte, S., Oliver, M., Auerbach, W., Moore, A., Forstner, J., Durie, P., Nadeau, J., Bear, C., & Tsui, L. C. (1996). Modulation of disease severity in cystic fibrosis transmembrane conductance regulator deficient mice by a secondary genetic factor. Nature Genetics, 12(3), 280–287. https://doi.org/10.1038/ng0396-280

207. Said, S. I., & Mutt, V. (1970). Polypeptide with broad biological activity: isolation from small intestine. Science (New York, N.Y.), 169(3951), 1217–1218. https://doi.org/10.1126/science.169.3951.1217

208. Said, S. I., Mutt, V., Yoshida, T., & Hara, N. (1975). Vasoactive polypeptides from normal lung. Chest, 67(2 Suppl), 44S. https://doi.org/10.1016/s0012-3692(15)53085-7

209. Said, S. I. (1991). VIP as a modulator of lung inflammation and airway constriction. The American Review of Respiratory Disease, 143(3 Pt 2), S22-4. https://doi.org/10.1164/ajrccm/143.3_Pt_2.S22

210. Said, S. I. (1991). Vasoactive Intestinal Polypeptide (VIP) in Asthma. Annals of the New York Academy of Sciences, 629(1 Advances in t), 305–318. https://doi.org/10.1111/j.1749-6632.1991.tb37985.x

211. Said, S. I. (2008). The vasoactive intestinal peptide gene is a key modulator of pulmonary vascular remodeling and inflammation. Annals of the New York Academy of Sciences, 1144, 148–153. https://doi.org/10.1196/annals.1418.014

212. Said, S. I. (1991). Vasoactive Intestinal Polypeptide (VIP) in Lung Function and Disease.

213. Said, S I., & Mutt, V. (1972). Isolation from Porcine-Intestinal Wall of a Vasoactive Octacosapeptide Related to Secretin and to Glucagon. European

Journal of Biochemistry, 28(2), 199–204. https://doi.org/10.1111/j.1432-1033.1972.tb01903.x

214. Said, S. I., & Rosenberg, R. N. (1976). Vasoactive intestinal polypeptide: Abundant immunoreactivity in neural cell lines and normal nervous tissue. Science, 192(4242), 907–908. https://doi.org/10.1126/science.1273576

215. Saint-Criq, V., & Gray, M. A. (2017). Role of CFTR in epithelial physiology. In Cellular and Molecular Life Sciences (Vol. 74, Issue 1, pp. 93–115). Birkhauser Verlag AG. https://doi.org/10.1007/s00018-016-2391-y

216. Salinas, D., Haggie, P. M., Thiagarajah, J. R., Song, Y., Rosbe, K., Finkbeiner, W. E., Nielson, D. W., & Verkman, A. S. (2005). Submucosal gland dysfunction as a primary defect in cystic fibrosis. The FASEB Journal, 19(3), 1–13. https://doi.org/10.1096/fj.04-2879fje

217. Sanlioglu, A. D., Karacay, B., Balci, M. K., Griffith, T. S., & Sanlioglu, S. (2012). Therapeutic potential of VIP vs PACAP in diabetes. In Journal of Molecular Endocrinology (Vol. 49, Issue 3). https://doi.org/10.1530/JME-12-0156

218. Sanlioglu, A.D., Dirice, E., Elpek, O., Korcum, A. F., Balci, M. K., Omer, A., Griffith, T. S., & Sanlioglu, S. (2008). High levels of endogenous tumor necrosis factor-related apoptosis-inducing ligand expression correlate with increased cell death in human pancreas. Pancreas, 36(4), 385–393. https://doi.org/10.1097/MPA.0b013e318158a4e5

219. Sato, K., & Sato, F. (1984). Defective beta adrenergic response of cystic fibrosis sweat glands in vivo and in vitro. Journal of Clinical Investigation, 73(6), 1763–1771. https://doi.org/10.1172/JCI111385

220. Sato, K., Cavallin, S., Sato, K. , & Sato, F. (1994). Secretion of ions and pharmacological responsiveness in the mouse paw sweat gland. Clinical Science, 86(2), 133–139. https://doi.org/10.1042/cs0860133

221. Sato, K., & Sato, F. (1988). Variable reduction in β-adrenergic sweat secretion in cystic fibrosis heterozygotes. The Journal of Laboratory and Clinical Medicine, 111(5), 504–510. https://doi.org/10.5555/uri:pii:0022214388900765

222. Savage, M. V, Brengelmann, G. L., Buchan, A. M., & Freund, P. R. (1990). Cystic fibrosis, vasoactive intestinal polypeptide, and active cutaneous vasodilation. Journal of Applied Physiology (Bethesda, Md.: 1985), 69(6), 2149–2154. https://doi.org/10.1152/jappl.1990.69.6.2149

223. Schäfer, M. K., Eiden, L. E., & Weihe, E. (1998). Cholinergic neurons and terminal fields revealed by immunohistochemistry for the vesicular acetylcholine transporter. II. The peripheral nervous system. Neuroscience, 84(2), 361–376. https://doi.org/10.1016/s0306-4522(97)80196-0

224. Schafer, M. K., Weihe, E., Erickson, J. D., & Eiden, L. E. (1995). Human and monkey cholinergic neurons visualized in paraffin-embedded tissues by immunoreactivity for VAChT, the vesicular acetylcholine transporter. Journal of Molecular Neuroscience: MN, 6(4), 225–235. https://doi.org/10.1007/BF02736782

225. Schemann, M., Sann, H., Schaaf, C., & Mäder, M. (1993). Identification of cholinergic neurons in enteric nervous system by antibodies against choline acetyltransferase. The American Journal of Physiology, 265(5 Pt 1), G1005-9. https://doi.org/10.1152/ajpgi.1993.265.5.G1005

226. Schemann, M., Schaaf, C., & Mäder, M. (1995). Neurochemical coding of enteric neurons in the guinea pig stomach. The Journal of Comparative Neurology, 353(2), 161–178. https://doi.org/10.1002/cne.903530202

227. Schofield, J. N., Day, I. N., Thompson, R. J., & Edwards, Y. H. (1995). PGP9.5, an ubiquitin C-terminal hydrolase; pattern of mRNA and protein expression during neural development in the mouse. Brain Research. Developmental Brain Research, 85(2), 229–238. https://doi.org/10.1016/0165-3806(94)00217-n

228. Schroeder, B. C., Cheng, T., Jan, Y. N., & Jan, L. Y. (2008). Expression Cloning of TMEM16A as a Calcium-Activated Chloride Channel Subunit. Cell, 134(6), 1019–1029. https://doi.org/10.1016/j.cell.2008.09.003

229. Semaniakou, A., Brothers, S., Gould, G., Zahiremani, M., Paton, J., Chappe, F., Li, A., Anini, Y., Croll, R. P., & Chappe, V. (2020). Disrupted local innervation results in less VIP expression in CF mice tissues. Journal of Cystic Fibrosis, 0(0). https://doi.org/10.1016/j.jcf.2020.06.013

230. Semaniakou, A., Croll, R. P., & Chappe, V. (2019). Animal models in the pathophysiology of cystic fibrosis. In Frontiers in Pharmacology (Vol. 9, Issue JAN). Frontiers Media S.A. https://doi.org/10.3389/fphar.2018.01475

231. Sharma, R. K., Addis, B. J., & Jeffery, P. K. (1995). The distribution and density of airway vasoactive intestinal polypeptide (vip) binding sites in cystic fibrosis and asthma. Pulmonary Pharmacology, 8(2–3), 91–96. https://doi.org/10.1006/pulp.1995.1011

232. Singh, V. K., & Schwarzenberg, S. J. (2017). Pancreatic insufficiency in Cystic Fibrosis. Journal of Cystic Fibrosis, 16, S70–S78. https://doi.org/10.1016/j.jcf.2017.06.011

233. Smith, D. J., Gaffney, E. A., & Blake, J. R. (2008). Modelling mucociliary clearance. Respiratory Physiology & Neurobiology, 163, 178–188. https://doi.org/10.1016/j.resp.2008.03.006

234. Smyth, R. L. (2000). Intestinal inflammation in cystic fibrosis. Archives of Disease in Childhood, 82(5), 394–399. https://doi.org/10.1136/adc.82.5.394

235. Snouwaert, J. N., Brigman, K. K., Latour, A. M., Malouf, N. N., Boucher, R. C., Smithies, O., & Koller, B. H. (1992). An animal model for cystic fibrosis made by gene targeting. Science, 257(5073), 1083–1088. https://doi.org/10.1126/science.257.5073.1083

236. Steele, P. A., Brookes, S. J., & Costa, M. (1991). Immunohistochemical identification of cholinergic neurons in the myenteric plexus of guinea-pig small

intestine. Neuroscience, 45(1), 227–239. https://doi.org/10.1016/0306-4522(91)90119-9

237. Sun, X., Olivier, A. K., Yi, Y., Pope, C. E., Hayden, H. S., Liang, B., Sui, H., Zhou, W., Hager, K. R., Zhang, Y., Liu, X., Yan, Z., Fisher, J. T., Keiser, N. W., Song, Y., Tyler, S. R., Goeken, J. A., Kinyon, J. M., Radey, M. C., Fligg, D., Wang, X., Xie, W., Lynch, T. J., Kaminsky, P. M., Brittnacher, M. J., Miller, S. I., Parekh, K., Meyerholz, D. K., Hoffman, L. R., Frana, T., Stewart, Z. A., & Engelhardt, J. F. (2014). Gastrointestinal pathology in juvenile and adult CFTR-knockout ferrets. American Journal of Pathology, 184(5), 1309–1322. https://doi.org/10.1016/j.ajpath.2014.01.035

238. Sun, X., Yi, Y., Xie, W., Liang, B., Winter, M. C., He, N., Liu, X., Luo, M., Yang, Y., Ode, K. L., Uc, A., Norris, A. W., & Engelhardt, J. F. (2017). CFTR influences beta cell function and insulin secretion through non-cell autonomous exocrine-derived factors. Endocrinology, 158(10), 3325–3338. https://doi.org/10.1210/en.2017-00187

239. Szema, A. M., & Hamidi, S. A. (2014). Gene Deletion of VIP Leads to Increased Mortality Associated with Progressive Right Ventricular Hypertrophy. Journal of Cardiovascular Disease, 2(3), 131–136. http://www.ncbi.nlm.nih.gov/pubmed/24860842

240. Szema, A. M., Forsyth, E., Ying, B., Hamidi, S. A., Chen, J. J., Hwang, S., Li, J. C., Dwyer, D. S., Ramiro-Diaz, J. M., Giermakowska, W., & Gonzalez Bosc, L. V. (2017). NFATc3 and VIP in idiopathic pulmonary fibrosis and chronic obstructive pulmonary disease. PLoS ONE, 12(1). https://doi.org/10.1371/journal.pone.0170606

241. Takahashi, T., Ohnishi, H., Sugiura, Y., Honda, K., Suematsu, M., Kawasaki, T., Deguchi, T., Fujii, T., Orihashi, K., Hippo, Y., Watanabe, T., Yamagaki, T., & Yuba, S. (2014). Non-neuronal acetylcholine as an endogenous regulator of proliferation and differentiation of Lgr5-positive stem cells in mice. The FEBS Journal, 281(20), 4672–4690. https://doi.org/10.1111/febs.12974

242. Tarique, A. A., Sly, P. D., Holt, P. G., Bosco, A., Ware, R. S., Logan, J., Bell, S. C., Wainwright, C. E., & Fantino, E. (2017). CFTR-dependent defect in alternatively-activated macrophages in cystic fibrosis. Journal of Cystic Fibrosis, 16(4), 475–482. https://doi.org/10.1016/j.jcf.2017.03.011

243. Tarran, R., Grubb, B. R., Parsons, D., Picher, M., Hirsh, A. J., Davis, C. W., & Boucher, R. C. (2001). The CF salt controversy: In vivo observations and therapeutic approaches. Molecular Cell, 8(1), 149–158. https://doi.org/10.1016/S1097-2765(01)00286-6

244. Taylor-Cousar, J. L., Munck, A., McKone, E. F., van der Ent, C. K., Moeller, A., Simard, C., Wang, L. T., Ingenito, E. P., McKee, C., Lu, Y., Lekstrom-Himes, J., & Elborn, J. S. (2017). Tezacaftor–Ivacaftor in Patients with Cystic Fibrosis Homozygous for Phe508del. New England Journal of Medicine, 377(21), 2013–2023. https://doi.org/10.1056/nejmoa1709846

245. Tizzano, E. F., Chitayat, D., & Buchwald, M. (1993). Cell-specific localization of CFTR mRNA shows developmentally regulated expression in human fetal tissues. Human Molecular Genetics, 2(3), 219–224. https://doi.org/10.1093/hmg/2.3.219

246. Tsukada, T., Horovitch, S. J., Montminy, M. R., Mandel, G., & Goodman, R. H. (1985). Structure of the Human Vasoactive Intestinal Polypeptide Gene. DNA, 4(4), 293–300. https://doi.org/10.1089/dna.1985.4.293

247. Tsutsumi, M., Claus, T. H., Liang, Y., Li, Y., Yang, L., Zhu, J., Cruz, F. Dela, Peng, X., Chen, H., Yung, S. L., Hamren, S., Livingston, J. N., & Pan, C. Q. (2002). A potent and highly selective VPAC2 agonist enhances glucose-induced insulin release and glucose disposal: A potential therapy for type 2 diabetes. Diabetes, 51(5), 1453–1460. https://doi.org/10.2337/diabetes.51.5.1453

248. Turton, K. B., Ingram, R. J., & Valvano, M. A. (2020). Macrophage dysfunction in cystic fibrosis: Nature or nurture? Journal of Leukocyte Biology. https://doi.org/10.1002/JLB.4RU0620-245R

249. Uc, A., Olivier, A. K., Griffin, M. A., Meyerholz, D. K., Yao, J., Abu-El-Haija, M., Buchanan, K. M., Vanegas Calderón, O. G., Abu-El-Haija, M., Pezzulo, A. A., Reznikov, L. R., Hoegger, M. J., Rector, M. V., Ostedgaard, L. S., Taft, P. J., Gansemer, N. D., Ludwig, P. S., Hornick, E. E., Stoltz, D. A., Ode, K. L., Welsh, M. J., Engelhardt, J. F., & Norris, A. W. (2015). Glycaemic regulation and insulin secretion are abnormal in cystic fibrosis pigs despite sparing of islet cell mass. Clinical Science, 128(2), 131–142. https://doi.org/10.1042/CS20140059

250. Umetsu, Y., Tenno, T., Goda, N., Shirakawa, M., Ikegami, T., & Hiroaki, H. (2011). Structural difference of vasoactive intestinal peptide in two distinct membrane-mimicking environments. Biochimica et Biophysica Acta - Proteins and Proteomics, 1814(5), 724–730. https://doi.org/10.1016/j.bbapap.2011.03.009

251. Vacas, E., Arenas, M. I., Muñoz-Moreno, L., Bajo, A. M., Sánchez-Chapado, M., Prieto, J. C., & Carmena, M. J. (2013). Antitumoral effects of vasoactive intestinal peptide in human renal cell carcinoma xenografts in athymic nude mice. Cancer Letters, 336(1), 196–203. https://doi.org/10.1016/j.canlet.2013.04.033

252. Valdehita, A., Bajo, A. M., Fernández-Martínez, A. B., Arenas, M. I., Vacas, E., Valenzuela, P., Ruíz-Villaespesa, A., Prieto, J. C., & Carmena, M. J. (2010). Nuclear localization of vasoactive intestinal peptide (VIP) receptors in human breast cancer. Peptides, 31(11), 2035–2045. https://doi.org/10.1016/j.peptides.2010.07.024

253. van Doorninck, J. H., French, P. J., Verbeek, E., Peters, R. H., Morreau, H., Bijman, J., & Scholte, B. J. (1995). A mouse model for the cystic fibrosis delta F508 mutation. The EMBO Journal, 14(18), 4403–4411. https://doi.org/10.1002/j.1460-2075.1995.tb00119.x

254. Van Goor, F., Hadida, S., Grootenhuis, P. D. J., Burton, B., Stack, J. H., Straley, K. S., Decker, C. J., Miller, M., McCartney, J., Olson, E. R., Wine, J. J., Frizzell, R. A., Ashlock, M., & Negulescu, P. A. (2011). Correction of the F508del-

CFTR protein processing defect in vitro by the investigational drug VX-809. Proceedings of the National Academy of Sciences of the United States of America, 108(46), 18843–18848. https://doi.org/10.1073/pnas.1105787108

255. Vankeerberghen, A., Cuppens, H., & Cassiman, J. J. (2002). The cystic fibrosis transmembrane conductance regulator: An intriguing protein with pleiotropic functions. Journal of Cystic Fibrosis, 1(1), 13–29. https://doi.org/10.1016/S1569-1993(01)00003-0

256. Verkman, A. S., Song, Y., & Thiagarajah, J. R. (2003). Role of airway surface liquid and submucosal glands in cystic fibrosis lung disease. In American Journal of Physiology - Cell Physiology (Vol. 284, Issues 1 53-1). American Physiological SocietyBethesda, MD. https://doi.org/10.1152/ajpcell.00417.2002

257. Vertex Announces Positive Phase 3 Study for TRIKAFTA® (elexacaftor/tezacaftor/ivacaftor and ivacaftor) in Children Ages 6-11 Years with Cystic Fibrosis to Support Submissions for Global Regulatory Approvals | Vertex Pharmaceuticals. (2020). Retrieved October 24, 2020, from https://investors.vrtx.com/news-releases/news-release-details/vertex-announces-positive-phase-3-study-trikaftar

258. Villanueva-Romero, R., Gutiérrez-Cañas, I., Carrión, M., González-Álvaro, I., Rodríguez-Frade, J. M., Mellado, M., Martínez, C., Gomariz, R. P., & Juarranz, Y. (2019). Activation of Th lymphocytes alters pattern expression and cellular location of VIP receptors in healthy donors and early arthritis patients. Scientific Reports, 9(1). https://doi.org/10.1038/s41598-019-43717-2

259. Wainwright, C. E., Elborn, J. S., Ramsey, B. W., Marigowda, G., Huang, X., Cipolli, M., Colombo, C., Davies, J. C., De Boeck, K., Flume, P. A., Konstan, M. W., McColley, S. A., McCoy, K., McKone, E. F., Munck, A., Ratjen, F., Rowe, S. M., Waltz, D., & Boyle, M. P. (2015). Lumacaftor–Ivacaftor in Patients with Cystic Fibrosis Homozygous for Phe508del CFTR. New England Journal of Medicine, 373(3), 220–231. https://doi.org/10.1056/nejmoa1409547

260. Wang, N., Freeman, R., & Gibbons, C. (2016). Sympathetic Adrenergic and Cholinergic Innervation of Sweat Glands across a Spectrum of Disease (P5.103). Neurology, 86(16 Supplement).

261. Wardi, A. H., & Allen, W. S. (1972). Alcian blue staining of glycoproteins. Analytical Biochemistry, 48(2), 621–623. https://doi.org/10.1016/0003-2697(72)90118-2

262. Waschek, J. A., Ellison, J., Bravo, D. T., & Handley, V. (1996). Embryonic expression of vasoactive intestinal peptide (VIP) and VIP receptor genes. Journal of Neurochemistry, 66(4), 1762–1765. https://doi.org/10.1046/j.1471-4159.1996.66041762.x

263. Wattchow, D. A., Furness, J. B., Gibbins, I. L., Little, K. E., & Carter, R. F. (1988). Vasoactive intestinal peptide immunoreactive nerve fibres are deficient in intestinal and nasal mucosa affected by cystic fibrosis. Journal of Gastroenterology and Hepatology, 3(6), 549–555. https://doi.org/10.1111/j.1440-1746.1988.tb00784.x

264. Werlin, S. L., Benuri-Silbiger, I., Kerem, E., Adler, S. N., Goldin, E., Zimmerman, J., Malka, N., Cohen, L., Armoni, S., Yatzkan-Israelit, Y., Bergwerk, A., Aviram, M., Bentur, L., Mussaffi, H., Bjarnasson, I., & Wilschanski, M. (2010). Evidence of intestinal inflammation in patients with cystic fibrosis. Journal of Pediatric Gastroenterology and Nutrition, 51(3), 304–308. https://doi.org/10.1097/MPG.0b013e3181d1b013

265. Widdicombe, J. H., & Wine, J. J. (2015). Airway Gland Structure and Function. Physiological Reviews, 95(4), 1241–1319. https://doi.org/10.1152/physrev.00039.2014

266. Wildhaber, J., Seelentag, W. K. F., Spiegel, R., & Schöni, M. H. (1996). Cystic fibrosis associated with neuronal intestinal dysplasia type B: A case report. Journal of Pediatric Surgery, 31(7), 951–954. https://doi.org/10.1016/S0022-3468(96)90419-4

267. Wilschanski, M., & Novak, I. (2013). The cystic fibrosis of exocrine pancreas. Cold Spring Harbor Perspectives in Medicine, 3(5). https://doi.org/10.1101/cshperspect.a009746

268. Wine, J. J. (2004). Submucosal Glands and Airway Defense. Proceedings of the American Thoracic Society, 1(1), 47–53. https://doi.org/10.1513/pats.2306015

269. Wine, J. J. (2007). Parasympathetic control of airway submucosal glands: Central reflexes and the airway intrinsic nervous system. https://doi.org/10.1016/j.autneu.2007.01.008

270. Wine, J.J., Char, J. E., Chen, J., Cho, H.-J., Dunn, C., Frisbee, E., Joo, N. S., Milla, C., Modlin, S. E., Park, I.-H., Thomas, E. A. C., Tran, K. V, Verma, R., & Wolfe, M. H. (2013). In vivo readout of CFTR function: ratiometric measurement of CFTR-dependent secretion by individual, identifiable human sweat glands. PloS One, 8(10), e77114. https://doi.org/10.1371/journal.pone.0077114

271. Wine, J.J. (2010). The development of lung disease in cystic fibrosis pigs. In Science Translational Medicine (Vol. 2, Issue 29). American Association for the Advancement of Science. https://doi.org/10.1126/scitranslmed.3001130

272. Winzell, M. S., & Ahrén, B. (2007). Role of VIP and PACAP in islet function. Peptides, 28(9), 1805–1813. https://doi.org/10.1016/j.peptides.2007.04.024

273. Wu, D., Lee, D., & Sung, Y. K. (2011). Prospect of vasoactive intestinal peptide therapy for COPD/PAH and asthma: A review. In Respiratory Research (Vol. 12, Issue 1, p. 45). BioMed Central Ltd. https://doi.org/10.1186/1465-9921-12-45

274. Wu, Y.-Z., Abolhassani, M., Ollero, M., Dif, F., Uozumi, N., Lagranderie, M., Shimizu, T., Chignard, M., & Touqui, L. (2010). Cytosolic phospholipase A2? mediates Pseudomonas aeruginosa LPS-induced airway constriction of CFTR -/- mice. In Respiratory Research (Vol. 11). https://doi.org/10.1186/1465-9921-11-49

275. Xia, C., Braunstein, Z., Toomey, A. C., Zhong, J., & Rao, X. (2018). S100 proteins as an important regulator of macrophage inflammation. In Frontiers in Immunology (Vol. 8, Issue JAN, p. 1). Frontiers Media S.A. https://doi.org/10.3389/fimmu.2017.01908

276. Xie, Y., Ostedgaard, L., Abou Alaiwa, M. H., Lu, L., Fischer, A. J., & Stoltz, D. A. (2018). Mucociliary transport in healthy and cystic fibrosis pig airways. Annals of the American Thoracic Society, 15(Supplement_3), S171–S176. https://doi.org/10.1513/AnnalsATS.201805-308AW

277. Xue, R., Gu, H., Qiu, Y., Guo, Y., Korteweg, C., Huang, J., & Gu, J. (2016). Expression of Cystic Fibrosis Transmembrane Conductance Regulator in Ganglia of Human Gastrointestinal Tract. Scientific Reports, 6, 30926. https://doi.org/10.1038/srep30926

278. Yoo, B. B., & Mazmanian, S. K. (2017). The Enteric Network: Interactions between the Immune and Nervous Systems of the Gut. In Immunity (Vol. 46, Issue 6, pp. 910–926). Cell Press. https://doi.org/10.1016/j.immuni.2017.05.011

279. Yu, R., Liu, H., Peng, X., Cui, Y., Song, S., Wang, L., Zhang, H., Hong, A., & Zhou, T. (2017). The palmitoylation of the N-terminal extracellular Cys37 mediates the nuclear translocation of VPAC1 contributing to its antiapoptotic activity. Oncotarget, 8(26), 42728–42741. https://doi.org/10.18632/oncotarget.17449

280. Zahm, J. M., Gaillard, D., Dupuit, F., Hinnrasky, J., Porteous, D., Dorin, J. R., & Puchelle, E. (1997). Early alterations in airway mucociliary clearance and inflammation of the lamina propria in CF mice. American Journal of Physiology - Cell Physiology, 272(3 41-3). https://doi.org/10.1152/ajpcell.1997.272.3.c853

281. Zhou, Z., Duerr, J., Johannesson, B., Schubert, S. C., Treis, D., Harm, M., Graeber, S. Y., Dalpke, A., Schultz, C., & Mall, M. A. (2011). The ENaC-overexpressing mouse as a model of cystic fibrosis lung disease. Journal of Cystic Fibrosis, 10(SUPPL. 2). https://doi.org/10.1016/S1569-1993(11)60021-0

282. Zielenski, J., Corey, M., Rozmahel, R., Markiewicz, D., Aznarez, I., Casals, T., Larriba, S., Mercier, B., Cutting, G. R., Krebsova, A., Macek M., J., Langfelder-Schwind, E., Marshall, B. C., Decelie-Germana, J., Claustres, M., Palacio, A., Bal, J., Nowakowska, A., Ferec, C., Estivill, X., Durie, P., & Tsui, L. C. (1999). Detection of a cystic fibrosis modifier locus for meconium ileus on human chromosome 19q13 [3]. In Nature Genetics (Vol. 22, Issue 2, pp. 128–129). Nat Genet. https://doi.org/10.1038/9635